THE
PHYSICAL REVIEW

A journal of experimental and theoretical physics established by E. L. Nichols in 1893

SECOND SERIES, VOL. 74, NO. 4 AUGUST 15, 1948

UNIVERSITY OF MICHIGAN LIBRARIES

Nuclear Spins of the Carbon Isotopes

F. A. JENKINS

Department of Physics, University of California, Berkeley, California

(Received May 3, 1948)

High dispersion spectrograms of the Swan bands of diatomic carbon are obtained from samples enriched to 50 percent and 40 percent, respectively, in C^{13} and C^{14}. The method of exciting an intense spectrum with microgram samples is described. To permit measurements of the alternating-intensity ratio, current densities in the source had to be limited so that the Λ-type doublets were well resolved. For C^{13}, photometric measurements of this ratio give 3:1, showing that the nuclear spin $I=\frac{1}{2}$. The antisymmetric rotational levels have the higher statistical weight (Fermi-Dirac statistics). For C^{14}, only the lines from symmetric levels appear. This shows clearly that $I=0$ for C^{14}, and that the nucleus obeys Einstein-Bose statistics. Wave numbers are given of lines in the R branches of the 0,0 band in the range $K=12$ to 20, due to all molecular species containing C^{12}, C^{13} and C^{14}. An isotope effect in the splittings of the electronic triplets is investigated, and found to agree with that calculated from the general term formula for $^3\Pi$ states.

1. INTRODUCTION

BECAUSE of the considerable interest in the spin of C^{14} from the standpoint of the theory of beta-decay, work was begun by the author in the fall of 1946 to develop a technique of determining it when sufficient quantities of this radioactive isotope should become available. These preliminary experiments were carried on with C^{13}, for which the spin determination was then in an unsatisfactory state. The only attempt to measure it, made by Townes and Smythe,[1] had shown that it was either $\frac{1}{2}$ or $\frac{3}{2}$, and the evidence rather favored the latter value. The first result of this work was the proof[2] that $I=\frac{1}{2}$ for C^{13}. Later it was shown[3] that $I=0$ for C^{14}. The purpose of this paper is to present the details of the two determinations.

Of the two methods of measuring nuclear spins by optical spectroscopy, that using hyperfine structure is most effective for the heavier elements, while that using alternating intensities in band spectra has thus far been the only feasible one for the lighter ones. This is because the light elements have smaller hyperfine splittings, and their lines have a greater Doppler broadening. Hence in the work of Townes and Smythe on C^{13}, it was logical to study the alternating intensities in the well-known Swan bands of diatomic carbon, C_2. This particular band system is not ideal for such observations, since it is of the rather complex type $^3\Pi$, $^3\Pi$. The intensity ratio to be measured is in this case the ratio of the two components in a set of narrow doublets, the so-called Λ-doublets. In the C_2

[1] C. H. Townes and W. R. Smythe, Phys. Rev. **56**, 1210 (1939).
[2] F. A. Jenkins, Phys. Rev. **72**, 169(A) (1947).
[3] F. A. Jenkins, Phys. Rev. **73**, 639 (1948).

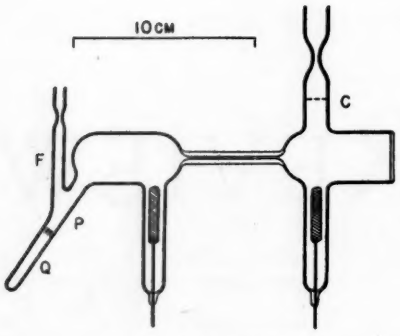

FIG. 1. Discharge tube.

bands, these have a separation of only 0.04A in the region where they are easily observable, and hence high resolving power is required. Townes and Smythe achieved ample instrumental resolving power by crossing a Lummer-Gehrcke plate with a large grating. This system was so wasteful of light, however, that they were obliged to run their source at large current densities; with a consequent increase in the intrinsic width of the lines. Therefore the Λ-doublets were not resolved in their work.

In the present investigation the method was essentially the same as that of Townes and Smythe, the chief improvement being the use of an excellent Wood grating. This is particularly bright in the second order green, where it has the same resolving power as the Lummer plate mentioned above. The saving of light permitted smaller currents in the source, and the Λ-doublets could then be resolved. Considerable study was also made of the best way of exciting the spectrum with very small amounts of carbon. It was first shown by R. C. Johnson[4] that a very intense source of the Swan bands is obtained in a sealed-off discharge tube of the conventional type containing about 20 mm of argon or helium, a trace of hydrogen, and small quantities of carbon or of any carbon-containing gas. This method of excitation was used by Wooldridge and the author[5] in measuring the enrichment of C^{13} in certain samples, and later by Brosi and Harkins.[6] The present work shows that it is an extremely efficient process, approaching in sensitivity that of the best methods of spectrographic detection of metals.

As regards the availability of samples of carbon enriched in the heavy isotopes, the author was fortunate at the outset in having several samples of methane enriched in C^{13} left over from a previous investigation,[5] and later he obtained some having a concentration as high as 35 percent of C^{13} through the kindness of Professor Smythe. Other concentrated samples of methane were later furnished through the good offices of Drs. A. V. Grosse and W. F. Libby, and finally a sizeable sample of $BaCO_3$ containing 52.5 percent of C^{13} became available. The latter is being used by Dr. Amos Newton of the University of California Radiation Laboratory for the determination of its enrichment in C^{14}, the sample having been produced at the Eastman Kodak Company. Besides these samples enriched by diffusion methods, others were used consisting of microgram amounts of elemental C^{13} separated in the large mass-spectrograph of the Radiation Laboratory, since it was thought that a similar separation of C^{14} from pile-bombarded materials might prove to be the most expeditious method. For the preparation of these samples of C^{13}, and later ones of C^{14}, the author is indebted to Drs. B. J. Moyer and W. L. Whitson. Recently, several milligrams of highly enriched C^{14} prepared by Norris and Snell[7] were made available through the Isotopes Division of the Atomic Energy Commission.

The spin of C^{13} was first definitely established using the samples from Professor Smythe, while the result for C^{14} was first obtained with the material from Norris and Snell. The mass-spectrographic samples, however, yielded as good a result a few days later.

2. EXPERIMENTAL PROCEDURE

The type of spectrum tube used in exciting the C_2 bands is shown in Fig. 1. It has solid aluminum electrodes, a 1 mm glass capillary, and a fused-on plane glass window. After being filled as described below, the tube was sealed off from the vacuum system, and would usually provide an intense source for many hours. The side-tube *P*, *Q*, of glass joined to a short piece of quartz

[4] R. C. Johnson, Phil. Trans. Roy. Soc. London **A226**, 157 (1926).
[5] D. E. Wooldridge and F. A. Jenkins, Phys. Rev. **49**, 404 (1936).
[6] A. R. Brosi and W. D. Harkins, Phys. Rev. **52**, 472 (1937).
[7] L. D. Norris and A. H. Snell, Phys. Rev. **73**, 254 (1948).

tubing Q by a graded seal, was required only when $BaCO_3$ was the starting material.

The first step in the preparation of a tube was the thorough removal of all impurities of ordinary carbon. This was accomplished by running the tube alternately with air and argon and by an occasional heating of all parts of the tube with a torch to near the softening point. If after filling with pure argon at 20 mm, the head of the green Swan band at λ5165 did not appear after 10 minutes' running at a current of 45 ma, the tube was judged to be clean.

Carbon was next deposited on the electrodes, either by decomposition of CH_4 or CO_2 with a discharge, or by slipping over one of the electrodes a cylinder of aluminum foil on which a film of carbon had been collected in the mass-spectrograph. When methane was used, it could be almost completely decomposed at a pressure of a few mm in half an hour. With CO_2 the process was very slow but could be greatly accelerated by adding an excess of hydrogen. When the original sample was in the form of $BaCO_3$, it was decomposed thermally in the quartz tube Q by heating the sample introduced through the filling tube F, with a torch to 1100°C.[8] When the deposit from the mass-spectrograph was used, the connecting tube was cracked off at the point C, the aluminum cylinder slipped over the electrode with forceps, and the tube re-sealed and evacuated prior to adding the argon.

To obtain high intensity of the Swan bands, it is essential that there be the proper amount of hydrogen in the tube, besides the carbon and argon. Apparently hydrocarbons must be formed in the discharge, and their subsequent decomposition gives the C_2 molecules. In the method here used, the necessary hydrogen is evolved from the aluminum electrodes, and could be controlled to some extent by the intensity of the discharge, which determines the heating of the electrodes. Too much hydrogen quenches the bands, and the tubes prepared by inserting aluminum foil were not as satisfactory, because the foil could not be adequately outgassed before sealing off. Mercury must of course be excluded, and this was done by using traps cooled in liquid nitrogen, or in dry ice and acetone when working with CO_2.

Some tests of the sensitivity of this mode of excitation were first made by introducing known, small amounts of ordinary CO_2. Although the ultimate limit of detection was not definitely established, it cannot lie far below 0.07 μg, with which amount the Swan bands were still obtained strong enough to yield a grating spectrogram. Several micrograms are required, however, to develop the bands to their full intensity, under which conditions the discharge in the capillary is an intense greenish-white color.

The spectrograph utilized a 21 foot aluminum-on-glass concave grating, ruled 30,000 lines to the inch for 5¼ in. Its dispersion was 0.568A/mm in the second order. The theoretical resolving power of 315,000 was somewhat greater than that needed for lines of the intrinsic width given by these tubes when they were excited by a current of 45 ma directly from a 20-kv transformer regulated by a rheostat in the primary. Exposures were from 10 minutes to 1 hour on Eastman "Experimental 2a-J" plates, which were kindly prepared at the author's request. These plates showed less fog and finer grain than the 103a-J plates first tried, though their sensitivity at λ5600 was about the same.

To permit the measurement of line intensities, the interesting portion of the 0,0 band, λλ5130–5142, was photographed through a step-weakener having eight steps 1.5 mm wide, of sputtered platinum on a crystal quartz plate. This was placed, with its steps perpendicular to the spectrum lines, immediately in front of the photographic plate. The astigmatism of the grating was large enough to give lines whose intensity was constant over the greater part of their height. The weakener was calibrated by measuring transmissions for the principal mercury lines with a photocell. Plate densities were measured with a Zeiss recording microphotometer. Relative intensities were always measured by the parallel displacement of the transmission curves, i/i_0, for each line along the $\log I$ axis.[9] This method of plate calibration automatically corrects for the most common errors in photographic photometry.

[8] L. D. Norris and M. G. Inghram, Phys. Rev. **73**, 350 (1948).

[9] Ornstein, Moll, and Burger, *Objektive Spektralphotometrie* (Vieweg, Braunschweig, Germany, 1932), pp. 46, 89.

UNIVERSITY OF MICHIGAN LIBRARIES

3. SPECTROGRAMS

No attempt was made to photograph and measure all the lines of the band systems because of the isotopic molecules $C^{12}C^{13}$, $C^{13}C^{13}$, $C^{12}C^{14}$ and $C^{14}C^{14}$. (These molecular species will for convenience be designated 12–13, 13–13, 12–14 and 14–14.) Since the primary interest was in finding the spins, attention was focused on that part of the band systems where the Λ-doublets are most easily observed. This proved to be the same as that selected by Townes and Smythe, namely the R branches of the 0,0 bands between rotational quantum numbers $K=12$ and 20. In this region the isotope shifts and the spacing of successive triplets of the R branch are fortunately so related that there is very little trouble with coincidence of lines of the several isotopic systems.

The advantage of observing this particular region will be clear from Fig. 2, in which the lower strip is enlarged 1.8× from the original plate, and the upper three, 11.1×. The isotope shifts, which here are primarily rotational isotope effects, place the important lines, those of 13–13 and 14–14, in favorable positions for observation. Higher rotational quantum numbers would show larger splittings of the Λ-doublets, but unfortunately the second band of the sequence, the 1,1 band, begins just beyond $R(19)$. At values of K below about 12, there is more confusion of the lines of the different molecules, and the Λ-doublets become too narrow to be resolved.

As will be seen in Fig. 2, the lines of 12–12 and 14–14 show no Λ-doubling. They are, however, alternately displaced toward higher and lower frequency from a smooth series by an amount equal to the Λ-doubling observed for the corresponding unsymmetrical 12–13 and 12–14 molecules. This effect may easily be seen on the spectrograms, since the doubling is negligible for the R_2 lines, and largest for R_3. Thus the spacing between the central and right-hand components of the electronic triplets is alternately wider and narrower. This "staggering" of the position of

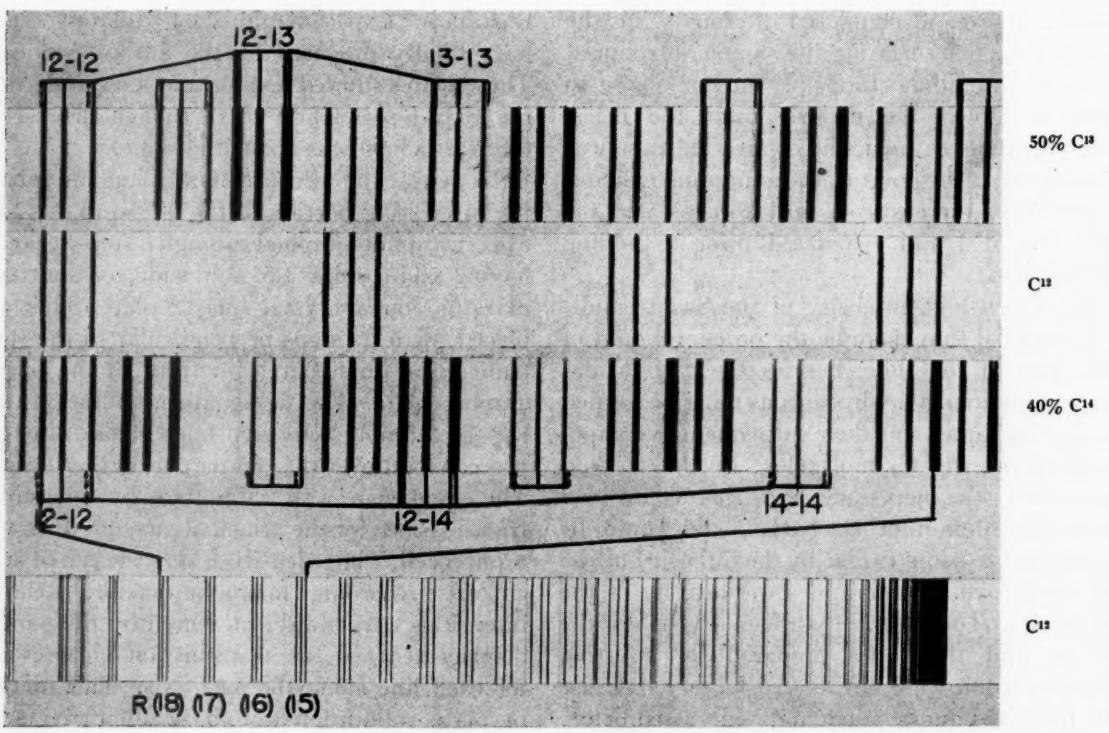

FIG. 2. Spectrograms of ordinary and isotopic carbon. Below is shown the complete 0,0 band of ordinary carbon. The middle of the upper three strips shows four triplets from this band greatly enlarged, while above and below, on the same scale, are the corresponding regions containing the bands due to carbon enriched in C^{13} and C^{14}, respectively. Triplets of the same K value in bands due to the three isotopic molecules have their leaders connected. Other triplets of the heaviest molecule are also marked with short leaders.

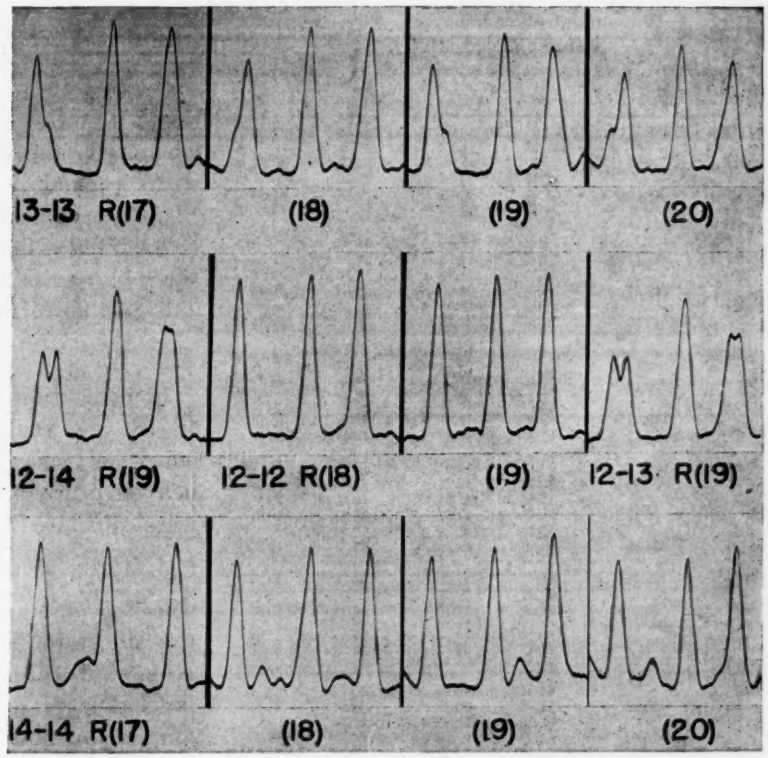

FIG. 3. Microphotometer traces of triplets of the R branch. Top, due to $C^{13}C^{13}$; middle, $C^{12}C^{13}$ and mixed molecules; bottom, $C^{14}C^{14}$.

the lines is well-known[10] in the ordinary Swan bands, and results from the fact that alternately one component and the other of the Λ-doublets is missing because the nuclear spin is zero. The 13–13 bands, on the other hand, show both components, with different intensities. This is a characteristic of the finite nuclear spin.

Three sets of plates were studied intensively. First, a set in which the measured intensities indicated a concentration of 33 percent C^{13} in the spectrum tube, which was made from the best Smythe sample. The lines of 12–13 and 13–13 were identified on these plates, and a detailed analysis made of the intensity contours of three of the R_3 Λ-doublets of 13–13. These indicated an intensity ratio of 3:1, and, since this ratio of the statistical weights is $(I+1)/I$, where I is the nuclear spin, the latter was reported[2] to be $\frac{1}{2}$ for C^{13}. The second set was made using the best sample of C^{14} from Norris and Snell, and showed 40 percent C^{14}. The complete absence of one component of the Λ-doublets was obvious on inspection, and therefore it was concluded[3] that $I=0$ for C^{14}. The last set was made with the richer C^{13} material from the Eastman Kodak Co., and permitted a measurement of the intensity ratio for eight doublets, the results of which agree with the previous conclusion, as will be shown below.

The first plates showed clear resolution of the Λ-doublets of R_3 in 12–13. This may be seen in the microphotometer curves shown in Fig. 3. The left-hand component of the triplet for $R(19)$ (center strip, at the right) has a measured splitting of 0.041A. That this is considerably greater than the theoretical limit of resolution of the grating, 0.0163A, proves the chief cause of the observed width of the lines to be in the light source, and not in the grating. In Fig. 3, it will be seen that there is even a beginning of resolution of the $R_1(19)$ doublet. The separation of this doublet as predicted from the "staggering" of the R_1 lines of the 12–12 bands (see below) is only 0.021A.

Since some interest may attach to the values of the isotope shifts from the standpoint of the theory of this effect in $^3\Pi$, $^3\Pi$ bands, the wave-numbers of all lines measured are given in Table I. These data are obviously very incomplete,

[10] J. D. Shea, Phys. Rev. **30**, 825 (1927).

UNIVERSITY OF MICHIGAN LIBRARIES

TABLE I. Wave-numbers of lines caused by various isotopic molecules.

K''	J''	12–12	12–13	13–13	12–14	14–14
	11(R_2)	19,435.13 *S*	19,431.58	19,428.06 *S*	19,428.54	19,421.84 *S*
		—— *A*	31.73	28.17 *A*	28.69	—— *A*
12	12(R_2)	36.15 *S*	32.60	29.04 *S*	29.59	22.87 *S*
		—— *A*	32.60	29.04 *A*	29.59	—— *A*
	13(R_1)	37.13 *S*	33.67	30.15 *S*	30.66	24.00 *S*
		—— *A*	33.67	30.15 *A*	30.66	—— *A*
	12	—— *A*	37.81	33.99 *A*	34.55	—— *A*
		41.77 *S*	37.97	34.13 *S*	34.71	27.55 *S*
13	13	—— *A*	38.79	34.99 *A*	35.54	—— *A*
		42.57 *S*	38.79	34.99 *S*	35.54	28.45 *S*
	14	—— *A*	39.75	35.95 *A*	36.52	—— *A*
		43.50 *S*	39.75	35.95 *S*	36.52	29.51 *S*
	13	48.29 *S*	44.27	40.21 *S*	40.80	33.17 *S*
		—— *A*	44.41	40.35 *A*	40.95	—— *A*
14	14	49.19 *S*	45.20	41.14 *S*	41.77	34.15 *S*
		—— *A*	45.20	41.14 *A*	41.77	—— *A*
	15	49.93* *S*	46.06	42.03 *S*	42.57	35.12 *S*
		—— *A*	46.06	42.03 *A*	42.57	—— *A*
	14	—— .	50.93	46.61 .	47.24	—— .
		55.38 .	51.08	46.74 .	47.38	39.27 .
15	15	—— .	51.83	47.51 .	48.13	—— .
		56.13 .	51.83	47.51 .	48.13	40.07 .
	16	——	52.60	48.29	48.94	——
		56.89	52.60	48.29	48.94	40.95
	15	62.41	57.83	53.25	53.90	45.27
		——	57.97	53.38	54.04	——
16	16	63.22	58.68	54.10	54.76	46.17
		——	58.68	54.10	54.76	——
	17	63.88	59.39	54.87	55.52	46.93
		——	59.39	54.87	55.52	——
	16	——	64.94	60.06	60.77	——
		69.93	65.08	60.19	60.91	51.80
17	17	——	65.76	60.88	61.60	——
		70.64	65.76	60.88	61.60	52.52
	18	——	66.40	61.51	62.24	——
		71.28	66.40	61.51	62.24	53.26
	17	77.41	72.27	67.12	67.85	58.20
		——	72.43	67.25	68.01	——
18	18	78.18	73.07	67.92	68.65	59.01
		——	73.07	67.92	68.65	——
	19	78.70	73.60	68.57	69.28	59.64
		——	73.71	68.57	69.28	——
	18	——	79.84	74.35	75.16	——
		85.25*	80.01	74.51	75.31	65.08
19	19	——	80.63	75.14	75.94	——
		86.07	80.63	75.14	75.94	66.76
	20	——	81.12	75.66	76.46	——
		86.64	81.22	76.66	76.55	66.40
	19	93.40	87.61	81.86	82.70	71.89
		——	87.77	82.02	82.85	——
20	20	94.08	88.18	82.64	83.47	72.65
		——	88.18	82.64	83.47	——
	21	94.64	88.76	83.22	83.93	73.19
		——	88.76	83.22	84.04	——

* Values from Shea (reference 10) appeared to be in error. More exact values are 19,450.01 and 19,485.46 cm^{-1}.

and could be greatly extended by further work on the plates. In the wave-length measurements, the iron arc standards were not used; instead the accurate wave-lengths of the 12–12 lines given by Shea[10] were used as reference lines. This was done partly for convenience, partly with the idea that since the shifts are more significant than the absolute values, wave-lengths measured relative to those of Shea would be most useful.

In Table I, *S* and *A* designate the symmetric and antisymmetric character of the wave functions of the states involved, exclusive of the part due to nuclear spin. Thus, in the upper electronic state, $^3\Pi_g$, the *S* states are those with + rotational functions,[11] and the *A* with − ones, whereas in the lower, $^3\Pi_u$, the correlation is *S* with −, and *A* with +. In both 12–12 and 14–14 the *A* states and lines are missing while in 13–13 the lines involving *A* states are considerably stronger than those involving *S* states. This will be further discussed below.

4. SPIN OF C^{13}

Identification of the lines due to 12–13 and 13–13 was easy when plates were compared which showed different concentrations of the heavier isotope. As a check, however, the shifts were calculated by the approximate relation

$$\Delta\nu=(\rho-1)\nu_v+(\rho^2-1)\nu_r, \qquad (1)$$

where $\rho=(\mu_1/\mu_2)^{\frac{1}{2}}\nu_v$ and ν_r were evaluated by the aid of the constants for 12–12 as given by King and Birge.[12] This gave shifts about 2.5 percent larger than the observed ones. For example, the line $R_2(18)$ of 12–13 is expected to have a vibrational shift of −1.40 cm^{-1} and a rotational shift of −3.88 cm^{-1}, total −5.28. The observed shift was −5.12 cm^{-1}. The origin of this discrepancy lies in the fact that the electronic and rotational energies are not properly separated by this method (see below). In predicting the shifts for other isotopic species, however, quite accurate results were obtained by assuming the calculated vibrational shift to be correct and applying rotational shifts proportional to ρ^2-1 relative to the observed rotational shift for 12–13.

The relative intensities of the bands due to 12–12, 12–13 and 13–13 are in the ratio $1:2r:r^2$, where r is the ratio of the numbers of atoms of C^{13} and C^{12}. From each plate, r was determined by measuring the relative intensity of several corresponding R_2 lines in the three bands. (These lines were chosen because they have a negligible Λ-doubling.) It was found that tubes prepared from the 35 percent material gave intensities corresponding to $r=0.5$, or a concentration of 33 percent, while those from the 52.5 percent sample gave 49 percent. This slight

[11] R. S. Milliken, Rev. Mod. Phys. **2**, 146 (1930).
[12] A. S. King and R. T. Birge, Astrophys. J. **72**, 38 (1930).

reduction from the initial concentrations resulted from unavoidable contamination with traces of ordinary carbon. When the amount of the sample was only a few micrograms, as with the mass-spectrograph deposits, this effect was more important. Even though these deposits must have consisted essentially of the pure single isotope, the greatest precautions had to be taken in order to obtain in this way a tube exhibiting a concentration higher than 30 percent of the heavier isotope.

For the measurement of the spin, the R_3 doublets were used since these have the widest splitting. Even for them, however, there was rarely an appreciable minimum between the two components because of the large difference in their intensities. The weaker component usually appeared merely as a shoulder on the side of the stronger one (see the left-hand component in upper strip of microphotometer traces in Fig. 3). In measuring the intensity ratio, two other difficulties exist, besides the lack of clear resolution. One is the presence of a number of weak lines of extraneous origin, some of which may coincide with the lines to be measured. Certain of these are the weak P branches returning from the band heads, but the most disturbing ones appear to be due to impurities, for example CN which will appear if any nitrogen is present. It was evidently the presence of a weak line of CN lying just on the short wavelength side of the line $R_3(19)$ that led Townes and Smythe to favor the higher value of the spin; it caused a spurious width for the weaker component. The other difficulty is the existence of a continuous background, which even on the best plates contributed about one-third the intensity of the weaker line. This line itself has only one-fourth of the total intensity of the R_3 doublet, which in 50 percent material is only one-half as strong as the unresolved R_2 doublet of 12–13. Hence the background is only 1/24 or 4 percent as intense as the strongest lines. Measuring it accurately, however, was one of the chief difficulties.

Since all of the three effects mentioned (lack of resolution, spurious lines, and background) tend to reduce the measured ratio of peak intensities below the true value, the following method was adopted. The peak intensities of the two components, the weaker of which was actually more of a shoulder than a peak, were measured for eight R_3 doublets of 13–13 and the intensity of the background subtracted from each. The ratio of the values for the two components were then plotted against rotational quantum number, as shown in Fig. 4 for the plate taken with 49 percent C^{13}. This should reveal the effect of spurious lines by large fluctuations, and the effect of lack of resolution by a decreasing ratio at lower rotational quantum numbers where the splittings are less. Both these effects are to be seen in Fig. 4. That the lines $R_3(14)$ and $R_3(20)$ have disturbing lines superposed on the weaker component was verified by examining other plates taken with a smaller concentration of C^{13}. It is clear, however, that the ratio approaches at large K the theoretical value of 3.0 for a spin $I=\frac{1}{2}$. The next higher possible spin, $I=\frac{3}{2}$, would give an intensity ratio of 1.67, in definite disagreement with these measurements.

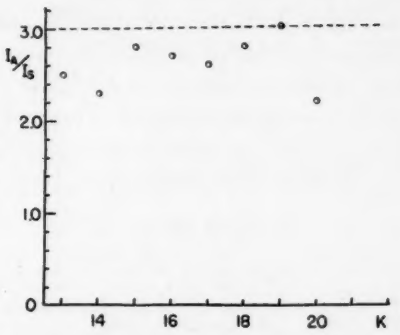

FIG. 4. Measured intensity ratios of the components of the Λ-doublets in $C^{13}C^{13}$.

These results appear to definitely establish that the spin of C^{13} is $\frac{1}{2}$. Although the exact value taken for the background has an important influence on the intensity ratios, it should be emphasized that no possible choice of background will bring the ratio down to 1.67. Without subtracting any background at all, the measured ratios are still about 2.0. Furthermore, a proof that there are no serious errors in the photometry is given by the fact that the intensities of corresponding R_2 lines of 12–12, 12–13 and 13–13 in the 50 percent sample came out very close to the theoretical values 1:2:1.

As regards the statistics obeyed by the C^{13} nucleus, it was concluded by Townes and Smythe,[1] and is verified here, that the A lines are the stronger, as required for Fermi-Dirac statistics. This may be seen directly in either

UNIVERSITY OF MICHIGAN LIBRARIES

Fig. 2 or Fig. 3 from the circumstance that for lines of the same rotational quantum number the component which is missing in 12–12 is the one which is the stronger in 12–13. The nucleus of C^{12} since it contains an even number of particles, obeys the Einstein-Bose statistics.

5. SPIN OF C^{14}

Band lines caused by C^{14} were first obtained with a tube containing a 2.7 μg deposit from the mass-spectrograph. Unavoidable contamination with ordinary carbon, however, resulted in an intensity of the 12–14 band corresponding to only 16 percent of C^{14}. This was sufficient to show lines due to 14–14, but they were so weak that it was difficult to identify them with any certainty among the many weak impurity lines. Shortly thereafter, a 2.6 mg sample of $BaCO_3$ furnished by Norris and Snell,[7] and reported to have[13] a concentration of approximately 19 percent, was tried. It was actually much richer than this, since the intensity measurements yielded 27 percent C^{14}. On these plates the 14–14 lines were plainly visible, and a comparison with the previous plates left no doubt as to their correct identification, since all of the true lines were about four times as strong. No doubling whatever of these lines could be detected, although the resolution was at least as good as on the C^{13} plates. Furthermore, a staggering of the R_3 lines was apparent, and it therefore seemed clear that the spin of C^{14} is zero as in C^{12}.

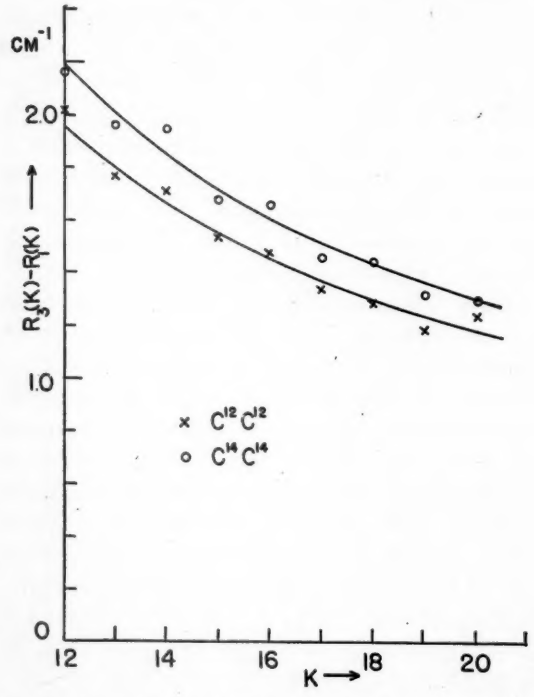

FIG. 5. Observed and calculated widths of the spin triplets.

Two further sets of plates were obtained showing still higher concentrations of C^{14}, one with a sample supposed[13] to contain about 27 percent of C^{14}, and another with a 5.8 μg sample from the mass-spectrograph. Photometric measurements on the first set, from which Figs. 2 and 3 were made, showed 40 percent C^{14}. The mass-spectrographic sample was split in two, and half put on each electrode. This, combined with extreme precautions to avoid contamination by ordinary carbon, resulted in a tube which also showed a concentration of 40 percent. These plates with greater enrichment served to confirm very definitely the results reached earlier. If the spin of C^{14} had been finite, the weaker component of the Λ-doublets would necessarily have been at least $\frac{1}{2}$ (or possibly $\frac{1}{3}$) the intensity of the stronger one, and could not conceivably have been overlooked. The 14–14 lines on these plates are nearly half as strong as those due to 12–12.

The statistics of the C^{14} nucleus is, as expected for a nucleus with an even number of particles, the same as for C^{12}, i.e., Bose-Einstein. This is determined from the fact that for lines of the same rotational quantum number, the staggering is in the same direction. Examination of Figs. 2 and 3, particularly a comparison of the lower two strips in Fig. 3, will show the definiteness of this effect.

6. ISOTOPE EFFECT

A more exact calculation of the isotope shifts than is given by Eq. (1) could be made with the aid of the theoretical term formulas for $^3\Pi$ states given by Budó.[14] In this paper are to be found also the rotational and electronic constants of the 0,0 band of C_2, upon which Budó tested the theory. Since there is now little reason to doubt the correctness of this theory, the complete calculations have not been made here. One feature of the observed shifts, however, is

[13] The author is informed by Mr. Norris that a corrected count on this sample gave the figure 22 percent. Similarly, the second sample used here should have been 32 percent instead of 27 percent. See L. D. Norris, Bull. Am. Phys. Soc. **23**, 46 (1948), paper T9.

[14] A. Budó, Zeits. f. Physik **98**, 437 (1935).

apparent from inspection of the plates, and can easily be compared with theory. This is the fact that the width of the spin triplets is not the same for lines of the different isotopic molecules having the same rotational quantum number. It increases with the mass of the molecule, and in 14–14 is some 10 percent greater than in 12–12. This effect may be seen in Fig. 2, and especially in Fig. 3, where the triplets $R(18)$ and $R(19)$ are placed one above the other for 12–12 and 14–14.

If the triplet splittings were purely electronic in origin, they would be the same for different isotopes, but it is well known that in multiplet electronic states there is an interaction between electronic and rotational motion. Hence for the correct evaluation of the effect of mass on these splittings, one must utilize the theoretical term formulas. In the present case a simplification results from the fact that in the range of rotational energies involved the spin is almost completely uncoupled from the molecular axis (case *b* coupling). With the assumption that the rotational energy is large compared to the multiplet splitting, one can show from Budó's equations that the over-all width of the triple levels, or the splitting of the levels $F_3(J=K-1)$ and $F_1(J=K+1)$ reduces to

$$F_3(K)-F_1(K)=\frac{BY(Y-4)}{4}\left(\frac{1}{K-\frac{1}{2}}+\frac{1}{K+\frac{3}{2}}\right). \quad (2)$$

Here $Y=A/B$ has the values -10.4 and -9.4 in the lower and upper states. Two isotopic species will have values of B in the ratio ρ^2, and of Y in the ratio $1/\rho^2$. Hence the splitting should involve a factor somewhat less than $1/\rho^2$. This is found to be the case.

Figure 5 is a plot of the measured triplet widths in the observed range of K values. The solid curves show the theoretical variation according to Eq. (2). The actual calculations, using the constants given by Budó, gave both of these curves 0.36 cm^{-1} lower, but this is because the line splittings are the differences between two much larger term splittings, and hence are very sensitive to the exact values of the constants. For comparison purposes, the computed values were therefore increased 0.36 cm^{-1}. The ratios between the line separations for 12–12 and 14–14 are in satisfactory agreement with theory, averaging 0.903 as compared to the computed 0.905. ρ^2 is 0.857. The scatter of the points in Fig. 5 is largely due to the staggering, which makes the splittings for even K larger than those for odd K.

7. DISCUSSION

The two values of the spin here determined, $I=\frac{1}{2}$ for C^{13} and 0 for C^{14} are definite, and consistent on the basis of comparison with the spins of known stable nuclei, but the latter value poses serious difficulties to the accepted theory of beta-decay. The half-life of C^{14} 5100 years, and the energy of its beta-rays, 155 kev, place it on the third Sargent curve so that the transition is at least twice forbidden. Therefore a large spin change is expected by the Gamov-Teller selection rules, but is not observed since the transition is $I=0\rightarrow1$.

No attempt will be made here to discuss possible explanations of this discrepancy. It is briefly treated in a forthcoming publication by A. Roberts,[15] who concludes that his observations on the microwave spectrum of OCS are consistent with $I=0$ for C^{14}.

It should be emphasized that the band spectrum method of determining nuclear spins is the only method that gives a positive result in cases where $I=0$, since in all other methods a vanishing magnetic moment or electric quadrupole moment, will give a null result regardless of the value of I. The success of the present experiment is an indication that the method may find other similar applications among stable or artificially radioactive isotopes that can only be obtained in small quantities.

ACKNOWLEDGMENTS

The author was encouraged to undertake this problem by discussions with Professors E. Segrè and J. R. Oppenheimer, and is particularly indebted to the latter for emphasizing the desirability of work on C^{14}. The investigation would not have been possible without the generous cooperation of the various persons who furnished the enriched samples. The contributions of W. R. Smythe, A. V. Grosse, W. F. Libby, A. Newton, B. J. Moyer, W. L. Whitson, L. D. Norris, and A. H. Snell have been mentioned in the Introduction. Some help on the preliminary experimental work was given by Mrs. W. G. Dauben.

[15] A. Roberts, Phys. Rev. **73**, 1405 (1948).

UNIVERSITY OF MICHIGAN LIBRARIES

The Slow Neutron Cross Section of H

W. B. JONES, JR.*
Laboratory of Nuclear Studies, Cornell University, Ithaca, New York
(Received April 25, 1948)

The total neutron cross section of water has been measured with a slow neutron velocity spectrometer in the energy interval 0.003 to 100 ev. A treatment of the data for energies above 0.8 ev gave a value of 20.0×10^{-24} cm² for the free neutron-proton cross section. Measurements of the total cross section of cyclohexane in the energy interval 0.8 to 100 ev were also made, and from these data a value of 20.1×10^{-24} cm² was obtained for the free neutron-proton cross section. Measurements of the oxygen and carbon cross sections were made in order that the data on water and cyclohexane could be corrected to obtain the bound proton cross sections. The values obtained for these cross sections for the high energy neutrons are: for oxygen, 3.7×10^{-24} cm², and for carbon, 4.7×10^{-24} cm². The data on water for energies below 0.8 ev yield evidence for the existence of a cross section for inelastic scattering of neutrons by water.

I. INTRODUCTION

REPORTED in this paper are some measurements of the neutron cross section of two hydrogenous materials. The measurements were made with the slow neutron velocity spectrometer at Cornell. The total cross section of water was measured in the energy range 0.003 to 100 ev. In the energy interval 0.8 to 100 ev, the water cross section was measured rather precisely in order to make a determination of the variation of the cross section with energy and to obtain an accurate value for the free neutron-proton scattering cross section. In order to obtain a check on the value of the neutron-proton cross section obtained from the measurements on water in the energy interval 0.8 to 100 ev, an equally precise measurement was made of the total cross section of cyclohexane, a hydrocarbon of well-known structure, in this energy interval. The cross sections of oxygen and carbon were also measured so that the cross sections of these nuclei could be accounted for in making the determinations of the neutron-proton cross section from the data on water and cyclohexane.

The neutron velocity spectrometer and the technique of determining the cross section of a material by measuring the transmission of a sample of the material have been described previously.[1,2] The modulating and timing apparatus used in making the measurements presented here were the same as those described in reference 2. The BF_3 ionization chamber used as the neutron detector was filled to two atmospheres of pressure with B^{10}-enriched BF_3. The geometrical arrangements used were somewhat different from the geometrical arrangements used in making the capture cross-section measurements described in the references.[1,2] The details of the geometry will be given in the discussion of the data obtained in the various energy intervals, because no single geometrical arrangement could be used throughout the energy range covered in the experiment. However, one important geometrical factor, namely, the source-detector distance, was held constant and equal to three meters for all the measurements reported here.

II. MEASUREMENTS IN THE 0.8- TO 100-EV INTERVAL AND THE NEUTRON-PROTON CROSS SECTION

The on-time chosen for the source and detector was 10 μsec. for all the measurements in this energy interval. Since the source-detector distance was 3 m, this on-time corresponds to 3.3 μsec./m. Thus, the half-width of the resolution function for the apparatus was about 3.5 μsec./m. This is rather poor resolution compared with the best resolution practicable with the apparatus used, but since the cross section measured varies so very slowly with neutron time of flight, better resolution is of no advantage. The poorer resolution gives the advantage of higher neutron counting rates than

* Present address: Research Laboratory, General Electric Company, Schenectady, New York.
[1] B. D. McDaniel, Phys. Rev. **70**, 832 (1946).
[2] W. B. Jones, Jr., Phys. Rev. **72**, 362 (1947).

obtained with the best resolution. The standard technique of using a thick Cd filter (0.9 g/cm²) to remove from the neutron beam the neutrons of energies less than 0.5 ev was employed so that a 2500-cycle/sec. repetition frequency could be used without difficulty with recycled neutrons.

The collimation arrangement used in this energy interval is shown in Fig. 1. Ordinarily, in making transmission measurements with the neutron spectrometer, the sample being studied is placed directly in front of the detector collimator section in the position where the filter is shown in Fig. 1, and the restricting aperture shown in the middle of the main part of the collimator is absent. Such an arrangement is satisfactory in a scattering experiment only if the detector collimator section is composed of a material which has a large ratio of absorption to scattering coefficient. A large ratio of absorption to scattering coefficients for the collimator material makes it unlikely that neutrons scattered by the sample being studied will be scattered by the collimator into the detector. The ratio of the absorption to scattering coefficients for B_2O_3 becomes smaller with increasing energy, and the ordinary arrangement was found to be unsatisfactory for scattering experiments at energies above 5 ev. For this reason, the collimation arrangement shown in Fig. 1 was used. It will be noted that, in this arrangement, for most of the solid angle into which neutrons can be scattered by the scatterer the scattered neutrons either must be scattered two or more times by the collimator or must pass through a large thickness of B_2O_3 in order to arrive at the detector.

Another geometrical effect which must be considered is that a certain fraction of the neutrons scattered through small angles by the scatterer are scattered into and detected by the detector. This "in-scattering" effect is determined by certain characteristics of the geometry, the thickness of the scatterer, and the characteristics of the scattering process.

A quantity characterizing the geometry with regard to the in-scattering effect is $\alpha=\omega_1\omega_2/4\pi\omega_3$, where ω_1 = the effective solid angle subtended at the source by the scatterer, ω_2 = the effective solid angle subtended at the scatterer by the detector, and ω_3 = the effective solid angle subtended at the source by the detector. For the geometry shown in Fig. 1, $\alpha=1.6\times10^{-3}$. If one measures the transmission of a scatterer which scatters neutrons isotropically in the laboratory coordinate system and which is sufficiently thin so that multiple scattering effects are not important, then

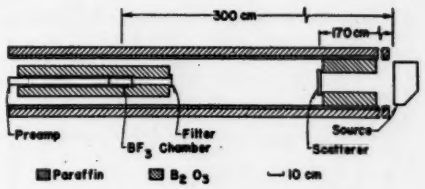

FIG. 1. Collimator arrangement for high energy measurements.

$$T_0=T+(1-T)\alpha,$$

where T_0 = the observed transmission, $T=e^{-n\sigma}$, n = the thickness of the scatterer in particles/cm², and σ = the scattering cross section in cm²/particle. It is assumed that the scattered neutrons which reach the detector have not undergone an energy change upon being scattered. If the scattering is elastic but not isotropic in the laboratory coordinate system, then one may write

$$T_0=T+(1-T)k\alpha,$$

where k is a quantity depending on the angular distribution of scattered neutrons in the laboratory system. Thus, for the scattering of neutrons by free protons, which is isotropic in the center of mass system, $k=4$.

Distilled water was used as one of the scattering materials. The cyclohexane used as the other scattering material was analyzed in the Cornell chemistry department and certified to have a hydrogen to carbon ratio of 2 and to have only traces of impurities besides hydrocarbons. These scattering materials were held in containers made of aluminum alloy 2S. The containers constrained the liquid scatterers to be of uniform thickness known to within 0.3 percent. A "blank" was provided with each scatterer holder which was of the same thickness as the two faces of the holder which "blank" was made from the same sheet of aluminum alloy used for the faces of the holder. The transmission of each container and "blank" was 0.96 for neutrons in the energy interval of interest here.

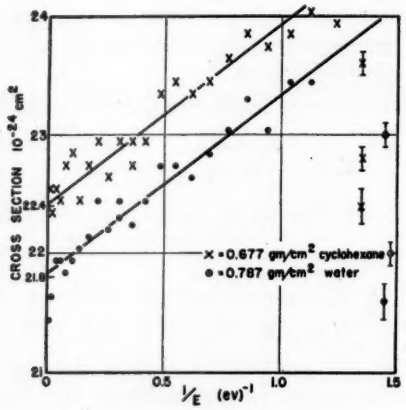

FIG. 2. Observed total cross section per hydrogen atom of cyclohexane and water *versus* reciprocal neutron energy. Curves shown are the best fitting straight lines for the two sets of data. Experimental probable errors for the points are shown at the right.

In Fig. 2 are shown the measured cross sections per hydrogen atom in water and in cyclohexane *versus* the reciprocal of the neutron energy. The ordinate scale is very much expanded in order to show the variation in cross section with the reciprocal energy. The data have been corrected for the in-scattering effect, assuming $k=4$. The correction was 0.25×10^{-24} cm² for both sets of data.

In order to determine the cross section which should be attributed to the hydrogen in the water and cyclohexane, it was necessary to measure the oxygen and carbon cross sections in this energy interval. For convenience, a solid compound containing oxygen was chosen for the oxygen cross-section measurement. Aluminum oxide was chosen. A pure aluminum "blank" was used which had the same mass of aluminum per cm² as in the aluminum oxide sample. The

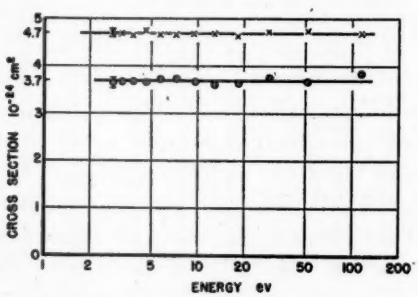

FIG. 3. ⊙ = cross section of oxygen from measurements on 11.6 g/cm² Al_2O_3. × = cross section of carbon from measurements on 4.11 g/cm² graphite. Probable errors are the same for all points in each set of data and are shown on only one point in each set.

aluminum oxide had the disadvantage that it is an adsorber of water, and some difficulty was experienced in drying the aluminum oxide. The aluminum oxide used in obtaining the data shown in Fig. 3 contained 0.7 percent water, and the data have been corrected for the effect of the water. A slab of very pure graphite machined to uniform thickness was used as the scattering material in the measurement of the carbon cross section. The data obtained for the carbon cross section are also shown in Fig. 3.

From a theory[3] assuming that hydrogen is anisotropically bound (to the oxygen or carbon), it is found that if the free neutron-proton cross section is constant and if the neutron energies are much greater than the maximum of the three energies associated with the hydrogen bond, then the neutron cross section of the bound hydrogen is given by

$$\sigma=\sigma_0(1+h\bar{\nu}/4E), \qquad (1)$$

where σ_0 = the free neutron-proton scattering cross section, h = Planck's constant, $\bar{\nu}$ = the mean of the three frequencies of vibration of the bound hydrogen, and E = the neutron energy.

Since the oxygen cross section and the carbon cross section are constant and the neutron-proton absorption cross section is small in the energy range being considered, one would expect that the relationship between the measured cross sections per H atom in water and cyclohexane and $1/E$ would be linear. Hence, the straight lines with the least square deviations from the points in the two sets of data shown in Fig. 2 were calculated, and these straight lines are shown in Fig. 2.

According to Eq. (1), the free neutron-proton cross section is given by the intercept on the cross-section axis of the curve of the bound hydrogen cross section as a function of reciprocal neutron energy. Since the oxygen and carbon cross sections are measured to be constant in the energy interval being considered, it is convenient to take the cross-section intercepts of the curves shown in Fig. 2 and correct these intercepts for the oxygen and carbon cross sections, for the water and cyclohexane, respectively, in order to obtain the free neutron-proton cross section. Using 3.7×10^{-24} cm² as the oxygen cross section,

[3] G. Placzek, private communication

the value obtained from the measurements on the water for the free neutron-proton cross section is 20.0×10^{-24} cm². Using 4.7×10^{-24} cm² as the carbon cross section, the value obtained from the measurements on cyclohexane for the free neutron-proton cross section is 20.1×10^{-24} cm². The *probable* error in these values due to all sources of error is believed to be no greater than $\pm0.3\times10^{-24}$ cm². These values for the free neutron-proton cross section agree with the values obtained by several authors[4] within their stated experimental errors. Other values for the free neutron-proton cross section have been obtained[5] which are much lower than the values obtained here, and it is believed that these low values must be considered incorrect.

The slopes of the two curves shown in Fig. 2 are very nearly equal to each other and equal to 1.5×10^{-24} cm² ev. This gives the $h\bar{\nu}$ the value of 0.3 ev. This is in fair agreement with a value of about 0.25 ev for $h\bar{\nu}$ obtained from the characteristic bond frequencies for the hydrogen.

III. MEASUREMENTS IN THE 0.05- TO 0.8-EV INTERVAL

The on-time used for the source and detector was 50 μsec. which corresponds to 16.7 μsec./m. No beam filter was used, and a repetition rate for the timing apparatus of 200 cycles/sec. was used without difficulty with recycled neutrons. Exploratory measurements indicated that the collimating system and geometry are not critical in this energy interval. It was convenient to make the final measurements with the same geometrical arrangement that was used for the high energy measurements (Fig. 1). The neutron moderator shown in Fig. 1 was modified for these measurements with a 2-cm slab of paraffin in front of the water moderator, used for high energy measurements, and with a sheet of thick Cd (0.9 g/cm²) between the paraffin and the water tank. This 2-cm slab of paraffin backed by thick Cd is referred to as the "tray."

[4] See, for example, L. J. Rainwater, W. W. Havens, Jr., J. R. Dunning, and C. S. Wu, Phys. Rev. **73**, 733 (1948); J. Marshall, *ibid.* **70**, 107A (1946); H. B. Hanstein, *ibid.* **59**, 489 (1941); V. W. Cohen, H. H. Goldsmith, and M. Hamermesh, *ibid.* **57**, 352 (1940); V. W. Cohen, H. H. Goldsmith, and J. Schwinger, *ibid.* **55**, 106 (1939).

[5] See, for example, L. Simons, Phys. Rev. **55**, 792 (1939); E. Amaldi, D. Bocciarelli, and G. C. Trabacchi, Ricerca Scient. **11**, 121 (1940).

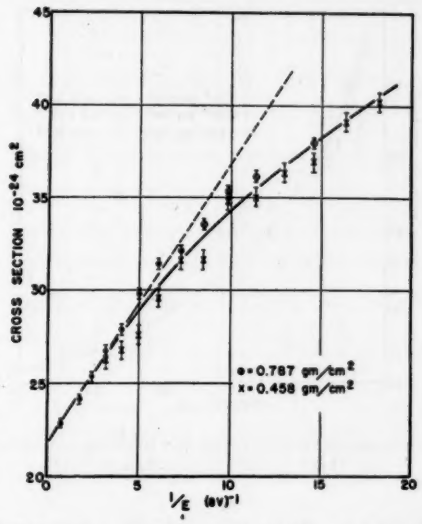

FIG. 4. Total cross section per hydrogen atom of water *versus* reciprocal energy. The dashed curve is the best fitting straight line for the high energy data on water shown in Fig. 2.

The data for this energy region are shown in Fig. 4. The cross section per hydrogen atom of the water is plotted *versus* $1/E$ so that a comparison can be made with the high energy data. The dashed curve is the best fitting straight line for the high energy data on water shown in Fig. 2. The correction of the data for the in-scattering effect was made assuming the scattering to be elastic; and to obtain a value for k, it was assumed that the neutron-hydrogen cross section is proportional to the square of the reduced mass.[6] The correction was less than 0.40×10^{-24} cm² for all points, and the correction was negligible for most of the points.

IV. MEASUREMENTS IN THE 0.003- TO 0.05-EV INTERVAL

The on-time used in the measurements in this energy interval for the neutron source and

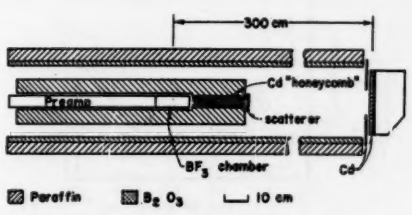

FIG. 5. Collimator arrangement for low energy measurements.

[6] H. A. Bethe, Rev. Mod. Phys. **9**, 122 (1937).

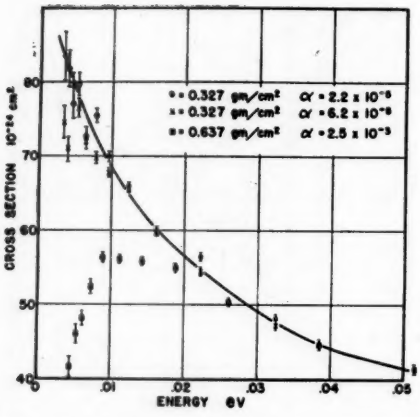

FIG. 6. Measured cross section per hydrogen atom of water for three geometrical arrangements.

detector was 250 μsec. which corresponds to 83 μsec./m. No beam filter was used, and a repetition rate for the timing apparatus of 200 cycles/sec. was used. The tray was used in conjunction with the neutron moderator. The mean life for the low energy neutrons emerging from the tray was 30 μsec.

It was found that for the measurements in this energy range, very good geometry was required in order to obtain consistent results. The collimation arrangement used is shown in Fig. 5. The effective area of the neutron source was determined by a circular hole in a thick sheet of Cd placed between the neutron source and the main section of the collimator. A honeycomb-shaped collimator made of Cd was placed in the region between the scatterer and the BF_3 chamber. By varying the size of the Cd honeycomb-shaped collimator, the geometry factor α could be varied. Data were obtained with three values of α: 2.5×10^{-3}, 6.2×10^{-5}, and 2.2×10^{-5}.

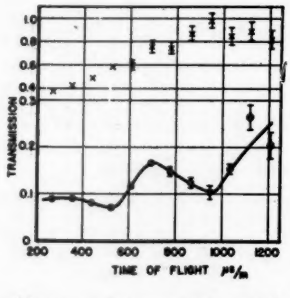

FIG. 7. Graphite test for geometry with $\alpha=2.5\times10^{-3}$. $\odot$ = measured transmission of 10 g/cm² graphite. $\times$ = measured transmission of 10 g/cm² graphite with 0.327 g/cm² water "filter" in neutron beam.

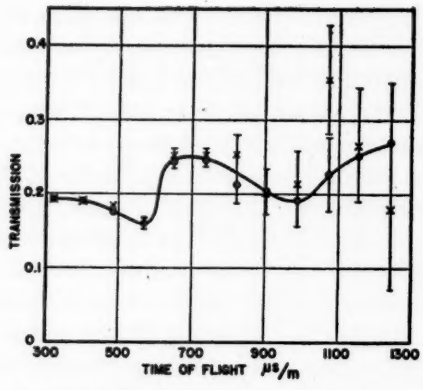

FIG. 8. Graphite test for geometry with $\alpha=6.2\times10^{-5}$. $\odot$ = measured transmission of 6.9 g/cm² graphite. $\times$ = measured transmission of 6.9 g/cm² graphite with 0.327 g/cm² water "filter" in neutron beam.

Shown in Fig. 6 are three sets of data obtained with the three values of α. The measured value of the cross section at low energy increases considerably as the geometry is improved. However, above approximately 0.03 ev, the measured value of the cross section is constant for values of α less than 2.5×10^{-3}.

Anisotropic scattering, predominantly in the forward direction, would give rise to the observed dependence of the measured cross section on α. One effect that would give rise to scattering of neutrons predominantly in the forward direction is inelastic scattering by the water molecule. In order to determine whether or not inelastic scattering was occurring, the following test was carried out. The transmission of a graphite scatterer was measured, and the well-known discontinuities due to interference phenomena were observed in the transmission with the three values of α. A water scatterer was then placed between the graphite scatterer and the neutron source, and with the water in this position, the transmission of the graphite was again measured. If a fraction of the neutrons which pass through the water have their energies changed and are scattered through angles sufficiently small so that they are not excluded from the detector by the collimator, the transmission discontinuities of the graphite will be "smeared." This smearing occurs because changing the energy of a neutron changes its time of flight (per unit distance). Hence, a neutron which loses energy in the water and is detected by the spectrometer to have a

time of flight τ will have had a time of flight less than τ between the neutron source and the water and a time of flight greater than τ between the water and the detector.

Shown in Fig. 7 are the results of this test with $\alpha=2.5\times10^{-3}$, and in Fig. 8 are the results with $\alpha=6.2\times10^{-5}$. The water "filter," when used, was placed between the neutron source and the position for the graphite scatterer and 10 cm from the position for the graphite scatterer. In Fig. 7, it is seen that when the water filter is in place, the transmission discontinuities of the graphite do not appear at all, and the measured transmission of the graphite is very large. Since the cross section of graphite for low energy neutrons is small, it can be concluded from the data in Fig. 7 that for $\alpha=2.5\times10^{-3}$, a fraction of the neutrons which reach the neutron detector after passing through the water have lost energy in the water. One cannot determine the initial energy of the inelastically scattered neutrons from these data. In Fig. 8, it is seen that there is very little smearing of the graphite transmission discontinuities with $\alpha=6.2\times10^{-5}$. It can be concluded that for $\alpha=6.2\times10^{-5}$, few of the neutrons which reach the detector after passing through the water have undergone an energy change in the water. The test was not carried out for $\alpha=2.2\times10^{-5}$, because the neutron intensity was too low to make a conclusive test practicable. However, it is to be expected that with $\alpha=2.2\times10^{-5}$, a smaller fraction of the neutrons which undergo an energy change would reach the detector than with $\alpha=6.2\times10^{-5}$. It is concluded, therefore, that the cross section per hydrogen of water at neutron energies below 0.03 ev is greater than or equal to the cross section measured with $\alpha=2.2\times10^{-5}$.

With $\alpha=2.2\times10^{-5}$, the data (Fig. 6) indicate that the cross section of the protons bound in water exceeds 80×10^{-24} cm^2 at sufficiently low energies. According to the theory given in reference 6, the maximum cross section of bound

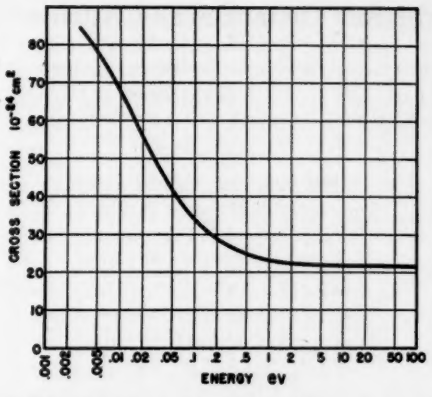

FIG. 9. Total cross section per hydrogen atom of water as a function of energy in the energy range studied. This curve is a composite of the solid curves shown in Figs. 2 (for water), 4, and 6.

protons should be four times the free neutron-proton cross section. In this theory, however, the low energy or thermal agitation of the molecule is not taken into account. The Doppler effect arising from the thermal agitation gives rise to an increase in the effective cross section. Also, the capture cross section of the proton is believed to obey the $1/v$ law, and thus the capture cross section will become appreciable at sufficiently low energy.

Shown in Fig. 9 is the total cross section per hydrogen atom of water for the neutron energy range in which measurements were made. This curve is composed of the solid curves shown in Figs. 2 (for water), 4, and 6.

It is a pleasure to express my thanks to Professor R. F. Bacher, who suggested the problem, and Professor H. A. Bethe for many valuable discussions relative to this investigation. I am especially indebted to Professor B. D. McDaniel for much aid in carrying out and interpreting the measurements. Thanks are also due to Mr. R. R. Meijer who rendered valuable assistance in making many of the measurements.

This work was supported in part by the Office of Naval Research.

Interatomic Distances and Nuclear Quadrupole Couplings in ClCN, BrCN, and ICN*

A. G. SMITH, HAROLD RING,** W. V. SMITH, AND WALTER GORDY
Department of Physics, Duke University, Durham, North Carolina

(Received May 10, 1948)

The following nuclear and molecular constants have been obtained from microwave measurements of the pure rotational spectra of ClCN ($J=2\rightarrow3$ transition), BrCN ($J=3\rightarrow4$), and ICN ($J=4\rightarrow5$). The moments of inertia from the ground vibrational states are, in g-cm^2 $\times10^{-40}$: for $Cl^{35}C^{12}N^{14}$, 140.5_{11}; for $Cl^{35}C^{13}N^{14}$, 141.2_{45}; for $Cl^{37}C^{12}N^{14}$, 143.4_{80}; for $Cl^{37}C^{13}N^{14}$, 144.2_{83}; for $Br^{79}C^{12}N^{14}$, 203.6_{21}; for $Br^{81}C^{12}N^{14}$, 204.7_{86}; for $Br^{79}C^{13}N^{14}$, 205.9_{64}; for $Br^{81}C^{13}N^{14}$, 207.1_{73}; for $I^{127}C^{12}N^{14}$, 260.0_{99}; and for $I^{127}C^{13}N^{14}$, 264.0_{72}. The interatomic distances in A for the ground vibrational states are $d_{CCl}=1.630$, $d_{CN}=1.163$, for ClCN; $d_{CBr}=1.789$, $d_{CN}=1.160$, for BrCN; and $d_{CI}=1.995$, $d_{CN}=1.159$, for ICN. Quadrupole couplings in mc/s evaluated from the hyperfine structure are: for Cl^{35}, -83.5; for Cl^{37}, -65.0; for Br^{79}, 686; for Br^{81}, 573; and for I^{127}, -2420.

THE microwave absorption of BrCN and ClCN caused by pure rotation of the molecules ($J=2\rightarrow3$ for BrCN for $J=1\rightarrow2$ for ClCN) was first reported by Townes, Holden, and Merritt.[1] The observed complex spectra were subsequently explained by Bardeen and the above authors[2] as a splitting in the rotational levels caused by nuclear quadrupole moments of the halides and of nitrogen. Rotational transitions of ICN ($J=4\rightarrow5$) and BrCN ($J=3\rightarrow4$) have been observed by Gordy, Smith, Smith, and Ring.[3] With increased precision of measurement, certain anomalies have been observed in these spectra,[4,5] which have been explained[5] as second-order interactions between levels of the same F and M_F but of different J.

In the earlier publications no accurate values for the interatomic distances have been given, and for ICN, since only one isotope was observed, it was necessary to assume the CN distance in order to obtain an estimate of the IC length. By observations on samples containing C^{13} isotope enriched to 15 percent and by frequency mea-

TABLE I. Hyperfine structure of the $J=3\rightarrow4$ rotational transition of cyanogen bromide, ground vibrational state.

Transition $F\rightarrow F'$	Frequency, mc/s Observed	Calculated*	Relative intensity Observed	Theoretical
	$Br^{79}C^{12}N^{14}$			
	$eqQ=686$	$\nu_0=32{,}961.79$ mc/s		
9/2→11/2	32,956.68	32,956.66	176	100
7/2→ 9/2	32,956.68	32,956.78		76.4
5/2→ 7/2	32,976.40	32,976.28	88	57.4
3/2→ 5/2	32,976.40	32,976.48		42.9
5/2→ 5/2	32,804.56	32,804.56	9	6.9
	$Br^{79}C^{13}N^{14}$			
	$eqQ=686$	$\nu_0=32{,}586.84$ mc/s		
9/2→11/2	32,581.73	32,581.71	176	100
7/2→ 9/2	32,581.73	32,581.84		76.4
5/2→ 7/2	32,601.46	32,601.33	88	57.4
3/2→ 5/2	32,601.46	32,601.53		42.9
	$Br^{81}C^{12}N^{14}$			
	$eqQ=573$	$\nu_0=32{,}774.38$ mc/s		
9/2→11/2	32,770.13	32,770.09	176	100
7/2→ 9/2	32,770.13	32,770.18		76.4
5/2→ 7/2	32,786.65	32,786.51	88	57.4
3/2→ 5/2	32,786.65	32,786.66		42.9
9/2→ 9/2	32,913.24	32,913.52	5	6.9
7/2→ 7/2	32,720.28	32,720.29	9	9.1
5/2→ 5/2	32,643.13	32,643.10	5	6.9
	$Br^{81}C^{13}N^{14}$			
	$eqQ=573$	$\nu_0=32{,}396.85$ mc/s		
9/2→11/2	32,392.59	32,392.56	176	100
7/2→ 9/2	32,392.59	32,392.65		76.4
5/2→ 7/2	32,409.06	32,408.98	88	57.4
3/2→ 5/2	32,409.06	32,409.12		42.9

* First- and second-order theories (references 2, 5) are both employed in calculating the nuclear interactions of the halogen. The nuclear interactions of the nitrogen are neglected.

* This research was supported by Contract No. W-28-099-ac-125 with the Army Air Forces, Watson Laboratories, Air Materiel Command and by a grant-in-aid from the Research Corporation of New York. Submitted by A. G. Smith in partial fulfillment of the requirements for the degree of Doctor of Philosophy in the Graduate School of Arts and Sciences, Duke University, Durham, North Carolina.

** Frederick Gardner Cottrell Fellow.

[1] C. H. Townes, A. N. Holden, and F. R. Merritt, Phys. Rev. **71**, 64 (1947).

[2] C. H. Townes, A. N. Holden, J. Bardeen, and F. R. Merritt, Phys. Rev. **71**, 664 (1947); J. Bardeen and C. H. Townes, *ibid.* **73**, 97 (1948).

[3] W. Gordy, W. V. Smith, A. G. Smith, and H. Ring, Phys. Rev. **72**, 259 (1947).

[4] O. R. Gilliam, H. D. Edwards, and W. Gordy, Phys. Rev. **73**, 635 (1948).

[5] J. Bardeen and C. H. Townes, Phys. Rev. **73**, 627 (1948).

TABLE II. Hyperfine structure of the $J=4\rightarrow5$ rotational transition of cyanogen iodide, ground vibrational state.

Transition $F\rightarrow F'$	Frequency, mc/s Observed	Calculated*	Relative intensity Observed	Theoretical
	$I^{127}C^{12}N^{14}$			
	$eqQ=-2420$	$\nu_0=32{,}255.55$ mc/s		
13/2→15/2	32,268.33	32,268.32	100	100
11/2→13/2	32,278.55	32,278.45	69	80.8
9/2→11/2	32,248.52	32,248.48	63	64.3
7/2→ 9/2	32,215.56	32,215.66	54	50.6
5/2→ 7/2	32,203.57	32,203.61	45	39.3
3/2→ 5/2	32,226.85	32,226.80	30	30.6
13/2→13/2	31,848.77	31,848.80	15	6.7
11/2→11/2	32,200.58	32,200.62	21	10.4
9/2→ 9/2	32,386.29	32,386.35	15	11.5
	$I^{127}C^{13}N^{14}$			
	$eqQ=-2420$	$\nu_0=31{,}770.35$ mc/s		
13/2→15/2	31,783.31	31,783.12	100	100
11/2→13/2	31,793.46	31,793.30	90	80.8
9/2→11/2	31,763.34	31,763.27	60	64.3
7/2→ 9/2	31,730.50	31,730.55	45	50.6
5/2→ 7/2	31,718.28	31,718.41	30	39.3
3/2→ 5/2	31,741.50	31,741.70	21	30.6

* First- and second-order theories (references 2, 5) are both employed in calculating the nuclear interactions of the halogen. The nuclear interactions of the nitrogen are neglected.

surements of increased accuracy[6] made with harmonics of a 10 mc signal monitored by WWV, we have been able to make unambiguous and accurate determinations of the structures of these molecules. In addition, determinations of certain of the nuclear quadrupole couplings have been obtained which are more accurate than those previously reported.

In Tables I and II are given the calculated and observed hyperfine structures of BrCN ($J=3\rightarrow4$ transition) and ICN ($J=4\rightarrow5$ transition) which are caused by the halogen nuclei. The much smaller nuclear coupling of the nitrogen causes a further splitting of these lines which becomes evident at very low pressures. These nitrogen effects were not investigated since the nitrogen nuclear coupling in each of these molecules has been carefully determined in other recent work.[3,7] The second-order theory of Bardeen and Townes[5] has been used with the first-order theory in calculating the positions of the BrCN and ICN lines, and in determining the nuclear quadrupole couplings of the bromine and the iodine. In the calculated hyperfine structure of ClCN ($J=2\rightarrow3$ transition), shown in Table III, the second-order effects are neglected since they are within the range of experimental error. However, the N as well as the Cl nuclear quadrupole coupling is

[6] Method to be described in a later publication by R. Unterberger and W. V. Smith.

[7] A. G. Smith, H. Ring, W. V. Smith, and W. Gordy, Phys. Rev. **73**, 633 (1948).

TABLE III. Hyperfine structure of the $J=2\rightarrow3$ rotational transition of cyanogen chloride, ground vibrational state.

Transition $F\rightarrow F'$	Frequency, mc/s Observed	Calculated	Relative intensity Observed	Theoretical
	$Cl^{35}C^{12}N^{14}$			
	$eqQ=-83.5$	$\nu_0=35{,}824.94$ mc/s		
7/2→9/2	35,825.95	35,825.95	169	100
5/2→7/2				68.6
3/2→5/2	35,820.65	35,820.80	68	44.8
1/2→3/2				28.0
7/2→7/2	35,805.09	35,805.05	15	11.4
5/2→5/2	35,835.74	35,835.75	21	14.6
	$Cl^{35}C^{13}N^{14}$			
	$eqQ=-83.5$	$\nu_0=35{,}638.77$ mc/s		
7/2→9/2	35,639.78	35,639.78	169	100
5/2→7/2				68.6
3/2→5/2	35,634.85	35,634.63	62	44.8
1/2→3/2				28.0
7/2→7/2	35,618.81	35,618.88	21	11.4
5/2→5/2	35,649.56	35,649.58	21	14.6
	$Cl^{37}C^{12}N^{14}$			
	$eqQ=-65.0$	$\nu_0=35{,}083.46$		
7/2→9/2	35,084.15	35,084.25	169	100
5/2→7/2				68.6
3/2→5/2	35,080.39	35,080.24	53	44.8
1/2→3/2				28.0
7/2→7/2	35,067.99	35,067.97	21	11.4
5/2→5/2	35,091.97	35,091.89	21	14.6
	$Cl^{37}C^{13}N^{14}$			
	$eqQ=-65.0$	$\nu_0=34{,}888.26$		
7/2→9/2	34,889.05	34,889.05		

* First-order theory only (reference 2) is employed in calculating the nuclear interaction of the halogen. The nuclear interaction of the nitrogen is taken into account in computing the center of gravity of the line.

TABLE IV. Nuclear quadrupole couplings in the cyanogen halides.

Molecule	Isotope	$eQ(\partial^2V/\partial z^2)$
ClCN	Cl^{35}	−83.5[a]
	Cl^{37}	−65.0[a]
	N^{14}	−3.67[b]
BrCN	Br^{79}	686[a]
	Br^{81}	573[a]
	N^{14}	−3.82[c]
ICN	I^{127}	−2420[a]
	N^{14}	−3.80[d]

[a] Values determined in present work. The coupling for I^{127} is identical with that recently obtained by Bardeen and Townes, reference 5.
[b] C. H. Townes *et al*, reference 2.
[c] C. H. Townes, privately communicated.
[d] A. G. Smith, *et al*, reference 7.

TABLE V. Frequencies ν_0 of hypothetical unsplit rotational lines and resulting moments of inertia of cyanogen halides in the ground vibrational state.

Molecule	J transition	ν_0(mc/s)	$I_B(10^{-40}$ g-cm$^2)$
$Cl^{35}C^{12}N^{14}$	2→3	35,824.94	140.5107*
$Cl^{35}C^{13}N^{14}$		35,638.77	141.2448
$Cl^{37}C^{12}N^{14}$		35,083.46	143.4804
$Cl^{37}C^{13}N^{14}$		34,888.26	144.2832
$Br^{79}C^{12}N^{14}$	3→4	32,961.79	203.6212
$Br^{81}C^{12}N^{14}$		32,774.38	204.7856
$Br^{79}C^{13}N^{14}$		32,586.84	205.9641
$Br^{81}C^{13}N^{14}$		32,396.85	207.1720
$I^{127}C^{12}N^{14}$	4→5	32,255.55	260.0994
$I^{127}C^{13}N^{14}$		31,770.35	264.0717

* Because Planck's constant is known to four places only, the last three figures given in the moment of inertia values have only relative significance.

TABLE VI. Molecular dimensions of the cyanogen halides in the ground vibrational state.

Molecule	CN distance (A)	CX distance (A)	Reference
ClCN	1.163	1.630	a, d
BrCN	1.160	1.789	b, d
ICN	1.159	1.995	c, d

[a] Using M_X for Cl^{35}=34.9800 a.m.u. and M_X for Cl^{37}=36.9775 a.m.u. as given by F. W. Aston, Proc. Roy. Soc. **A163**, 391 (1937).
[b] Using M_X for Br^{79}=78.9417 a.m.u. and M_X for Br^{81}=80.9400 a.m.u. as given by F. W. Aston, Nature **141**, 1096 (1938).
[c] Using M_X for I^{127}=126.932 a.m.u. as given by F. W. Aston, Proc. Roy. Soc. **A115**, 487 (1927).
[d] Other constants used: $h=6.624\times10^{-27}$ erg-sec., mass of atom of unit atomic mass $=1.6599\times10^{-24}$ g, and M_C for C^{12}=12.00386 a.m.u., all as given by R. T. Birge, Rev. Mod. Phys. **13**, 233 (1941); M_C for C^{13}=13.0074 a.m.u. as given by an average of M. L. E. Oliphant, Nature **137**, 396, 407 (1936), and J. D. Cockcroft and W. B. Lewis, Proc. Roy. Soc. **A49**, 883 (1936), M_N=14.0075 as given by M. S. Livingston and H. A. Bethe, Rev. Mod. Phys. **9**, 373 (1937).

here taken into account. The most noticeable effect of the N coupling is to split the $F=3/2\rightarrow5/2$ and $3/2\rightarrow3/2$ lines so that the latter is too weak to detect and the frequency determination of the former is less accurate than it is for the rest of the lines.

In Table IV are listed the values of the halogen nuclear quadrupole couplings determined here and the previously determined values for nitrogen. The ratio of the quadrupole moment of Br^{79} to that of Br^{81} is here determined as 1.197 and that of Cl^{35} to Cl^{37} as 1.274. These ratios compare favorably with the values 1.197 and 1.273 found in a similar manner from CH_3Br and CH_3Cl respectively.[8]

Table V gives the moments of inertia which were calculated from the spectral data, while in Table VI are shown the internuclear distances obtained. In calculating these distances from the moments of inertia it is assumed that the internuclear distances in the ground vibrational state are the same for a given molecule containing different isotopes. Though not strictly true, the assumption probably does not introduce an error in the third figure. The various atomic weights and other constants used in the calculations are listed in the tables.

The carbon to halogen internuclear distances in these halogen cyanides are appreciably shorter than those found for the corresponding distances in the methyl halides.[8] This pronounced effect, which was detectable in the earlier less accurate measurements, may be attributed largely to resonance between the electronic structures $X^+=C=N^-$ and $X-C\equiv N$ which gives the XC bond some double bond character. This type of resonance would also reduce the bond order of the CN, and one would therefore expect a somewhat longer CN bond length than that for a normal CN triple bond. This expected lengthening of the CN bond, which should be much less pronounced than the shortening of the XC bond,[9,10] is revealed for the first time in the measurements reported here. The added triple bond radii[11] of C and N, 1.149A, are definitely shorter than the CN lengths listed in Table VI.

[8] W. Gordy, J. W. Simmons, and A. G. Smith, Phys. Rev. **73**, 243 (1948).

[9] L. Pauling, *Nature of the Chemical Bond* (Cornell University Press, Ithaca, New York, 1939), p. 164.
[10] R. S. Mulliken, C. A. Rieke, and W. G. Brown, J. Am. Chem. Soc. **63**, 41 (1941).
[11] L. Pauling, reference 9, p. 154.

Reaction Constants for $Li^7(p,n)Be^7$

RICHARD TASCHEK AND ARTHUR HEMMENDINGER
Los Alamos Scientific Laboratory, Los Alamos, New Mexico
(Received May 5, 1948)

Absolute values for the reaction cross section of $Li^7(p,n)Be^7$ are given for proton energies between 1.86 Mev and 2.5 Mev. Detailed angular distributions and their analyses are presented and the use of the reaction as a variable energy neutron source is discussed.

I. INTRODUCTION

THE experimental work described below is the result of a cooperative effort by many members of the Van de Graaff group at Los Alamos; the names of the members of this group would appear with those of the writers except for length. They are: Dudley Williams,* Richard Christian,** Arthur Schelberg,*** Harold Argo,**** Roland Perry,** Rubby Sherr,† and Howard Kratz.†† The detailed analyses of the angular distributions were developed and carried out by Frederick Reines.

Following the exploratory work of Hanson, Benedict,[1] and others at the University of Wisconsin during 1942, which had established the general trend of cross section, angular distribution, and monoergic nature of the reaction $Li^7(p,n)Be^7$ to proton energies in excess of 3.0 Mev, this source of neutrons was extensively used at Los Alamos with little further investigation of the reaction itself. The detailed study reported below was undertaken to establish precisely the nature of the reaction, since it is one of the most versatile sources of neutrons available.

The compound system Li^7+p has been studied over a considerable energy interval but the complete experimental picture is not yet known. Information is available about the particle reaction[2–7a]

$$Li^7+p\rightarrow He^4+He^4+17.5\text{ Mev}, \quad (1)$$

the γ-ray emission[8,9]

$$Li^7+p\rightarrow Be^8+\gamma+17\text{ Mev} \quad (2)$$

with its resonance at 440-kev proton energy, and the inelastic scattering process[10]

$$Li^7+p\rightarrow Li^{7*}+p, \quad (3)$$

$$Li^{7*}\rightarrow Li^7+h\nu(450\text{ kev}). \quad (4)$$

The reaction considered in the present study is

$$Li^7+p\rightarrow Be^7+n+Q; \quad (5)$$

$$Be^7+e^K\xrightarrow[K\text{ capture}]{43\text{ day}}Li^{7*}+\eta_0\rightarrow\begin{cases}Li^7+h\nu+\eta_0 & \text{about 10 percent}\\ Li^7+\eta_0 & \text{about 90 percent.}\end{cases} \quad (6)$$

The excited state of Li^{7*} is presumably the same as in the inelastic scattering case.

The first studies of the trend of this reaction with incident proton energy were made by Wells, Haxby, Shoupp, and Stephens[11] who established, according to their energy scale, that the threshold was at 1.86 Mev, giving a $Q=-1.63$ Mev. This value has been used

* Now at Ohio State University, Columbus, Ohio.
** Now at Argonne National Laboratory, Chicago, Illinois.
*** Now at Indiana University, Bloomington, Indiana.
**** Now at Institute for Nuclear Studies, University of Chicago, Chicago, Illinois.
† Now at Princeton University, Princeton, New Jersey.
†† Now at General Electric Laboratories, Schenectady, New York.

[1] A. O. Hanson, CF-618 (1943); D. L. Benedict and A. O. Hanson, CF-638 (1943).
[2] Herb, Parkinson, and Kerst, Phys. Rev. **48**, 118 (1935).
[3] L. J. Haworth and L. D. P. King, Phys. Rev. **54**, 38 (1938).
[4] Rumbaugh, Roberts, and Hafstad, Phys. Rev. **54**, 657 (1938).
[5] Young, Ellett, and Plain, Phys. Rev. **58**, 498 (1940).
[6] Swartz, Rossi, Jennings, and Inglis, Phys. Rev. **65**, 80 (1944).
[7] J. M. Blair and A. O. Hanson, CF-624 (1943).
[7a] Rubin, Fowler, and Lauritsen, Phys. Rev. **71**, 212L (1947).
[8] Hafstad, Heydenburg, and Tuve, Phys. Rev. **50**, 504 (1936).
[9] W. A. Fowler and C. C. Lauritsen, Phys. Rev. **56**, 841 (1938).
[10] Hudson, Herb, and Plain, Phys. Rev. **57**, 587 (1940).
[11] Wells, Haxby, Shoupp, and Stephens, Phys. Rev. **58**, 1035 (1940).

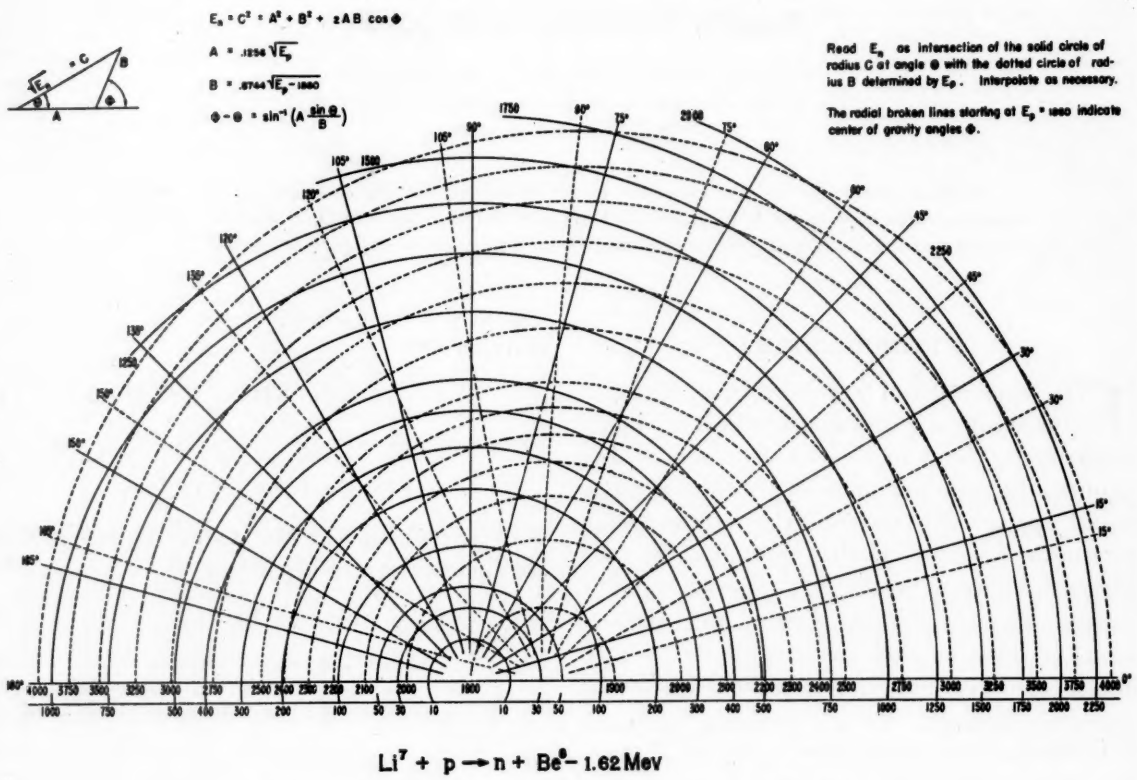
$E_p = C^2 + A^2 + B^2 \pm 2AB\cos\Phi$
$A = .1256\sqrt{E_p}$
$B = .8744\sqrt{E_p - 1880}$
$\Phi - \Theta = \sin^{-1}\left(A\frac{\sin\Theta}{B}\right)$
Read E_p as intersection of the solid circle of radius C at angle Φ with the dotted circle of radius B determined by E_p. Interpolate as necessary.
The radial broken lines starting at E_p = 1880 indicate center of gravity angles Φ.
$Li^7 + p \rightarrow n + Be^8 - 1.62\,Mev$

FIG. 1. Energy-angle nomograph for the $Li^7(p,n)Be^7$ reaction.

throughout all the work done at Los Alamos with this source, notwithstanding Hanson and Benedict's[12] value of 1.88_3 Mev at threshold obtained with a curved plate electrostatic analyzer. Recent observations at Los Alamos with a more highly developed electrostatic analyzer[13] corroborate the higher value but further independent methods should be used to clarify this discrepancy.

The other reactions mentioned have not been studied at energies above the threshold for the neutron emission. The question of an excited state in Be^7, which might lead to another group of neutrons at proton energies above some 400 kev above the threshold has not been investigated *per se*, but evidence from proton recoil distributions[14,15] indicates that, up to proton energies of at least 1 Mev above the threshold, no other group than the initial one is present to more than approximately ten percent of the initial group intensity. This excited state is surmised from the expected similarity of the isobars Li^7 and Be^7.

II. SOURCE

In all the work reported below the Los Alamos Van de Graaff generator[13] was used. This machine provides up to 60 μa of magnetically analyzed protons or deterons at a maximum usable energy of 2.7 Mev with an energy control of about ± 1.5 kev and a focus approximately 2 mm in diameter at a distance of 1.5 meters from the analyzing magnet.

Unseparated metallic lithium targets were used for all experiments; these targets, evaporated onto 0.25-mm thick tantalum caps in a separate vacuum system were especially designed to reduce scattering material around the neutron source to a minimum, the 0.25 mm of tantalum being the only material between the lithium film and the outside in the forward direction. For very large proton currents these targets were approximately 3.8 cm in diameter and rotated

[12] A. O. Hanson and D. L. Benedict, Phys. Rev. **65**, 33 (1944).
[13] J. L. McKibben and D. H. Frisch, Phys. Rev. **70**, 117A (1946).
[14] P. G. Koontz and T. A. Hall, LA-128 (1944).
[15] P. G. Koontz and T. A. Hall, MDDC-31 (1946).

eccentrically in a fine air-water spray to dissipate the 100 watts of power, while for currents of 1 or 2 μa small (19 mm in diameter) air-cooled stationary targets were used with no observable loss of lithium as monitored by the neutron flux. The large proton currents available allowed extremely thin (2 to 5 kev) lithium deposits to be used with sufficient neutron yield to make most experiments easily possible. Target thicknesses were measured, for routine work, by the proton energy increment between threshold and the first knee or maximum of the neutron yield at 0°, as measured by a flat energy response counter[16] subtending solid angles as small as 3×10^{-3} steradian (half-angle about 2°) and, subsequent to this, calibration of a counter by the forward yield at 2.05 Mev (see Fig. 3). For the small stationary targets, on which the lithium deposit was very uniform, chemically determined weights were used to measure the surface density of lithium. It was found that carbon deposits made the energy increment method inaccurate for lithium mass determination of the thinnest targets, since the thickness measured in this way grew with time, although for targets thicker than 30 kev the inaccuracy was negligible.

In Fig. 1 is shown an energy-angle nomograph, due to McKibben,[17] for this reaction. This chart will aid in the discussion below since most observations were made on neutrons emerging from the source with different energies because varying proton energies and neutron angles were used. It may be noted here (as can be seen from the nomograph) that for all proton energies, except just at threshold, up to 40 kev above the threshold the neutrons appear double-valued in energy at each angle within a forward cone of less than 2π solid angle; this effect is due to the large center of mass velocity. Above 1.90-Mev proton energy the neutrons have a single energy at each angle and by using large angles (near 120°) experiments may be done with neutrons as low as 5 kev in energy, providing the intensity is sufficient.

Time did not permit an extensive investigation of the angular distribution of neutrons within the double-valued region, but a method using the $N^{14}(n,p)C^{14}$ reaction[18,19] as a detector was devised which appears promising for the resolution of the two groups down to a neutron energy difference of approximately 20 kev, where the neutron energies individually are in the range 2 kev to 100 kev. It will be seen, however, that the ratios of the solid angle factors from center of gravity to laboratory coordinates are in the ratio of the energies of slow to fast groups of neutrons at a given angle (Appendix I); this means that a roughly isotropic distribution in the center of mass system would result in an observationally unfavorable yield for the slow group in the laboratory system, particularly after the cone mentioned above has become large.

Appendix II describes a method of obtaining the energy dependence of a given neutron cross section by taking advantage of the neutron cone in this reaction.

Since the neutrons emerge with varying energies over 4π solid angle, it is highly advisable to keep neighboring scattering and moderating material as far from the source as possible. The present source is located over a pit with a distance of eight feet to ground level, thin fiberboard walls at about twelve feet forward, 2-foot thick concrete walls about ten feet away on either side and, most unfavorably, the edge of the pit about five feet behind the source at four feet above pit floor.

III. REACTION CROSS SECTION

Method

The absolute value of the reaction cross section was determined by a comparison of the total neutron flux from the $Li^7(p,n)Be^7$ source with the total neutron flux from a standardized RaBe source. The source strength for the RaBe source standard was determined by Walker[20] and is known to approximately ±5 percent. From the magnitude of the cross section of $Li^7(p,n)Be^7$ it seems likely that the reverse process could be carried out, i.e., a spectrochemical determination of the mass of Be^7 formed in a long bombardment of a thick Li target would calibrate a RaBe source for neutron flux since approximately 10^{-7} g

[16] A. O. Hanson and J. L. McKibben, Phys. Rev. **72**, 673 (1947).
[17] J. L. McKibben, Phys. Rev. **70**, 101A (1946).
[18] B. T. Feld, Phys. Rev. **70**, 429L (1946).
[19] H. H. Barschall and M. E. Battat, Phys. Rev. **70**, 245 (1946).
[20] R. L. Walker, LA-400 (1945).

of Be^7 can be formed in 48 hours of bombardment (Appendix III).

In the present experiment the fluxes of the two sources were compared at two proton energies, 1.95 Mev and 2.25 Mev, by means of the activities induced in a large "manganese bath." The particular variations in the technique of manganese bath measurements here used were developed and reported in detail by Turner.[21] Briefly, a cubical Lucite container approximately 70 cm on a side contained a solution of 200 g/liter of $MnSO_4$; the 155-minute Mn^{56} activity was excited either by the RaBe source or the $Li^7(p,n)Be^7$ source introduced into the center of the solution on a diagonal of the cube through a horizontal tube of 19-mm diameter. After sufficient exposure of the solution the whole bath was vigorously stirred and approximately a liter of the solution withdrawn in a cylindrical Lucite container. This container was filled to a fixed height, lowered into a lead shield, and a thin-walled (4-mil) Al Geiger counter, carried vertically on the lead lid for the shield, lowered into the solution. The activity was usually followed for more than one half-life with alternate measurements of background being made on a geometrically identical sample of the solution withdrawn before irradiation. Before immersion in the solution, the Geiger counter was thinly coated with ceresin wax to prevent corrosion. The counters were systematically checked for calibration constancy with uranium glass "standards."

Exposures with the RaBe sources used were made for about 12 hours, giving approximately 99 percent saturated activity. Activities induced with the $Li^7(p,n)Be^7$ source required only one or two hours exposure for high counting rates.

It seemed particularly desirable to make total reaction cross-section measurements at closely spaced energies, since the neutron yield was known to vary rapidly with proton energy. Only one, or at most two, exposures of the manganese bath could be made per day, it being necessary to wait for the strong activity from the lithium neutrons to decay considerably before a second run could be made without large corrections. For this reason and the added one of much greater convenience, advantage was taken of the 43-day γ-activity induced in the target itself from decay of the Be^7. The following procedure was adopted:

1. After an exposure of the manganese bath to the $Li^7(p,n)Be^7$ source, which measured directly the total number of neutrons emitted during the course of a run, the bath was rolled off the target and a Geiger counter in a lead shield with a hole and spacer in it for introduction of the target was rolled up to it on a trolley and the Be^7 activity due to the same run measured.
2. In this way, the Be^7 activity counted in a standard geometry was calibrated against the Mn bath and further flux measurements at the same or different proton energies could subsequently be made in terms of the easily measured Be^7 activity rather than by using the cumbersome Mn bath.

For the targets used it had been ascertained that:

1. No Be^7 activity was induced in the Li when protons below the threshold energy of $Li^7(p,n)Be^7$ were used;
2. No activity of any kind was induced in the Ta backing material with protons of energies up to the maximum used in this experiment;
3. No long-lived activity was induced in a block of metallic Li when bombarded with neutrons up to 1-Mev maximum energy;
4. Neither Li nor Ta gave long-lived activities when immersed in slow neutron fluxes corresponding to those met with in the Mn bath for equal lengths of time;
5. The ratios of Be^7 to Mn^{56} activities due to the same run were constant, independent of neutron energies between 30 kev and 1 Mev within experimental error of about six percent.

The last two inches of the small target tubes were made of Ta and at the end of this was the 10-mil Ta cap on which the Li was evaporated. It was found necessary to make this much of the target of Ta to avoid troublesome n, γ-activities induced in such metals as Al, Fe, and Cu when the target was immersed in the strong slow neutron flux of the Mn bath.

It was determined that the small targets were uniformly deposited by making one of these in two annular segments of approximately equal area and analyzing each separately. The chemically determined mass per unit area for the outside ring was within two percent of that of the central disk. Later experience showed, however, that the mass measurements after bombardment on the thinnest targets were not reliable, the error being an approximately constant one and probably a result of the fact that some lithium penetrated rather deeply into the Ta

[21] C. M. Turner, LA-445 (1945).

TABLE I. Mn bath exposures to $Li^7(p,n)Be^7$ source.

E_p (Mev)	Target no.	ρ, surface density of Li in mg/cm²	A_0, Mn^{56} activity at zero time in counts/min.	I, weighted current in μ coul./min.	$A_{Mn}=A_0/I$ in counts/μ coul.	$\sigma_{Li(p,n)}\times10^{33}$ cm² from Eq. (7)
2.25	1	0.105	1675	25.85	64.79	0.508
2.25	2	0.106	963	15.94	60.40	0.470
2.25	2	0.106	3002	47.69	62.94	0.489
						av. 0.489±2.7%
1.95	1	0.105	2201	73.61	29.90	0.234_4
1.95	2	0.106	467	14.66	31.86	0.247_2
1.95	2	0.106	830	28.60	29.02	0.225_5
1.95	3	0.142	940	23.05	40.75	0.236
1.95	3	0.142	1150	28.72	40.10	0.232_3
						av. 0.238±2.8%

E_p (Mev)	Target no.	A_1, Be^7 activity arising from irradiation in counts/min.	Total proton charge q during run in μ coul.	$A_{Be}=A_1/q$ in counts/μ coul.-min.	$R=A_{Mn}/A_{Be}$	A_{Be}/target thickness in counts/min./μ coul. mg/cm²
2.25	1	601	7311	0.0822	788	0.783
2.25	2	320	3958	0.0811	745	0.766
2.25	2	1122	14,005	0.0803	784	0.757
						av. 0.769±4%
1.95	1	1200	29,549	0.0407	735	0.387
1.95	2	171	3632	0.0472	676	0.445
1.95	2	348	8051	0.0432	673	0.407
1.95	3	304	5966	0.0509	801	0.358
1.95	3	382	7598	0.0503	797	0.354
					av. 750±6%	av. 0.390±7.5%

backing material and was not measured in the chemical analysis. This appeared clearly in a series of nine targets bombarded with 2.25-Mev protons for approximately equal times. These targets varied by a factor of 25 between thinnest and thickest in chemically determined mass of lithium. For the targets thicker than 0.08 mg/cm² the Be^7 activity/mg/cm² was independent of the thickness to within the experimental error of ~eight percent in the two measurements and only these targets were used for the absolute comparisons.

In terms of the quantities which are directly measured in the Mn bath experiment, it can readily be shown that the $Li^7(p,n)Be^7$ cross section at the proton energy E is

$$\sigma(E)=\frac{A_0}{A_s}\cdot\frac{[1-\exp(-t_R/\tau)]Q_{RaBe}(1-L)1.983\times10^{-33}}{\sum_i(\Delta q_i/\Delta t_i)[1-\exp(-\Delta t_i/\tau)][\exp(-t_i^*/\tau)]\rho}\ \text{cm}^2, \tag{7}$$

where

A_0 = observed zero time activity of Mn^{56} due to a run on $Li(p,n)$ neutrons (zero time is defined as the end of the irradiation),

A_s = observed zero time activity of Mn^{56} due to RaBe neutrons,

Q_{RaBe} = number of neutrons/minute from the RaBe source,

L = fraction of RaBe neutrons leaking from Mn bath,

t_R = duration of RaBe exposure,

τ = decay period of Mn^{56} = 224.2 minutes,

ρ = surface density of normal lithium on target in mg/cm²,

$T=\sum_i\Delta t_i$ is the total exposure time in a given run to $Li(p,n)$ neutrons,

Δq_i = charge in micro-coulombs due to protons striking the target in subinterval Δt_i,

t_i^* = time elapsed from end of Δt_i to end of irradiation.

The numerical factor 1.983×10^{-33} is determined by the constants: charge of the proton, Avogadro's number, atomic weight of normal lithium, and the isotopic constitution of lithium.

TABLE II. Standardization of Mn bath.

Run no. and data	Q_{RaBe} source strength in n/min.	t_R exposure length in min.	A_s bath activity at zero time in c/min.	k bath constant in counts/neutron
1 (4–9–46)	5.37×10^8	1369	1210	2.33×10^{-6}
2 (4–17–46)	5.37×10^8	1566	1220	2.35×10^{-6}
3 (4–20–46)	3.48×10^8	1347	802	2.39×10^{-6}
4 (5–16–46)	3.48×10^8	1600	869	2.57×10^{-6}
				$k_{Av}=2.41\times10^{-6}\pm3\%$

IV. MEASUREMENTS

In Eq. (7) the summation is necessary because over the whole irradiation time T it was difficult to keep the proton current sufficiently constant to use simply the induced activity per microcoulomb derived from dividing the infinite exposure activity by the total charge from the protons during the run. The summation is over the proton current to the target during short intervals suitably weighted to account for bath decay during irradiation. Thus, in Table I, which gives the results of the eight Mn bath measurements on the $Li(p,n)$ source, the quantity

$$A_{Mn}=\frac{A_0}{\sum_i(\Delta q_i/\Delta t_i)[1-\exp(-\Delta t_i/\tau)][\exp(-t_i^*/\tau)]}=\frac{A_0}{I} \tag{8}$$

is the infinite exposure specific activity of the Mn bath and is independent of duration or intensity of the irradiation on a given target at a fixed proton energy.

In Table II are shown the individual Mn bath standardizations obtained with the two different secondary standard RaBe sources used which determine the bath constant

$$k=A_s/Q_{RaBe}(1-L). \tag{9}$$

The leakage factor L used was 0.03, based upon early calculations of RaBe spectrum leakage corrected for new bath size and revised estimate of the spectrum; whatever errors are in this estimate are considerably smaller than the remainder of the experimental errors. It will be noted that the last calibration was done at the end of the Mn bath experiment and, in its deviation from the other three runs, may indicate a small change in bath constant during this time; since the effect was small, no correction was made. For the four runs the average value of k in counts per neutron was $2.41\times10^{-6}\pm3$ percent.

For the data taken by the Be^7 method, the

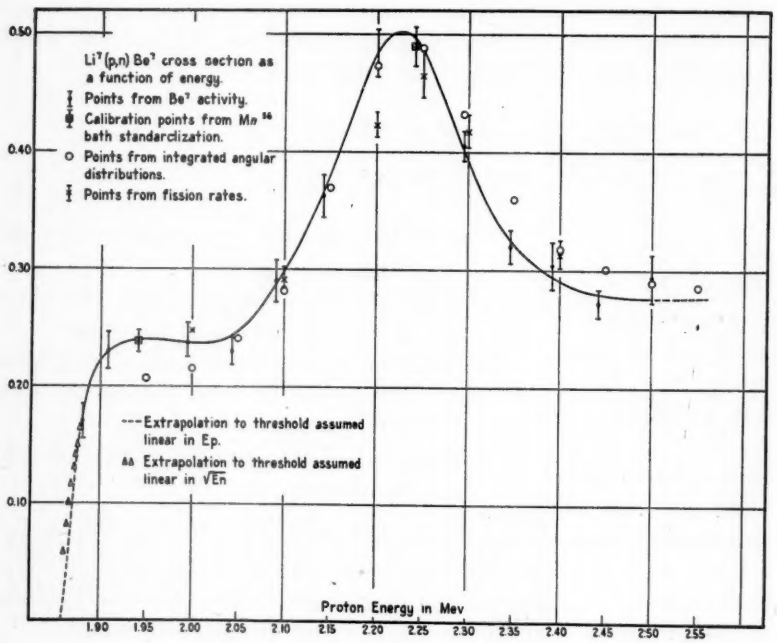

FIG. 2. $Li^7(p,n)Be^7$ reaction cross section in units of 10^{-24} cm² as a function of proton energy.

cross sections obtained for target thicknesses above 0.08 mg/cm² were consistently reliable, while for much lighter targets the chemical weights were untrustworthy. However, for almost all targets at least one measurement of the activity for an exposure at $E_p = 2.25$ Mev, the standardization energy, was made. In this case, the ratio of Be^7 activity at any energy above threshold to that of 2.25 Mev was completely independent of target thickness and excellent agreement was obtained in all cases.

The total $Li^7(p,n)Be^7$ cross section thus obtained is shown in Fig. 2. The proton energies at which the cross sections are plotted are corrected for target thickness, which varied from 5 to 20 kev. The errors shown on the Be^7 points are the mean deviations of two or more runs at the given energy.

In the same figure the circles are data obtained by integration of the angular distributions discussed in the next section and normalized to the Mn bath data at 2.25 Mev. These data will be discussed in more detail in the next section; the errors are estimated to be about ±5 percent except at the lowest energies where they may be larger, due to changes in detector sensitivity and background.

The crosses in Fig. 2 represent data taken with a U^{235} fission foil subtending a half-angle of 18° at the zero degree position. From the known weight and cross sections of the U^{235}, and the angular distributions of the next section which gave the fraction of all the neutrons emitted causing the measured fission rate, the cross section of the $Li^7(p,n)Be^7$ reaction was calculated assuming a target thickness of 0.012 mg/cm². This target thickness cannot be more than an estimate, since it was obtained from a rise curve which will be discussed in more detail in the next section, but the agreement is fairly good in absolute value. The errors here indicated are the statistical errors in the fission counts.

The absolute value of the $Li^7(p,n)Be^7$ cross section is good to about ±12 percent over-all; this arises from an estimated ±5 percent error in mass determination, ±6 percent in absolute source strength of the secondary RaBe standards, and about ±2 percent in activity measurements. The relative values of the cross section as a function of energy are somewhat better than this and the curve drawn through the Be^7 points is estimated to be good to ±6 percent at individual points.

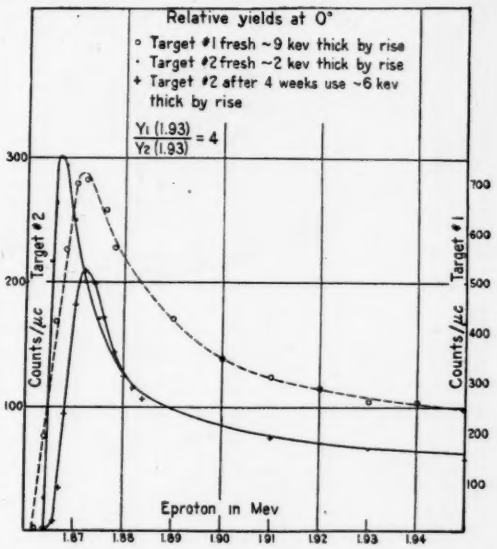

FIG. 3. Neutron yields in the forward direction as a function of proton energy for different target thicknesses.

V. ANGULAR DISTRIBUTION

Method

The angular distribution of the neutrons from the $Li^7(p,n)Be^7$ reaction was measured with a counter, whose response was nearly independent of neutron energy, over a range of proton energies from 1.95 Mev to 2.25 Mev in 50-kev steps. The same rotating target was used for all these measurements, and a second (monitor) counter similar to the one mentioned above was kept at zero degrees to the beam in order to be sure that no systematic changes in neutron flux occurred. The movable counter subtended a solid angle of 1.06×10^{-2} steradian (half-angle approximately 3.5°) and the monitor an angle of 0.32×10^{-2} steradian (half-angle approximately 2°).

A very thin target was used in order to get maximum resolution in the angular distribution data. In Fig. 3 is shown a plot of the forward yield of neutrons for two targets near threshold as measured by the monitor counter. The curves for both targets show the yield and rise-width thickness ratios to be the same while both targets are fresh, but after four weeks' use of target 2 in the angular distribution measure-

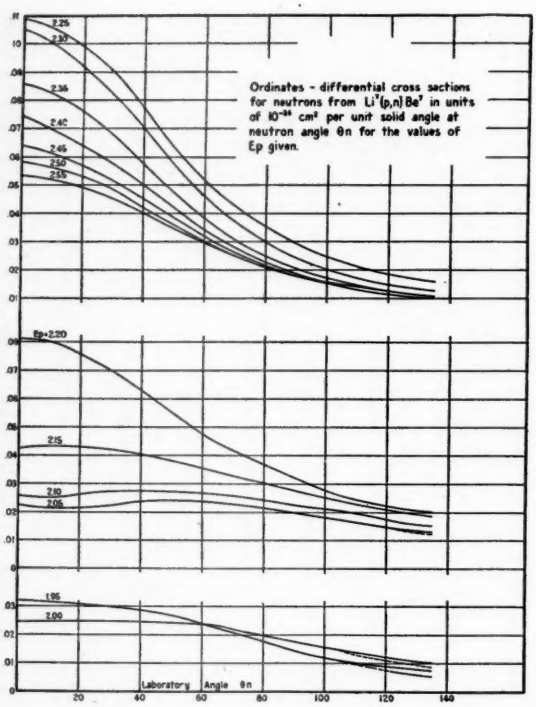
Ordinates - differential cross sections for neutrons from Li⁷(p,n)Be⁷ in units of 10⁻²⁴ cm² per unit solid angle at neutron angle θn for the values of Ep given.
Laboratory Angle θn

FIG. 4. Laboratory angular distributions in 10^{-24} cm^2 per unit solid angle as a function of laboratory angle at the listed proton energies.

ments, the yield ratio at 1.93 Mev is still the same but the rise-width has increased from about 2 kev to an apparent 6 kev. Since the yield at the flat portion of the curve remained the same, no lithium was lost or gained and the increased rise width was due to an inert contaminant, undoubtedly a carbon deposit.

Since changing angles was less convenient than changing energies, the movable counter was set at a fixed angle and the yield at that angle was measured as the energy was changed from 1.95 Mev to 2.55 Mev in 50-kev steps. In this manner the angular range from 0° to 135° was covered in approximately 15° intervals.

Serious difficulties were expected at 135° for the lowest proton energies. Two background effects at 1.95 Mev and 2.00 Mev may interfere with the direct neutrons at 135°, since the yield of neutrons here is small compared to those going at the same time in the forward direction. One of these effects is due to room and floor scattering, the other to direct back scattering with little energy loss from the target backing material. The latter effect was determined to be negligible for the present backing material of 10-mil Ta, by observing that approximately 1 cm of Ta in addition to the target cap was necessary immediately in front of it before an appreciable change in counting rate was made at 135°.

The effect of the sea of scattered and degraded neutrons was determined by observing the deviation from r^{-2} dependence of intensity on distance from the source. This type of measurement was first done at a forward angle (65°) to locate the "effective center" of the counter, since here the direct neutron flux completely overshadows backgrounds at the distances involved and the counter length is an appreciable fraction of the closest distances to the source. The intercept of the linear counting rate curve plotted against r^{-2} gave the background counting rate correction necessary at the distance where the angular distribution measurement was made. Corrections were necessary only at 135° and at the proton energies 1.95, 2.00, and 2.05 Mev; the corrected yields were, respectively, 68 percent, 83 percent, and 93 percent of the observed.

A further correction to the yields at 135°, for the lowest proton energies, should have been made for change in counter sensitivity. The neutron energies here are between 15 and 25 kev and previous experience with this type of counter has indicated that a loss in sensitivity of at least 10 percent is quite usual at these energies. However, since no actual sensitivities for these particular counters had been determined, no correction has been made. It is believed that the sensitivities of the two counters used is independent of neutron energy to ±5 percent in the energy range from about 50 kev to 850 kev, the maximum energy occurring in this experiment.

VI. RESULTS

In Fig. 4 are shown the angular distributions as measured in the laboratory coordinate system. The cross section is given in 10^{-24} cm^2 per unit solid angle for neutrons at the neutron angle in question. This has been done by calculating, from the measured angular distribution, the fraction of all the neutrons passing through the counter at 0° and 2.25 Mev, where the Mn bath absolute cross section was measured, and normalizing the observed counting rate to the

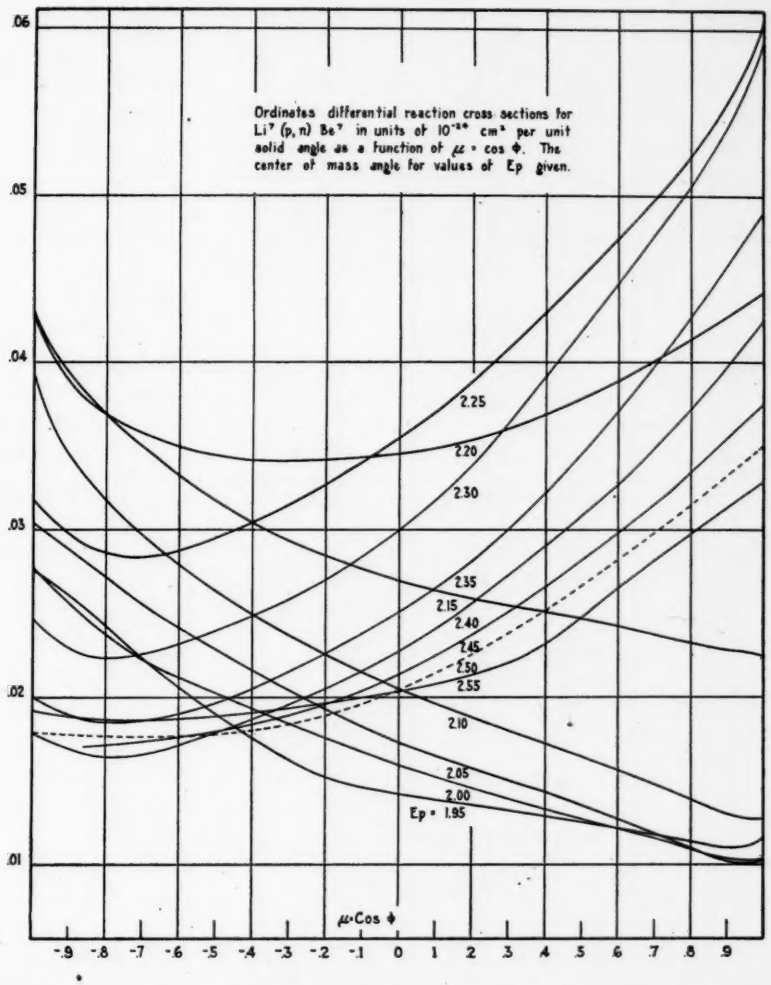

FIG. 5. Angular distributions in the center of mass system in units of 10^{-24} cm² per unit solid angle as a function of the cosines of the center of mass angle at the listed proton energies.

differential cross section obtained from the fraction and the total cross section.

From Fig. 4 it is immediately apparent that although the total cross section is not exceedingly large, the strong forward asymmetry of neutron yield, which comes primarily from center of mass motion at low neutron energies and from the effect of the resonance at high energies, makes this a particularly strong neutron source for forward observations.

Figure 5 shows the center of mass differential cross sections as a function of the cosine of the center of mass angle. Laboratory system yields were converted to center of mass by means of the following relationships holding for the $Li^7(p,n)Be^7$ reaction:

$$\phi=\theta+\sin^{-1}(\sin\theta/\gamma), \tag{10}$$

$$\gamma=7((E_p-E_{th})/E_p)^{\frac{1}{2}}, \tag{11}$$

$$\sigma(\phi)\sin\phi d\phi=\sigma(\theta)\sin\theta d\theta, \tag{12}$$

where ϕ = neutron angle in the center of mass system, θ = neutron angle in the laboratory system, E_p = energy of the incident proton, E_{th} = energy of the incident proton at the threshold; $d\Omega_{lab}/d\Omega_{cm}=\sin\theta d\theta/\sin\phi d\phi$ = ratio of solid angles in center of mass system to that in the laboratory system. For 0° and 180°

$$\frac{d\Omega_{lab}}{d\Omega_{cm}}=\frac{\gamma(\gamma^2-\sin^2\theta)^{\frac{1}{2}}}{\gamma^2+\cos 2\theta+2\cos\theta(\gamma^2-\sin^2\theta)^{\frac{1}{2}}}. \tag{13}$$

For all other angles

$$d\Omega_{lab}/d\Omega_{cm}=\cos(\phi-\theta)(\sin\theta/\sin\phi)^2. \tag{14}$$

The angular distributions in the center of mass system can be accurately fitted with a simple power series of the form

$$\sigma(\phi)=A(E)+B(E)\cos\phi+C(E)\cos^2\phi, \tag{15}$$

but a more adequate representation in terms of Legendre polynomials has been devised. This

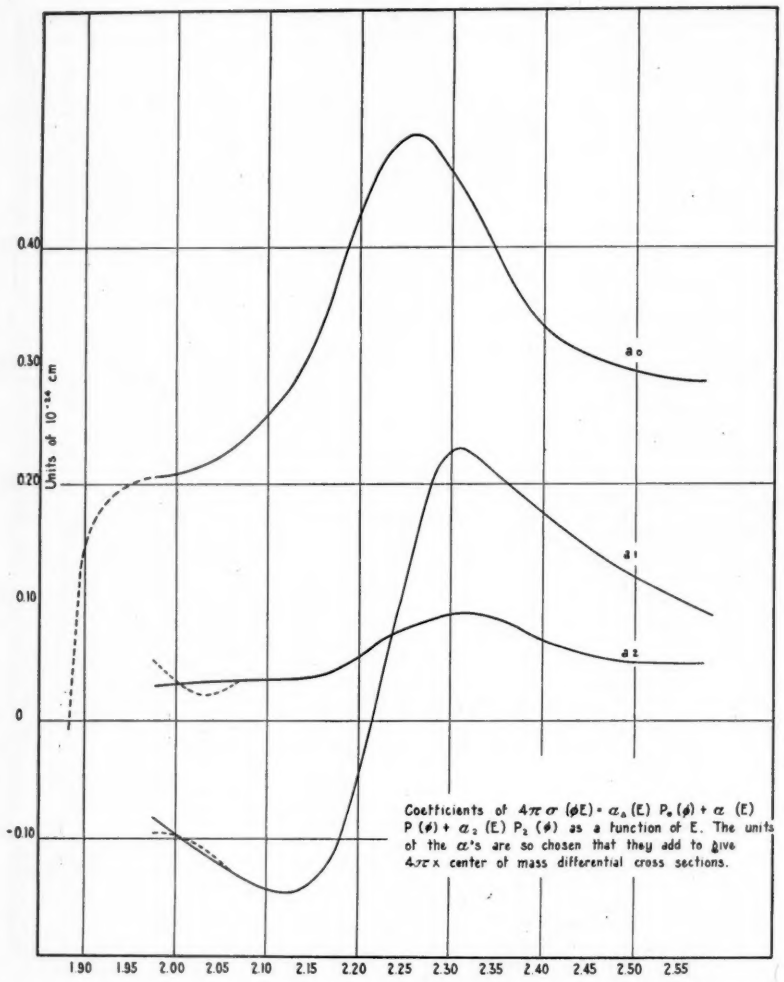
0.40
0.30
0.20
0.10
0
-0.10
Units of 10^{-24} cm
a_0
a_1
a_2
Coefficients of $4\pi\sigma(\phi E) = \alpha_0(E) P_0(\phi) + \alpha_1(E) P_1(\phi) + \alpha_2(E) P_2(\phi)$ as a function of E. The units of the α's are so chosen that they add to give 4π x center of mass differential cross sections.
1.90 1.95 2.00 2.05 2.10 2.15 2.20 2.25 2.30 2.35 2.40 2.45 2.50 2.55

FIG. 6. Energy dependence of the coefficients a_0, a_1, and a_2 of the Legendre polynomial fit to the center of mass angular distributions. The units of the a's have been adjusted to give 4π times the center of mass differential cross sections, at a chosen value of ϕ and E_p.

method has the great advantage of giving a fit to the data which is insensitive to the exact shape of the curve, and therefore to experimental errors, since it depends on the integral properties of the curve when advantage is taken of the orthogonal nature of the functions. Moreover, the resolution of the data is immediately into the partial waves of which the emitted wave may be assumed to be composed. For this method of analysis

$$\sigma(\cos\phi, E) = a_0(E)P_0(\mu) + a_1(E)P_1(\mu) + a_2(E)P_2(\mu), \quad (16)$$

where $\mu = \cos\phi$ and $P_i(\mu)$ is the Legendre polynomial of order i. The derivation of this expansion and its use in determining the energy dependent coefficients are given in Appendix IV.

The coefficients a_0, a_1, and a_2 are plotted in Fig. 6 as a function of the proton energy. It is immediately apparent that the energy dependence is a resonance process. From the analysis $2a_0(E)$ is the total cross section for the process and there is good agreement between this curve and the one from the Be^7 method except at the very lowest energies (see Fig. 2) where it is believed the angular distribution measurements are most inaccurate.

It would be of considerable interest to investigate how the coefficients a_0, a_1, and a_2 approach the threshold below 1.95 Mev, the lowest energy studied here. There is some indication that a_1 and a_2 are approaching zero as threshold is approached but there are no experimental data to support this; a_0 should be proportional to total cross section for which Be^7 measurements were made down to 1.883 Mev. Below this energy

total yield measurements are difficult of interpretation since target thicknesses must be held to a minimum. At the high energy of the threshold for this reaction it does not seem necessary that the P wave be zero at threshold. Since the lowest energy Be^7 measurement gave a yield only about 70 percent of the next at 25-kev higher energy, it seemed reasonable to extrapolate the total yield to zero at threshold.

The curves of forward yield in Fig. 3 show such a sharp rise just above threshold that there may be some question of a resonance there in the reaction yield. One might expect that very near threshold the cross section would be proportional to the neutron velocity in the center of mass system. Figure 7 shows a plot of $\sigma/(E_n)^{\frac{1}{2}}$ as a function of $(E_n)^{\frac{1}{2}}$ where $(E_n)^{\frac{1}{2}}$ is proportional to the neutron velocity in the center of mass system. The solid portion of this curve is drawn through points obtained from the actual data taken above 1.883 Mev. Below this the dotted curves arise from the two extrapolations of the data to zero at threshold shown in Fig. 2 between 1.860 and 1.883 Mev. It is seen that $\sigma/(E_n)^{\frac{1}{2}}$ is very sensitive to the exact extrapolation and the dependence of σ on $(E_n)^{\frac{1}{2}}$ must wait on very precise data in this region.

Although the possibility of a resonance near threshold is thus not ruled out, the general trend of the total yield makes it seem unlikely or weak. The rapid decrease in forward yield may be explained by the center of mass motion, which makes the neutrons come out in a cone near threshold, the solid angle included in the cone increasing more rapidly than ΔE_p, the proton energy increment above threshold. Thus the function

$$\frac{\Delta E_p}{1-\cos\theta_{\text{cone edge}}}$$

is rather rapidly decreasing and the forward yield will go down as this ratio if the total yield is proportional to ΔE_p. In addition to this, the angular distribution in the center of mass system may be such as to reduce the forward yield. Even for a spherically symmetric yield in the center of mass system, the solid angle factor alone will reduce the laboratory yield in the forward direction as ΔE_p becomes larger, since ratio of solid angles of slow to fast group decreases in the same way as the ratio of the energies of these groups.

We wish to thank Mr. William Ashley of the analytical chemistry group for his work on the weight analysis of the many lithium targets used.

This paper is based on work performed under U. S. Government Contract No. W7045-eng 36 at the Los Alamos Scientific Laboratory of the University of California.

APPENDIX I

Energy and Angle Relationships in Double Group Region

Using Eqs. (10), (11), and (13),

$$E_n(\theta)=(E_p/64)(\gamma^2+2\gamma\cos\phi+1)$$

gives the energy in the laboratory system as a function of the center of mass angle ϕ. Then for $\theta=0°$ and $\phi=0°$, i.e., for the *fast* group:

$$E_n^F(0°)=(E_p/64)(\gamma+1)^2,$$

and for $\theta=0°$, $\phi=180°$ which occurs only near threshold and results in the *slow* group:

$$E_n^S(0°)=(E_p/64)(\gamma-1)^2,$$

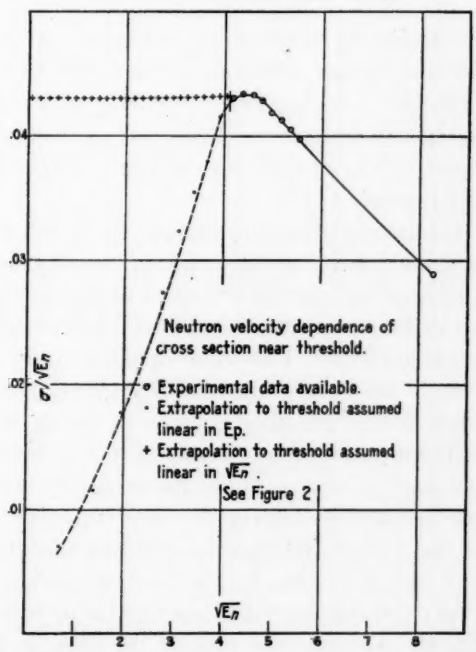

FIG. 7. Reaction cross section as a function of neutron velocity in the center of mass system extrapolated to threshold according to linear or quadratic dependence of σ on E_p.

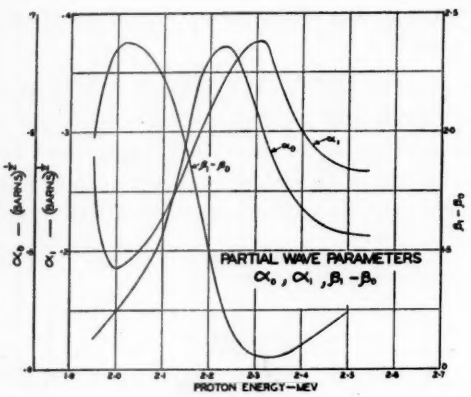

FIG. 8. Partial wave parameters α_0, α_1, and $\beta_1-\beta_0$ as a function of energy.

and the solid angle factor for 0° observation is

$$\Omega_S/\Omega_F=(\gamma-1)^2/(\gamma+1)^2=E_S/E_F.$$

This solid angle factor varies from unity just at threshold to as little as 0.01 at energies where the cone angle is large. At the edge of the cone, however, there is always only one energy neutron present.

APPENDIX II

A 30-Kev Neutron Source

The following method of measuring a cross section for 30-kev neutrons if the cross section is known for a higher neutron energy is a result of the special properties of the $Li^7(p,n)Be^7$ reaction and has been used successfully to measure cross sections.

If the bombarding proton energy is set very close to threshold of the reaction, small energy fluctuations will produce bursts of neutrons of very nearly 30 kev in energy, all lying within a very narrow cone. This cone opens to only 40° half-angle at 16 kev above threshold so that a thin foil or thin gas-filled counter of the element, for which the low energy cross section is desired, placed as close as possible to the essentially point source will always receive the *total* neutron yield from the source. If now the foil has a uniform surface density (this is always true for a gas counter) and the total neutron yield is monitored by the Be^7 activity, the ratio of the cross section at this energy to the cross section for, say, 1 Mev neutrons is found. For the 1-Mev neutrons the cross section must be known and the angular distribution of the neutrons measured, since here the Be^7 activity monitors total flux while the counter receives only a fraction of this. Often the angular distribution for the case where the $Li^7(p,n)Be^7$ reaction gives 1-Mev neutrons at zero degrees can be done with the detector in question since the minimum neutron energies at this proton energy are still about 400 kev.

APPENDIX III

Amount of Be^7 Formed

At a bombarding energy of 2.6 Mev a thick target density will be approximately 6 mg/cm²; a slightly thicker target should be used so that forward Be^7 recoils will not hit the backing material. Assuming an average cross section of 0.3 barn, which is conservative, and a mean energy loss of the protons in the lithium of 130 kev per mg/cm², also conservative, one finds

$$\frac{\text{No. } Be^7 \text{ atoms formed}}{\text{Microcoulomb}}\cong 6.25\times10^{12}\times0.3\times10^{-24}\times5.7\times\frac{6.03}{7}\times10^{20}$$

$$=9.2\times10^{8}.$$

On the Los Alamos machine a 50 μa beam can easily be maintained for long periods of time; thus 48 hours of exposure would give 8.0×10^{15} atoms or 0.09 microgram of Be^7 formed, neglecting decay. Because of the 43-day half-life this exposure may be made over several days period, the decay rate being only about 1.6 percent per day, for which corrections can be accurately made.

Spectrochemical techniques seem capable of determining Be to an accuracy of five percent in concentrations of less than one part per million. If this accuracy can be slighly improved, this would provide a straightforward method of measuring the total flux of neutrons from the source during such an exposure. In particular, manganese bath activities taken over selected portions of such a run would then be standardized and RaBe source strengths could be measured in terms of their activities induced in the same bath. If chemical separation of Be from the bulk of the Li is necessary, the ratio of Be^7 activities in two

samples allows a simple determination of the separation efficiency.

APPENDIX IV

Method of Analysis of Angular Distributions

The method developed below is due to Frederick Reines of the Theoretical Division.

The observed neutron intensity $I(\mu, E)$ in the center of mass system is plotted as a function of $\mu=\cos\phi$ at each proton energy E.

At a given energy E, the amplitude of the neutron wave is

$$f(\mu)=\sum_{i=0}^{m}a_iP_i(\mu), \tag{1}$$

where P_i is the Legendre polynomial of the first kind and $a_i=\alpha_i\exp[i\beta_i]$. Then

$$I(\mu)=|f(\mu)|^2=\sum_{\substack{i=0\\ i\neq j}}^{m}\sum_{j=0}^{m}a_iP_i(\mu)a_j^*P_j(\mu). \tag{2}$$

In terms of α_i and β_i this becomes

$$I(\mu)=\sum_{\substack{i=0\\ i\neq j}}^{m}\sum_{j=0}^{m}\alpha_i\alpha_j\cos(\beta_i-\beta_j)P_iP_j+\sum_{i=0}^{m}\alpha_i^2P_i^2, \tag{3}$$

and using the theorem

$$P_iP_j=\sum_{r=0}^{i}C_rP_{i+j-2r}, \quad i\geq j, \tag{4}$$

where

$$C_r=(A_{i-r}A_rA_{j-r}/A_{i+j-r})\cdot(2i+2j-4r+1)/(2i+2j-2r+1),$$

$$A_r=[1\cdot3\cdot5\cdots(2r-1)]/r!,$$

it is possible to write $I(\mu)$ as a *linear* expansion in the P's instead of products. Thus

$$I(\mu)=\sum_{\substack{i=0\\ i\neq j}}^{m}\sum_{j=0}^{m}\alpha_i\alpha_j\cos(\beta_i-\beta_j)\sum_{r=0}^{i}C_rP_{i+j-2r}+\sum_{i=0}^{m}\alpha_i^2\sum_{r=0}^{i}C_rP_{2(i-r)}, \tag{5a}$$

and by collecting coefficients,

$$I(\mu)=a_0P_0+a_1P_1+\cdots+a_mP_m.$$

From the orthogonality properties of the Legendre polynomials one finds

$$\int_{-1}^{+1}IP_n\,d\mu=\sum_{i=0}^{m}[2\alpha_i/(2i+1)]=a_0 \quad \text{for} \quad n=0 \tag{6a}$$

$$=[2/(2n+1)]\left\{\sum_{\substack{i=0\\ i\neq j}}^{m}\sum_{j=0}^{m}\alpha_i\alpha_j\cos(\beta_i-\beta_j)C_{[(i+j-m)/2]}+\sum_{i=0}^{m}\alpha_i^2C_{i-(m/2)}\right\} \quad \text{for} \quad n\neq0$$

$$=a_n[2/(2n+1)].$$

Thus from the plot of the experimental $I(\mu)$ one can immediately calculate the coefficients from

$$a_n=[(2n+1)/2]\int_{-1}^{+1}IP_n\,d\mu, \tag{7}$$

without recourse to the *detailed* shape of the curve.

For the present data the calculations were carried out through a_6; however, all coefficients beyond a_2 were zero to within the experimental error of <6 percent, i.e. only S and P waves were sufficient to describe the distributions up to 2.55 Mev.

In terms of the α's and β's the coefficients are

$$a_0(E)=\alpha_0^2(E)+\alpha_1^2(E)/3,$$
$$a_1(E)=2\alpha_0(E)\alpha_1(E)\cos(\beta_1-\beta_0),$$
$$a_2(E)=\tfrac{2}{3}\alpha_1^2(E),$$

and the total cross section is given by $2a_0$. Curves are shown in Fig. 8 for the energy dependence of the partial wave parameters α_0, α_1, and $\beta_1-\beta_0$.

It should be noted that in the case in which an admixture of more than S and P waves is required to describe the distribution there are more unknowns than equations, rendering impossible a unique assignment of amplitudes and phases.

PHYSICAL REVIEW VOLUME 74, NUMBER 4 AUGUST 15, 1948

The Influence of Relaxation on the Two Velocity Field Model of Helium II

WILLIAM BAND AND LOTHAR MEYER,
Institute for the Study of Metals, The University of Chicago, Chicago, Illinois
(Received May 10, 1948)

In a previous paper (see reference 1) we have introduced the concept of a time of relaxation in discussing disturbances of thermal equilibrium between the populations of the "superfluid" state and the normal states in helium II, in order to relate second sound with heat conductivity.

For a complete discussion of the unrelaxed, the fully relaxed, and the transition region, we need at least one more independent variable than the two which specify the thermodynamic state of a system of one component in internal equilibrium. In a Taylor expansion of the energy as a function of such a set of three variables the coefficients at partial or zero relaxation will differ from the ordinary values calculated from equilibrium thermodynamics. The wave equations ordinarily deduced are therefore modified.

Expressions are obtained for the velocities of propagation of both sounds at infinite frequency (zero relaxation) and at zero frequency (full relaxation). At zero frequency, second sound reduces to thermal diffusion. Normal sound undergoes a sharp Einstein dispersion-and-attenuation at the lambda temperature where the relaxation time passes abruptly through the critical value for all generally used frequencies. The theory is used to compute x, the fraction of normal particles, from thermodynamic data and second sound velocity. The energy per normal particle is obtained as a function of temperature from x and the thermodynamic data on total heat content.

IN a previous paper[1] we have introduced the concept of a time of relaxation in discussing disturbances of thermal equilibrium between the populations of the "superfluid" state and the normal states in helium II, in order to relate second sound with the heat conductivity. For a complete discussion of the unrelaxed state (infinite frequency), the fully relaxed state (thermal equilibrium at zero frequency) and the transition region (partially relaxed states), we need at least one more independent variable than the two which specify the thermodynamical state of a system of one component when it is in internal equilibrium. Appropriate variables seem to be ρ, the density of the whole liquid, x, the fraction of the liquid in the normal states

$$x=\rho_x/\rho, \tag{1}$$

where ρ_x is the density of the normal component, and σ the entropy per unit mass of normal component:

$$\sigma=S/x, \tag{2}$$

where S is the entropy per unit mass of the liquid, contributed by the normal component. It will be assumed with Tisza[2] and Landau[3] that S is the whole entropy of the mixture. In this case the above three independent variables, ρ, x, σ, are sufficient to define the state of the system when it is not in a state of internal (thermal) equilibrium. In the case of full internal equilibrium ρ and x become equivalent to V and T, respectively, while σ ceases to be independent because in (2) both x and S are now definite functions of T. At the other extreme, in the entire absence of relaxation (infinite frequency) the entropy per normal particle remains constant as there is no time for interaction:

$$\Delta\sigma=0. \tag{3}$$

In a Taylor expansion of the variation of any function of the three variables, ρ, x and σ, only two variables will again appear explicitly; however, the coefficients at zero relaxation will differ from the ordinary equilibrium coefficients that apply to full relaxation. For a fully relaxed system, the variation of the energy may be written:

$$\Delta_r E=(\partial E/\partial\rho)_x\Delta\rho+(\partial E/\partial x)_\rho\Delta x + \text{second-order terms.} \tag{4}$$

As long as we consider only variations around an energy minimum, i.e., a state of equilibrium, the first-order terms vanish identically, and only second-order derivatives remain. For the completely unrelaxed case where (3) applies the variations of energy become, therefore,

$$\Delta_u E=\tfrac{1}{2}(\partial^2 E/\partial\rho^2)_{x,\sigma}\Delta\rho^2+(\partial^2 E/\partial x\partial\rho)_\sigma\Delta x\Delta\rho+\tfrac{1}{2}(\partial^2 E/\partial x^2)_{\rho\sigma}\Delta x^2. \tag{5}$$

[1] W. Band and L. Meyer, Phys. Rev. **73**, 226 (1948).
[2] L. Tisza, Phys. Rev. **72**, 838 (1947).
[3] L. Landau, J. Phys. U.S.S.R. **5**, 711 (1941).

The second derivatives here have two suffixes to show that they are not the ordinary equilibrium partial derivatives for which σ would not be constant. These unrelaxed derivatives are evaluated in Appendix A.

To study the partially relaxed system in the intermediate region between the above two extremes we introduce a generalized temperature, T_x, defined by

$$T_x=(\partial E/\partial S)_{x\rho}=(1/x)(\partial E/\partial\sigma)_{x\rho} \quad (6)$$

(in any degree of relaxation). In Appendix A, it is shown that the first variation of energy can be expressed in the form

$$\Delta E=T_x\Delta S-P_x\Delta V+\mu_x\Delta x, \quad (7)$$

where

$$P_x\equiv\rho^2(\partial E/\partial\rho)_{x\sigma}=P+(T_x-T)(\partial P/\partial T)_v \quad (8)$$

and

$$\mu_x=(C/x')(1-T_x/T). \quad (9)$$

Here P_x is a generalized pressure, μ_x plays the part of a chemical potential for the mixture, C is the specific heat, and x' is $\partial x/\partial T$. In the fully relaxed limit $T_x\to T$, $P_x\to P$, and $\mu_x\to 0$.

The quantities $(\partial T_x/\partial T)_{x\sigma}$ and $(\partial T_x/\partial T)_{\rho\sigma}$ are related to each other. As already assumed, the heat content per gram, Q, of helium II is due to the normal particles only, so

$$Q=x\epsilon, \quad (10)$$

where ϵ is the mean energy per gram of normal particles. The specific heat per gram is then

$$C=dQ/dT=(dx/dT)\epsilon+(d\epsilon/dT)\cdot x. \quad (11)^*$$

In the completely unrelaxed case, variations of x at constant ρ and σ are not capable of altering ϵ because of absence of interaction with the superfluid. This means that, comparing equal variations in energy, relaxed and unrelaxed:

$$\Delta_u E=C\Delta T=x'\epsilon\cdot\Delta T_x)_{\rho\sigma}. \quad (12)$$

On the other hand, in an unrelaxed variation of ρ, keeping x constant, only ϵ can vary, so that

$$\Delta_u E=\epsilon'\cdot x\cdot\Delta T_x)_{x\sigma}. \quad (13)^{**}$$

Comparing (12) and (13) we find, writing a suffix "u" again to indicate the completely unrelaxed values:

$${}_u(\partial T_x/\partial T)_{\rho\sigma}=C/x'\epsilon, \quad {}_u(\partial T_x/\partial T)_{x\sigma}=C/\epsilon' x, \quad (14)$$

or by (10)

$${}_u(\partial T_x/\partial T)_{\rho\sigma}=xC/x'Q, \quad (15)$$

and

$${}_u(\partial T_x/\partial T)_{x\sigma}=1/[1-(x'Q/xC)]. \quad (16)$$

Consider two local adiabatic compressions, one ideal with full relaxation, the other actual with incomplete relaxation; they are accompanied by temperature increase T and T_x, respectively. The quantity

$$\chi=T_x-T \quad (17)$$

is a measure of the lack of internal equilibrium in the incompletely relaxed compression. Following Frenkel,[4] the tendency of the system to return to internal equilibrium will be assumed proportional to χ and we write

$$d\chi/dt=-\chi/\tau_2+(d\chi/dt)_\infty \quad (18)$$

which, with Frenkel's operator

$$A_2\equiv 1+\tau_2 d/dt, \quad (19)$$

leads after some algebraic work (given in Appendix B) to the following result: The effective value $(\partial T_x/\partial T)^*$ under partial relaxation is given by

$$(\partial T_x/\partial T)^*-1=[(\partial T_x/\partial T)_u-1](1-A_2^{-1}), \quad (20)$$

where the expression $(\partial T_x/\partial T)_u$ appearing on the right side represents its value under complete absence of relaxation (infinite frequency).

This relation permits us to express the elastic coefficients of (5) for the partially relaxed case in terms of the values they have in the completely unrelaxed limit.*** The thermodynamic part of the problem is then solved. The general results, derived in Appendix B, are expressible in terms

* We neglect the small difference between C_p and C_v in helium II.

** In writing ϵ' here, it is assumed that the increase of ϵ resulting from the work performed on the system during increase in density is distributed over the different excited states of the normal component with sufficient rapidity: the term "unrelaxed" refers only to the equilibrium between the superfluid and the excited states as a whole. This assumption will have to be confirmed by measurements on the dispersion of ordinary sound below the lambda-point.

[4] J. Frenkel, *Kinetic Theory of Liquids* (Oxford University Press, Cambridge, 1946).

*** These coefficients, which are physically real quantities, appear in this operator-type relaxation theory as complex quantities essentially because we have chosen to ignore the fact that additional terms in $\Delta\sigma^2$ would appear in (5) for the partially relaxed case.

of directly measurable (i.e., fully relaxed or thermal equilibrium) quantities, as follows:

$$(\partial^2 E/\partial x^2)_{\rho\sigma}^* = S/xx' + (C/Tx'^2 - S/xx') \times (1 - xC/x'Q)(1 - A_2^{-1}),$$
$$(\partial^2 E/\partial x \partial \rho)_\sigma^* = (\partial P/\partial T)_v [ST/xC + (1/x') \times (1 - xC/x'Q)(1 - A_2^{-1})], \quad (21)$$
$$\rho^2 (\partial^2 E/\partial \rho^2)_{x\sigma}^* = \rho^2 (\partial^2 E/\partial \rho^2)_s + (\partial P/\partial T)_v \times (\partial T/\partial \rho)_s (xC/x'Q - 1)^{-1} (1 - A_2^{-1}).$$

The Lagrangian method, first used in this connection by Tisza,[2] lends itself most naturally to the derivation of wave propagation in terms of these "elastic" coefficients. The details of the argument are given in Appendix C.

Instead of assuming that the x particles obey a mass continuity law which would be the case only in the completely unrelaxed limit, the following relation is obtained:

$$\Delta x/x = (x'Q/xC) \nabla \cdot \bar{u}_x (\partial T_x/\partial T)_{\rho\sigma}^*, \quad (22)$$

which reduces, by (20) to the mass continuity

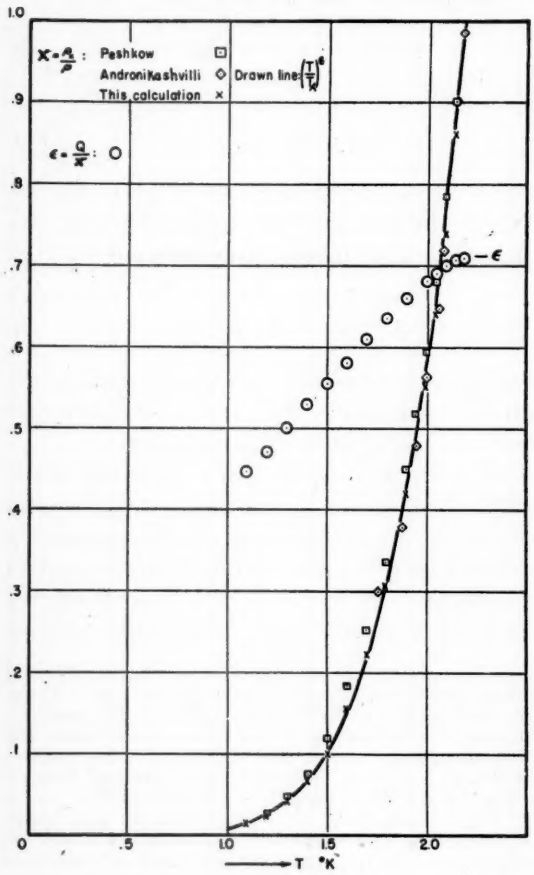

FIG. 1.

at zero relaxation, but becomes the conservation of heat at full relaxation.

To the ordinary Lagrangian is added a dissipation function to take account of the rate at which momentum is being lost by collisions between opposing streams of superfluid and normal part. This loss appears in terms of a relaxation time τ_1 not necessarily identical with the equilibrium relaxation time introduced above in (18). The normal viscosity of the x fluid can also be included in this analysis, but it is found that it contributes only terms which are entirely negligible up to frequencies as high as 10^{11} cycles per sec.

Limiting the solutions of the wave equations to steady oscillations depending on time only through the factor $\exp(2\pi i \nu t)$, the operator $(1 - A_2^{-1})$ becomes equivalent finally to the factor

$$(1 - A_2^{-1}) = 1/[1 + 1/(2\pi i \nu \tau_2)]. \quad (23)$$

This factor is directly responsible for a dispersion and attenuation in both ordinary and second sound. The relaxation time τ_1 enters only the second sound propagation, and is identical with the relaxation time previously introduced.[1]

The velocity of normal sound V_n is found to be:

$$V_n^2 = V_{n0}^2 + K/(1 + 1/2\pi i \nu \tau_2), \quad (24)$$

where V_{n0} is the ordinary (relaxed) velocity of normal sound and

$$K = (T/\rho^2 C)(\partial P/\partial T)_v^2/(xC/x'Q - 1). \quad (25)$$

This is a typical Einstein[5] dispersion, with a peak attenuation given by

$$\alpha_{\max} = \tfrac{1}{2}\pi \nu K/V_{n0}^3. \quad (26)$$

The sharp peak in attenuation observed by Pellam and Squire[6] in the neighborhood of the lambda-temperature may be due to the circumstance that τ_2 suddenly rises from times much smaller in order of magnitude than $1/2\pi\nu$ above T_λ to times considerably longer than this value below T_λ. Pellam and Squire report a peak attenuation "at least 3.5 per cm for 15 Mc." Equation (26) gives $\alpha_{\max}$ equal to 10 per cm. at this frequency.† The wave equation obtained

[5] A. Einstein, Sitz. Berl. Akad. **1920**, p. 380.
[6] J. R. Pellam and C. F. Squire, Phys. Rev. **72**, 1245 (1947).
† The attenuation in the helium II region well below the lambda-point may be due to the dispersion mentioned in the footnote to Eq. (13).

for second sound is

$$(\partial^2 Z/\partial t^2)+(1/\tau_1)(\partial Z/\partial t)=V_s^2\nabla\nabla\cdot Z, \quad (27)$$

Z being the relative displacement of the x-fluid and V_s^2 is in general complex, depending on $2\pi i\nu\tau_2$. At high frequencies, however,

$$(\partial^2 Z/\partial t^2)=V_{s\infty}^2\nabla\nabla\cdot Z, \quad (28)$$

where

$$V_{s\infty}^2=[x(1-x)/(x')^2](C/T)\times[ST/Q+(1-xc/x'Q)]. \quad (29)$$

At very low frequencies τ_2 again drops out and the second sound wave approaches a diffusion type equation as $\nu\to 0$,

$$(\partial Z/\partial t)/\tau_1=[x'(1-x)/x^2](SQ^2/C^2)\nabla\nabla\cdot Z. \quad (30)$$

This change-over is expected to set in as soon as $2\pi\nu\tau_1<1$, and occurs for all ordinary frequencies at T_λ. The applications of (30) to experimental evidence will be given in the following paper.

The expression (29) for the velocity of propagation of second sound has been used to compute x as a function of T from known data on C, S, Q[7,††] and the published measurements of V_s by Peshkov[8] and by Lane, Fairbank, and Fairbank.[9] Equation (29) can be written in the form of a differential equation

$$(x'/x)^3-A(1/x-1)(x'/x)+B(1/x-1)=0, \quad (31)$$

where

$$A=C(1+ST/Q)/TV_s^2,$$

and

$$B=C^2/QTV_s^2 \quad (32)$$

are known functions of T between 1.1°K and T_λ. It would be ideally possible to obtain a unique solution for $x(T)$ from this equation if A and B were known over the entire temperature range from 0°K to T_λ, and if it could be assumed that $x(T)$ varied continuously from zero at 0°K to unity at T_λ. Data actually available permit only a selection of a family of curves which behave reasonably near T_λ and appear to go nicely towards zero as temperature falls. Since only half the temperature range is covered by the data, this family of curves is not sufficient to force a unique selection of one curve, although in fact the range of values of x is only a few percent.

TABLE I.

T °K	C cal./g deg.	Q cal./g	S cal./g deg.	V_s m/sec.	x	ϵ cal./g
1.0	0.023	0.00329	0.00383			
1.1	0.0411	0.00645	0.00684	18.2±.3	0.0143	0.451
1.2	0.0705	0.01194	0.01160	18.7±.1	0.025	0.478
1.3	0.116	0.02109	0.01892	18.95	0.042	0.502
1.4	0.176	0.03560	0.02964	19.82	0.067	0.531
1.5	0.269	0.05737	0.04477	20.09	0.104	0.552
1.6	0.391	0.0902	0.06582	20.33	0.157	0.575
1.7	0.525	0.1359	0.09324	20.35	0.222	0.612
1.8	0.691	0.1964	0.1278	19.90	0.307	0.640
1.9	0.918	0.2784	0.1714	18.68	0.420	0.663
2.0	1.218	0.3745	0.2260	16.69	0.552	0.678
2.05	1.41	0.4407	0.2583	14.94	0.641	0.688
2.10	1.66	0.5162	0.2951	12.25	0.738	0.699
2.15	2.05	0.6073	0.3383	8.05±.3	0.860	0.706
2.18	2.85	0.6776	0.3701	4.25±.4		
2.186		0.71	0.390	0	1.00	0.71

The final selection of the curve for $x(T)$ was made as follows. From some preliminary selection of the $x(T)$ curve, and the data on Q, we derive the curve for $\epsilon(T)$ by Eq. (10). From the two curves $x(T)$ and $\epsilon(T)$ we obtain graphically the sum $\epsilon'/\epsilon+x'/x$. By Eq. (11) we then have

$$C/Q=\epsilon'/\epsilon+x'/x. \quad (33)$$

By successive approximation, the selection of the $x(T)$ curve was improved until agreement with (33) lay within 1 percent for all temperatures from 1.1°K up to about 1.95°K. Above this temperature the difference rose to about 10 percent at the lambda-point; this may be due to the experimental uncertainties in C and Q near T_λ, or to errors in the graphical determination of x' and ϵ' near T_λ where both curves change their slopes very strongly. The results are shown in Fig. 1, and Table I, where the values of C, S, and Q are also given.

Peshkov[8] has published values for $x(T)$ deduced from Landau's theory of second sound[10] and using his measurements of the velocity. In that theory, entire absence of relaxation was assumed in setting up mass continuity equations, but the fully relaxed (equilibrium) "elastic coefficients" were used.

Andronikashvilli[11] has also deduced values of $x(T)$ from his measurements of the inertia of

[7] W. H. Keesom, *Helium* (Amsterdam, New York, 1942).

†† Q and S have been calculated by numerical integration of the Leyden measurements on C by A. P. Keesom and W. K. Westmyze (see reference 7).

[8] V. Peshkov, J. Phys. U.S.S.R. 10, 389 (1946).

[9] C. T. Lane, H. A. Fairbank, and W. M. Fairbank, Phys. Rev. 71, 600 (1947).

[10] L. Landau, J. Phys. U.S.S.R. 10, 91 (1947).

[11] E. Andronikashvilli, J. Phys. U.S.S.R. 10, 201 (1946).

He II. His points lie about 5 to 10 percent below those of Peshkov, which is just about the limit of the experimental errors. The values calculated in the present paper, using non-equilibrium "elastic coefficients" are slightly lower than Andronikashvilli's, but are much nearer to the latter than those of Peshkov, the relative difference from Peshkov's being about 10 percent.††† Our results can, to a first approximation, be represented by a $(T/T_\lambda)^6$ curve up to about 1.8°K, and above this temperature they tend rather towards a 6.5 or 7th power curve.

The writers are happy to express their gratitude to Professor Clarence Zener for helpful discussions.

APPENDIX A

Thermodynamics

In general, any function of three variables ρ, x, and σ can be expanded:

$$\Delta F=(\partial F/\partial\rho)_{x\sigma}\Delta\rho+(\partial F/\partial x)_{\rho\sigma}\Delta x+(\partial F/\partial\sigma)_{x\rho}\Delta\sigma+\cdots. \quad (A1)$$

Under zero relaxation, $\Delta\sigma=0$, which reduces (A1) to its first two terms. Under full relaxation the expansion also reduces to two terms, because here $\Delta\sigma$ has its equilibrium value:

$$\Delta\sigma=(\partial\sigma/\partial\rho)_x\Delta\rho+(\partial\sigma/\partial x)_\rho\Delta x+\cdots. \quad (A2)$$

In what follows, partial first derivatives with one suffix will indicate equilibrium derivatives; first derivatives with two suffixes indicate that the equilibrium represented by (A2) cannot be *assumed*. In particular for internal equilibrium we also have

$$\Delta F=(\partial F/\partial\rho)_x\Delta\rho+(\partial F/\partial x)_\rho\Delta x+\cdots, \quad (A3)$$

and this must be identical with the result of using (A2) in (A1). Therefore it follows that

$$(\partial F/\partial x)_{\rho\sigma}=(\partial F/\partial x)_\rho-(\partial F/\partial\sigma)_{x\rho}(\partial\sigma/\partial x)_\rho, \quad (A4)$$

$$(\partial F/\partial\rho)_{x\sigma}=(\partial F/\partial\rho)_x-(\partial F/\partial\sigma)_{x\rho}(\partial\sigma/\partial\rho)_x. \quad (A5)$$

Writing E for F in (A4), it is then easy to show that

$$(\partial E/\partial x)_{\rho\sigma}=\mu_x+\sigma T_x, \quad (A6)$$

where μ_x and T_x have been defined in the text. Also from (A5) with E replacing F, we derive

$$\rho^2(\partial E/\partial\rho)_{x\sigma}=\rho^2(\partial E/\partial\rho)_x+T_x(\partial P/\partial T)_v. \quad (A7)$$

This last equation yields Eq. (8) in the text, while from (A6), (9) and (8) and the thermodynamic relation

$$P=\rho^2(\partial E/\partial\rho)_T+T(\partial P/\partial T)_v, \quad (A8)$$

Eq. (7) of the text also follows at once.

To evaluate the second derivatives of E the first derivatives given by (A6) and (A7) are substituted for F in (A4) and (A5). Thus (A4) gives

$$(\partial^2E/\partial x^2)_{\rho\sigma}=(\partial[\mu_x+\sigma T_x]/\partial x)_\rho-(\partial\sigma/\partial x)_\rho(\partial[\mu_x+\sigma T_x]/\partial\sigma)_{\rho x}. \quad (A9)$$

In the first term, the relaxed derivative, we may already set $\mu_x=0$ and $T_x=T$, so obtaining simply $(\partial\sigma T/\partial x)_\rho$. Again from (A4) with σT_x in place of F we have

$$(\partial\sigma T/\partial x)_\rho-(\partial\sigma/\partial x)_\rho(\partial\sigma T_x/\partial\sigma)_{\rho x}=(\partial\sigma T_x/\partial x)_{\rho\sigma}=\sigma(\partial T_x/\partial x)_{\rho\sigma}.$$

Using this in the second term on the right of (A9) we obtain

$$(\partial^2E/\partial x^2)_{\rho\sigma}=\sigma(\partial T_x/\partial x)_{\rho\sigma}-(\partial\sigma/\partial x)_\rho(\partial\mu_x/\partial\sigma)_{\rho x}=\sigma(\partial T_x/\partial x)_{\rho\sigma}+(\partial\mu_x/\partial x)_{\rho x}-(\partial\mu_x/\partial x)_\rho. \quad (A10)$$

The last term here again vanishes because $\mu_x=0$ for the relaxed condition implied in the single suffix, while from (9)

$$(\partial\mu_x/\partial x)_{\rho\sigma}=C[1-(\partial T_x/\partial T)_{\rho\sigma}]/T\cdot(x')^2. \quad (A11)$$

Finally, therefore, evaluating the expression *at* the origin of the variations—namely, at $T_x=T$, we find

$$(\partial^2E/\partial x^2)_{\rho\sigma}=(S/xx')(\partial T_x/\partial T)_{\rho\sigma}+C[1-(\partial T_x/\partial T)_{\rho\sigma}]/T\cdot(x')^2$$

or

$$\boxed{(\partial^2E/\partial x^2)_{\rho\sigma}=[C/T\cdot(x')^2]\times[ST/Q+(1-xC/x'Q)]}. \quad (A12)$$

From (8) and (A7) and (A8)

$$\rho^2(\partial^2E/\partial\rho^2)_{\sigma x}=(\partial P/\partial\rho)_T-2P/\rho-[1-(\partial T_x/\partial T)_{x\sigma}](\partial T/\partial\rho)_s(\partial P/\partial T)_v \quad (A13)$$

when evaluated at $T_x=T$. This can be written

††† A comprehensive discussion of the different methods used to compute the fraction x has been given by J. G. Daunt at the Washington Meeting of the American Physical Society, May 1947, which will be published soon. We wish to thank Professor Daunt for sending us a copy of this report.

in the form

$$\rho^2(\partial^2E/\partial\rho^2)_{x\sigma}=\rho^2(\partial^2E/\partial\rho^2)_x+(\partial T/\partial\rho)_s \times(\partial P/\partial T)_v/[xC/x'Q-1]. \quad \text{(A14)}$$

From (8) we may write

$$\rho^2(\partial^2E/\partial x\partial\rho)_\sigma=(\partial P/\partial x)_{\rho\sigma} -(1/x')[1-(\partial T_x/\partial T)_{\rho\sigma}](\partial P/\partial T)_v.$$

But

$$(\partial P/\partial x)_{\rho\sigma}=\sigma(\partial P/\partial S)_\rho=-(S/x)(\partial T/\partial V)_s,$$

so that we have, finally,

$$\rho^2(\partial^2E/\partial x\partial\rho)_\sigma=-(S/x)(\partial T/\partial V)_s -(1/x')[1-xC/x'Q](\partial P/\partial T)_v. \quad \text{(A15)}$$

APPENDIX B

Relaxation Theory

As stated in the text, Eqs. (17) and (18), the quantity $\chi=T_x-T$ is a measure of the lack of internal equilibrium, and we assume

$$d\chi/dt=-\chi/\tau_2+(d\chi/dt)_\infty, \quad \text{(B1)}$$

where $(d\chi/dt)_\infty$ is the value expected at zero relaxation, $\tau_2=\infty$. But we can write

$$(d\chi/dt)_\infty=(d\Delta\rho/dt)(\partial\chi/\partial\rho)_{x\sigma} +(d\Delta x/dt)(\partial\chi/\partial x)_{\rho\sigma}, \quad \text{(B2)}$$

where $\Delta\rho$ and Δx are the first-order variations present in the wave. Note that $\Delta\sigma=0$ at zero relaxation. However, by definition of χ we have

$$(\partial\chi/\partial\rho)_{x\sigma}=[(\partial T_x/\partial T)_{x\sigma}-1](\partial T/\partial\rho)_s,$$

and

$$(\partial\chi/\partial x)_{\rho\sigma}=[(\partial T_x/\partial T)_{\rho\sigma}-1](\partial T/\partial x)_{\rho\sigma}. \quad \text{(B3)}$$

For variations at constant x we may therefore write (B1) as

$$d\chi_x/dt=-\chi_x/\tau_2+(\partial T/\partial\rho)_s \times[(\partial T_x/\partial T)_{x\sigma}-1](d\Delta\rho/dt), \quad \text{(B4)}$$

and for variations at constant ρ

$$d\chi_\rho/dt=-\chi_\rho/\tau_2+(\partial T/\partial x)_\rho \times[(\partial T_x/\partial T)_{\rho\sigma}-1](d\Delta x/dt). \quad \text{(B5)}‡$$

‡ As we are not interested eventually in the *shape* of the attenuation curve, we assume for simplicity that the relaxation times for the two processes, (B4) and (B5), are identical.

Introduce the Frenkel operator defined by Eq. (19) in the text, such that

$$\tau_2d/dt=A_2-1,$$

then (B4) and (B5) can be solved formally for χ_x and χ_ρ:

$$\chi_x=(\partial T/\partial\rho)_s[(\partial T_x/\partial T)_{x\sigma}-1](1-A_2^{-1})\Delta\rho,$$
$$\chi_\rho=(\partial T/\partial x)_\rho[(\partial T_x/\partial T)_{\rho\sigma}-1](1-A_2^{-1})\Delta x. \quad \text{(B6)}$$

At full relaxation, $\tau_2\to0$, $A_2\to1$ and χ_x, χ_ρ both vanish. At zero relaxation, $\tau_2\to\infty$, $A_2^{-1}\to0$, and therefore

$$\chi_x\to(\partial T/\partial\rho)_s[(\partial T_x/\partial T)_{x\sigma}-1]\Delta\rho,$$
$$\chi_\rho\to(\partial T/\partial x)_\rho[(\partial T_x/\partial T)_{\rho\sigma}-1]\Delta x. \quad \text{(B7)}$$

It is now clear from a comparison between (B6) and (B7) that in the general (partially relaxed) case $[(\partial T_x/\partial T)-1](1-A_2^{-1})$ replaces $[(\partial T_x/\partial T)-1]$, as stated in the text, no matter whether x or ρ is kept constant.

Using (20) in the equation preceding (A12), we obtain for the general (partially relaxed) case the following expression for the "elastic coefficient" which determines the velocity of second sound propagation:

$$(\partial^2E/\partial x^2)_{\rho\sigma}=S/xx'+(C/Tx'^2-S/xx') \times[1-(\partial T_x/\partial T)_{\rho\sigma}](1-A_2^{-1}). \quad \text{(B8)}$$

By (15) this reduces to the expression given in the text, (21). Similarly, using (20) in (A13) yields the third expression in (21) for the elastic coefficient determining the velocity of ordinary sound. Finally, with the same substitution, (A15) gives the cross term coefficient in (21).

APPENDIX C

The Lagrangian Equations of Wave Motion

Using the two velocity field model, the Lagrangian per unit mass in the completely unrelaxed case is written

$$L_u=\tfrac{1}{2}x\bar{u}_x^2+\tfrac{1}{2}(1-x)\bar{u}_z^2-\Delta_uE, \quad \text{(C1)}$$

where $\bar{u}_x$ and $\bar{u}_z$ are the velocities of the two components, normal, and superfluid, and Δ_uE is obtained from (5) in the text. Following Tisza[2] we use coordinates for the center of mass and relative displacement:

$$\langle\dot{\eta}\rangle=x\bar{u}_x+(1-x)\bar{u}_z, \quad \text{(C2)}$$
$$\langle\dot{\xi}\rangle=\bar{u}_x-\langle\dot{\eta}\rangle=(1-x)(\bar{u}_x-\bar{u}_z), \quad \text{(C3)}$$

then the Lagrangian is

$$L_u=\tfrac{1}{2}\langle\dot{\eta}\rangle^2+\tfrac{1}{2}[x/(1-x)]\langle\xi\rangle^2-\Delta_u E. \quad \text{(C4)}$$

To express $\Delta_u E$ in terms of $\bar{\eta}$ and $\bar{\xi}$ we write the mass continuity equations, assuming zero relaxation, in the forms given by Tisza:[2]

$$\Delta\rho/\rho=-\nabla\cdot\bar{\eta}, \quad \text{(C5)}$$

$$\Delta x/x=-\nabla\cdot(\bar{\eta}+\bar{\xi}). \quad \text{(C6)}$$

It is then more convenient to use in place of $\bar{\xi}$ the variable

$$\bar{\zeta}=(x/(1-x))^{\frac{1}{2}}\bar{\xi}. \quad \text{(C7)}$$

Using (C5), (C6), (C7) in (C4) with (5), we finally obtain for this limiting case

$$L_u=\tfrac{1}{2}\langle\dot{\eta}\rangle^2+\tfrac{1}{2}\langle\dot{\zeta}\rangle^2+f_u(\nabla\cdot\bar{\eta})^2+g_u(\nabla\cdot\dot{\zeta})^2 +h_u(\nabla\cdot\bar{\eta})(\nabla\cdot\bar{\zeta}), \quad \text{(C8)}$$

where

$$\begin{aligned} f_u&=-\tfrac{1}{2}\rho^2(\partial^2E/\partial\rho^2)_{x\sigma}-\tfrac{1}{2}x^2(\partial^2E/\partial x^2)_{\rho\sigma},\\ g_u&=-\tfrac{1}{2}x(1-x)(\partial^2E/\partial x^2)_{\rho\sigma}, \quad \text{(C9)}\\ h_u&=-(x(1-x))^{\frac{1}{2}}\rho(\partial^2E/\partial x\partial\rho)_\sigma -2x(x(1-x))^{\frac{1}{2}}(\partial^2E/\partial x^2)_{\rho\sigma}. \end{aligned}$$

Turning now to the fully relaxed limit, we can no longer use (C6), but are obliged instead to use the conservation of energy in the form

$$C\dot{T}=-\epsilon\nabla\cdot(x\bar{u}_x) \quad \text{(C10)}$$

or, from (C3),

$$C\Delta T=-\epsilon x\nabla\cdot(\bar{\xi}+\bar{\eta}), \quad \text{(C11)}$$

so that

$$\begin{aligned} \Delta x/x&=-(\epsilon x'/C)\nabla\cdot(\bar{\xi}+\bar{\eta}),\\ &=-(x'Q/xC)\nabla\cdot(\bar{\xi}+\bar{\eta}). \quad \text{(C12)} \end{aligned}$$

This modifies the Lagrangian which will have the same form as (C8) except that the coefficients f, g, h have new values which we may denote as follows:

$$\begin{aligned} f_r&=-\tfrac{1}{2}\rho^2(\partial^2E/\partial\rho^2)_x-\tfrac{1}{2}x^2(\partial^2E/\partial x^2)_\rho(x'Q/xC),\\ g_r&=-\tfrac{1}{2}x(1-x)(\partial^2E/\partial x^2)_\rho(x'Q/xC)^2, \quad \text{(C13)}\\ h_r&=-(x(1-x))^{\frac{1}{2}}\rho(\partial^2E/\partial x\partial\rho)(x'Q/xC) -2x(x(1-x))^{\frac{1}{2}}(\partial^2E/\partial x^2)_\rho(x'Q/xC)^2, \end{aligned}$$

where it is to be noted the partial derivatives are now all fully relaxed ones.

For the general case intermediate between the above two limits we note first that it is necessary to employ the general expressions given in (21) instead of the limiting forms for the elastic coefficients. In addition to this however, it is necessary to choose the correct generalization of the two limiting expressions of the conservation equation, (C6) and (C12), respectively. From (15) and (20) it is immediately clear that the required generalization is simply

$$\Delta x/x=(\partial T_x/\partial T)_{\rho x}(x'Q/xC)\nabla\cdot(\bar{\eta}+\bar{\xi}), \quad \text{(C14)}$$

since this reduces to the correct expression at each limit, zero and full relaxation.

Using (C14) in place of (C6) or (C12), the Lagrangian retains the same form as before but now the coefficients f, g, h, must be replaced by the following expressions:

$$\begin{aligned} f^*&=-\tfrac{1}{2}\rho^2(\partial^2E/\partial\rho^2)^*-\tfrac{1}{2}x^2(\partial^2E/\partial x^2)^* \times(x'Q/xC)(\partial T_x/\partial T)_{\rho\sigma}{}^*,\\ g^*&=-\tfrac{1}{2}x(1-x)(\partial^2E/\partial x^2)^* \times(x'Q/xC)^2[(\partial T_x/\partial T)_{\rho\sigma}{}^*]^2, \quad \text{(C15)}\\ h^*&=-(x(1-x))^{\frac{1}{2}}\rho(\partial^2E/\partial x\partial\rho)^* \times(x'Q/xC)(\partial T_x/\partial T)_{\rho\sigma}{}^* -2x(x(1-x))^{\frac{1}{2}}(\partial^2E/\partial x^2)^* \times(x'Q/xC)^2[(\partial T_x/\partial T)_{\rho\sigma}{}^*]^2. \end{aligned}$$

In general, terms with the asterisk contain the operator A_2.

The cross terms, h^*, represent coupling between the two sounds, but can be formally eliminated by transforming to new coordinates:

$$\begin{aligned} \bar{Y}&=\bar{\eta}\cos\theta+\bar{\zeta}\sin\theta,\\ \bar{Z}&=\bar{\zeta}\cos\theta-\bar{\eta}\sin\theta, \end{aligned} \quad \text{(C16)}$$

where

$$\tan2\theta=h^*/(f^*-g^*).$$

The Lagrangian now becomes

$$L^*=\tfrac{1}{2}\langle\dot{Y}\rangle^2+\tfrac{1}{2}\langle\dot{Z}\rangle^2+F^*(\nabla\cdot\bar{Y})^2+G^*(\nabla\cdot\bar{Z})^2, \quad \text{(C17)}$$

where

$$F^*=f^*+h^{*2}/4f^*, \quad G^*=g^*-h^{*2}/4f^*. \quad \text{(C18)}$$

From a numerical point of view the differences between F^* and f^*, and G^* and g^*, are practically negligible, so that actually this coupling can be neglected.

The components of the two vectors $\bar{Y}$ and $\bar{Z}$ are six dependent variables, say Y_i and Z_i, $i=1, 2, 3$; and the four independent variables are the position coordinates and time, x_i, t. Write for the partial derivatives

$$Y_{ij}=\partial Y_i/\partial x_j, \quad Z_{ij}=\partial Z_i/\partial x_j; \quad \text{(C19)}$$

then the Lagrangian has the general form

$$L^*(x_i, t; Y_i, Z_i, Y_{ij}, Z_{ij}, \dot{Y}_i, \dot{Z}_i) \text{ per cm}^3. \quad \text{(C20)}$$

The dynamical law, in absence of dissipation, has the variational form

$$\delta\int\int\int\int L^*dx_1dx_2dx_3dt=0,$$

and the Euler equations solving this are simply

$$\begin{aligned}&\partial L^*/\partial Y_i-\textstyle\sum_j(\partial/\partial x_j)(\partial L^*/\partial Y_{ij})\\&\qquad-(d/dt)(\partial L^*/\partial\dot{Y}_i)=0 \text{ all } i,\\&\partial L^*/\partial Z_i-\textstyle\sum_j(\partial/\partial x_j)(\partial L^*/\partial Z_{ij})\\&\qquad-(d/dt)(\partial L^*/\partial\dot{Z}_i)=0 \text{ all } i.\end{aligned}\tag{C21}$$

If there is dissipation, the rate of loss of momentum appears on the right of these equations.

Following the ideas already introduced,[1] we shall now assume that there is a dissipation of relative momentum by relaxation interference between the opposing streams of superfluid and normal part. The relative momentum is $(\partial L^*/\partial Z_i)$, so that we may define the relaxation time as τ_1 where the loss of momentum occurs at the rate $(\partial L^*/\partial Z_i)/\tau_1$. This loss appears only in the equation for $\bar{Z}$, not in that for $\bar{Y}$, in (C21). Writing out this modified form of (C21), using (C17), we find the two wave equations:

$$\begin{aligned}&(\partial^2\bar{Y}/\partial t^2)+2F^*\nabla\nabla\cdot\bar{Y}=0,\\&(\partial^2\bar{Z}/\partial t^2)+2G^*\nabla\nabla\cdot\bar{Z}=-\langle\dot{Z}\rangle/\tau_1.\end{aligned}\tag{C22}$$

The first of these is the wave equation for ordinary sound, and includes dispersion and attenuation effects in the expression for F^*. The second equation is the propagation of second sound, including the relaxation term which is eventually responsible for the degeneration to diffusion.

Consider steady-state solutions $\bar{Y}$, $\bar{Z}$, depending on time only through the factor $\exp(2\pi i\nu t)$, then the operator $(1-A_2^{-1})$ contained in F^* and G^* becomes equivalent to multiplication by the complex factor

$$(1-A_2^{-1})=1-1/(1+2\pi i\nu\tau_2).\tag{C23}$$

This vanishes when $\tau_2\to 0$ in full relaxation, and becomes unity when $\tau_2\to\infty$ for zero relaxation.

Second Sound

Case 1: $2\pi\nu\tau_2\gg 1$

From (21) we have in this case

$$\begin{aligned}(\partial^2E/\partial x^2)^*\to&(\partial^2E/\partial x^2)_{\rho\sigma}\\&-[(\partial^2E/\partial x^2)_{\rho\sigma}-S/xx']/2\pi i\nu\tau_2\end{aligned}\tag{C24}$$

gives the partially relaxed coefficient in terms of the unrelaxed one. Also from (15) and (20) we have in this case

$$\begin{aligned}(\partial T_x/\partial T)_{\rho\sigma}^*\to&xC/x'Q\\&+(1-xC/x'Q)/2\pi i\nu\tau_2.\end{aligned}\tag{C25}$$

Now use (C24) and (C25) in (C15) and (A12), the result is

$$-2g^*=V_{s\infty}^2(1+1/2\pi i\nu\tau_3)^{-1},\tag{C26}$$

where $V_{s\infty}$ is given by (29) in the text, and where

$$\begin{aligned}1/\tau_3=(1/\tau_2)\{&3-2x'Q/xC\\&-S(1-x)/x'V_{s\infty}^2\}.\end{aligned}\tag{C27}$$

Evidently the velocity of propagation of second sound at infinite frequency is $V_{s\infty}$ as stated in the text. Dispersion effects can only be expected if the frequency is such that the relaxation time given in (C27) is small enough to compare with $1/2\pi\nu$.

Case 2: $2\pi\nu\tau_2\to 0$

Equation (21) now gives

$$(\partial^2E/\partial x^2)^*\to S/xx',\tag{C28}$$

and (20) gives, of course,

$$(\partial T_x/\partial T)^*\to 1.$$

Now (C15) yields immediately

$$-2g^*=x(1-x)(S/xx')(x'Q/xC)^2$$

so the wave equations becomes

$$(\partial^2\bar{Z}/\partial t^2)+\langle\dot{Z}\rangle/\tau_1=V_{s0}^2\nabla\nabla\cdot\bar{Z},\tag{C29}$$

where

$$V_{s0}^2=x'(1-x)SQ^2/x^2C^2.\tag{C30}$$

If now also $2\pi\nu\tau_1\to 0$, then $(\partial^2\bar{Z}/\partial t^2)\ll\langle\dot{Z}\rangle/\tau_1$ and (C29) reduces to the diffusion Eq. (30) as stated in the text.

Ordinary Sound

Neglecting terms of the order g^*/f^*, or V_s^2/V_n^2, we find for the velocity of propagation V_n of ordinary sound, from (C22) and (C15)

$$V_n^2=-2F^*=\rho^2(\partial^2E/\partial\rho^2)^*\tag{C31}$$

or from (21)

$$V_n^2=V_{n0}^2+K/(1+1/2\pi i\nu\tau_2),$$

where K is as given in the text, Eqs. (24) and (25).

Case 1: $2\pi\nu\tau_2 \gg 1$

Here

$$V_n^2 = V_{n0}^2 + K + iK/2\pi\nu\tau_2, \qquad \text{(C32)}$$

so that at infinite frequency

$$V_{n\infty}^2 = V_{n0}^2 + K. \qquad \text{(C33)}$$

The attenuation coefficient arising from (C32), and entering the solution of the wave equation in the form

$$\bar{Y} = \bar{Y}_0 e^{-\alpha x} \exp 2\pi i\nu(t - r/V_n),$$

where r is position, is

$$\alpha = K/2\tau_2 V_{n0}^3. \qquad \text{(C34)}$$

Case 2: $2\pi\nu\tau_2 \ll 1$

Here

$$V_n^2 = V_{n0}^2 + K \cdot 2\pi i\nu\tau_2, \qquad (35)$$

and at zero frequency

$$V_n^2 = V_{n0}^2, \qquad \text{(C36)}$$

while the attenuation coefficient for this frequency range is

$$\alpha = 2\pi^2\nu^2\tau_2 K/V_{n0}^3. \qquad \text{(C37)}$$

The peak attenuation occurs at the frequency given by

$$2\pi\nu\tau_2 = (V_{n0}^2/(V_{n0}^2 + K))^{\frac{1}{2}},$$

which is practically unity. The peak attenuation coefficient is then

$$\alpha_{\max} = \tfrac{1}{2}\pi\nu K/V_{n0}^3, \qquad \text{(C38)}$$

as stated in the text.

PHYSICAL REVIEW VOLUME 74, NUMBER 4 AUGUST 15, 1948

Relaxation Theory of Thermal Conduction in Helium II

LOTHAR MEYER AND WILLIAM BAND
Institute for the Study of Metals, The University of Chicago, Chicago, Illinois

(Received May 10, 1948)

The equation for thermal diffusion derived in the foregoing paper agrees with the relaxation equation for second sound used previously (see reference 3), if the second sound velocity is corrected to zero frequency. The relaxation time τ is calculated to a higher accuracy. The peculiar property of the heat current in being proportional to the cube root of the temperature gradient can be phenomenologically reduced to the relation

$$u_s^2\tau_s = J,$$

where u_s is the velocity of the superfluid balancing the mass flow of normal particles transporting the energy. τ_s is a relaxation time derived from τ, the relaxation time responsible for the damping of second sound, by the conditions for frequency balance. J appears to be a simple function of temperature only, approaching $h/m\pi$ at temperatures below 1°K. The equations lead to a qualitative understanding of the reduction of thermal conductivity by mass flow found by Kapitza.

IN the previous paper[1] it has been shown that the wave equation for second sound degenerates into a diffusion equation approaching zero frequency and becomes

$$\langle\dot{\bar{Z}}\rangle/\tau_1 = V_{s0}^2\nabla\nabla\cdot\bar{Z}\,;\quad V_{s0}^2 = x'(1-x)SQ^2/x^2C^2, \quad (1)$$

where x is the fraction of the liquid in the normal (excited) states, $\bar{Z}$ is the relative displacement vector of the normal fluid, τ_1 is the relaxation time for momentum exchanges between the two component streams. Take the divergence of this equation: assume very small amplitude and absence of ordinary sound, then we shall have, by (C6) of the previous paper,

$$\nabla\cdot\bar{Z} \propto \Delta x/x.$$

Thus:

$$(1/\tau_1)(\partial/\partial t)(\Delta x) = V_{s0}^2\nabla\nabla\cdot(\Delta x). \quad (2)$$

Here there is full relaxation so we have $\Delta x = x'\Delta T$,

[1] W. Band and L. Meyer, Phys. Rev. **74**, 386 (1948).

where $\Delta T = T - T_0$, T_0 being constant. Thus (2) can be written

$$(1/\tau_1)(\partial T/\partial t) = V_{s0}^2 \nabla^2 T. \quad (3)$$

If this is compared with the equation for conservation of heat flow,

$$\rho C(\partial T/\partial t) = -\nabla \cdot W.$$

W being the heat current density, Eq. (3) yields*

$$\nabla \cdot W = -\rho \tau_1 C V_{s0}^2 \nabla \cdot \nabla T, \quad (4)$$

or

$$W = -\rho \tau_1 C V_{s0}^2 \nabla T. \quad (5)$$

From the experimental fact[2] that a heat current W in helium II is proportional to the cube root of the temperature gradient

$$W \propto (\nabla T)^{\frac{1}{3}}, \quad (6)$$

Eq. (5) means that

$$\tau_1 \propto 1/W^2, \quad (7)$$

because τ_1 is the only quantity in (5) which can depend on W in order to fulfill (6). As the heat flow is due to the diffusion of the normal particles (velocity u_x) with a density ρ_x and energy content ϵ, we can also write[3]

$$W = \rho_x \epsilon u_x. \quad (8)$$

Under the assumption that the energy content of the normal particles is the heat content of helium II, we get

$$\rho_x \epsilon = \rho Q = \rho \int_0^T C dT.$$

This permits us to calculate u_x from measurements on W and C.

Using (8) in (7) we find

$$\tau_1 \propto 1/W^2 \propto 1/u_x^2,$$

or

$$\tau_1 u_x^2 = \text{constant for constant temperature.} \quad (9)$$

The relaxation time τ_1 in itself is due to two processes: transitions from the superfluid state into the normal state with a time τ_s and the inverse process with a time τ_x. As both processes contribute to the disturbance of the opposing streams, the total disturbance is obtained by adding the two frequencies:

$$1/\tau_1 = 1/\tau_s + 1/\tau_x. \quad (10)$$

In the steady state the number of particles passing from one state to the other must be

TABLE I.

T °K	W cal./cm² sec. at 10^{-3} deg./cm	u_x cm/sec.	$u_x\tau_x = u_s\tau_s$ 10^{-4} cm	V_{s0} m/sec.	J
1.0	0.0134	28.1			
1.1	0.0217	23.2	9.8	17.00	0.0099
1.2	0.0347	20.1	8.1	17.06	0.0125
1.3	0.0533	17.4	6.5	17.20	0.0148
1.4	0.0791	15.3	5.5	17.41	0.0183
1.5	0.112	13.5	4.8	17.52	0.0225
1.6	0.155	11.9	4.2	17.66	0.0270
1.7	0.210	10.6	4.0	17.72	0.0363
1.8	0.258	9.0	3.7	17.23	0.0447
1.9	0.285	7.0	3.3	16.00	0.0510
2.0	0.275	5.0	2.9	14.14	0.0546
2.05	—	—	—	12.65	—
2.10	0.196	2.6	2.3	10.95	0.0552
2.15	—	—	—	7.75	—
2.186	—	—	—	—	—

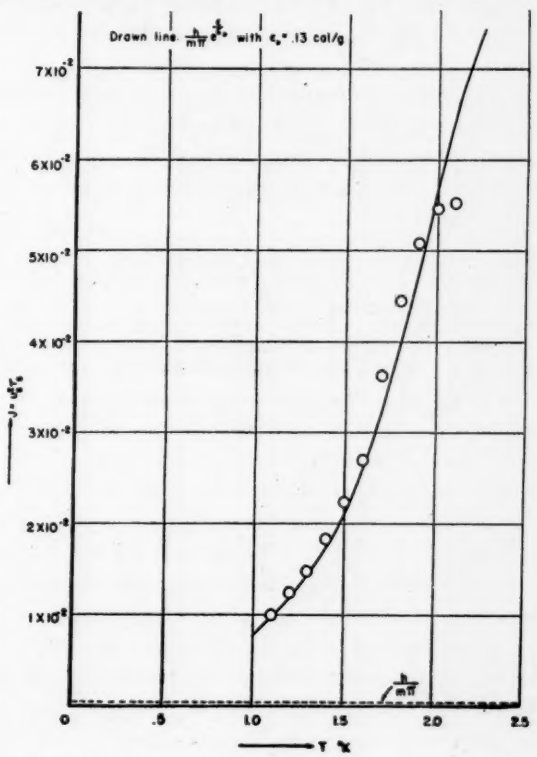

FIG. 1.

* If, as is later found to be the case, $1/\tau_1 \propto \dot{Z}^2$ or W^2, a factor 3 must be inserted on the left side of (2) on taking the divergence of (1). Similarly, a factor 3 must be inserted on the right side of (5) on integrating (4). These two factors cancel each other, so the result (5) is correct in any case.

[2] W. H. Keesom, B. F. Saris, and L. Meyer, Physica **7**, 870 (1940).

[3] W. Band and L. Meyer, Phys. Rev. **73**, 229 (1948).

equal in both directions:**

$$\rho_x/\tau_x=\rho_s/\tau_s. \tag{11}$$

The condition that the center of mass stays at rest is

$$\rho_x u_x+\rho_s u_s=0. \tag{12}$$

Equations (10)–(12) enable us to replace τ_1 and u_x in (8) by τ_s and u_s leading to

$$\tau_s u_s^2=J(T). \tag{13}$$

The evaluation of this function is given in Table I and Fig. 1.

The somewhat surprising result is that the values of $J(T)$ tend to approach $h/m\pi$ at temperatures below 1°K. However, as the velocities u_x and u_s in (12) are only drift velocities, this result cannot be related to the uncertainty principle, but must be considered as a transition probability relation. The whole $J(T)$ curve can be represented, purely empirically, by the equation

$$\tau_s u_s^2=(h/m\pi)\exp\epsilon/\epsilon_0, \tag{13a}$$

where ϵ is the energy per excited particle (see reference 1) and ϵ_0 is a constant having the value 0.13 cal./g; m is the mass of the helium atom.

Equation (13) leads also to a simple understanding of the peculiar behavior of the heat current observed by Kapitza[4] in the presence of mass flow. In this case Eq. (11) remains valid, but (12) must be replaced by

$$\rho_s u_s+\rho_x u_x=\rho u, \tag{12a}$$

where ρu is the net mass flow. Express u_s in terms of u_x and u by means of (12a) and use the result in (13), then because of (8) and the equation derived from (10) and (11), namely,

$$1/\tau_1=\rho/\rho_x\tau_s,$$

it is found that (13) is equivalent to

$$J/\tau_1=(\rho/\rho_x)\{(\rho u/\rho_s)^2+(\rho_x W/\rho_s\rho Q)^2 +2(\rho_x\rho/\rho_s^2)(uW/\rho Q)\}. \tag{13b}$$

Use this in (12a) in the form*

$$\tfrac{1}{3}\rho C V_{s0}^2 d\nabla T=(1/\tau_1)dW \tag{14}$$

and integrate the result; we obtain

$$K^3\nabla T=(\rho/\rho_x)^2(\rho Q u)^2 W +(\rho/\rho_x)(\rho Q u)W^2+W^3, \tag{15}$$

where K is the normal coefficient under zero mass flow.

It is clear from (15) that if ρQu is the same order of magnitude as W—as it was in the measurements reported by Kapitza—and if the temperature is low enough to make ρ_x/ρ considerably less than unity, there should be a great increase in thermal resistance due to the mass flow, qualitatively independent of the direction of u. At temperatures sufficiently near T_λ the effect should change sign with the direction of mass flow. For very large heat currents ($W\gg\rho Qu$) the effect should become very small. The conclusions are all in agreement with Kapitza's observations.

We hope to be able to discuss the meaning of Eq. (13) in a later paper. We want to thank Professor E. A. Long for valuable discussions.

** This equation is strictly true only at zero temperature gradient. If account is taken of the fact that the normal particles are moving towards lower temperature where their number is less, it is easy to calculate from (13) the departure from the cube root law at higher heat currents. It is found that significant increases in thermal resistance are to be expected if the temperature gradients are higher than 0.01°/cm.

[4] P. L. Kapitza, J. Phys. U.S.S.R. **5**, 58 (1941).

PHYSICAL REVIEW VOLUME 74, NUMBER 4 AUGUST 15, 1948

Resonances in $Li^7(p,n)Be^7$

G. BREIT AND I. BLOCH
Yale University, New Haven, Connecticut*

(Received May 3, 1948)

A qualitative and schematic discussion of the theory of the angular distribution of neutrons emitted in the reaction $Li^7(p,n)Be^7$ is presented. Evidence concerning existence of quasi-stationary states is discussed with the conclusion that there are indications of two such states, one at ~2.2-Mev incident proton energy and another below the reaction threshold. Both levels are probably of odd parity. The existence of the level below threshold is based on less direct evidence than that of the level at ~2.2 Mev. It is assumed that Be^7 is left either in its ground state or another state of the same parity.

I. INTRODUCTION AND NOTATION

IN this section the general reasons for considering the interpretation to be a likely one will first be outlined, and formulas for the angular distribution will also be derived. Considerations of orders of magnitude indicate that the reaction is caused to a considerable degree by the action of s protons. Since the interpretation makes use of a resonance to s protons, the additional reasons for considering them as playing an important part will now be mentioned. Comparison of the observed cross section[1] with those shown in Fig. 10 of Rumbaugh, Roberts, and Hafstad[2] shows that it is in the class of "probable" reactions in the terminology of Goldhaber.[3] An extrapolation of the curve for $Li^7(p,\alpha)He^4$ indicates in fact a cross section of only about 2×10^{-27} cm^2 at 1.86 Mev while the $Li^7(p,n)Be^7$ reaction shows a cross section of about 1.2×10^{-24} cm^2 at 2-Mev proton energy. The order of magnitude is the same as that of $Li^7(d,n)2He^4$, which is one of the most probable reactions of protons with Li. It is generally considered as likely that $Li^7(p,\alpha)He^4$ is caused by p protons and the classification of $Li^7(p,n)Be^7$ among the more probable $L=0$ reactions appears to be a natural one. The comparison made above is sensitive to the incident proton energy, E_p, because the cross section vanishes at the threshold of the reaction. A somewhat more quantitative argument will, therefore, be given. On the hypothesis of s waves for incident protons and ejected neutrons and of direct transitions produced by the deviation of the Hamiltonian from spherical symmetry one obtains the following approximate formula for the expected cross section

$$\sigma\cong E_n^{\frac{1}{2}}(2M)^{\frac{1}{2}}|H_{if}|^2/(2\pi v_p\hbar^4). \quad (1)$$

All symbols with the exception of the matrix element are explained in the section on notation at the end of this section. The matrix element H_{if} corresponds to wave functions asymptotic to plane waves of unit density for large internuclear distances. The quantity H_{if} will be interpreted as the result of integrating an unknown energy V through a sphere of radius $\hbar/[3(Mm)^{\frac{1}{2}}c]\cong3\times10^{-13}$ cm and the approximate value of $\sigma=0.24\times10^{-24}$ cm^2 will be fitted for the bombarding energy of 2 Mev. One finds by means of Eq. (1)

$$\sigma\cong2.5(E_n/E_p)^{\frac{1}{2}}(V/20mc^2)^2\times10^{-24}\text{ cm}^2, \quad (1')$$

and hence for $(8/7)E_p=2$ Mev, $(8/7)E_n=2-1.86=0.14$ Mev there follows $V\cong12\ mc^2$. This is a rather large energy for the volume assumed. If the proton and neutron were taken to be in states $L=1$, appreciable barrier penetration effects would enter and the interaction energy V would become unreasonably high. The estimates of effects of barrier penetrability will be made in two ways corresponding to the employment of the regular and irregular functions. Different results are obtained by the two methods, but both indicate that the $L=0$ reaction is the more likely. One way of making the estimate consists in taking the square of the ratio of the regular functions for the neutron in states $L=1$ and

* Assisted by Contract N6ori-44, Task Order XVI, of the Office of Naval Research.

[1] R. Taschek and A. Hemmendinger, Phys. Rev. **74**, 373 (1948).

[2] L. H. Rumbaugh, R. B. Roberts, and L. R. Hafstad, Phys. Rev. **54**, 657 (1938).

[3] M. Goldhaber, Proc. Camb. Phil. Soc. **30**, 561 (1934).

$L=0$ as a measure of relative probabilities of escape. For $E_n=0.35\ mc^2$ the value of kr is ~ 0.26 and the ratio of probabilities of neutron escape is estimated to be $(0.26/3)^2 \cong 1/130$. This should be combined with a factor for proton entry which also favors the $L=0$ process. In view of the relatively high proton energy barrier penetrability is not a simple matter of proton entry. It nevertheless appears safe to claim that the value of V would have to be at least 11 times greater for $L=1$ than for $L=0$, so that the unreasonably large $V\sim 130\ mc^2$ would be required. On the basis of the irregular function the ratio of probabilities of escape is $(0.26)^2=1/14$ and an interaction energy V of $\sim 46\ mc^2$ would be needed. If the assumptions appropriate to the applicability of the irregular function are more nearly applicable than those of the regular one, the possibility of a major part of the reaction occurring through the p waves is perhaps not excluded at $E_n=0.35\ mc^2$ but is nevertheless improbable because $45\ mc^2$ through a sphere of radius 3×10^{-13} cm is a questionably high value. The combined evidence makes it reasonable to attribute the main part of the reaction for $E_n\sim 0.2$ Mev to the ejection of s neutrons and the entry of s protons.

The experimentally observed angular distribution shows an appreciable component of the $B\cos\Theta$ type even at lower energies than have just been considered. It is natural to interpret the large asymmetry at low energies as an interference effect of s and p neutrons. The relatively large magnitude of the coefficient B is then explained as arising partly through the largeness of the s part of the neutron wave through a cross product between the s and p waves. The large slope of the graph of B as a function of the energy occurs at nearly the same energy as the maximum of A which corresponds to the spherically symmetric part of the angular distribution. This fact also fits in with the explanation of the variation in B being primarily due to an s wave resonance and arising as the result of a rapid variation of the phase of the s wave.

The statistical mixture of the initial states can be represented as

$$\psi_i=[R_0+R_1\Upsilon_1{}^0+\cdots][\Sigma_{\mu=-2}^{+2}\epsilon_\mu{}^{(2)}2_\mu + \Sigma_{\mu=-1}^{+1}\epsilon_\mu{}^{(1)}1_\mu] \quad (2)$$

in terms of symbols explained at the end of this section. The statistical factors ϵ are subject to rules of statistical averaging summarized by

$$\langle \epsilon_\lambda{}^{(i)*}\epsilon_\mu{}^{(j)}\rangle = \delta_{ij}\delta_{\lambda\mu}/8, \quad (2.1)$$

which correspond to a unit probability for the incident state. Independent of any detailed hypothesis concerning the mechanism of the reaction one can be sure that any R_02_μ in the incident wave cannot give rise to $R'_01'_{\mu'}$ or to $R'_02'_{\mu'}$ for $\mu'\neq\mu$ but can be responsible for the appearance of $R'_02'_\mu$ in the neutron wave. Similarly, the state R_01_μ cannot give rise to $R'_02'_{\mu'}$ or to $R'_01'_{\mu'}$ for $\mu'\neq\mu$ but can give $R'_01'_\mu$. It is also a general consequence of conservation of angular momentum that the states $R'_02'_\mu$ arising from any R_02_μ have the same coefficient, which is besides independent of μ, and that the states $R'_01'_\mu$ arise from the R_01_μ with an amplitude which is independent of μ, provided the states 1_μ, $1'_\mu$ are defined in the same convention, i.e., provided they transform similarly under rotations. It does not follow, however, either from conservation of angular momentum or other general relations that the states $R'_01'_\mu$ arise from the R_01_μ with the same strength as the $R'_02'_\mu$ arise from the R_02_μ.

Inasmuch as the appearance of the experimental results suggests resonance involving s neutrons, it is natural to suppose that a state of the compound nucleus having total angular momentum with either the value 1 or 2 is involved, and that there is an inequality in the strengths of the transitions leading to the states $R'_01'_\mu$, $R'_02'_\mu$ which have just been discussed. It is not clear from the experimental results on angular distributions that there is a decided preference for attributing an angular momentum of either 1 or 2 to the resonances. The calculations will be made, therefore, without specialization in this particular.

The peak in the coefficient A is an indication that one deals with an s resonance, and the anomalous dispersion-like shape of the curve for the coefficient B suggests that the rapid change of the phase of the s wave with energy is being brought into evidence in the experiments through interference with neutron p waves. The coefficient C can have to do partly with quadratic effects of the p waves or with linear effects of d

waves. A theoretical understanding of the behavior of C is clearly more complicated and less certain than that of A and B. It involves an understanding of the variations of amplitudes of the p and d waves which, on account of the nuclear spins, involve states with various values of total angular momenta. No attempt is made, therefore, to understand the variation of C with energy in a really quantitative manner. The number of available parameters is great enough to make a precise fit to the experiments of little value.

Disregarding temporarily the complexities resulting from the many factors which enter into the variation of C with energy, there are still the following inherent uncertainties of present theories which make a truly quantitative understanding of the coefficients A, B somewhat difficult.

(a) Even the variation of the coefficient A with energy cannot be simply specified by a formula of the dispersion type unless one either calculates the many body problem involved or else has assurance through empirical evidence that one is dealing with a single level resonance case.

On account of the difficulty of ascertaining the actual situation it will be assumed that the variation of the resonant s wave with energy is of the single level with background type.[4]

(b) The p waves enter through the coefficient B. Their variation with energy is hard to predict. It will be assumed below that the variation of the p waves with energy is not important within the range of energies covered by experiment and that the main variations of B with energy result from the presence of cross product terms with the s wave.

(c) Higher levels of even parity giving rise to transitions to neutron p waves have unknown locations. These are influential in determining the p wave background which interferes with the resonant s state.

The many inherent uncertainties of the problem make it desirable to discuss below the way in which the interpretation lacks definiteness rather than try to arrive at a best fit to experiment. The calculations are carried out only schematically in certain respects as will be seen in the next section. The notation used is summarized below.

[4] G. Breit and E. Wigner, Phys. Rev. **49**, 519 (1936); H. A. Bethe and G. Placzek, *ibid.* **51**, 450 (1937); G. Breit, *ibid.* **58**, 506 (1940); *ibid.*, 1068; *ibid.* **69**, 472 (1946); E. P. Wigner, *ibid.* **70**, 15 (1946); *ibid.* 606; E. P. Wigner and L. Eisenbud, *ibid.* **72**, 29 (1947).

NOTATION

R_L = radial function for relative motion of Li^7 and H^1 with orbital angular momentum $L\hbar$.

Υ_L^M = angular function for relative motion of Li^7 and H^1 with orbital angular momentum $L\hbar$ and projection $M\hbar$ on line of relative motion of H^1 with respect to Li^7. The angular function is normalized to give unity for integration over angles.

2_μ, 1_μ = spin functions of compounded spin of Li^7 and H^1 corresponding, respectively, to resultants $2\hbar$, $\hbar$, and to projections $\mu\hbar$ on line of flight. They are linear combinations of products of spin functions for the incident proton and spin functions for the ground state of Li^7. The latter are solutions of the complete wave equation for the relative motion and spins; it is taken for the ground state.

$\epsilon_\mu^{(2)}$, $\epsilon_\mu^{(1)}$ = statistical factors describing the statistical mixture of spin states 2_μ, 1_μ. The orthogonality conditions for products of these factors and their complex conjugates are stated as Eq. (2.1).

R_L', Υ'^M_L, $2_\mu'$, $1_\mu'$ are defined for Be^7 and n^1 in the same way as corresponding unprimed quantities have been defined for Li^7 and H^1.

E_p = energy of relative motion of Li^7 and H^1.

E_n = energy of relative motion of Be^7 and n^1.

E_0 = resonance energy; $E=E_p-E_0$.

v_p = relative velocity initially.

v_n = relative velocity finally.

m = electronic mass.

r = internuclear distance.

λ = wave-length of relative motion.

$k=2\pi/\lambda$.

θ = angle between line from the center of mass to proton and the line of flight.

Θ = angle between line from center of mass to neutron and the line of flight.

A, B, C = coefficients in formula $A+B\cos\Theta+C(3\cos^2\Theta-1)/2$ for the cross section per unit solid angle in the center of mass system.[5]

ψ_i = wave function of initial state (Li^7+p).

ψ_f = wave function of final state (Be^7+n).

M = mass of proton or neutron.

H = Hamiltonian function of the 8 particles.

II. CALCULATIONS

The Li^7 nucleus will be treated schematically as containing only one neutron which matters for the reaction. This neutron will be supposed to be in a central field, and the other particles of Li^7 are supposed to be in closed shells and not to

[5] A, B, C, are equivalent, respectively, to the quantities a_0, a_1, and a_2 in Eq. (16) of reference 1.

influence the p wave background. Similarly, in Be^7 only one proton is supposed to matter. The orbital p wave functions of the internal neutron in Li^7 are denoted by

$$b_m \quad (m=1, 0, -1),$$

while the p wave orbital functions of the proton incident on Li^7 are designated by

$$A_m.$$

The motion of the center of mass is not explicitly considered. Similarly, the proton wave functions in Be^7 are denoted by

$$a_m$$

and the p wave functions of the emerging neutron by

$$B_m.$$

The magnetic quantum number m is defined here with respect to the line of flight, and among the A_m only the function A_0 enters the expressions for the incident wave. In order to simplify the considerations it will be supposed that for the purpose of discussing transitions of the p states it will suffice to consider only the part of the forces of the ordinary and Majorana type, neglecting the spin dependence of nuclear forces and spin-orbit interactions as well. The incident wave and the Li^7 nucleus can be considered to form states of definite orbital angular momentum $L=0$, 1, 2. Transitions from this state to an intermediate state Q of the compound nucleus can take place only if the orbital angular momentum of Q is also L, because of the simplifying assumption concerning dominance of the part of the potential involving coordinates alone. The state Q can disintegrate into states of the Be^7+n system which also have orbital angular momentum L. Since spin dependence of nuclear forces was assumed to have a negligible effect on the p wave, no distinction is made between singlets and triplets in this part of the calculation. The presence of energy differences in the denominators of formulas for the amplitudes of final states brings the position of the states of the compound nucleus into the final result, and the number of adjustable parameters is greatly increased since the positions of the levels are unknown. In the interests of simplicity only two cases will be considered, each of which is admittedly extreme in its assumptions. The first (case I) is that in which the S, P, D states of Q belonging to the same configuration fall in very closely spaced multiplets. The second (case II) corresponds to the idealization of having the P states so far above the S and D states of the same configuration that their presence can be neglected. The S and D states in case II are supposed to fall close together. Case II is intended to represent a condition which is emphasized by Majorana forces. The incident states of definite orbital angular momentum L with magnetic quantum number M are contained among the nine functions

$$X^L{}_M=\Sigma_\mu C^L{}_{\mu,\,M-\mu}A_\mu b_{M-\mu}, \tag{3}$$

where the $C^L{}_{\mu,\,M-\mu}$ are appropriate coefficients for the composition of angular momenta. Similarly, the emerging states are contained among the nine functions

$$Y^L{}_M=\Sigma_\mu C^L{}_{\mu,\,M-\mu}B_\mu a_{M-\mu}. \tag{3.1}$$

The function A_0 is the term $R_1\Upsilon_1{}^0$ in Eq. (2). From Eq. (3) one obtains the relation

$$A_0 b_M=\Sigma_L C^L{}_{0,\,M}X^L{}_M \tag{3.2}$$

by means of which the incident wave can be expressed in terms of the compounded orbital angular momentum functions $X^L{}_M$. By conservation of angular momentum every $X^L{}_M$ gives rise only to a $Y^L{}_M$ with the same L and M. The coefficients with which the $Y^L{}_M$ arise for the same L but different M can also be shown to be the same. On the other hand, the coefficients depend in general on L.

The transitions are pictured as occurring through the intermediate stage of forming a compound nucleus in states $Q^L{}_M$ which in turn give rise to final states $Y^L{}_M$. The matrix elements of the Hamiltonian giving transitions through the $Q^L{}_M$ of a multiplet depend, in general, on the multiplet and on L. Taking into account all of these dependences is somewhat complicated in the general case, and the calculations have been made in the simplified way of neglecting the variations with L except for the omission of the effect of $L=1$ for case II.

One has then as a result of the collision

$$A_0 b_M \rightarrow P\Sigma_L C^L{}_{0,\,M}Y^L{}_M, \tag{3.3}$$

where P is a number independent of L and where terms for $L=1$ are omitted for case II. For case I one finds simply

$$A_0 b_M \rightarrow P a_0 B_M. \tag{3.4}$$

This is a consequence of the fact that the conditions for case I can be obtained by dealing with degenerate intermediate states so that the calculation could be performed by decoupling the proton and neutron in the intermediate state. For case II one obtains instead of Eq. (3.4)

$$\begin{aligned} A_0 b_1 &\rightarrow P(a_0 B_1 + a_1 B_0)/2, \\ A_0 b_0 &\rightarrow P a_0 B_0, \\ A_0 b_{-1} &\rightarrow P(a_0 B_{-1} + a_{-1} B_0)/2. \end{aligned} \tag{3.5}$$

The wave function of Li^7 with magnetic quantum number M will be denoted by Li_M and is

$$Li_M = \Sigma_\mu C^{1}_{\mu, M-\mu} \nu_\mu b_{M-\mu}, \tag{3.6}$$

where ν_μ is the spin function of the neutron with projection μ. Similarly, the wave function of Be^7 in its state with total angular momentum $\frac{3}{2}$ will be written as Be_M and is

$$Be_M = \Sigma_\mu C^{\frac{3}{2}}_{\mu, M-\mu} \pi_\mu a_{M-\mu}, \tag{3.7}$$

where π_μ is the spin function of the proton with magnetic quantum number μ. While, energetically, transitions to the excited state of Be^7 are possible, they do not occur with a large enough probability to be observed and they will be, therefore, left out of account. For this reason in Eq. (3.7) only states with spin $i=\frac{3}{2}$ are considered for Be^7. The statistical wave function representing the incident state contains a term

$$\omega_M{}^\mu A_0 \pi_\mu Li_M, \tag{3.8}$$

where $\omega_M{}^\mu$ is a statistical factor analogous to $\epsilon_\lambda{}^{(i)}$ of Eq. (2) but corresponding to the strong field condition of proton and Li.

Substitution of Li_M by means of Eq. (3.6) gives then an expression involving proton and neutron spin functions as well as internal neutron functions b. By means of Eq. (3.3) one obtains the function for the emerging neutron wave which contains internal proton functions a, neutron orbital functions B, as well as the proton and neutron spin functions. According to Eq. (3.7) the scalar product of any $\pi_\mu a_{M-\mu}$ with Be_M is $C^{1}_{\mu, M-\mu}$, and the amplitude of the part of the wave function containing Be_M as a factor is, therefore, $C^{1}_{\mu, M-\mu}$ to within a factor independent of M. The contributions to the coefficients of the

$$\omega_M{}^\mu Be_{M'} \tag{3.9}$$

containing p waves B_1, B_0, B_{-1} have been obtained in the manner just described. To these contributions there have been added the s waves which arise partly through the supposed resonance.

The contributions to the statistical wave function containing neutron s waves are supposed here to arise as follows. The spins of the incident proton and the Li^7 nucleus compound themselves so as to form states of angular momenta 2 and 1:

$$d^J{}_M = \Sigma_\mu c^J{}_{\mu, M-\mu} \pi_\mu Li_{M-\mu} \quad (J=1, 2) \tag{4}$$

and, similarly, the spins of the emerging neutron and of Be^7 give states

$$e^J{}_M = \Sigma_\mu c^J{}_{\mu, M-\mu} \nu_\mu Be_{M-\mu} \quad (J=1, 2). \tag{4.1}$$

The functions $d^J{}_M$, $e^J{}_M$ have already occurred in Eq. (2) in another notation. The two notations are related by

$$\begin{aligned} d^J{}_M &= 2_M, \ J=2; \quad e^J{}_M = 2'_M, \ J=2; \\ d^J{}_M &= 1_M, \ J=1; \quad e^J{}_M = 1'_M, \ J=1. \end{aligned} \tag{4.1'}$$

By means of Eq. (4) the part of the incident statistical wave function with assigned projections of spins of proton and of Li^7 can be expressed as

$$\omega_M{}^\mu \pi_\mu Li_M = \omega_M{}^\mu \Sigma_J c^J{}_{\mu, M} d^J{}_{M+\mu}. \tag{4.2}$$

The state $d^J{}_M$ can give rise to $e^J{}_M$. Since J and M are, respectively, the total angular momentum and its projection, the matrix elements for the transitions are independent of M. They can depend on J, however. The emerging s states arise, therefore, according to the scheme

$$\omega_M{}^\mu \pi_\mu Li_M \rightarrow \omega_M{}^\mu \Sigma_J c^J{}_{\mu, M} S_J e^J{}_{M+\mu}, \tag{4.3}$$

where the S_J depend only on the energy and on J. By means of Eq. (4.1) the emerging wave which is represented by the right side of Eq. (4.3) can be expressed in terms of some coefficients multiplying the expression $\omega_M{}^\mu Be_{M'}$. Combining these contributions with those which arose in the consideration of p waves in connection with Eq. (3.9), one obtains the whole statistical wave function ordered according to spin orientations

of Be^7 and of the emerging neutron. Adding the intensities of the waves for each of these terms and remembering that states with different final spin orientations do not interfere with each other,[6] one finds that

$$I_{\mathrm{I}}=\frac{5}{8}|S_2|^2+\frac{3}{8}|S_1|^2+\frac{5}{24}(B_0^*S_2+B_0S_2^*)$$
$$-\frac{1}{24}(B_0^*S_1+B_0S_1^*)$$
$$+\frac{2}{9}(|B_1|^2+|B_0|^2+|B_{-1}|^2), \quad (5)$$

$$I_{\mathrm{II}}=\frac{5}{8}|S_2|^2+\frac{3}{8}|S_1|^2+\frac{5}{12}(S_2B_0^*+S_2^*B_0)$$
$$-\frac{1}{12}(S_1B_0^*+S_1^*B_0)$$
$$+\frac{1}{3}|B_0|^2+\frac{1}{18}(|B_1|^2+|B_{-1}|^2), \quad (5.1)$$

where the intensities for cases I and II are distinguished by corresponding subscripts. The factor P has been set equal to unity since no attempt has been made to calculate its magnitude. In Eq. (5) (case I) the quadratic terms in the p waves combine to give a spherically symmetric combination. In Eq. (5.1), however, there is left over a quadratic term which can be confused with a d wave. Changing the scale of the p waves in Eq. (5), one obtains

$$I_{\mathrm{I}}=\frac{5}{8}|S_2|^2+\frac{3}{8}|S_1|^2+\frac{5}{12}(B_0'^*S_2+B_0'S_2^*)$$
$$-\frac{1}{12}(B_0'^*S_1+B_0'S_1^*)$$
$$+\frac{8}{9}(|B_1'|^2+|B_0'|^2+|B_{-1}'|^2), \quad (5.2)$$

which is identical in form with Eq. (5.1) except for the quadratic terms in the p waves.

Besides the effect of the s and p waves there is probably also an effect of d waves produced partly as the result of the incident s and d waves. No attempt will be made here to treat the d wave for emerging neutrons quantitatively. It differs appreciably between cases I and II and the uncertainties in the determination of s and p wave parameters are so large that one may consider the experimental value of the coefficient of $P_2(\cos\Theta)$ to be reasonable.

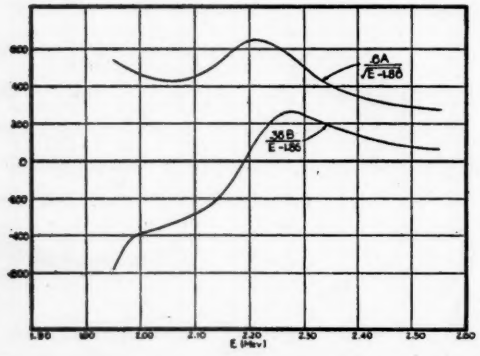

FIG. 1. Experimental angular dependence of neutron intensity plotted against proton energy and corrected for part of the expected effect of neutron velocity (see the beginning of Section III of the text). A and B are determined by the observed neutron intensity

$$I(\Theta)=AP_0(\cos\Theta)+BP_1(\cos\Theta)+CP_2(\cos\Theta).$$

[6] Reference 1 contains a determination of the amplitudes and phase difference of neutron s and p waves which would give the observed neutron intensity in the absence of spin effects.

III. DISCUSSION AND CONCLUSIONS

It is impractical to try to predict purely theoretically the energy dependence of all the parameters that enter the resonance theory of nuclear reactions. Since the reaction studied here has a threshold close to the region within which the data lie, it would be wrong to omit the more obvious parts of the dependence on the neutron velocity. The emerging s wave is expected to have an intensity proportional to the neutron velocity v_n, the p wave to v_n^3, and the cross product terms between s and p waves to v_n^2. Besides there should be other dependences contained in the usual Γ_n of the denominators of dispersion formulas. Neglecting these, the correction for neutron velocity can be made by dividing the experimental A, B, respectively, by $(E-1.86)^{\frac{1}{2}}$, $E-1.86$. The result of doing so is shown in Fig. 1 in which the quantities

$$A'=0.6A(E-1.86)^{-\frac{1}{2}}, \quad B'=0.36B/(E-1.86)$$

are plotted against E. The values of A and B used here are nearly but not precisely equal to

the values of a_0 and a_1, given by the more systematic analysis of Reines.[1]

It is seen that both A' and B' show a strong variation with energy at $E=1.86$ Mev, suggesting that there might be a resonance below the threshold in addition to the pronounced resonance at about 2.2 Mev. The increase in B' towards the threshold is then explicable as being a consequence of the increase in A' in the same region.

In Fig. 2 there are plotted for comparison graphs of $a+qb$ with

$$a=1/(1+x^2), \quad b=x/(1+x^2).$$

For a simple one-level resonance with background one expects the quantities A', B' to vary with energy approximately as $a+qb$. The quantity

$$x=(E-E_0)/\Gamma,$$

where E_0 is the resonance energy and 2Γ is the half-value breadth. In making the comparison the following considerations enter:

(a) If either S_2 or S_1 is represented by single level resonance with background, i.e., if it is of the form

$$[\alpha/(E-E_0+i\Gamma)]+\beta,$$

then only the part of the right side of Eqs. (5.1), (5.2) containing $|S_2|^2$ or $|S_1|^2$ contains α and β. There is besides, however, an additional background of an additive character in the expected variation of the coefficient A with energy. The comparison of Figs. 1 and 2 has to be made, therefore, by suitably translating the figures up and down before superposing them.

(b) The quantity Γ can be expected to vary with energy. For energies slightly above threshold the variation with energy of the part of Γ having to do with neutron escape is expected to be given by a simple proportionality to v_n. This, however, is the only simple obvious dependence, and deviations from the simple formula can be expected.

(c) The coefficient B' is also expected to be representable only in part by graphs of the type drawn in Fig. 2. The presence of cross product terms involving both S_2, S_1 brings in an additive background term here as well.

(d) In view of the fact that the phases of S_2, S_1, B_0 occurring in Eqs. (5.1), (5.2) have no special relation to each other the coefficient q of $a+qb$ which depends on these phases has to be inferred from experiment.

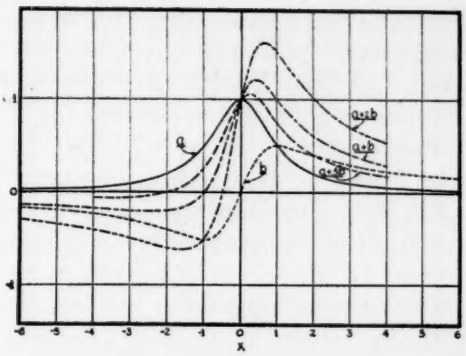

FIG. 2. Approximate energy dependence of the quantities A' and B' of Section III (plotted as ordinates in Fig. 1) to be expected in the case of a one-level resonance with background. Here $a=1/(1+x^2)$ and $b=x/(1+x^2)$; for comparison of these curves with those of Fig. 1, x is to be taken as $(E-E_0)/\Gamma$, where E_0 is the resonance energy and 2Γ is the half-value breadth.

(e) The resonance level does not, in general, lie[4] at a maximum of either A or B.

(a) Comparison of Figs. 1 and 2 shows that: (a) Experiment is not in agreement with the simple one level with background theory. This is especially true for the marked variations in both A' and B' close to the threshold. It is believed, on the other hand, that the region close to threshold is subject to especially large experimental uncertainties.

(b) For 2.20 Mev$<E<$2.60 Mev there is a marked similarity of the curves of Fig. 2 with those of Fig. 1. The behavior of A' suggests a value of q close to zero. The behavior of B' speaks for $1/q$ close to zero. Such values of q would be obtained if β were small and if there were no phase difference between α and B_0.

(c) If the assignment of q considered in (b) above should be the right one, then subtraction from B' of a negative contribution to the left of the node and representing b of Fig. 2 leaves a part which is appreciable only above the threshold and fits in qualitatively with the increase of A' close to the threshold.

(d) The parts of A', B' to the right of the node of B' fit in reasonably well with the expected variations of a and b. Thus, for example, the maximum of b falls at $x=1$, which should be also

the point at which a has a value equal to one-half of its maximum value. The maximum of B' falls at about 2.28 Mev. Taking the value of A' at 2.60 Mev as an approximate base line for A', the half-value point of A' falls at $\sim$2.32 Mev, which may be looked at as agreeing reasonably well with 2.28 Mev, since there are so many uncertain factors in the adjustment of the curves to each other.

The tentative interpretation just discussed is defective in reproducing the exact shape of the right side of curve b of Fig. 2. Thus, e.g., the value of b for $x=2$ is 0.8 of its value at the maximum which falls at $x=1$. On the other hand, the value of B' at $2.19+2(2.88-2.19)=2.37$ Mev is $165/250=0.66$ of the value at the maximum. The quantity B' is thus seen to decrease relatively somewhat faster beyond the maximum than b. The fit could be improved in a number of ways. Thus, for example, one can leave the zero line of B' undisplaced but fit the curve for B' to the right of its node by a curve of type $a+qb$, with a finite positive q, to the right of the node of B'. For $q=1$ the distance from the node to the maximum is 1.4, the point distant from the node by twice this amount is at $x=1.8$, and the ratio of $a+b$ at $x=1.8$ to its maximum value is $0.66/1.21=0.55$, which is less than the corresponding number for the curve b. For $q=2$ this number is 0.63, which is close to the experimental value. The fit can also be improved by displacing the zero line of B' and various combinations of the two ways can be used.

It is clear that the presence of several adjustable parameters in Eqs. (5.1), (5.2) would make a fit by one or another type of curve very questionable. This situation is further aggravated by the presence of unknown variations in the backgrounds. In addition, the cross product terms which matter for B are affected by both the phase and the amplitude of the nonresonant s wave.

(e) It is believed in view of the arguments just presented that the experimental material contains evidence of the presence of a quasi-stationary level at an energy corresponding to $\sim$2.2-Mev incident proton energy and that the half-value breadth $2\Gamma\sim200$ kev. It is also believed that there is an indication of another level which is stable towards dissociation into Be^7+n but unstable towards disintegration into Li^7+p. The behavior of the angular distribution coefficients A, B suggests that in both cases there is resonance to s protons and it is probable, therefore, that the compound nucleus is in an odd state for both of them.

(f) It was assumed throughout that Be^7 is left in its ground state after neutron emission. A reason for this assumption is the apparent absence of a second group of neutrons which would be expected to appear if Be^7 were left in an excited state analogous to the 450-kev level of Li^7. It should be pointed out, however, that this assumption is based on incomplete evidence. It is difficult to exclude the possibility of a weak neutron component of smaller energy which might be setting in $\sim8\times450/7=514$ kev above threshold and would confuse the interpretation. On the other hand, there is no special evidence in the curves of Fig. 1 for supposing that such a neutron group begins to appear at $\sim1.86+0.51=2.37$ Mev. Both A' and B' decrease smoothly in this region.

It is more difficult to deal with the possibility of an excited level of Be^7 at a quite low energy taking part in the process. If it did, the parity of the level might even be different. On the other hand, it is somewhat improbable that there should be a level of a different parity so close to the ground level of Be^7.

Angular Distribution of Alphas from $Li^6(d,\alpha)\alpha$ and $Li^7(p,\alpha)\alpha$

N. P. HEYDENBURG, C. M. HUDSON,* D. R. INGLIS,** AND W. D. WHITEHEAD, JR.***
Carnegie Institution of Washington, Department of Terrestrial Magnetism, Washington, D. C.

(Received May 10, 1948)

The intensity of the reaction $Li^6(d,\alpha)\alpha$ is observed to vary with angle as $1+A(E)\cos^2\theta+B(E)\cos^4\theta$, as expected from the Bose statistics of the product alphas, with $A(E)$ rising gradually beginning just below 1 Mev to a broad maximum a little below unity at a bombarding energy E in the neighborhood of 2 Mev. The coefficient $B(E)$ remains zero up to almost 1.5 Mev and rises to a positive value of about 0.35 at higher energies. The yield curve observed at right angles to the beam displays a sharp maximum at 0.75 Mev and there is evidence of approach to another peak at or just beyond the highest bombarding energy employed, 3.75 Mev. The substitution of a proportional counter for the ionization chamber used in earlier work has made possible improvement over our earlier observations of the angular distribution of the reaction $Li^7(p,\alpha)\alpha$ in the neighborhood of 3 Mev, where difficulty was experienced in the discrimination against pile-up of scattered protons, and the new results show a node in the curve for $A(E)$ at 2.7 Mev. A peak in the yield curve of this reaction is found at 3 Mev, which is about 3 Mev lower in the compound nucleus Be^8 than the lower peak observed in the reaction $Li^6(d,\alpha)\alpha$. There is great similarity in the trends of the angular distributions of the two reactions, but their coefficients $B(E)$ have opposite signs in the energy regions investigated, and both $A(E)$ and $B(E)$ rise from zero more gradually in $Li^6(d,\alpha)\alpha$ than in $Li^7(p,\alpha)\alpha$ as the bombarding energy increases from low values.

I. INTRODUCTION

BECAUSE the pair of alphas resulting from the reaction $Li^6(d,\alpha)\alpha$ and from the reaction $Li^7(p,\alpha)\alpha$ obey Bose statistics, their angular distribution is observed to display fore-and-aft symmetry, and it may be expanded in even powers of the cosine of the angle of deflection θ in the center-of-mass coordinate system:

$$Y(\theta)=Y(90°)(1+A\cos^2\theta+B\cos^4\theta+\cdots).$$

The simplest theoretical discussion[1] of the Li^7 reaction, which considers only entering protons with the lowest possible angular momentum, accounts for the existence of a term in $\cos^2\theta$ but no higher terms. A more nearly complete theory,[2] treating also the entering protons in $Li^7(p,\alpha)\alpha$ or deuterons in $Li^6(d,\alpha)\alpha$ of somewhat higher angular momentum, accounts also for the term in $\cos^4\theta$. The angular distribution of the reaction $Li^6(d,\alpha)\alpha$ has been previously observed[3] only at 0.2 Mev and it was shown to be spherically symmetrical at this low bombarding energy. The $Li^7(p,\alpha)\alpha$ reaction has been observed in several laboratories,[4-7] with results not completely in accord in detail but consistently indicating a rapid rise of the coefficient $A(E)$ from zero at a small bombarding energy to a maximum near 1 Mev and a subsequent gradual decline. The most recent of those papers, which was by the present authors, disclosed the existence of a term in $\cos^4\theta$ having a coefficient $B(E)$ of order of magnitude $-\frac{1}{2}$ in most of the energy range from 1 to 3 Mev. That paper also showed that $A(E)$ falls off apparently toward zero just beyond the range of observation. In that work, the observations at the highest energies were rendered more uncertain than the rest because the range of the scattered protons is there about the same as that of the alphas, at least at some angle, and the scattered protons were so numerous that the possibility of their piling up to make pulses as large as the alphas was not completely eliminated. In view of the similarity and the relative simplicity of these two reactions, it seemed desirable to investigate the $Li^6(d,\alpha)\alpha$ at least as completely as the other reaction has been, and in the course of this work a rather definite improvement in

* Office of the Chief of Ordnance, War Department, Washington, D. C.
** Johns Hopkins University, Baltimore, Maryland.
*** Carnegie Institution Fellow.

[1] C. L. Critchfield and E. Teller, Phys. Rev. **65**, 10 (1941).
[2] D. R. Inglis, Phys. Rev. **74**, July 1 (1948).
[3] R. O. Haxby, J. S. Allen, and J. H. Williams, Phys. Rev. **55**, 140 (1939).
[4] V. S. Young, A. Ellett, and G. J. Plain, Phys. Rev. **58**, 498 (1940).
[5] C. D. Swartz, H. H. Rossi, B. Jennings, and D. R. Inglis, Phys. Rev. **65**, 80 (1944).
[6] S. Rubin, W. A. Fowler, and C. C. Lauritsen, Phys. Rev. **71**, 212 (1947).
[7] N. P. Heydenburg, C. M. Hudson, D. R. Inglis, and W. D. Whitehead, Jr., Phys. Rev. **73**, 241 (1948).

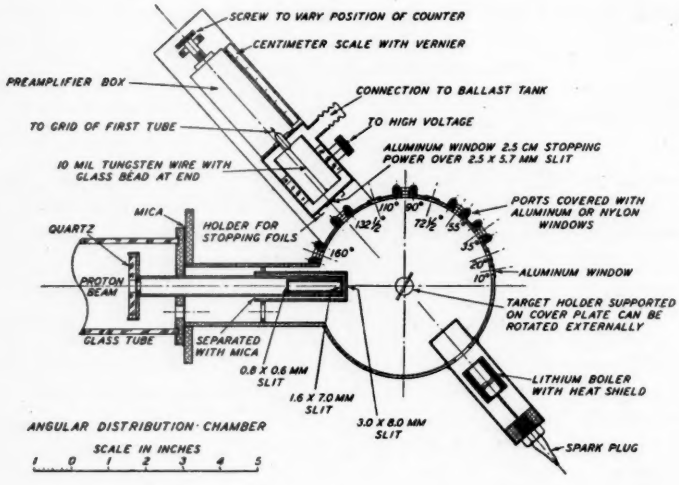
SCREW TO VARY POSITION OF COUNTER
CENTIMETER SCALE WITH VERNIER
PREAMPLIFIER BOX
CONNECTION TO BALLAST TANK
TO GRID OF FIRST TUBE
TO HIGH VOLTAGE
ALUMINUM WINDOW 2.5 CM STOPPING POWER OVER 2.5 X 5.7 MM SLIT
10 MIL TUNGSTEN WIRE WITH GLASS BEAD AT END
PORTS COVERED WITH ALUMINUM OR NYLON WINDOWS
MICA
QUARTZ
HOLDER FOR STOPPING FOILS
ALUMINUM WINDOW
PROTON BEAM
TARGET HOLDER SUPPORTED ON COVER PLATE CAN BE ROTATED EXTERNALLY
GLASS TUBE
SEPARATED WITH MICA
0.8 X 0.8 MM SLIT
1.6 X 7.0 MM SLIT
3.0 X 8.0 MM SLIT
LITHIUM BOILER WITH HEAT SHIELD
ANGULAR DISTRIBUTION CHAMBER
SCALE IN INCHES
SPARK PLUG

FIG. 1. Target chamber.

experimental technique was introduced which has made it possible to repeat with increased accuracy some of our earlier observations on $Li^7(p,\alpha)\alpha$ in the high energy range.

II. APPARATUS AND TECHNIQUE

The present series of observations were made entirely with the large pressurized statitron, and most of the technique employed was closely similar to that described in our earlier papers.[7,8] The only essential change was the substitution of a proportional counter for the shallow ionization chamber used in the earlier work. The pulses obtained from the proportional counter are of much shorter duration than those from the ionization chamber, so the probability of pile-up of the smaller proton pulses was greatly reduced.

The proportional counter is of rather conventional design, with a collecting electrode consisting of a 10 mil (0.025 cm) tungsten wire 2.5 cm long, supported from one end by a Kovar-seal insulator and protected at the other end by a small glass bead. A potential of 750 volts is applied to an insulated cylinder surrounding this, 2.5 cm in inside diameter and about 3 cm long. The particles enter through a 2×5 mm thin aluminum window in the end of the counter beyond the glass bead. The window is very near the axis, the nearest edge is a little less than 1 mm from the axis, and the alignment is sufficiently uncertain that particles might hit the wire. This does not intefere seriously with discrimination of particle energies, however, because the dimensions of the region of gas multiplication are much smaller than the dimensions of the window and only a very small fraction of the primary ionization takes place within the region of avalanche formation.

The proportional counter as we have been using it gives pulses of much shorter duration than the ionization chamber for several reasons, including the higher potential gradient in the significant region, the greater mobility in the reduced pressure and the smallness of the region (a few diameters of the inner wire) in which the significant potential drop takes place. But perhaps a more important cause of the slow pulses observed with the ionization chamber was that the amplifier was purposefully slowed down to filter out the high frequency noise and thereby increase the small pulse-to-noise ratio. This was done because most of the noise was high frequency noise after the microphonics had been eliminated by attention to the mechanical construction and mounting. The slow amplifier meant that positive ion current as well as electron current contributed to the pulses. With the proportional counter the pulses are large enough that the high-frequency noise makes no trouble. In our ionization chamber the tracks pass normal to the plane of the plates. In the proportional counter the incident particles are collimated parallel to the central wire, but in a region wide

[8] N. P. Heydenburg and D. R. Inglis, Phys. Rev. **73**, 230 (1948). *Erratum:* An error occurred in an expansion of a transformation formula which was included supposedly for future convenience but was not employed in the calculations of that paper. The last expression for $g(E,\theta)$ on page 235 should read

$$g(E,\theta)=1-2(V/v_r)\cos\theta+(V/v_r)^2[(5/2)\cos^2\theta-\tfrac{1}{2}]+\cdots.$$

enough that they have various distances from it. Such a geometry would not be satisfactory for a simple ionization chamber with fast detection of electron motions only, because the contribution of an ion motion to the pulse size depends on the potential gradient through which it falls. (This is the so-called "electron collection," which really means *detection* of the *current* induced in the circuit by the *motion* of the electrons in the chamber.) Thus the pulse size would depend critically on the position of the particle path in the ionization chamber. In the proportional counter on the other hand the pulse size with a fast amplifier is a fairly reliable indication of the number of primary ions formed outside of the avalanche region, both because the primary electrons are a small fraction of all the electrons and because the primary electrons fall through a small potential difference outside the avalanche region. The important condition is that each primary electron forms an avalanche and each avalanche starts at about the same distance from the central wire. Within the proportional counter, the input circuit to the discriminator was given a time constant of about three microseconds.

The counter was filled with argon to a pressure of 9 cm Hg. As an aid to keeping the purity of the argon as constant as possible in spite of possible minute leaks, the counter itself was connected to a gas reservoir of about two liters capacity by a flexible metal tube, with manometers and filling valve mounted on the reservoir. During recent operation the gain of the proportional counter has remained sensibly constant for several weeks without refilling, so this precaution may have been unnecessary.

The proportional counter is mounted as shown in Fig. 1 on a carriage with a radial vernier screw mechanism which in turn is mounted on a supporting arm pivoted about an axis through the target, just as the ionization chamber was mounted in the earlier work. On the face of the proportional counter is a foil holder for the mounting of absorbing foils. The foils are used for the gross adjustments of range and the carriage is retracted to change the air path for fine adjustment.

The target backing used for the $Li^7(p,\alpha)\alpha$ was thin Beryllium foil, of a thickness approximately 3 to 5×10^{-5} cm, in order to reduce the intensity of scattered particles to a minimum. This foil was cemented across a hole about 1 cm in diameter in a frame of rather thin sheet copper, and was mounted so as to permit rotation about an axis normal to the beam and to the plane of observation. The target backing for the $Li^6(d,\alpha)\alpha$ reaction was thin silver leaf, stopping power about 1 mm. The target was normally set with its plane at about 66° from the beam direction. With it in this position the alphas could be observed at 10°, 20°, and 35° after traversing the backing. The window at 55° was considered too close to grazing and was ordinarily not used with the target in this position. Instead the target was turned to the complimentary 114° position for observation at this angle. The beam encounters the same effective target thickness at these two complimentary positions, as was verified by observing the same intensity for both target positions at the forward angles.

III. RESULTS

The excitation curves obtained by measuring the yield at 90° to the incident beam, as functions of bombarding energy, are shown for both reactions in Fig. 2. It is seen that the reaction $Li^6(d,\alpha)\alpha$ exhibits a striking resonance at 0.75 Mev and shows evidence of the existence of another resonance very near the highest bombarding energy attained, 3.75 Mev. The reaction $Li^7(p,\alpha)\alpha$ on the other hand displays but one

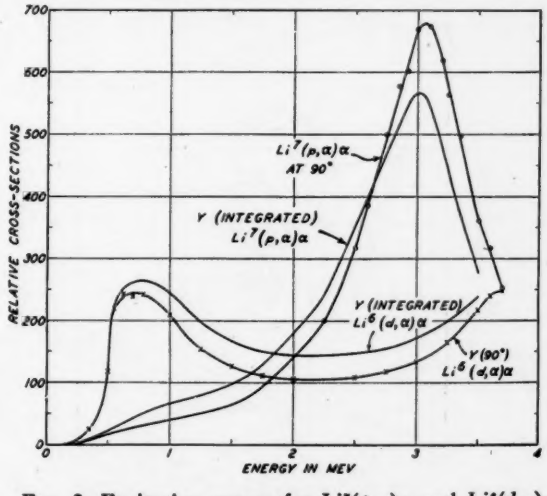

FIG. 2. Excitation curves for $Li^7(p,\alpha)\alpha$ and $Li^6(d,\alpha)\alpha$, obtained with thin evaporated targets. Both the 90° intensity and the average intensity are shown.

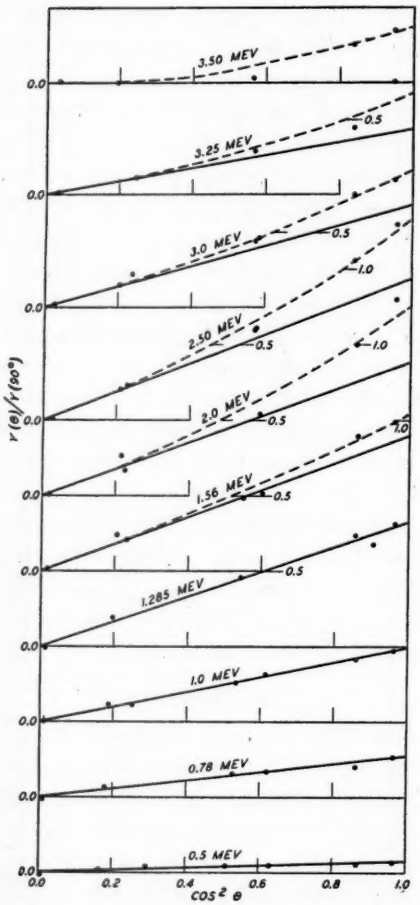

FIG. 3. Relative yields as functions of $\cos^2\theta$ for various deuteron energies for the reaction $Li^6(d,\alpha)\alpha$. The angle θ is the deviation from the deuteron beam in the center-of-mass system.

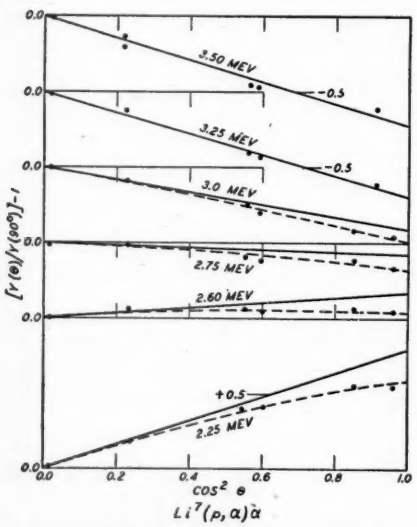

FIG. 4. Relative yields as functions of $\cos^2\theta$ for various proton energies for the reaction $Li^7(p,\alpha)\alpha$.

distinct resonance, at 3 Mev. The scale of ordinates in the figure is arbitrary because of the exact thickness of the thin targets, made by evaporation and used in the same vacuum, is unknown, but it is the same scale of nuclear cross sections for both curves, since this only requires knowledge of the (natural) relative abundance of the two isotopes in the target employed for intercomparison. The total yield curves, obtained from the 90° yields by integrating over all directions with the angular distributions reported below, are also shown in Fig. 2.

In Fig. 3 the angular distributions for $Li^6(d,\alpha)\alpha$ at the various energies are shown by plotting the observed yields, relative to the observed 90° yield, as dependent on $\cos^2\theta$. In such a plot a straight line would indicate that $B(E)$ is zero and the slope of the line would be $A(E)$. Each plotted point has been obtained by first varying the range adjustment enough to verify the position of the peak of the range curve, the bias being sufficient (in almost all cases) to count only alphas near the end of their range in the proportional counter, and then returning to take at least a thousand counts at the peak positions at all angles possible at a given energy. The angles and intensities have of course been transformed to the center-of-mass coordinate system.[8] Observations made at forward and backward angles having about the same value of $\cos^2\theta$ are plotted as nearby points, and the fact that they fall consistently on the same curve is a demonstration of the fore-and-after symmetry. It is seen that there is some scattering of the points, and this makes it impossible to determine $A(E)$ and $B(E)$ uniquely from them. Because of this inevitable uncertainty, we have simply drawn "by eye" a roughly parabolic curve which fits the points reasonably well. The slope of the tangent to this curve at $\cos^2\theta=0$ is then taken as $A(E)$ and the difference between the intercepts, at $\cos^2\theta=1$, of the curve itself and of this tangent is $B(E)$. The prevalently upward initial slope corresponds to positive $A(E)$ and the upward curvature to positive $B(E)$.

Similar results for the reaction $Li^7(p,\alpha)\alpha$ in the energy range between 2 and 3.5 Mev are shown in Fig. 4. These data are the result of repeating, with the more refined technique possible with the

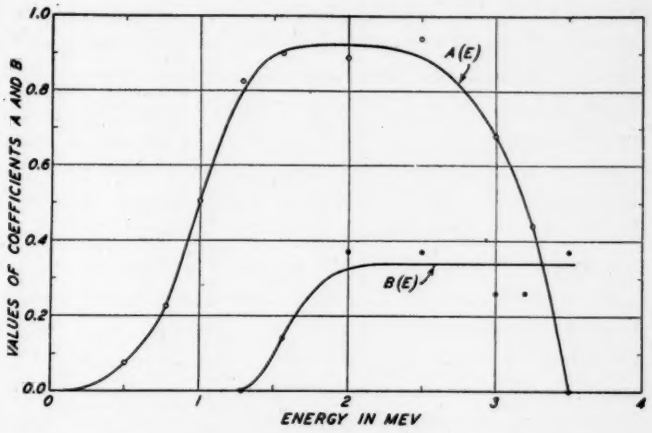

FIG. 5. Variations of $A(E)$ and $B(E)$ with bombarding energy E for the reaction $Li^6(d,\alpha)\alpha$.

proportional counter, measurements made earlier with an ionization chamber.[7] Our earlier data were questionable just in this energy range, and particularly between 3 and 3.5 Mev, because here the scattered protons have about the same range as the alphas and it becomes more difficult to discriminate against pile-up when both kinds of particles are at the end of their range in the chamber. Even with the results observed with the proportional counter and shown in Fig. 4, it may be noted that the data are missing at some angles because of this difficulty.

The variations of $A(E)$ and of $B(E)$ with bombarding energy E are shown in Fig. 5 for the reaction $Li^6(d,\alpha)\alpha$ and in Fig. 6 for the reaction $Li^7(p,\alpha)\alpha$. It is seen that the plotted values scatter some about the solid curves in Figs. 5 and 6, which were drawn in an attempt to fit the data as well as possible with reasonably smooth curves, but the arbitrariness in the simultaneous selection of $A(E)$ and $B(E)$ is sufficient that the observations may be considered compatible with the curves. In the case of the reaction $Li^7(p,\alpha)\alpha$ theoretical formulas for the energy variation of $A(E)$ and of $B(E)$ have been given by one of us.[2] They are

$$A(E)=(C_0E^2+C_1E+C_2)/(E^2+C_3E+C_4), \quad (1)$$

$$B(E)=(C_5E^2+C_6)/(E^2+C_3E+C_4). \quad (2)$$

We find we can make a reasonable fit to the general trend of the observed results by selecting the arbitrary parameters as follows (with E expressed in Mev):

$$C_0=-1.75, \quad C_1=-2.8C_0, \quad C_2=0.27C_0,$$
$$C_3=-1.91, \quad C_4=2.15, \quad C_5=0.4, \quad C_6=-1.2.$$

The values of $A(E)$ and $B(E)$ resulting from this choice are shown as the dot-dash curve in Fig. 6. The solid curves were drawn to fit the points as well as possible without reference to the theory. It is seen that the fit is almost as good as was made in reference 2 to our earlier results by use of the same formulas but a different choice of parameters. The high-energy node which did not appear except by extrapolation in the earlier results has now been brought within the observed range. The observation of this node makes particularly apparent the inadequacy in this rather extended range of energies, of the earlier theory[1] based on entering p protons alone, since that theory predicts no node beyond the one at

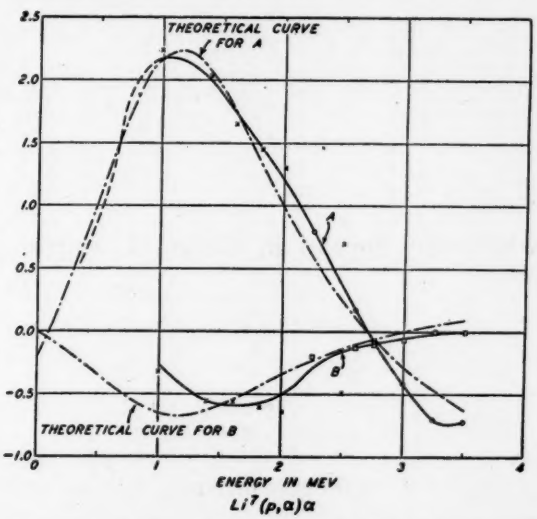

FIG. 6. Variation of $A(E)$ and $B(E)$ with bombarding energy E for the reaction $Li^7(p,\alpha)\alpha$. The dot-dashed curves were obtained from theoretical formulas given by Inglis. The crossed points are taken from our earlier data (see reference 7). The circled points are the latest measurements.

low energy. It should also be noted that the present choice of parameters makes the intensity become negative at some angles at high energies beginning at about 7 Mev, so this choice would not be acceptable in a strict theory. However, Eqs. (1) and (2) result from a simplifying assumption concerning the barrier penetrabilities which is expected to be valid only in the region of fairly low energies, and is even being stretched in our application up to above 3 Mev. Since the theory with this assumption is not applicable at high energies, improper behavior there need not be used as a criterion. The assumption becomes gradually worse with increasing energy, and the choice of parameters has been influenced by a desire to defer the negative intensities to energies considerably above the present observations; otherwise a slightly better fit could have been obtained.

The theory is also based on the assumption that the reaction in this energy region is influenced mainly by two compound states, one narrow with $j=2$ and one very broad with $j=0$. Our excitation curve indicates a fairly narrow state of even parity in the neighborhood of 3 Mev bombarding energy, presumably the state with $j=2$, and the broad state would not be expected to give rise to an observable resonance. The reactions $Li^7(p,\gamma)Be^8$ and $Li^7(p,n)Be^7$ and the excitation of Li^7 by scattered protons indicate[9] the existence of four compounds states in the range of bombarding energies up to 2.5 Mev. Since we do not observe that they affect the reaction $Li^7(p,\alpha)\alpha$ they are apparently states of odd parity. If we may use this as an indication of expected level density for the states of even parity also, we might consider the two states employed by the theory as rather few for so extended an energy range. This consideration leads us to suggest that the slight discrepancy between theoretical and experimental values of $A(E)$ above 2 Mev, which appears to be barely significant from the point of view of experimental accuracy, might be in part the influence of some higher compound state not included in the theory. This might in particular be true of the sudden upward bend in the experimental curve near 3.25 Mev, if this is real. The very slight discrepancy near 2.5 Mev gives no indication of another state since it could easily arise from inadequacy of the simplifying assumption concerning penetrabilities, or it could be eliminnated by readjustment of parameters if no attempt were made to extend the fit above 3 Mev. It is satisfactory both that the assumptions made in the theory concerning the compound states are compatible with our observed excitation curve and that the theory, even with its assumption concerning penetrabilities, follows the general trend of the angular distribution data over so broad an energy range as well as it does.

We wish again to express our gratitude to Dr. Hugh Bradner of the University of California for supplying thin Be foils.

[9] C. M. Hudson, R. G. Herb, and G. J. Plain, Phys. Rev. **57**, 587 (1940); Taschek and Hemmendinger, unpublished; W. F. Hornyak and T. Lauritsen, Rev. Mod. Phys. **20**, 191 (1948).

PHYSICAL REVIEW VOLUME 74, NUMBER 4 AUGUST 15, 1948

Discharge Spread in Geiger Counters with Methane and Methane/Argon Fillings

C. BALAKRISHNAN, J. D. CRAGGS, AND A. A. JAFFE
Metropolitan-Vickers Electrical Company, Ltd., Research Department, Manchester, England

(Received April 13, 1948)

Further measurements with a split-cathode Geiger counter filled with methane and methane/argon mixtures are described.

I. INTRODUCTION

IN earlier papers[1,2] some experiments on discharge spread caused by photon effects in divided cylinder Geiger counters have been described.

In these experiments it was shown that the absorption of photons capable of ejecting electrons from the cathode in self-quenching gases is not

[1] J. D. Craggs and A. A. Jaffe, Nature **159**, 369 (1947).
[2] J. D. Craggs and A. A. Jaffe, Phys. Rev. **72**, 784 (1947).

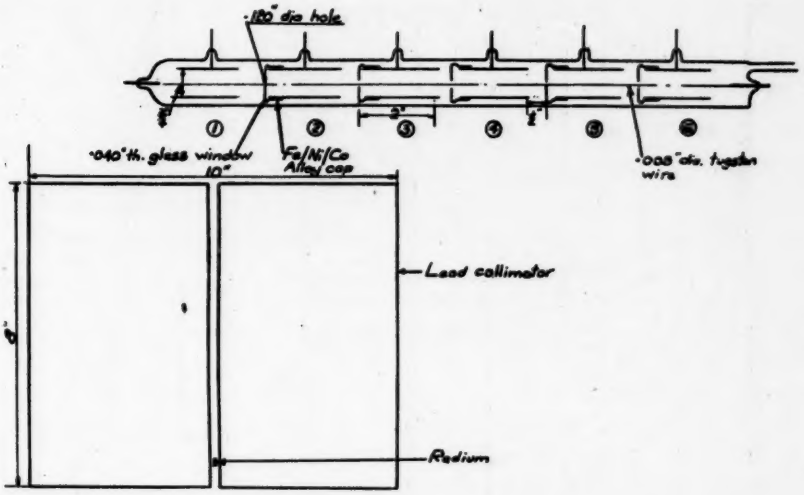

FIG. 1. 6-cylinder window counter.

complete. It must be emphasized, however, that this finding does not, in the least, invalidate the general and reasonable assumption that the discharge spreads along the wire in a Geiger counter because of photo-ionization in the gas near the wire with subsequent build-up of further avalanche processes. The same general type of mechanism is supposed to be responsible for streamer propagation in corona and spark discharges (Loeb).

The discharge propagation along the wire is accountable to absorption of highly absorbable radiations which, by virtue of the distances involved in the split-cathode counter work, cannot easily be responsible for discharge spread over a jump of some centimeters in length.

Two types of counter tube were described (*loc. cit.*), *viz.*: (a) one consisting of open-ended cylinders arranged in line along a common wire and (b) a counter containing cylinders with thick glass end windows through which the common wire passed. The windows served to collimate the photon beam from one of the end cylinders which was irradiated with an external (radium) source of gamma-rays. The gamma-ray beam was carefully collimated with a large lead block, so that the experimental arrangement was as shown in Fig. 1.

In the present work only the window-cylinder counter was used, and the preliminary results described with it in the earlier paper[2] were extended to include measurements with other gases.

So far as is known, in all similar previous work that has been made with counters (generally only two tubes have been used) to observe photo-ionization effects, the cathode photo-emission effect has not been separated from that resulting from photo-ionization in the counter gas.[3–5]

The purpose of the present paper is to provide further data required for the elucidation of the effects encountered in self-quenched ("fast") Geiger counters.[6,7]

II. APPARATUS AND EXPERIMENTAL METHOD

The experimental arrangement is shown in Fig. 1. The counter tube consisted of 6 copper cylinders (initially cleaned with chromic acid and not deliberately oxidized) 2 inches in length, 0.75 in. in internal diameter, and spaced 0.5 in. apart. The windows (B.T.H. C40 glass) were 0.040 in. in thickness and had circular central apertures 0.120 in. in diameter surrounding the wire (0.005-in. diameter tungsten). Each cylinder except that at one end of the set had one window in it. The windows were necessarily made of an electrical non-conductor, and C40 glass was convenient for the purpose of sealing onto Fe/Ni/Co alloy caps which were slipped over the ends of the copper cylinders. The glass windows were sufficiently

[3] E. Greiner, Zeits. f. Physik **81**, 543 (1933).
[4] S. C. Curran and J. E. Strothers, Proc. Camb. Phil. Soc. **35**, 654 (1939).
[5] F. Alder, E. Baldinger, P. Huber, and F. Metzger, Helv. Phys. Acta **20**, 73 (1947).
[6] S. A. Korff and R. D. Present, Phys. Rev. **65**, 274 (1944).
[7] M. E. Rose and S. A. Korff, Phys. Rev. **59**, 850 (1941).

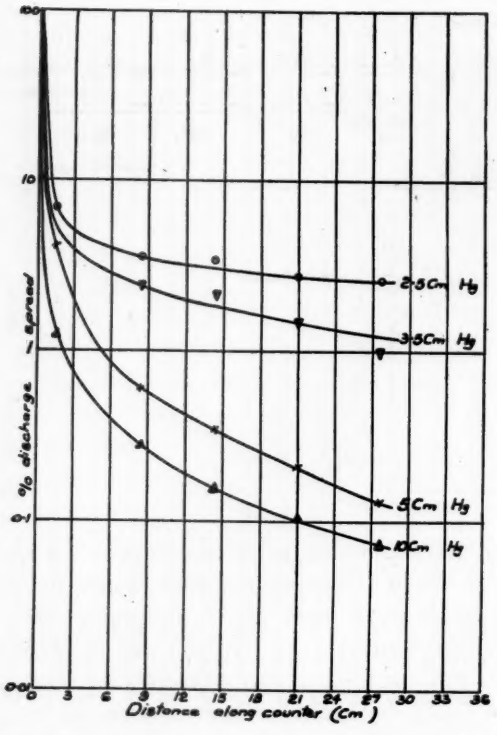

FIG. 2. Discharge spread in methane-filled split-cathodes counter (methane pressures are marked on the curves).

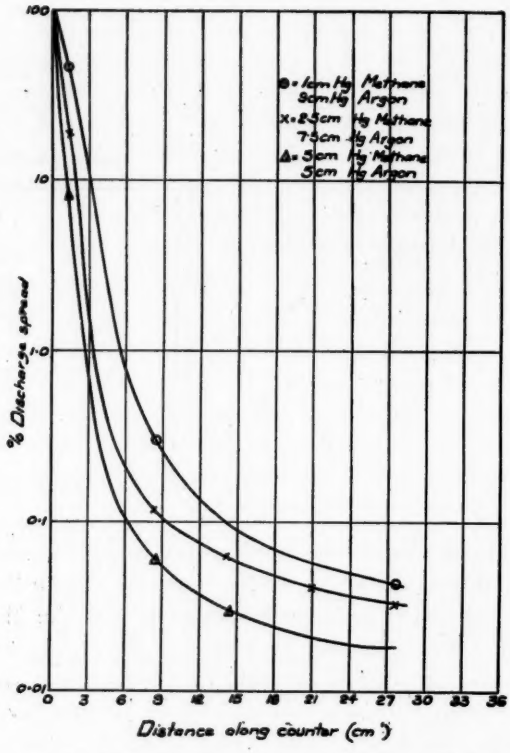

FIG. 3. Discharge spread in argon/methane-filled split-cathode counter.

thick to absorb effectively radiations whose wave-lengths were ~2000A or less (see Section IV).

The method was to irradiate an extreme cylinder and to count double coincidences between this cylinder and the others taken in turn. The circuits are briefly described in the earlier paper[2] and present no unusual features. In that paper also the precautions taken to eliminate random and cosmic-ray coincidences are described.

III. EXPERIMENTAL RESULTS

Figure 2 shows some data obtained with methane of good cylinder grade obtained from the Safety in Mines Research Board. The operating voltages were as shown in Table I.

TABLE I.

Gas	Press cm Hg	Starting voltage	Working voltage
Methane	2.5	1350	1400
	3.5	1420	1470
	5	1650	1700
	10	2000	2100
Argon/methane	9/1	1070	1720
	7.5/2.5	1250	1300
	5/5	1380	1480

Data for argon/methane mixtures are plotted in Fig. 3. The argon was of cylinder grade and contained about 1 percent of nitrogen with, of course, small traces of the other rare gases. Check experiments were made by varying the voltage on the intervening cylinders from zero up to values just less than the starting value (Table I), to ensure that the coincidence counts were not due to electrons diffusing from the first cylinder into those further along the counter tube. Since the photon flux from the irradiated cylinder should fall off with an inverse square variation with distance, the curves shown in Figs. 2 and 3 should be corrected, using the dimensions given in Fig. 1.

IV. DISCUSSION OF RESULTS

It must be stated at once that the conditions of operation for the methane and methane/argon fillings are not strictly comparable, in that the operating voltages are not the same for equal pressures. It is, unfortunately, not feasible to obtain such comparable conditions with counters,

since the over voltage also should be adjusted in cases to be compared. No serious attempts were made in the present experiments to obtain conditions in which the absorption of quanta in argon/methane and methane could be compared, since the efficiency of production of quanta of a given energy, even in rigidly defined discharge conditions, of field strength, gas pressure, and gas purity, is not known.

The experiments are therefore intended to show only basic qualitative trends and to have relevance only to general counter theory. It is hoped in a later paper to describe experiments made with simple gases, with which more fundamental data may be obtained.

The paper of Korff and Present[6] discusses clearly the general mechanisms of photon quenching in fast counters. They point out that the general type of excitation process leading to photon production is different in the two cases of simple (atomic) and complex (polyatomic) gases since, for the latter, inelastic electron collisions will tend to give rotational and vibrational excitation, thus reducing the number of ultraviolet photons emitted, and even electronic excitation will generally result in decomposition of the molecule rather than photon emission. In a simple gas the proportion of excitations leading to emission of short wave-length quanta will be much higher than in a complex gas. In a mixture of gases such as argon ($V_i=15.7$ volts) and methane ($V_i=14.5$ volts) the energetic photons should therefore be produced mostly in the argon, despite its higher ionization potential, and the methane will serve to absorb these photons and thus prevent them from reaching the cathode of the counter.[6,7]

The continuous absorption in methane extends from about 1450A to shorter wave-lengths[8] and therefore, unless the work function of the cathode is less than about 8.5 V, photoelectric emission from the cathode will be unlikely. Evidence exists[2,9] that ordinary metals might in certain circumstances show such high work functions. Korff and Present[6] state that the ultraviolet photons from argon have wave-lengths lying between 1070A and 790A (corresponding to the level at about 11.5 ev and to the ionization potential which is 15.7 ev) so that methane could absorb them. It seems, however, that the argon spectrum would include radiations lying on both sides of the above band, but the main postulate, i.e., the ability of methane to absorb most of the argon radiations, seems reasonable. We do not propose, however, to discuss the photon energies obtainable by excitation in argon/methane mixtures.

A new feature of the results of Figs. 2 and 3 is the greater absorption of the radiations in argon/methane relative to methane even for the same total pressure and for a methane concentration of only 10 percent. Further, the partial pressure of methane (Fig. 3) affects the absorption only slightly. The absorption in 2.5 cm Hg methane is much less than with the same amount of methane added to 7.5 cm Hg argon.

Separate measurements with argon as filling gas (to be described in a later paper on photoionization effects in monatomic and diatomic gases) show that the absorption of argon radiations in argon is very small compared with that shown in Fig. 3. These results should be compared with those of Liebson,[10] who worked with argon/CH_2Br_2 and argon/C_2H_5OH. Liebson used a different experimental technique and did not eliminate the cathode effect.*

In the earlier paper the great reduction in discharges spread through a divided counter because of the use of windows was demonstrated. It is suggested that such a counter if made with glass beads on the wire[11] would show practically zero spreading and might be useful in applications to directional counting with split counters.[12]

V. CONCLUSIONS

The study of discharge spreading by photoionization of the gas in Geiger counters containing methane and methane/argon mixtures tends to support Korff's view that the photo-ionizing radiations are produced mainly in the argon and are quenched by the methane. The higher absorption and lower extent of discharge spreading in argon/CH_4, as compared with CH_4 only at the same pressure, would tend to show that absorption in argon is predominant when CH_4 is present,

[8] H. Sponer and E. Teller, Rev. Mod. Phys. **13**, 75 (1941).
[9] R. Geballe, Phys. Rev. **66**, 316 (1944).
[10] S. H. Liebson, Phys. Rev. **72**, 602 (1947).
* This paper was written before Liebson's paper appeared, but it is thought necessary to refer to the latter.
[11] H. G. Stever, Phys. Rev. **61**, 38 (1942).
[12] W. E. Ramsey, Phys. Rev. **61**, 96 (1942).

but the probable differences in the spectra obtained in the two cases make detailed interpretation difficult.

VI. ACKNOWLEDGMENTS

The authors are indebted to Mr. F. R. Perry for his interest in and encouragement of the work and to Sir Arthur P. M. Pleming, C.B.E., D. Eng., Director of Research and Education, and to Mr. B. G. Churcher, M.Sc., M.I.E.E., Manager of Research Department, Metropolitan-Vickers Electrical Company, Ltd., for permission to publish this paper.

PHYSICAL REVIEW VOLUME 74, NUMBER 4 AUGUST 15, 1948

Penetrating Particles in Extensive Air Showers

J. E. TREAT AND K. I. GREISEN
Cornell University, Ithaca, New York

(Received May 3, 1948)

Penetrating particles in extensive air showers have been studied at 4300- and 3260-m elevations. The particles capable of penetrating 14 cm lead are about 1 per 30 shower particles at 3260 m and 1 per 25 at 4300 m. The number of penetrating particles is reduced by a factor 1.8 when the lead is increased from 15.5 to 39 cm, and the density of the penetrating particles diminishes by a factor 1.7 between 4300 and 3260 m elevation. These facts imply the penetrating particles are very numerous and have too low average energy to be mesons coming from the top of the atmosphere. Further experiments show that they are not produced multiply in lead shields above the counters. This fact, together with the independence of their number on the atomic number of the absorber, seems to indicate they are not produced by photons.

SECTION A

IN order to extend our knowledge about the penetrating particles in extensive air showers, experiments were performed last summer at Echo Lake and Mt. Evans, Colorado (elevations 3260 and 4300 meters, respectively), in which the particles of the showers were recorded with unshielded counters and with counters under lead. The counter and lead arrangement used for a large part of the data taken at Echo Lake and all of the data taken at Mt. Evans are shown in Fig. 1. For brevity in reference we shall call this experiment *A*.

In experiment *A* the area of the shielded counters was held constant at 293 cm² each, but the area of the unshielded counters was changed periodically among the values 48, 98, and 293 cm².

The counters had brass walls, ½ mm thick, were one inch in diameter and were filled with a self-quenching gas mixture. Almost all were 16 inches in length and had an active area of 98 cm². The largest counter area referred to above, 293 cm², was composed by connecting three such counters in parallel. The smallest area, 48 cm², was obtained with single counters eight inches in length and one inch in diameter. The circuits and the counter plateaus were checked daily during the course of the experiments.

As Fig. 1 shows, the counter separations were about two meters. Cocconi, Loverdo, and Tongiorgi[1] have shown that the number of showers recorded with a counter arrangement similar to that of experiment *A* is not sensitive to changes of the counter-separation between two and eight meters.

The lead shielding the lower counters was composed of lead pigs, cut so as to nest tightly together, and covered with lead sheets. The counters were not perfectly shielded with lead at the ends, but the lead below, on the sides and above the counters was much longer than the counters themselves (see Fig. 1b). The smallness of the counter area facing the ends, the small solid angle of the openings and the low intensity at large zenith angles combine to make the relative probability of a shower particle entering the counter through the unshielded ends less than 10^{-3}. The lead below the counters was five

[1] G. Cocconi, A. Loverdo, and V. Tongiorgi, Phys. Rev. 70, 841 and 852 (1946).

cm thick, that at the sides was ten cm thick and that above the counters was fourteen cm thick, sufficient to exclude electrons of energy below about 3×10^{10} ev in the vertical direction. For cascade showers in air arising from primaries of energy 10^{12} to 10^{15} ev at the top of the atmosphere, the fraction of the electrons above 3×10^{10} ev at Echo Lake is less than 10^{-3}.

The apparatus was housed in a light canvas tent so that there should be essentially no shower-producing material above the unshielded counters. The counters were all far enough apart so that showers produced in the lead, whether of electrons or penetrating particles, would not likely discharge more than one counter. Hence the coincidences recorded were in general due to multiplication of the showers in the air and not in local materials.

Impulses from the four unshielded counters were fed into a discriminator circuit (with 0.9 microsecond resolving time) which selected fourfold and threefold coincidences (denoted by $4S$ and $3S$, respectively, where S stands for "soft rays"). Similarly, the impulses from the shielded counters were fed into a discriminator that selected fourfold, threefold and twofold coincidences and single pulses (denoted by $4H$, $3H$, $2H$, and $1H$, respectively, where H stands for "hard rays"). Coincidences denoted by nS or nH include all coincidences of at least n counters; thus $3S$ includes both threefold and fourfold coincidences, etc. Hence, in computing standard errrors of a ratio of rates such as $3S/4S$, it must be kept in mind that the $3S$ and $4S$ counts were not independent.

TABLE I. Coincidences recorded in experiment A. (Fig. 1.)

	Echo Lake (3260 m)			Mt. Evans (4300 m)		
Area° (cm²)	48	98	293	48	98	293
Time (min.)	10,102	10,167	5585	4569	2538	1427
$3S$	1173	3059	7325	910	1304	3400
$3S+1H$	509	1013	1181	408	409	550
$3S+2H$	164	276	242	194	142	104
$3S+3H$	78	95	68	86	54	32
$3S+4H$	29	32	22	40	18	10
$4S$	298	829	2267	271	377	1031
$4S+1H$	182	407	591	190	196	292
$4S+2H$	92	165	180	125	94	84
$4S+3H$	56	77	60	67	38	27
$4S+4H$	26	26	20	35	14	10
$2H$	1442	1404	861	1276	697	388
$2H$*	1010	970	620	920	500	280
$3H$	123	110	78	125	78	34
$4H$	31	33	22	41	19	10
total time		25,854			8534	
total $2H$*		2600			1700	
total $3H$		311			237	
total $4H$		86			70	

° Area refers to unshielded counters. Area of shielded counters was fixed at 293 cm².
* Corrected for chance coincidences with 0.9 microsec. resolving time.

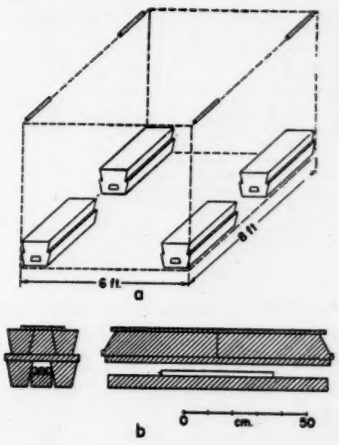

FIG. 1. Arrangement of counters and lead in experiment A.

Pulses from the two discriminator circuits were fed into coincidence units which selected (with a 3.5-microsecond resolving time) coincidences of the S counters with the H counters. Thus thirteen different coincidence combinations were recorded simultaneously, as listed in Table I, which contains all of the data of experiment A.

Conclusions Drawn from Experiment A

1. Density Distribution for All Shower Particles

In Fig. 2, the logarithms of the $3S$ and $4S$ coincidence rates are plotted against the logarithms of the counter area. Within statistical errors (too small to appear outside the circles), the data are in agreement with straight lines, all of the same slope, 1.40, as drawn in Fig. 2. This characteristic of the showers has been observed before[1-3] and indicates that the frequency of incident showers, as a function of the total particle density, Δ (capable of penetrating $\frac{1}{2}$ mm of brass), follows the equation $f(\Delta)d\Delta=K\Delta^{-\gamma}d\Delta$ with $\gamma=2.4$ and $K(4300)/K(3260)=1.8$.

On the assumption that the form of the fre-

[2] P. Auger and J. Daudin, J. de phys. et rad. **6**, 233 (1945).
[3] J. Daudin and A. Loverdo, J. de phys. et rad. **8**, 233 (1947).

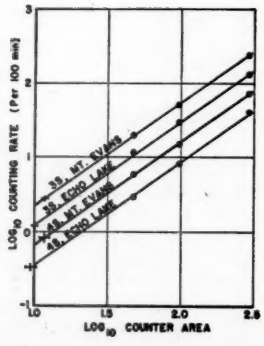

FIG. 2. Dependence of threefold and fourfold coincidence rates of the unshielded counters on counter area. Crosses indicate threefold and fourfold coincidence rates of shielded counters of area 293 cm².

quency-density relation is a power law as given above, an independent value for γ can be derived from the ratio of threefold to fourfold coincidences.[2,3] Since the probability of missing a counter is $e^{-A\Delta}$ and the probability of hitting a counter is $1-e^{-A\Delta}$ (A being the counter area), we have

$$(4S)=\int_0^\infty (1-e^{-A\Delta})^4 K\Delta^{-\gamma}d\Delta$$
$$=KA^{\gamma-1}(-\gamma)![-4+6(2)^{\gamma-1}-4(3)^{\gamma-1}+(4)^{\gamma-1}].$$
$$(3S)=\int_0^\infty [(1-e^{-A\Delta})^4+4e^{-A\Delta}(1-e^{-A\Delta})^3]K\Delta^{-\gamma}d\Delta$$
$$=KA^{\gamma-1}(-\gamma)![-6(2)^{\gamma-1}+8(3)^{\gamma-1}-3(4)^{\gamma-1}].$$

The ratio is a function of γ alone. Experimentally, we find the average ratio $(4S)/(3S)=0.296\pm0.004$, whereas if $\gamma=2.40$ (derived from the slopes in Fig. 2) the ratio should be 0.340.

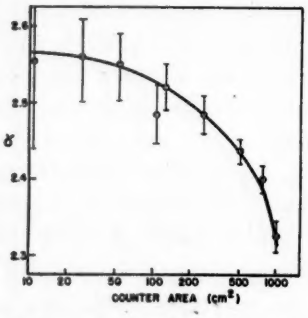

FIG. 3. Variation of effective value of γ with counter area, as computed from data of Cocconi, Loverdo and Tongiorgi (reference 1).

The experimental ratio $(4S)/(3S)$ would indicate $\gamma=2.55$. Thus, the two determinations of γ are not in good agreement.

Auger and Daudin[2] have made measurements of γ by observing the ratio of threefold to twofold coincidences between counters of surface area about 150 cm². They found γ to be a decreasing function of altitude, varying linearly with the pressure and having the values 2.66 at 50 m, 2.58 at 980 m, 2.50 at 2060 m, and 2.46 at 2860m. They have made the observation that even at a fixed altitude γ must not be a true constant, but must decrease slowly as Δ decreases; otherwise the total number of particles must diverge.

Recently, Maze, Fréon, and Auger[4] have confirmed the decrease of γ with altitude, with measurements in an airplane. They report $\gamma=2.67\pm0.01$ at sea level and 2.41 ± 0.05 at 22,000 ft. Calculations by Cocconi,[5] however, indicate that the cascade theory would predict an increase of γ with altitude, rather than a decrease as found by the above authors.

Cocconi, Loverdo, and Tongiorgi[1] have measured threefold and fourfold coincidence rates as functions of counter area over a wide range of areas. At 2200 meters' elevation, the dependence of counting rates upon area indicates $\gamma=2.45$ before correction. A correction for showers generated in the roof raised this value to 2.55. However, if one examines their ratios of threefold to fourfold coincidences, one finds that γ apparently depends on the counter area, as indicated by the graph in Fig. 3. This variation is as predicted by Auger and Daudin[2] and has been discussed in considerable detail by Daudin and Loverdo.[3] The same trend appears in our data but is not so apparent because we did not vary the counter area by so large a factor.

A possible source of error in the value of γ deduced from the variation of coincidence rates with counter area arises from the fact that the counters of different area were not of the same shape. The largest counters (in the experiments of Cocconi *et al.* as well as our own) were made up of several cylinders placed side by side and resembled plane areas, while the smaller counters were single cylinders and thus more nearly re-

[4] R. Maze, A. Fréon, and P. Auger, Phys. Rev. **73**, 418 (1948).
[5] G. Cocconi, Phys. Rev. **72**, 964 (1947).

sembled spherical detectors. Thus the effective area of the counters, for showers incident with a large zenith angle, is reduced by a larger factor for the larger counters. This makes the variation of counting rate with counter area appear less strong than it should; i.e., it reduces the apparent value of γ.

Another source of error is the barometric fluctuations. The counting rates with different counter areas were measured at different times. Since the barometric coefficient for extensive showers is very high (10 to 20 percent per cm Hg), the apparent variation of counting rate with area may have been appreciably influenced by pressure variations. These would not have any effect, however, on the determination of γ through the ratio $4S/3S$, because the $4S$ and $3S$ rates with any given counter area were measured simultaneously.

Because of all the above considerations, we do not think the discrepancy between the values of γ deduced in our experiment is large. In fact, both values are in agreement with measurements of other authors. It was not our purpose to determine γ with great precision, but rather the relative numbers of penetrating and soft particles in the showers, and in the analysis given below, a variation of 0.1 in the value of γ is not serious. Therefore, in the calculations to follow we shall take $\gamma = 2.5$.

2. *All Extensive Air Showers Contain Penetrating Particles, and All Extensive Penetrating Showers Are Accompanied by Extensive Electron Showers*

This conclusion is in agreement with that of Cocconi, Loverdo, and Tongiorgi.[1]

In Table II we list the relative numbers of $3H$ and $4H$ coincidences that were accompanied by threefold and fourfold coincidences of the unshielded counters. It may be seen that when three of the counters under lead were struck, the probability was not very large that the fourth counter be struck also; but the probability was very high that three or all four of the unshielded counters be discharged. When all four counters under lead were struck, it was a relatively rare event for one or more than one of the unshielded counters to be missed, even when the area of the unshielded counters was $\frac{1}{6}$ that of the counters under lead. These facts imply that practically all of the extensive showers of penetrating particles were accompanied by extensive electron showers, and that the number of electrons was large compared with the numbers of particles that could penetrate 14 cm of lead.

TABLE II. Relative numbers of extensive penetrating showers accompanied by coincidences of unshielded counters.

Location	Area* cm²	$\frac{3H+3S}{3H}$	$\frac{3H+4S}{3H}$	$\frac{4H+3S}{4H}$	$\frac{4H+4S}{4H}$
Echo Lake	48	78/123	56/123	29/31	26/31
Mt. Evans	48	86/125	67/125	40/41	35/41
Echo Lake	98	95/110	77/110	32/33	26/33
Mt. Evans	98	54/78	38/78	18/19	14/19
Echo Lake	293	68/78	60/78	22/22	20/22
Mt. Evans	293	32/34	27/34	10/10	10/10

* This area refers to the unshielded counters. The area of the counters under lead was held constant at 293 cm².

In principle, one could calculate the average ratio of soft particles to hard particles from the data of Table II. The results, however, would depend sensitively on the very small numbers of the $3H$ and $4H$ counts that were not accompanied by a $3S$ or $4S$ coincidence. Evidence will be presented below that a comparatively large number of locally generated penetrating showers occurred, not associated with extensive air showers. Mostly, these were not recorded in Experiment *A* because of the large counter separations; but if a small fraction of the local penetrating showers succeeded in discharging more than one of the counters under lead, they could be responsible for many of the penetrating showers in which $3S$ and $4S$ coincidences were not recorded.

In Fig. 4 are shown the relative numbers of $3S$ and $4S$ coincidences in which various numbers of penetrating particles were recorded. These ratios are functions of the area of the unshielded counters, because the average density of particles in the showers that are recorded increases as the area is reduced, thus increasing the relative chance of detecting penetrating particles. The $3S$ and $4S$ coincidences could not have been appreciably affected by local showers, because the counting rates were high and the counters were well separated with no shower producing material above them (see Fig. 1).

The solid curves in Fig. 4 have all been calcu-

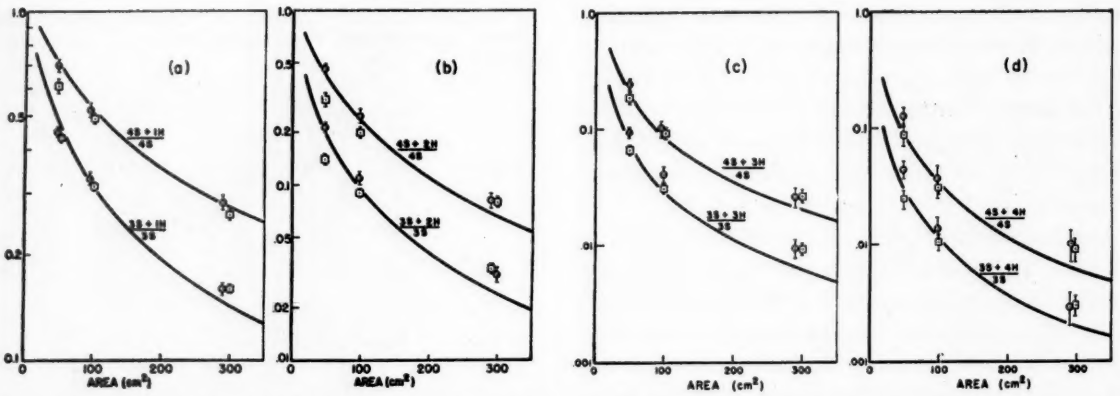

FIG. 4. Relative numbers of S showers (in unshielded counters) that are accompanied by H counts (in the shielded counters), as functions of the area of the unshielded counters. Circles give data at 4300 m; squares give data at 3260 m elevation. Solid curves are calculated for one penetrating particle per 29 shower particles.

lated under the assumption that the ratio of soft particles to penetrating particles is a constant throughout the showers. To illustrate the calculations we give the deduction of the formula representing the $4S+1H$ coincidence rate:

$$(4s+1H)=\int_0^\infty (1-e^{-A\Delta})^4(1-e^{-A'\Delta/N})K\Delta^{-\gamma}d\Delta$$

$$=KA^{\gamma-1}\int_0^\infty (1-e^{-x})^4(1-e^{-\beta x})x^{-\gamma}dx,$$

$$\text{with } \beta=A'/AN$$

$$=KA^{\gamma-1}(-\gamma)![-4+6(2)^{\gamma-1}-4(3)^{\gamma-1}$$

$$+(4)^{\gamma-1}-(\beta)^{\gamma-1}+4(1+\beta)^{\gamma-1}$$

$$-6(2+\beta)^{\gamma-1}+4(3+\beta)^{\gamma-1}-(4+\beta)^{\gamma-1}].$$

In these equations A is the area of the unshielded counters and A' is the total area of all four counters under lead, N is the ratio of all particles in the shower to the penetrating particles, and $K\Delta^{-\gamma}d\Delta$ is the frequency of showers with total particle density between Δ and $\Delta+d\Delta$. The curves have been drawn corresponding to $N=29$.

The agreement of the calculations with the experimental results is apparently satisfactory. The agreement would be better if we had used a slightly lower value for N at Mt. Evans and a slightly higher value at Echo Lake. It may be seen from Fig. 4 that almost all the points for the higher elevation lie above the points for the lower elevation, indicating relatively more penetrating particles in the showers at the higher elevation.

Perfect agreement between the data and the calculated curves should not be expected, for neither N nor γ is more than an empirical constant. In particular, the relative number of mesons and electrons might be expected to vary with the geometric distance from the core of the shower and with the energy of the shower. As one increases the area of the unshielded counters, one does not change appreciably the average distance to the core of the showers recorded, but one decreases the average primary energy because smaller showers are recorded.

The associated production of electron showers and showers of penetrating particles has been observed in the cloud chamber by Fretter.[6] He observed no examples of production of penetrating showers by electronic radiation, but found that in more than half of the examples of penetrating showers, high energy electronic radiations was simultaneously produced. We think it is likely that the Auger showers in the atmosphere are fundamentally the same as the showers observed by Fretter, differing from them only in the magnitude of the energy and the total number of particles. In the large Auger showers

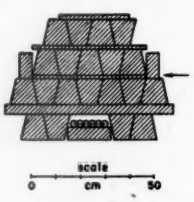

FIG. 5. Arrangement of shielded counter and lead in experiment B. In part of this experiment, the lead above the level of the arrow was removed.

[6] W. B. Fretter, Phys. Rev. **73**, 41 (1948).

which we recorded, our data seem to indicate that all penetrating showers involve simultaneous production of electronic radiation, and all electronic showers involve simultaneous production of showers of penetrating particles.

3. *Further Evaluation of N*

If one accepts the conclusion that all extensive penetrating showers are associated with extensive electron showers, the most direct way to evaluate the ratio of electrons to penetrating particles is as follows. The probability of a coincidence being recorded is a function only of the product $A\Delta$, the area of the counters times the density of shower particles. Therefore, the area of the unshielded counters which would give the same threefold and fourfold coincidence rates, as are obtained with the counters under lead, bears a ratio to the area of the shielded counters which is the same as the ratio of penetrating particles to total particles per square meter. This principle is independent of the precise form of the frequency-density distribution law.

In Fig. 2, the crosses indicate the $3H$ and $4H$ coincidence rates found at Echo Lake and Mt. Evans. Extrapolation of the $3S$ and $4S$ counting rate *vs.* area curves shows that the $3S$ and $4S$ rates would equal the $3H$ and $4H$ rates if the area of the unshielded counters were reduced to 11.9 cm² at Echo Lake, or 9.9 cm² at Mt. Evans. Since the area of the unshielded counters was 293 cm², N must equal 30 at Echo Lake and 25 at Mt. Evans. These results are in very good agreement with the data given in Fig. 4.

4. *Variation with Altitude*

The chief purpose of these experiments was to gain some indication as to whether the penetrating particles in Auger showers are principally of local origin, as has been concluded by several authors,[7-9] or are produced at high altitude in the act which initiated the shower, as might be concluded from the theory of Lewis, Oppenheimer, and Wouthuysen[10] or inferred from recent data of Cocconi and Greisen.[11] By local production we mean production in the lead immediately surrounding the counters by the photons in the air showers.

TABLE III. Absorption of the penetrating particles in extensive air showers.

Pb thickness Time (min.)	15.5 cm 3614	39 cm 7639
$3S$	1077	2225
$4S$	326	679
$3S+H$	154	189
$4S+H$	72	115
$(3S+H)/3S$	0.143 ± 0.011	0.085 ± 0.006
$(4S+H)/4S$	0.22 ± 0.023	0.169 ± 0.014

It was thought that if the penetrating particles are of local origin, they would appear to be in equilibrium with the photons and electrons of the showers, whereas if they are of distant origin, the relative number of electrons and penetrating particles should vary with altitude. In fact, if the penetrating particles are mesons produced near the top of the atmosphere, they should be of high average energy at Echo Lake and should not change much in number between Mt. Evans and Echo Lake.

Experimentally, we find the average ratio of $3H$ and $4H$ coincidence rates of Mt. Evans (4300 m) to those at Echo Lake (3260 m) is 2.32 ± 0.18. This is an even larger change than occurs in the $3S$ and $4S$ rates, for which the average ratio between Mt. Evans and Echo Lake is 1.79 ± 0.03. Therefore, the density of "penetrating" particles in the showers is reduced even more than the density of electrons in traveling from Mt. Evans down to Echo Lake. The same result appears in the sections above where the average ratio of electrons to penetrating particles was shown to be about 29 at Echo Lake but only 24 at Mt. Evans.

If the frequency of extensive penetrating showers with density between Δ and $\Delta+d\Delta$ varies as $\Delta^{-\gamma}d\Delta$ with the same value of γ as that which applies for all particles in the showers, the density of penetrating particles must be reduced, between 4300 and 3260 meters elevation, by a factor $(2.32\pm0.18)^{1/\gamma-1}=1.75\pm0.09$. Ordinary mesons occurring singly and not associated with extensive showers decrease in intensity only by a factor of 1.3 between the same two elevations.

The strong reduction in average density of penetrating particles between the two elevations

[7] G. Cocconi and C. Festa, Nuovo Cimento **3**, 293 (1946).
[8] D. Broadbent and L. Janossy, Proc. Roy. Soc. **190**, 497 (1947), and **192**, 364 (1948).
[9] G. Salvini and G. Tagliaferri, Phys. Rev. **73**, 261 (1948).
[10] H. W. Lewis, J. R. Oppenheimer, and S. A. Wouthuysen, Phys. Rev. **73**, 127 (1948).
[11] G. Cocconi and K. Greisen, Phys. Rev. **74**, 62 (1948).

may be an effect either of absorption and decay, or of scattering and initial angular divergence. In either case, it is entirely inconsistent with the hypothesis that the particles are mesons produced near the top of the atmosphere in the act which initiated the shower. It does not, of course, prove that the particles are locally produced by the gamma-rays. But if the particles are locally produced, the absorption appears even more pronounced, for the "true" absorption must be partially compensated by production of some particles between Mt. Evans and Echo Lake. In other words, if the penetrating particles are locally produced mesons, their spectrum is very soft.

SECTION B

Absorption of the Penetrating Particles

A second experiment was performed at Echo Lake in order to measure the absorption of the penetrating particles of the extensive air showers in lead. The four unshielded counters were of 98 cm² area arranged as in experiment *A*. Under lead we had a single counter of area 586 cm², composed of six counters in parallel, as shown in Fig. 5. The thickness of lead above this counter was alternately 15.5 and 39 cm of lead. We shall refer to this absorption experiment as experiment *B*.

The data recorded are given in Table III. From the ratio $(3S+H)/3S$ with 15.5 cm of lead, we deduce (as outlined above in part *b* of Section *A*) the value 44 ± 4 for N, the ratio of the total number of shower particles to those capable of penetrating 15.5 cm of lead. Similarly, from the data with 39 cm of lead we deduce $N=83\pm7$, the ratio of all particles to those capable of penetrating 39 cm of lead. Since the total number of particles above the absorber is independent of the amount of lead, the factor of absorption between 15.5 and 39 cm is given by the ratio of these two values of N, which equals 0.54 ± 0.07. From the ratio $(4S+H)/4S$ with 15.5 and 39 cm lead, one deduces a smaller absorption (0.72 ± 0.13), but the statistical error is considerably larger. Since the fourfold coincidences are counted with the threefold coincidences in the $3S$ and $3S+H$ rates, the average absorption factor is 0.54 ± 0.07.

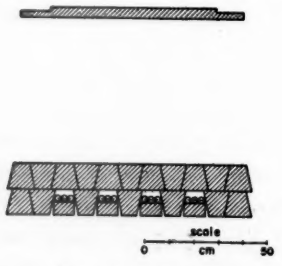

FIG. 6. Arrangement of shielded counters and lead in experiment C_1.

If the penetrating particles are mesons incident on the lead from the air, this absorption in lead appears very strong. From the data of Rossi and collaborators,[12] the ordinary mesons not associated with air showers are much less strongly absorbed at Echo Lake. Of those which can penetrate 15.5 cm only 17 percent are absorbed in an additional 23 cm of lead. On the other hand, if the penetrating particles are locally produced in the lead, the absorption must be at least as great as if they are incident from the air.

The implications are: (1) Whether the "penetrating" particles are produced locally or not, their average range in lead is not very great. (2) If the particles are locally produced in the lead, the primaries that produce them also have a short range. (3) If the particles are ordinary mesons, the mean energy is too small to be consistent with the hypothesis that the mesons are produced at the top of the atmosphere. Thus, the strong absorption in lead is consistent with the strong decrease in the atmosphere, and leads to the same conclusion.

The results of this experiment incidentally imply that the quantity N, referred to above, is a function of the amount of absorber placed above the shielded counters, and hence must be expected to vary from one experiment to another in which a different absorber thickness is used.

SECTION C

Search for Local Production of the Penetrating Particles in Extensive Showers

Experiment C_1 differed from Experiment *A* in that the shielded counters were placed much closer together, as shown in Fig. 6, and part of the lead shielding above the counters was raised about two feet. These changes were made to

[12] B. Rossi, K. Greisen, J. C. Stearns, D. K. Froman, and P. G. Koontz, Phys. Rev. 61, 675 (1942).

enhance the detection of multiple groups of penetrating particles locally produced in the lead. With the counter arrangement of Fig. 6, it was possible for a single particle striking the lead to generate a shower of penetrating particles which would discharge several of the shielded counters. In experiment A such an event was highly improbable.

A fixed area, 98 cm², was used for the unshielded counters in Experiment C, and the experiment was performed only at 3260 m elevation. Table IV summarizes the results, together with the comparable data of experiment A.

These data show no evidence for an increase in the fraction of the Auger showers ($3S$ and $4S$ coincidences) in which groups of penetrating particles were recorded. Therefore, we must conclude either that the penetrating particles observed in the showers are not produced locally, or that the penetrating particles are produced singly rather than in groups. In the latter case, the probability of detecting a coincidence of several shielded counters with the unshielded ones would not be strongly affected by the separation of the counters.

Experiment C_2 differed from C_1 only in that two of the counter groups under the lead were disconnected. The two remaining counter groups under lead were alternately adjacent groups and more distant groups. This experiment was made in order to investigate further the effect of the counter separations. The data are given in Table V. The spacings listed in the top row were measured from center to center of the counters. The minimum amount of lead between the counters, in experiment C_2 as well as in C_1, was 8 cm.

The statistical errors in experiment C_2 are large, but nevertheless the data show that the penetrating showers accompanying extensive air showers do not depend strongly on the separation of the counters. Considering both experiments C_1 and C_2, one may say that a coincidence of two counters under lead, caused by the particles in an extensive air shower, is just as likely to occur when the counters are two meters apart as when they are six inches apart. This is in diagreement with the experimental results of Salvini and Tagliaferri,[9] but in agreement with other experiments of Cocconi and Greisen.[11] In addition to indicating that the penetrating particles are not produced locally (or are produced singly), it confirms our belief that the "penetrating particles" are not high energy electrons in the core of the showers.

TABLE IV. Comparison of experiment C_1 and experiment A with 98 cm² area of unshielded counters.

	Experiment C_1	Experiment A
Time (minutes)	4106	10167
$3S$ rate*	27.7 ±0.8	30.1 ±0.5
$4S$ rate	8.3 ±0.4	8.2 ±0.3
$2H$ rate**	306.0 ±3	10.0 ±0.3
$3H$ rate	11.1 ±0.5	1.20 ±0.07
$4H$ rate	0.61 ±0.12	0.33 ±0.04
$(3S+1H)/3S$	0.268±0.013	0.331±0.009
$(4S+1H)/4S$	0.45 ±0.03	0.49 ±0.02
$(3S+2H)/3S$	0.084±0.008	0.090±0.005
$(4S+2H)/4S$	0.18 ±0.02	0.20 ±0.014
$(3S+3H)/3S$	0.032±0.005	0.031±0.003
$(4S+3H)/4S$	0.073±0.014	0.093±0.010
$(3S+4H)/3S$	0.009±0.003	0.010±0.002
$(4S+4H)/4S$	0.029±0.009	0.031±0.006

* All rates are per 100 minutes.
** Corrected for chance coincidences.

In sharp contrast to the above conclusions regarding the penetrating showers *accompanying* extensive air showers, we reach very different conclusions for the penetrating showers *not accompanied* by air showers. In Tables IV and V it may be seen that the $2H$, $3H$, and $4H$ coincidence rates were very strongly increased when the counter separation was reduced, whereas the number of these coincidences associated with air showers remained constant.

With the small counter separations, a significant fraction of the $2H$, $3H$, and $4H$ coincidences were without doubt caused by single ordinary mesons travelling almost horizontally, and by knock-on electrons produced by such mesons in the lead. In order to discover whether

TABLE V. Coincidence rates as function of counter spacing, with only two counter groups under lead.

Counter spacing	7 inches	14 inches	21 inches
Time (minutes)	365	1051	587
$3S$*	31 (114)	26 (269)	28 (165)
$3S+1H$	8.5 (31)	5.3 (56)	7.7 (45)
$3S+2H$	1.4 (5)	1.1 (12)	1.4 (8)
$4S$	7.7 (28)	7.3 (77)	7.0 (41)
$4S+1H$	2.7 (10)	2.7 (28)	3.4 (20)
$4S+2H$	0.6 (2)	0.8 (8)	1.2 (7)
$2H$**	100 (366)	18 (199)	7.3 (47)

* Rates are per 100 minutes. The numbers in parentheses tell the numbers of counts recorded.
** Correction for chance coincidences was 0.7 count per 100 minutes

TABLE VI. Coincidence rates with two counter groups under 29 cm Pb.

Counter spacing	7 inches	
Time (minutes)	850	
$3S$	28	(239)*
$3S+1H$	2.9	(25)
$3S+2H$	0.35	(3)
$4S$	8.9	(76)
$4S+1H$	1.5	(13)
$4S+2H$	0.2	(2)
$2H$	79**	(676)

* Rates are per 100 minutes. The numbers in parentheses indicate the numbers of counts recorded.
** Correction for chance coincidences was one percent of rate.

or not all of the increase in counting rates could be so explained, experiment C_2 was repeated with twice as much lead above the counters (see Fig. 7). The data are given in Table VI. If the $2H$ coincidences were almost entirely due to mesons travelling horizontally, the rate should not have been affected by increasing the amount of lead above the counters. If anything, the $2H$ rate should have been increased since the amount of lead on the sides was reduced. Instead, we find that the $2H$ rate was diminished from 100 ± 5 (see Table V) to 79 ± 3.

Thus we have evidence for very large numbers of penetrating showers locally produced in the lead, but not accompanied by extensive air showers.[11] The absorption between 15 and 29 cm indicates that neither the primaries nor the secondaries have a very long range in lead. The $2H$ coincidence rates with different counter separations (Table V) indicate that the secondaries in these showers have a very wide angular spread. The small ratios of $3H$ to $2H$ and $4H$ to $3H$ indicate that the number of particles is in general small in such showers.

The nearly isotropic distribution of the particles and the great frequency of the penetrating showers not accompanied by extensive air showers make it seem plausible that they have caused some of the coincidences of the shielded counters even in experiment A where the counters were two meters apart. This may account particularly for many of the twofold coincidences of H counters observed in experiment A unaccompanied by $3S$ or $4S$ coincidences.

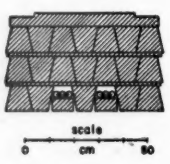

FIG. 7. Arrangement of shielded counters and lead used in part of experiment C_2 (data in Table VI).

DISCUSSION

It has been shown that the extensive showers contain many penetrating particles which cannot be mesons coming from the top of the atmosphere because their density diminishes too rapidly with atmospheric depth and with increasing thickness of the lead that they are required to penetrate. In fact, the relative density of penetrating and soft particles is almost the same at 4300 as at 3260 meters' elevation, and not very different at these elevations from the values found by Cocconi and by Broadbent and Janossy[8] at 2200 meters and at sea level. It seems thereby implied that the penetrating particles are of comparatively local origin, produced in the air not many radiation lengths above the point of observation. On the other hand, no evidence could be found for production of groups of penetrating particles, by the particles in extensive air showers, in a lead shield. These facts seem to present a contradiction, because phenomena that take place abundantly nearby in the air should also occur abundantly in the lead.

Suggestions for resolving the contradiction are: (1) the penetrating particles may be produced locally by photons in the air showers, but the production may be mostly of single particles rather than groups; or (2) the particles responsible for the production of the penetrating particles may have a short mean path in air, and be very much more abundant a few thousand meters above the point of observation than at the point of observation.

Under these conditions the penetrating particles could be mesons with rather large angular divergence and moderately low energies. This suggestion fits in well with a sort of cascade multiplication of the penetrating particles, which has passed its maximum before reaching 5000 meters' elevation. Intermediate particles involved in such cascade multiplication may be both nucleons and heavy mesons, as has been suggested by one of us.[13]

While the first alternative for resolving the

[13] K. Greisen, Phys. Rev. **73**, 521 (1948).

contradiction may seem more easily digestible, it meets with difficulty in accounting for the experimental results of Cocconi,[7] Janossy, and Broadbent,[8] and Salvini and Tagliaferri,[9] who found that the number of penetrating particles in extensive air showers, recorded under absorbers of different atomic number, was independent of Z. As has been pointed out by Ferretti,[14] this would imply a cross section for meson production proportional to Z^2.

[14] B. Ferretti, Nuovo Cimento **3**, 301 (1946).

The authors wish to thank Professor H. A. Bethe and especially Dr. G. Cocconi for helpful discussions of the problems associated with air showers. They are grateful to Professors B. E. Cohn and M. Iona of Denver University for assistance in the arrangements for performing the experiment, and to the cosmic-ray group of M.I.T. for the supply of electrical power on Mt. Evans.

The work here reported was in part supported by the Office of Naval Research.

PHYSICAL REVIEW VOLUME 74, NUMBER 4 AUGUST 15, 1948

The Beta- and Gamma-Spectra of Gallium Irradiated by Slow Neutrons*

S. K. HAYNES

Oak Ridge National Laboratory, Oak Ridge, Tennessee and Vanderbilt University, Nashville, Tennessee

(Received April 28, 1948)

The beta- and gamma-ray spectra of gallium irradiated with slow neutrons have been investigated with a thin-magnetic-lens spectrometer. Probable beta-ray end points for Ga^{72} at 3.15 Mev (9.5 percent), 2.52 Mev (8 percent), 1.48 Mev (10.5 percent), 0.955 Mev (32 percent), and 0.64 Mev (40 percent) were found. A conversion line occurring in about 0.5 percent of the disintegrations was observed at 0.68 Mev. Gamma-rays of 2.51 Mev (26.5 percent), 2.21 Mev (33 percent), 1.87 Mev (7.8 percent), 1.59 Mev (4.5 percent), 1.05 Mev (4.5 percent), 0.84 Mev (100 percent), and 0.63 Mev (24 percent) were also found for Ga^{72}. A nearly complete decay scheme for Ga^{72} is suggested.

The beta-ray spectrum of Ga^{70} (20.5 min.) has also been observed with the spectrometer. The Kurie plot is linear from the end point of 1.65 Mev to 0.4 Mev. No evidence of conversion lines in this energy interval was found.

I. INTRODUCTION, Ga^{72}

IN 1935 Amaldi *et al.*[1] reported a 23-hour strong gamma-ray activity in gallium irradiated with a slow neutrons. Chemical identification, assignment of the activity to Ga^{72}, and accurate measurement of the half-life (14.1 hr) were accomplished by Sagane[2] who observed hard beta-radiation as well as the hard gamma-radiation. This isotope has also been produced by $Ga(d,p)$,[3] $Ge(n,p)$,[4] $Ge(d,\alpha)$[4] and by decay of the uranium fission product Zn^{72}.[5]

The maximum end point of the beta-ray spectrum was first reported to be 1.71 Mev by Sagane *et al.*[6] using a cloud chamber. Livingood and Seaborg,[7] using absorption methods, later reported an end point at 2.6 Mev. Siegel and Glendenin,[5] using absorption in Al, reported two groups of beta-rays with end points of 3.1 Mev (35 percent) and 0.8 Mev (65 percent) while Mitchell *et al.*[8] by the same method found 2.3 Mev and 0.77 Mev. In a preliminary report[9] on the present work in which a lens spectrometer was used, the author reported five apparent end points, 3.15 Mev (9.5 percent), 2.52 Mev (8 percent), 1.48 Mev (10.5 percent), 0.95 Mev

* All of the experimental work and a major portion of the analysis for this paper was performed under Contract W35-058 Eng 71 with the Atomic Energy Commission.

[1] E. Amaldi, O. Agostino, E. Fermi, B. Pontecorvo, F. Rasetti, and E. Segrè, Proc. Royal Soc. **A149**, 522 (1935).

[2] R. Sagane, Phys. Rev. **53**, 212 (1938); **55**, 31 (1939).

[3] J. J. Livingood and G. T. Seaborg, Phys. Rev. **54**, 51 (1938).

[4] R. Sagane, G. Miyamoto, and M. Ikawa, Phys. Rev. **59**, 904 (1941).

[5] J. M. Siegel and L. E. Glendenin, Rev. Mod. Phys. **18**, 513 (1946); CC-2835, June 1945; Plutonium Project Record Vol. **9B**, 7.1 (1946).

[6] R. Sagane, R. S. Kojima, and G. Miyamoto, Proc. Phys. Math. Soc. Japan **21**, 728 (1939).

[7] J. J. Livingood and G. T. Seaborg, Rev. Mod. Phys. **12**, 30 (1940).

[8] A. C. G. Mitchell, E. T. Jurney, and M. Ramsey, Phys. Rev. **71**, 324 (1947).

[9] S. K. Haynes, Report MonP-368, Clinton Laboratories, Sept. 1, 1947; also Phys. Rev. **73**, 187 (1948).

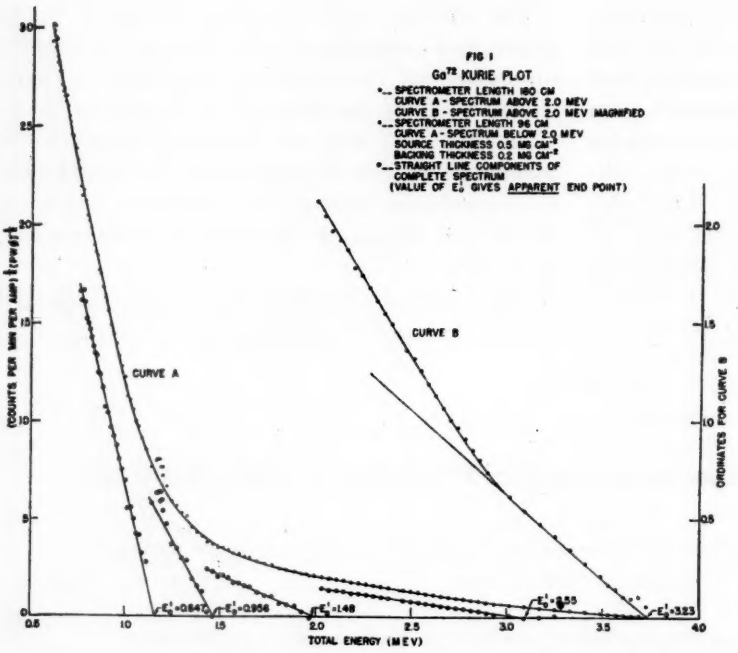
FIG 1
Ga72 KURIE PLOT
CURVE A - SPECTRUM ABOVE 2.0 MEV
CURVE B - SPECTRUM ABOVE 2.0 MEV MAGNIFIED
SPECTROMETER LENGTH 96 CM
CURVE A - SPECTRUM BELOW 2.0 MEV
SOURCE THICKNESS 0.5 MG CM-2
BACKING THICKNESS 0.2 MG CM-2
STRAIGHT LINE COMPONENTS OF COMPLETE SPECTRUM
(VALUE OF E0' GIVES APPARENT END POINT)
CURVE A
CURVE B
(COUNTS PER MIN PER ΔMP) (r/mg)2
ORDINATES FOR CURVE B
TOTAL ENERGY (MEV)

FIG. 1. Kurie Plot of the beta-radiation from Ga^{72} showing the resolution into five straight line components. The reality of the components cannot be judged from this curve alone. The energies of the upper two end points have not been corrected for resolving power.

(32 percent), and 0.64 Mev (40 percent), of which certainly all but perhaps the one at 1.48 Mev represented real end points. More recently, Mitchell *et al.*[10] have reported three end points at 3.09 Mev, 2.2 Mev, and 0.79 Mev.

Mandeville[11] first measured the gamma-rays using Compton recoils in a spectrometer. He found two of equal intensity at 1.17 Mev and 2.65 Mev. Miller and Curtiss[12] using photoelectrons in a lens spectrometer reported gamma-rays of 0.64 Mev, 0.84 Mev, and 2.25 Mev, with intensity ratios of roughly 1 to 6 to 6. Coincidence absorption measurements by Mitchell *et al.*[8] gave 2.4 Mev and 0.82 Mev for the gamma-rays. The same method used by Mandeville and Scherb[13] gave 2.29 Mev. Wattenberg[14] studying photoneutrons reported an energy of 2.50 Mev and at least one other line above the photoneutron threshold for Be. In the preliminary reports[9] of this work using a lens spectrometer lines were reported at 2.51 Mev (26 percent), 2.21 Mev (31.5 percent), 1.87 Mev (7.5 percent), 1.05 Mev (4.5 percent), 0.84 Mev (100 percent), 0.63 Mev (18.5 percent) and possibly one at 1.60 Mev (4.5 percent). Mitchell *et al.*,[10] also using a lens spectrometer, have reported gamma-rays at 0.64 Mev, 0.71 Mev, 0.84 Mev, 2.15 Mev and one of higher energy. Deutsch and Siegbahn[15] first observed a conversion line at 0.72 Mev. This was later reported by the author[9] as 0.68 Mev, and by Mitchell *et al.*[10] to be 0.71 Mev. Bowe, Goldhaber *et al.*[16] have found the half-life of this conversion line to be 0.5×10^{-6} sec. and believe it to arise from a $0\rightarrow0$ transition with no parity change and, therefore, to be 100 percent converted. If this interpretation of the conversion line is correct, the 0.71 Mev gamma-ray reported by Mitchell *et al.*,[10] if real, cannot be associated with the same transition as the conversion line.

Beta-gamma-coincidences as a function of beta-ray absorption[8,13] not only substantiate the complexity of the beta-ray spectrum but also indicate that very few if any of the beta-transitions go to the ground state of Ge^{72}. The latter conclusion is also supported by the figure of 2.6 Mev of gamma-ray energy per beta-particle given by Barker.[17]

[10] A. C. G. Mitchell, B. D. Kern and D. J. Zaffarano, Phys. Rev. **73**, 1220A (1948). *Note added in proof*: See Phys. Rev. **73**, 1431 (1948) for a fuller report of this work.
[11] C. E. Mandeville, Phys. Rev. **64**, 147 (1943).
[12] L. C. Miller and L. F. Curtiss, CP-3102, June 1945, and Phys. Rev. **70**, 983 (1946).
[13] C. E. Mandeville and M. Scherb, Phys. Rev. **72**, 520 (1947).
[14] A. Wattenberg, Phys. Rev. **71**, 497 (1947).
[15] M. Deutsch and K. Siegbahn, Private communication quoted in reference 15.
[16] J. C. Bowe, M. Goldhaber, R. D. Hill, W. E. Meyerhof, and O. Sala, Phys. Rev. **73**, 1219 (1948).
[17] E. C. Barker, Phys. Rev. **72**, 167 (1947).

This paper will present the experimental evidence both for the previously published conclusions[9] and for some new results which make it possible to suggest an almost complete decay scheme for Ga^{72}.

II. BETA-RAY SPECTRUM OF Ga^{72}

The beta-ray spectrum of Ga^{72} was run four times on a thin lens spectrometer under experimental conditions which differed as to source thickness, baffle system, and spectrometer length (distance from source to counter).

Two sources were used. Source *A* consisted of 1 mg/cm² gallium evaporated[18] onto 1 mil polystyrene (~3 mg/cm²). The layer of gallium was 9 mm in diameter and the polystyrene film 12 mm in diameter. After 16 hours irradiation in the Clinton pile, this source was cemented onto a thin walled lucite cylinder 12 mm in diameter and about 5 cm long which was mounted in the source holder of the spectrometer. Source *B* had the same diameter as source *A* and was prepared and irradiated in the same way. After removal from the pile the source was placed upside down on a 0.2 mg/cm² Formvar film 1 inch in diameter. The polystyrene and more than $\frac{2}{3}$ of its almost negligible activity were then dissolved off, leaving 0.5 mg/cm² of gallium on the Formvar film. In every case the 20 minute activity of Ga^{70} was allowed to decay completely before the Ga^{72} measurements were started.

Three baffle systems were used. Baffle system *A* was essentially that of Deutsch *et al.*[19] Baffle system *B* consisted of about 10 aluminum baffles with edges bevelled to present a minimum scattering surface to the beam. Notches which act as electron catchers were also machined in the surface of the central lead absorber. Baffle system *C* was similar to system *B* but arranged for a spectrometer length of 180 cm.

The 180 cm length was used to investigate the high energy end of the spectrum since the upper energy limit of the spectrometer with a length of 100 cm was 2.6 Mev. In all runs at 100 cm the inner and outer radii of the annular aperture were 6.6 cm and 7.6 cm respectively. With a 9 mm diameter source the resolving power was about 3.5 percent. In the run at 180 cm the radii of the aperture were 2.6 cm and 7.6 cm while the resolving power was about 10 percent. The counter window had a thickness of about 2.5 mg/cm² in all cases. Calibration of the spectrometer was made with annihilation radiation from Cu^{64} using photoelectrons from a gold radiator. The radiator was approximately 0.8 mg/cm² thick and of the same diameter as the gallium beta-ray sources. The spectrometer constant was also calculated from the coil constants and the calculated and measured values agreed to within less than one percent.

Figure 1 shows a Kurie plot of the complete beta-ray spectrum. The high energy portion was run with source *A* and spectrometer length of 180 cm while the low energy portion was run with source *B* and baffle-system *B*. In the course of the four runs (the other two were source *A*,

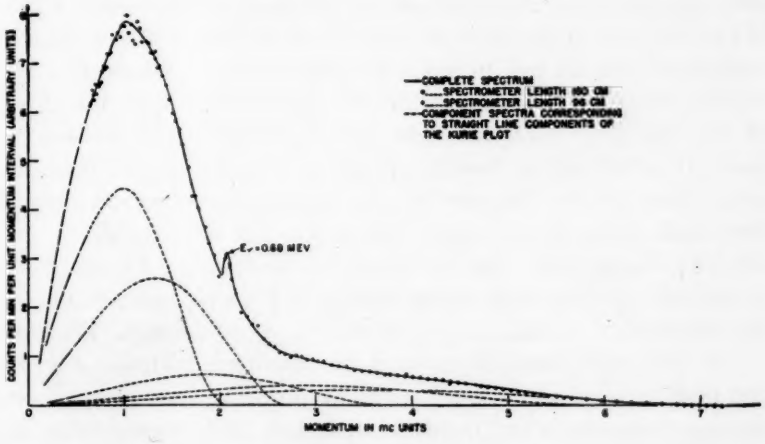

FIG. 2. Normal beta-ray spectrum of Ga^{72} showing the possible component spectra and the conversion line at 0.68 Mev.

[18] S. K. Haynes, Phys. Rev. **71**, 832 (1947).
[19] M. Deutsch, L. G. Elliott, and R. D. Evans, Rev. Sci. Inst. **15**, 179 (1944).

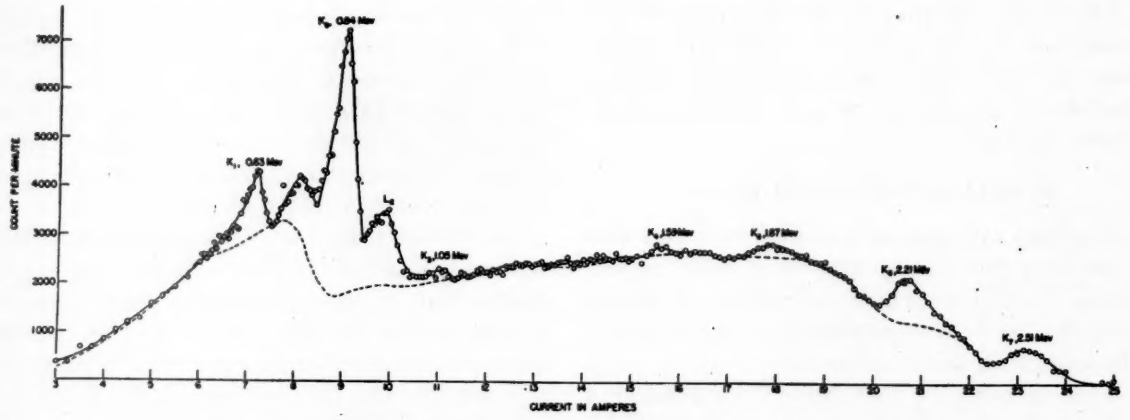

FIG. 3. Photoelectron plus Compton electron spectrum of Ga^{72} using a uranium radiator of thickness 74.9 mg/cm². Broken line shows the estimated background from the copper capsule.

Baffle-system *A* and source *A*, Baffle-system *B*) it was shown that the shape of this spectrum above 0.2 Mev is: (1) independent of change in source thickness, (2) independent of a change of baffle-system, and (3) has a half life of 14.1±0.5 hours at all points. In the first run the spectrum was observed five times over an interval of more than 30 hours. Spectroscopic analysis of the sources, observation (3), the known half lives, activation cross sections, and end points of possible impurities show that impurities cannot contribute appreciably to the spectrum. The spectrum shown in Fig. 1, above 0.2 Mev, is, therefore, characteristic of Ga^{72} and, except for finite resolving power, is independent of instrumental effects.

The curve obviously represents a complex beta-ray spectrum. Since the half life and energies of Ga^{72} are not in the allowed range, each of the component spectra has an unknown shape which renders difficult, if not impossible, the separation of the complete spectrum into its component parts. It is instructive, however, to see how many end points can be obtained on the assumption that each component beta-particle group has a straight Kurie plot. By the usual method of extraction the five end points shown in Fig. 1 are obtained.

The two upper energies given in the figure are too high because of the poor resolving power of the spectrometer when the 180 cm length and full aperture were used and because of the short energy interval (less than 20 percent of the full energy) available for drawing the straight Kurie line. The upper energy was corrected by assuming a Gaussian resolving function with a 10 percent half-width and applying it to a linear Kurie plot. The best straight line was drawn through the upper 20 percent of the resulting curve. The difference between the resulting end point and the original assumed end point gives the correction to be subtracted which in this case was 0.08 Mev. The corrected Kurie line was then used in a redetermination of the second highest end point. The corrected value of the latter was 2.52 Mev as against the initial value of 2.55 Mev. The corrected energies for the two upper end points and the *average* of four runs for the three lower end points are as follows: 3.15 Mev (9.5 percent), 2.52 Mev (8 percent), 1.48 Mev (10.5 percent), 0.955 Mev (32 percent), and 0.64 Mev (40 percent). These intensities are based on the assumption of a straight line Kurie plot and may, therefore, be subject to correction; in fact, the decision as to the existence of all these end points must depend on the gamma-ray spectrum and on coincidence measurements, if such are feasible.

Figure 2 shows the plot of counts per unit momentum interval against momentum in mc units. The conversion line which appears at 0.68 Mev in Fig. 1 can be shown from Fig. 2 to occur in approximately 0.5 percent of the disintegrations. Each of the five straight line components of the Kurie plot is shown by a broken line in Fig. 2.

III. GAMMA-RAY ENERGIES OF Ga^{72}

The gamma-ray source of Ga^{72} consisted of a cylinder of metallic gallium 0.140-inch in diameter and 0.070-inch in length. The temperature of this cylinder was kept below its melting point of 30°C during all manipulations. After irradiation in the pile to a source strength of 10 to 20 millicuries the solid metallic gallium was transferred to a cylindrical copper capsule with side wall thickness of 0.025-inch and an end wall thickness of 0.060-inch. These thicknesses were the smallest which were sufficient to stop all beta-rays which could enter the spectrometer and hence gave a minimum background of Compton electrons. Complete runs were made with the gallium filled capsule alone and also with a uranium radiator of the same diameter as the capsule (0.190-inch) and 74.9 mg/cm² thick. Partial runs were made with uranium radiators[20] 12.8 mg/cm², 21.9 mg/cm², and 42.2 mg/cm² thick. Calibration runs on annihilation radiation from Cu^{64} were made with uranium radiators of 12.8 mg/cm², 21.9 mg/cm², 74.9 mg/cm² and with a gold radiator of 0.8 mg/cm². One run was made on Na^{24} with a uranium radiator of 74.9 mg/cm² in order better to understand the shape of the photoelectron lines and of the Compton distributions from two widely separated gamma-rays of equal intensity. Observations of this type on other elements were prevented by lack of time.

In Fig. 3 the Compton plus photoelectron counting rate using a 74.9 mg/cm² uranium radiator is plotted against lens current which is proportional to electron momentum. Points were taken at currents separated by about 0.5 percent and about 10^4 counts were taken per point except between 18.5 and 14.5 amp. Each of the points between 18.5 and 16.5 amperes represents the average of six runs or a total of about 6×10^4 counts per point. Two additional runs were made from 16.5 to 14.5 amperes (not included in Fig. 3) as well as one extra run on the Compton distribution in order to decide whether or not a line existed at 1.59 Mev. Figure 4 shows the photoelectron spectrum alone (including all the data between 16.5 and 14.5 amp) obtained by subtracting the Compton distribution. This subtraction is not as straightforward as it might appear, for a uranium radiator of thickness 74.9 mg/cm² scatters the Compton electrons coming from the copper in such a manner as to reduce

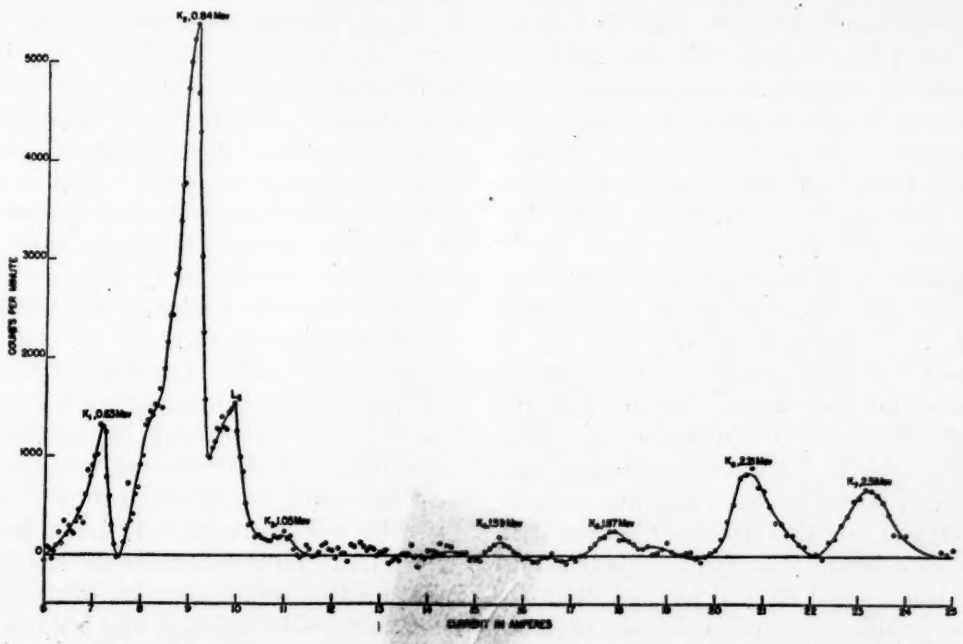

FIG. 4. Photoelectron spectrum of Ga^{72} from a uranium radiator of thickness 74.9 mg/cm².

[20] The author wishes to express his indebtedness to Dr. L. F. Curtiss of the Bureau of Standards for the uranium foil from which these radiators were made.

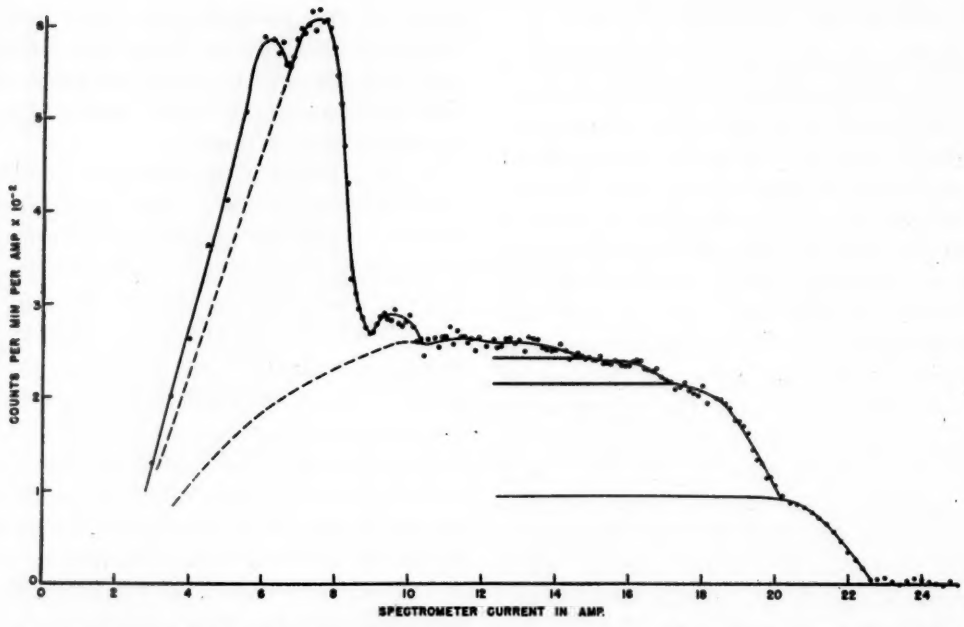

FIG. 5. Electron distribution from Ga^{72} in a bare copper capsule. Each counting rate has been divided by the current to get counts per unit momentum interval.

the Compton counting rate (evaluated in between the photoelectron lines) to about 70 percent of its value with no uranium radiator. Enough points between lines were available to establish the amount to be subtracted to within less than 100 counts per min. from 25 amp to 11 amp and below 6 amp. Since no reference points could be found between 6 and 11 amp, the amount to be subtracted in this region may be off by several hundred counts per minute, particularly below 8.5 amp where the Compton electrons from the strong line at 0.84 Mev become very important.

The data shown in Fig. 4 are fairly conclusive evidence for the existence of the seven lines indicated. It is extremely unlikely that any of these lines could arise from an impurity for the whole curve has been shown to decay with the 14.1 hour half-life of Ga^{72}. Moreover, an examination of a table of the known radioactive elements reveals that none has a half-life, gamma-ray spectrum, activation cross section and probable abundance (as shown by spectroscopic analysis) which could account for these lines.

Further evidence for the existence of these lines and also further information about their relative intensities can be obtained by comparing the electron distribution (chiefly Compton) from Ga^{72} in the bare copper capsule with that of Na^{24} with a 74.9 mg/cm² radiator. Figure 5 shows the curve of counts per unit current against current for Ga^{72} in a bare copper capsule. The Compton distributions of the four strongest gamma-rays are clearly evident. The corresponding curve for Na^{24}, Fig. 6, shows that: (1) the Compton distribution from the 2.76 Mev line is horizontal from 22 amp (~2.3 Mev) to 13 amp (~1.2 Mev) where it begins to turn downward toward the origin; (2) the height of the Compton distribution at its maximum is roughly proportional to the intensity of the gamma-ray from 22 amp (~2.3 Mev) at least to 11 amp (~1.0 Mev). The fact that the Compton distribution from Ga^{72} is not horizontal between 17 amp where it should level off for the 2.21 Mev gamma-ray and 13 amp is strong evidence for the existence of at least two weak gamma-rays in this interval. By comparison with the curve for Na^{24}, the approximate horizontal levels indicated by the curve of Fig. 5 have been drawn in. It should be strongly emphasized that the shape of the steps in Fig. 5 is not justified by the accuracy of the points but is necessitated by the fact that a single gamma-ray can only give a step function with a horizontal or declining top as shown by the curve for Na^{24}. The upward trend between 17 amp and 13

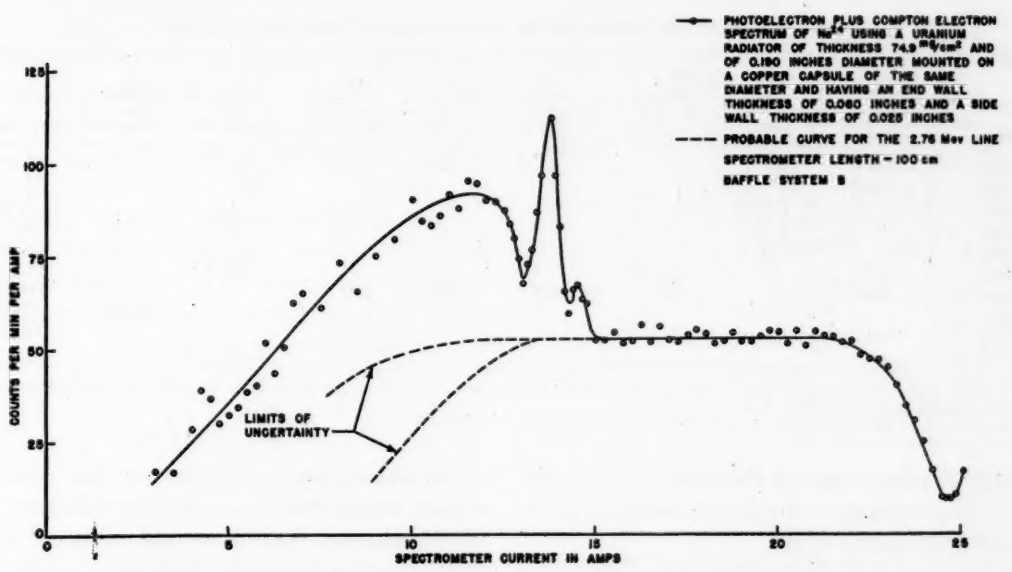
PHOTOELECTRON PLUS COMPTON ELECTRON SPECTRUM OF Na24 USING A URANIUM RADIATOR OF THICKNESS 74.9 mg/cm2 AND OF 0.190 INCHES DIAMETER MOUNTED ON A COPPER CAPSULE OF THE SAME DIAMETER AND HAVING AN END WALL THICKNESS OF 0.060 INCHES AND A SIDE WALL THICKNESS OF 0.025 INCHES
PROBABLE CURVE FOR THE 2.76 Mev LINE
SPECTROMETER LENGTH = 100 cm
BAFFLE SYSTEM B
COUNTS PER MIN PER AMP
LIMITS OF UNCERTAINTY
SPECTROMETER CURRENT IN AMPS

FIG. 6. Photoelectron plus Compton electron spectrum of Na^{24} showing the horizontal top of the Compton distribution from the 2.76 Mev line. Each counting rate has been divided by the current to get counts per unit momentum interval.

amp in Fig. 5 is well outside of experimental error. The energies of the gamma-rays deduced from the Compton end points shown are not very accurate but are in agreement within experimental error with those obtained from the photoelectron lines. The possibility of a very weak additional gamma-ray is indicated by the fact that between 13 amp and 10 amp the curve does not begin to fall as does the sodium curve. The energy of this gamma-ray would be about 1.2 Mev. However, much more data would be necessary to establish its existence beyond doubt. The rounded peak between 9 and 10 amp is attributed in part to the copper photoelectron yield of the strong 0.84 Mev line and to a lesser extent to the Compton distribution of the weak 1.05 Mev line.

In order to separate the lines below one million electron volts, a run was made with the 12.8 mg/cm² thick uranium radiator. The results are shown in Fig. 7 where the background of Compton electrons from the bare copper has been subtracted out. If a photoelectron line exists corresponding to the 0.68 Mev transition observed in the beta-ray spectrum its intensity is probably less than two percent, indicating a minimum conversion coefficient of the order of 25 percent. This photoelectron line would be difficult to detect for it falls very close to the maximum of the Compton distribution of the 0.84 Mev line and not far from the L shell photoelectron line of the 0.63 Mev gamma-ray line. These results are not in contradiction with the hypothesis of a 0→0 transition with no parity change since the conversion coefficient may well be 100 percent. When considered in conjunction with its half life $(0.5\times10^{-6}$ sec)[16] and energy,

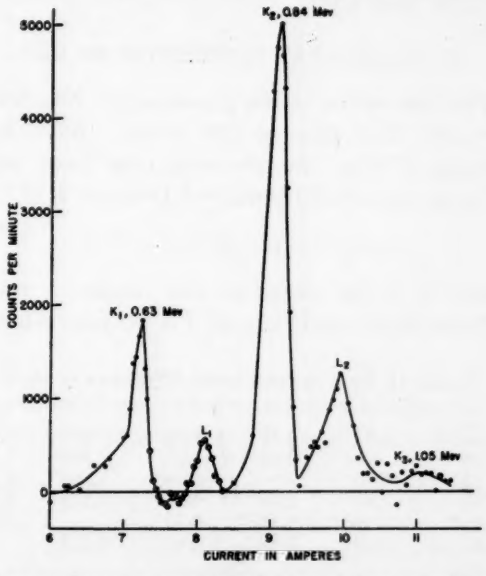

FIG. 7. Photoelectron distribution at low energies with a uranium radiator of thickness 12.8 mg/cm². Open circles represent three times as much data as full black circles.

TABLE I. Gamma-ray intensities of Ga^{72} in percent of the 0.84 Mev line.†

Line	1 Compton	2 Compton*	3 Photo 12.8 mg/cm²	4 Photo 21.9 mg/cm²	5 Photo 42.2 mg/cm²	6 Photo 74.9 mg/cm²	7 Photo 74.9 mg/cm²*	8 Conversion line	9 Average
2.51 Mev	(24)	26.5*		31.5	23	(26.5)	26.5*		26.5±4%*
2.21 Mev		34*					32*		33 ±5%*
1.87 Mev		7.9*					7.6*		7.8±2%*
1.59 Mev		4.5*					4.6*		4.5±2%*
(1.20) Mev?		(<2)*							(<2%)*
1.05 Mev			((4.2))				(4.6)*		(4.5±2%)*
0.84 Mev	100		100	100	100	100			100%
0.68 Mev			(<2)					0.5%	<2%
0.63 Mev	(31)		24			(18.5)			24±5%

† One or more parentheses about a figure indicates one or more known uncertainties in the figure. In averaging, each parentheses reduce the weight of the observation by a factor of 2.
* Figures so denoted are based upon a 26.5 percent intensity of the 2.51 Mev line.

the order of magnitude of the conversion coefficient of this transition eliminates assignment to it of any finite value of Δl.

The energies of the gamma-rays given in Table I were obtained from the complete run with a 74.9 mg/cm² uranium radiator. Corrections of the order of 0.5 percent were subtracted from the several lines of highest energy as a result of analysis of the positions of the photoelectron lines in the following runs: (1) the four calibration runs with annihilation radiation mentioned above, (2) runs with 74.9 mg/cm², 42.2 mg/cm², 21.9 mg/cm² and 12.8 mg/cm² uranium radiators on the 0.84 Mev line, and (3) runs with all but the 12.8 mg/cm² radiator on the 2.51 Mev line.

IV. GAMMA-RAY INTENSITIES OF Ga^{72}

The intensities of the gamma-rays relative to the 0.84 Mev line as 100 percent have been calculated from the photoelectron lines using the semi-empirical formula of Deutsch *et al.*[21]

$$n_p = Ct_r\tau[(kt_r/\beta^3\Delta p)^2+1]^{-\frac{1}{2}} \qquad (1)$$

where n_p is the observed line height, t_r is the radiator thickness in g/cm², τ is the photoelectric mass absorption coefficient for the gamma-ray under consideration, β is the velocity of the photoelectron relative to the velocity of light, Δp is the momentum resolution width of the spectrometer, and k and C are empirical constants. The constant k was determined for the 0.84 Mev line and the 2.51 Mev line by use of radiators of several thicknesses.

TABLE II. Beta-ray end point differences in Mev.

Beta-ray	3.15	2.52	1.48	0.955	0.64
3.15	—	0.63*	1.67	2.205*	2.51*
2.52	0.63*	—	1.04*	1.565*	1.88*
1.48	1.67	1.04*	—	0.525	0.84*
0.955	2.205*	1.565*	0.525	—	0.315
0.64	2.51*	1.88*	0.84*	0.315	—

The intensities have also been calculated from the maximum height of the Compton distribution in accord with observations on Na^{24}. Each of these methods applied respectively to the complete runs with 74.9 mg/cm² U radiator and with no radiator should give the relative intensities of the lines above 1.5 Mev fairly accurately. Neither will give an accurate comparison between this group of lines and the 0.84 Mev line for the following reasons: (1) For the complete photoelectron spectrum with the 74.9 mg/cm² radiator, the height of the photoelectron lines below one Mev is an unreliable index of intensity both because the Compton background is uncertain in this region and because Eq. (1) has not been adequately tested for such a thick radiator in this region. (2) Since no test of the relative heights of Compton distributions with lines of known intensity below one Mev was made with the geometry used in these experiments the maximum heights of the Compton distributions may not be a reliable measure of intensity in this range.

The two runs on the 0.84 Mev and the 2.51 Mev lines with uranium radiators of 42.2 mg/cm² and 21.9 mg/cm² are within the range in which Eq. (1) may be expected to hold. The intensity of the 2.51 Mev line relative to

[21] M. Deutsch, L. G. Elliott, and R. D. Evans, Rev. Sci. Inst. 15, 193 (1944).

the 0.84 Mev line was chiefly obtained from these two runs with less weight given to the determinations with the 74.9 mg/cm² radiator and the relative heights of the Compton distributions as shown in Table I, columns 1, 4, 5, 6, and 9.

Using the value of 26.5 percent for the intensity of the 2.51 Mev line, the intensities of the lines at 2.21 Mev, 1.87 Mev, and 1.59 Mev are readily obtained as shown in columns 2 and 7 of Table I. The excellent agreement in the relative intensities in columns 2 and 7 is very strong evidence for the existence of the lines at 1.87 Mev and 1.59 Mev. The intensity of the 1.05 Mev line cannot be obtained from the Compton distribution because the copper photoelectron yield of the 0.84 Mev line also falls between 9 and 10 amperes. It can be roughly estimated from the runs with the 12.8 mg/cm² and 74.9 mg/cm² radiators as shown in columns 3 and 7 of Table I. The intensity of the 0.68 Mev line is less than 2 percent as previously discussed and as shown in column 3 of the table. The most accurate value for the intensity of the 0.63 Mev line is that obtained from the 12.8 mg/cm² radiator, for with this radiator not only does Eq. (1) hold but the Compton background is observable between lines. Less reliable figures are obtained from the Compton distribution and also from the data taken with the 74.9 mg/cm² radiator (previously published).[9]

V. DECAY SCHEME AND DISCUSSION

As stated in Section II the Kurie plot of the beta-ray spectrum can be separated into five linear components with the following end points and intensities: 3.15 Mev (9.5 percent), 2.52 Mev (8 percent), 1.48 Mev (10.5 percent), 0.955 Mev (32 percent), and 0.64 Mev (40 percent). In order to get an indication of the validity of these apparent end points, all possible energy differences between them are taken and compared with the gamma-ray energies (Table II). The differences indicated by an asterisk in Table II correspond closely to gamma-ray energies in Table I. On each line the values to the right of the blank diagonal represent transitions into the state determined by the end point at the left hand end of the line while values to the left of the diagonal represent transitions out of this

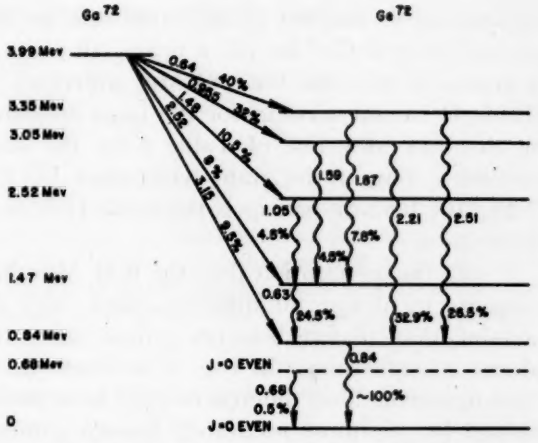

FIG. 8. A nearly complete proposed decay scheme for Ga^{72}.

state. Every energy of beta-ray has at least two differences associated with it which correspond to gamma-ray energies. Hence, as a preliminary hypothesis, all five beta-ray groups will be assumed to exist.[22]

The difference between the highest and lowest energy beta-ray end points is about 2.5 Mev and since Barker[17] has obtained a figure of 2.6 Mev of gamma-ray energy per beta-particle, it follows that none of the beta-ray groups reported here can go to the ground state of Ge^{72}. As stated above, this inference is also supported by coincidence work.[8,13] The most logical assumption is, therefore, that the very intense 0.84 Mev

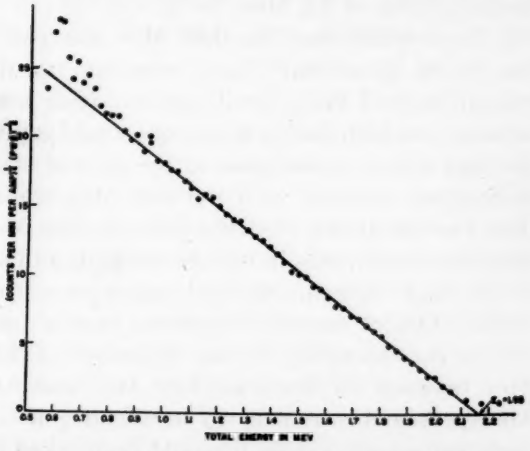

FIG. 9. A Kurie Plot of the Ga^{70} beta-ray spectrum.

[22] Further support for the existence of the 1.48 Mev beta-ray group comes by private communication from M. Goldhaber who finds that the beta-rays which precede the 0.68 Mev delayed conversion electrons seem to have an end point at roughly 1.5 Mev. No delayed gamma-rays were found.

gamma-ray is emitted in the transition to the ground state of Ge^{72} for all or nearly all disintegrations. In any case the 0.84 Mev difference in Table II cannot account for the large intensity of the 0.84 Mev line of Table I for the only transition out of the state terminated by the 1.48 Mev beta-ray group is the weak 1.05 Mev gamma-ray.

Using the assumption that the 0.84 Mev line appears in almost all disintegrations, and assuming that all five beta-ray groups exist, the decay scheme shown in Fig. 8 is obtained. In this figure the level differences have been determined by the most accurately known gamma-rays and the intensities of both beta-ray groups and gamma-ray lines are those reported above. The agreement between beta-ray end points and level values is excellent while the agreement between the incoming and outgoing intensities of each state is surprisingly good. It would appear that the 1.48 Mev beta-ray group is not as intense as the linear Kurie-plot would indicate and that some of the beta transitions assigned to this group actually belong to the 3.15 Mev group. Probably some of the transitions assigned by linear Kurie plot to the 0.64 Mev group actually belong to the 0.955 Mev group. The value obtained for the average gamma-ray energy per beta-particle from Table I and Fig. 8 is 2.64 $\pm$0.16 Mev which is in good agreement with Barker's value of 2.6 Mev.[17]

It is probable that the 0.68 Mev conversion line (0$\rightarrow$0 transition)[16] is a transition to the ground state of Ga^{72}, for if the transition were between two high energy levels, one would expect the high energy transitions to the ground state to compete strongly with the 0.68 Mev transition. Further strong evidence that the 0.68 Mev transition terminates in the ground state of Ge^{72} is the fact that no delayed gamma-rays are found.[22] One or more weak gamma-rays of total energy corresponding to the difference of 1.84 Mev between the levels at 2.52 Mev and 0.68 Mev presumably remain to be found.[22] If one such gamma-ray exists, it would be masked by the stronger line at 1.87 Mev. If the 1.2 Mev line of Table I actually exists, an additional weak line between 0.65 and 0.75 Mev probably also is present. Such a line has been reported by Mitchell *et al.*[10]

No coincidence experiments were performed on Ga^{72}. For verification of such a complicated decay scheme, it appears that coincidence experiments involving one or more spectrometers will be necessary. More accurate data on gamma-ray intensities will also be helpful.

VI. BETA-RAY SPECTRUM OF Ga^{70}

In the course of the work on Ga^{72} it was possible to make two 20 minute irradiations of Source *A* and to investigate the beta-ray spectrum of Ga^{70} (20.5 min. half life).[23] After inserting the source in the spectrometer as rapidly as possible, the lens current was varied in steps of 0.25 amp while counts were recorded during 0.5 min at each step. More than one step per minute was made so that the complete spectrum was run in about an hour (three half lives). The spectrum was then rerun in order to establish the amount of 14.1 hour activity to be subtracted out. One run was made from high energy to low and one from low to high. The Kurie plot of the resulting spectrum (Fig. 9) has an end point at 1.65 Mev and is linear down to about 0.4 Mev. Further investigation would be necessary to ascertain whether the deviation from a straight line below 0.4 Mev is due to scattering, another group of beta-rays, or non-linearity of the Kurie plot of the 1.65 Mev beta-ray group. No conversion lines were detected above 0.6 Mev. Below this energy the spacing and accuracy of the experimental points are not sufficient to show conversion lines. No attempt to measure the gamma-ray spectrum of Ga^{70} was made.

VII. ACKNOWLEDGMENTS

The author wishes to express his appreciation to many members of the staff both at Clinton National Laboratory and at Vanderbilt University for their help and advice. Particular recognition is due Dr. A. H. Snell who suggested the problem and whose continued counsel was of very great value. Many helpful discussions were held with Dr. E. Greuling and Mr. P. W. Levy. Special thanks are due to Miss T. Arnette who helped operate the spectrometer and made many calculations.

[23] E. C. Barker, private communication.

PHYSICAL REVIEW VOLUME 74, NUMBER 4 AUGUST 15, 1948

Phenomenological Theory of Exchange Currents in Nuclei

R. G. SACHS
University of Wisconsin, Madison, Wisconsin
(Received May 10, 1948)

On the assumption that the interaction between nuclear particles involves a space exchange operator, it is shown that an addition must be made to the conventional current density for the nucleons in order to establish the equation of continuity within the nucleus. A general expression is found for this exchange current and the corresponding exchange magnetic moment. This phenomenological theory has application to the calculation of magnetic moments of nuclei and to the calculation of transition probabilities for the absorption and emission of radiation by nuclei. In this paper, application is limited to the exchange moments of H^3 and He^3. It is found that the exchange moments are six or seven times too small to account for the observed moments. In view of results obtained by Villars, it is concluded that the important contributions to the magnetic moment are directly related to the properties of the field (meson field) which describes the nuclear interaction, so the exchange moment may be of use for obtaining direct information concerning the nature of this field.

I. INTRODUCTION

As a result of recent measurements[1] of the magnetic moments of the nuclear three-body systems H^3 and He^3, consideration has been given to the possibility that there exist exchange currents in nuclei.[2] The term exchange current is used here to denote the net flow of charge between nucleons which may be considered to be a consequence of the charge exchange nature of their interaction potentials. A current of this type is expected to introduce a contribution to the magnetic moment with the result that the magnetic moments of nuclear systems could not, in general, be obtained by simply adding the spin and orbital contributions of the nucleons.

It was first suggested by Siegert[3,4] that the existence of exchange forces in nuclei implies the existence of an exchange current. He showed that under certain circumstances, one would expect the exchange current to be proportional to the exchange potential. The arguments presented by Siegert were based on a field theoretical description of the nuclear interaction, although his final result is independent of the properties of the nuclear field other than the interaction potential it produces. This suggests strongly that Siegert's exchange current is a property associated with the exchange potential which is quite independent of the nature of the field producing the potential. It will be shown below that this is indeed the case.

It is not to be assumed that this is the only contribution to the exchange current. For example, the anomalous contributions to the magnetic moments of the neutron and proton may be due to a charge bearing field, and the corresponding currents may be to some extent independent of the neutron-proton interaction potential. In general, then, one expects the exchange current to contain two terms, one depending in some way on the details of the field describing the interactions between nucleons.

Villars[2] has shown that for a specific type of nuclear field (pseudoscalar symmetric) one can account for the observed exchange moment of H^3 and He^3. It is to be expected that other types of field could also account for the observations.[5] In spite of the apparent agreement, the situation cannot be considered to be completely satisfactory because the field theories lead to unsatisfactory interaction potentials. An explanation of the exchange moments based on the "field independent" exchange current described above would not labor under this difficulty since it can be directly expressed in terms of the phenomenological potentials. Therefore, the contribution of this exchange current to the magnetic moments of H^3 and He^3 is estimated below. It is found that the result is not in agreement with observa-

[1] H. L. Anderson and A. Novick, Phys. Rev. **71**, 372 (1947); *ibid.* **73**, 919 (1948); F. Bloch, A. C. Graves, M. Packard, and R. W. Spence, *ibid.* **71**, 373, 551 (1947).
[2] F. Villars, Phys. Rev. **72**, 256 (1947); Helv. Phys. Acta **20**, 476 (1947).
[3] A. F. Siegert, Phys. Rev. **52**, 787 (1937).
[4] W. E. Lamb and L. I. Schiff, Phys. Rev. **53**, 651 (1938).
[5] A. Thellung and F. Villars, Phys. Rev. **73**, 924 (1948), have considered vector fields and a Møller-Rosenfeld mixture with negative results.

tions, so one may conclude that the exchange currents do depend in a detailed way on the nature of the nuclear fields. This would seem to indicate that the exchange moments may be a means for determining experimentally the transformation properties of the nuclear fields. However, a satisfactory comparison of this nature does not seem feasible until there is developed a field theory that leads to reasonable interaction potentials which may then be used to fix the constants in the theory.

In order to establish the relationship between exchange current and exchange potential, use will be made of Wheeler's velocity dependent formulation of the exchange potential.[6] The resulting theory of the interaction between the nuclear system and the electromagnetic field is applicable to radiation problems as well as to the magnetic moment problem. The consequences of the theory with respect to the emission and absorption of radiation by nuclei have not been investigated but it is hoped that that investigation will be carried out in time.

II. FORMULATION OF THE PROBLEM

We consider only the Majorana type of exchange interaction since it can be shown that a spin exchange operator in the interaction does not introduce any additional contributions to the exchange current. The exchange operator will be denoted by P_{jk}; this operator exchanges the position coordinates of the jth and kth particles.

If the usual expression of the equation of continuity which arises from the Schroedinger equation is considered, it becomes immediately obvious that an exchange potential requires the addition of a term in the exchange current. In the usual way we find

$$\frac{\partial}{\partial t}|\psi|^2+(ih/2M)\sum_j \operatorname{div}_j(\psi \operatorname{grad}_j\psi^*-\psi^* \operatorname{grad}_j\psi) = (i/h)(\psi V\psi^*-\psi^* V\psi). \quad (1)$$

For ordinary potentials the expression on the right vanishes, but for exchange potentials of the form $V=\sum J_{jk}P_{jk}$, with $J_{jk}=J(\mathbf{r}_j-\mathbf{r}_k)$, it will not vanish except for very special types of wave function. However, in the special case of the deuteron, it will always vanish since the wave functions are necessarily either symmetric or antisymmetric for interchange of the two nucleons. The wave functions of other nuclei will usually contain both symmetric and antisymmetric terms.

Although Eq. (1) shows clearly that the exchange current can be expected to depend directly on the exchange potential, it is not the most convenient form for establishing the exact relationship. For that purpose we look into the question of the gauge invariance of the Schroedinger equation involving exchange potentials.

It is well known that gauge invariance usually implies charge conservation. Stated more precisely, if it is possible to obtain the field equations (Schroedinger equation) from a gauge invariant Lagrangian, then a "natural" expression for the current density can usually be obtained by applying an infinitesimal gauge transformation to the Lagrangian and identifying the equation resulting from invariance under this transformation with the equation of continuity for charge and current.

If, then, the Schroedinger equation involving an exchange potential can be obtained from a Lagrangian formalism, the requirement of gauge invariance will lead directly to an expression for the exchange current. The problem is, therefore, reduced to that of obtaining the Lagrangian which will properly describe the exchange interactions between nucleons in the presence of an external electromagnetic field.

III. THE LAGRANGIAN DENSITY

In the absence of external fields, the Lagrangian density, L, may be taken to be

$$L=-ih(\psi, \partial\psi/\partial t) +\sum_k(h^2/2m_k)(\operatorname{grad}_k\psi, \operatorname{grad}_k\psi) +\sum_k\sum_{j<k}(\psi, J_{jk}P_{jk}\psi), \quad (2)$$

where the labels j and k denote particular nucleons and J_{jk} is the potential function which depends on the distance between the particles j and k and may be an operator involving the spins of those particles. The scalar product notation includes only the sum over spin coordinates; thus $(\psi, \partial\psi/\partial t)=\sum_\sigma\psi_\sigma^*\partial\psi_\sigma/\partial t$, etc. The condition

$$\delta\int L dt d\tau_1 d\tau_2\cdots d\tau_N=0, \quad (3)$$

[6] J. A. Wheeler, Phys. Rev. **50**, 643 (1936).

in which ψ^* is varied but ψ is kept constant, clearly leads to the Schroedinger equation

$$i\hbar\partial\psi/\partial t = -\sum_k(\hbar^2/2m_k)\nabla_k^2\psi + \sum_k\sum_{j<k} J_{jk}P_{jk}\psi, \quad (4)$$

which is the required form. The conjugate complex of Eq. (4) is obtained if ψ is varied and ψ^* is held fixed in Eq. (3). To show this it is necessary to note that

$$\int(\psi, J_{jk}P_{jk}\delta\psi)d\tau_j d\tau_k = \int(J_{jk}P_{jk}\psi, \delta\psi)d\tau_k d\tau_j \quad (5)$$

in virtue of the symmetry of the integration with respect to the variables $\mathbf{r}_j$ and $\mathbf{r}_k$. It is assumed, of course, that J_{jk} is symmetric in the coordinates of the two particles and Hermitian.

In the presence of an external electromagnetic field described by a vector potential $\mathbf{A}$ and a scalar potential φ, the first two terms in the Lagrangian density given by Eq. (2) are to be modified by the substitution

$$\begin{aligned}&\mathrm{grad}_k\psi\rightarrow\mathrm{grad}_k\psi-(ie_k/\hbar c)\mathbf{A}_k\psi,\\ &\frac{\partial\psi}{\partial t}\rightarrow\frac{\partial\psi}{\partial t}+(i/\hbar)\sum_k e_k\varphi_k\psi,\end{aligned} \quad (6)$$

where e_k is the charge of the kth particle (e for protons, 0 for neutrons) and $\mathbf{A}_k=\mathbf{A}(\mathbf{r}_k)$, $\varphi_k=\varphi(\mathbf{r}_k)$. Then these two terms are invariant under the gauge transformation

$$\begin{aligned}&\mathbf{A}\rightarrow\mathbf{A}+\mathrm{grad}G, \quad \varphi\rightarrow\varphi-\partial G/\partial(ct),\\ &\psi\rightarrow\psi e\{i\sum_k e_kG_k/\hbar c\},\end{aligned} \quad (7)$$

where $G_k=G(\mathbf{r}_k)$ and $e\{x\}$ is used to denote e^x.

The third term in the Lagrangian Eq. (2) is certainly not gauge invariant as it stands since

$$P_{jk}\psi e\{i\sum_m e_mG_m/\hbar c\} = e\{(i/\hbar c)(\sum_{m\neq j,k}e_mG_m+e_jG_k+e_kG_j)\}P_{jk}\psi.$$

Only those terms for which $e_j=e_k$ (i.e., involving exchange of two protons or two neutrons) behave in such a way as to leave $(\psi, J_{jk}P_{jk}\psi)$ unchanged. In order to obtain the appropriate gauge-invariant modification of this term it is convenient to express the exchange operator as a differential operator as proposed by Wheeler.[6] Wheeler called attention to the fact that the function $P_{jk}\psi(\mathbf{r}_j, \mathbf{r}_k)$ may be expanded in Taylor series about the point $(\mathbf{r}_j, \mathbf{r}_k)$ with the result:

$$\begin{aligned}P_{jk}\psi=\sum_{(n)}(-1)^{n_4+n_5+n_6}&\times\frac{(x_k-x_j)^{n_1+n_4}(y_k-y_j)^{n_2+n_5}(z_k-z_j)^{n_3+n_6}}{n_1!n_2!n_3!_4!n_5!n_6!}\\ &\times\left(\frac{\partial}{\partial x_j}\right)^{n_1}\left(\frac{\partial}{\partial y_j}\right)^{n_2}\left(\frac{\partial}{\partial z_j}\right)^{n_3}\\ &\times\left(\frac{\partial}{\partial x_k}\right)^{n_4}\left(\frac{\partial}{\partial y_k}\right)^{n_5}\left(\frac{\partial}{\partial z_k}\right)^{n_6}\psi.\end{aligned}$$

It is to be noted that this equation may be put into simpler form by treating $\mathbf{r}_{kj}$ and $\mathbf{r}_{jk}$ as constant vectors in the equation

$$P_{jk}\psi=\sum_n\frac{1}{n!}(\mathbf{r}_{kj}\cdot\mathrm{grad}_j+\mathbf{r}_{jk}\cdot\mathrm{grad}_k)^n\psi, \quad (8)$$

and setting

$$\mathbf{r}_{kj}=\mathbf{r}_k-\mathbf{r}_j, \quad \mathbf{r}_{jk}=\mathbf{r}_j-\mathbf{r}_k=-\mathbf{r}_{kj}, \quad (9)$$

after each term in the series has been expanded. If we now denote by D_{kj} the differential operator $(\mathbf{r}_{kj}\cdot\mathrm{grad}_j)$, Eq. (8) takes the simple operational form

$$P_{jk}\psi=e\{D_{kj}+D_{jk}\}\psi. \quad (10)$$

Using this operator, the last term in the Lagrangian is given by

$$L_P=\sum_k\sum_{j<k}(\psi, J_{jk}e\{D_{kj}+D_{jk}\}\psi). \quad (11)$$

The gauge-invariant modification which takes into account the effect of external electromagnetic fields is now obvious. According to Eq. (6), the required substitution is

$$D_{kj}\rightarrow D_{kj}-(ie_j/\hbar c)(\mathbf{r}_{kj}\cdot\mathbf{A}_j). \quad (12)$$

Setting

$$f_{kj}=-(e_j/\hbar c)(\mathbf{r}_{kj}\cdot\mathbf{A}_j), \quad (13)$$

the potential term in the Lagrangian becomes in place of Eq. (11)

$$L_P(f)=\sum_k\sum_{j<k}(\psi, J_{jk}\times e\{D_{kj}+D_{jk}+if_{kj}+if_{jk}\}\psi). \quad (14)$$

This expression is clearly gauge invariant. Thus

the complete gauge-invariant Lagrangian density is

$$L=-i\hbar(\psi,\partial\psi/\partial t)+(\psi,\textstyle\sum_k e_k\varphi_k\psi)$$
$$+\textstyle\sum_k(1/2m_kc^2)([\hbar c\,\mathrm{grad}_k\psi-ie_k\mathbf{A}_k\psi],$$
$$\cdot[\hbar c\,\mathrm{grad}_k\psi-ie_k\mathbf{A}_k\psi])$$
$$+\textstyle\sum_k\sum_{j<k}(\psi,J_{jk}$$
$$\times e\{D_{kj}+D_{jk}+if_{kj}+if_{jk}\}\psi). \quad (15)$$

IV. PROPERTIES OF THE EXCHANGE OPERATOR

In order that the Schroedinger equations for ψ and ψ^* which are produced by the Lagrangian Eq. (15) be consistent with each other, it is necessary that the operator $e\{D_{kj}+D_{jk}+if_{kj}+if_{jk}\}$ be Hermitian. To establish this property it will be convenient to consider some of the properties of the operator $\exp(D+g)$, where

$$D=(\boldsymbol{\alpha}\cdot\mathrm{grad}), \quad (16)$$

with $\boldsymbol{\alpha}$ a constant vector, and g a function of the point $\mathbf{r}$.

We first note that if ds is the element of length along a path parallel to $\boldsymbol{\alpha}$, then

$$D=\alpha(d/ds). \quad (17)$$

If we define a function $\Gamma(\mathbf{r})$ to be the line integral

$$\Gamma=\frac{1}{\alpha}\int^{r} g\,ds \quad (18)$$

along a straight line path parallel to $\boldsymbol{\alpha}$ and passing through the point $\mathbf{r}$, we find that

$$D\Gamma=g. \quad (19)$$

Now any function F which defines a differentia operator $F(D)$ through a power series will have the property

$$F(D+g)\psi=e^{-\Gamma}F(D)e^{\Gamma}\psi. \quad (20)$$

Proof: From Eq. (19) it follows that

$$De^{\Gamma}\psi=\psi(De^{\Gamma})+e^{\Gamma}(D\psi)=e^{\Gamma}(D+g)\psi.$$

Iterating this result, we find

$$D^ne^{\Gamma}\psi=e^{\Gamma}(D+g)^n\psi,$$

or

$$e^{-\Gamma}D^ne^{\Gamma}\psi=(D+g)^n\psi.$$

The validity of this equation for each term in he series $F(D)$ leads immediately to the result Etq. (20).

A further result which will prove to be useful is that for any two functions φ and χ

$$e^D(\varphi\chi)=e^D\varphi e^D\chi. \quad (21)$$

Proof: e^D is a displacement operator such that $e^D\varphi(\mathbf{r})=e^D\varphi(\mathbf{r}+\boldsymbol{\alpha})$ if $\mathbf{r}$ is a point on the path along which the operator D is defined. Thus

$$e^D\varphi\chi=\varphi(\mathbf{r}+\boldsymbol{\alpha})\chi(\mathbf{r}+\boldsymbol{\alpha})=e^D\varphi e^D\chi.$$

If we now apply Eq. (21) to Eq. (20) with $F(D)$ replaced by the special function e^D, we find

$$e^{D+g}\psi=e^{-\Gamma}e^De^{\Gamma}\psi)=(e^{-\Gamma}e^De^{\Gamma})e^D\psi. \quad (22)$$

It is to be noted that the factor $(e^{-\Gamma}e^De^{\Gamma})$ is just a multiplicative factor consisting of a series of derivatives of g.

Now to return to the physical problem. The operator appearing in Eq. (14) can clearly be written as

$$e\{D_{kj}+D_{jk}+if_{kj}+if_{jk}\}=e\{D_{kj}+if_{kj}\}e\{D_{jk}+if_{jk}\}$$

since the two differential operators affect different coordinates. Then, from Eq. (22) it is found that

$$e\{D_{kj}+D_{jk}+if_{kj}+if_{jk}\}\psi$$
$$=[e\{-i\Phi_{kj}-i\Phi_{jk}\}e\{D_{kj}+D_{jk}\}$$
$$\times e\{i\Phi_{kj}+i\Phi_{jk}\}]e\{D_{kj}+D_{jk}\}\psi, \quad (23)$$

or, according to Eq. (10),

$$=[e\{-i\Phi_{kj}-i\Phi_{jk}\}P_{jk}e\{i\Phi_{kj}+i\Phi_{jk}\}]P_{jk}\psi,$$

where

$$\Phi_{kj}=\frac{1}{r_{kj}}\int^{r_j} f_{kj}ds_j=-(e_j/\hbar c)\left(\frac{\mathbf{r}_{kj}}{r_{kj}}\cdot\int^{r_j}\mathbf{A}_jds_j\right),$$

according to the definition of f_{kj}. Thus

$$\Phi_{kj}=-(e_j/\hbar c)\int^{r_j}A_j^sds_j, \quad (24)$$

where A^s is the component of $\mathbf{A}$ along the path of integration, which is parallel to $\mathbf{r}_{kj}$. Similarly,

$$\Phi_{jk}=-(e_k/\hbar c)\int^{r_k}A_k^sds_k.$$

Since ds_k is parallel to $\mathbf{r}_{jk}=-\mathbf{r}_{kj}$ it is antiparallel to ds_j and both integrals can be expressed in terms of the same path which we choose to be parallel to ds_j. It is to be noted that the sign of

the component A^s of the vector is changed by this transformation of paths so

$$\Phi_{kj}+\Phi_{jk}=-\left[(e_j/\hbar c)\int^{r_j}A^s ds+(e_k/\hbar c)\int^{r_k}A^s ds\right]. \quad (25)$$

Now

$$P_{jk}(\Phi_{kj}+\Phi_{jk})=-\left[(e_j/\hbar c)\int^{r_k}A^s ds+(e_k/\hbar c)\int^{r_j}A^s ds\right].$$

So Eq. (23) becomes

$$e\{D_{kj}+D_{jk}+if_{kj}+if_{jk}\}\psi=e\left\{[i(e_k-e_j)/\hbar c]\int_{r_j}^{r_k}A^s ds\right\}P_{jk}\psi, \quad (26)$$

since

$$\int^{r_k}A^s ds-\int^{r_j}A^s ds=\int_{r_j}^{r_k}A^s ds. \quad (27)$$

To establish the hermiticity of the operator we observe that the quadratic form $(\psi_a, e\{D_{kj}+D_{jk}+if_{kj}+if_{jk}\}\psi_b)$ involves integrals of the type

$$I_{ab}=\int\int\psi_a{}^*e\left\{[i(e_k-e_j)/\hbar c]\int_{r_j}^{r_k}A^s ds\right\}\times P_{jk}\psi_b d\tau_j d\tau_k.$$

In the integration, the variables $\mathbf{r}_j$ and $\mathbf{r}_k$ may be interchanged without altering the value of the integral. Thus

$$I_{ab}=\int\int P_{jk}\left[\psi_a{}^*e\left\{[i(e_k-e_j)/\hbar c]\times\int_{r_j}^{r_k}A^s ds\right\}\right]\psi_b d\tau_j d\tau_k.$$

Since

$$P_{jk}\int_{r_j}^{r_k}A^s ds=-\int_{r_j}^{r_k}A^s ds,$$

as can be seen from Eq. (27),

$$I_{ab}=\int\int\psi_b e\left\{-[i(e_k-e_j)/\hbar c]\int_{r_j}^{r_k}A^s ds\right\}\times P_{jk}\psi_a{}^* d\tau_j d\tau_k=I_{ba}{}^*. \quad (28)$$

This establishes the desired result since integration over the variables referring to other particles will not alter the essential relationship.

V. THE EQUATIONS OF MOTION AND THE EXCHANGE CURRENT

Making use of Eq. (26), the Lagrangian density Eq. (15) may now be expressed in the form

$$L=-i\hbar(\psi,\partial\psi/\partial t)+(\psi,\textstyle\sum_k e_k\varphi_k\psi)+\sum_k(1/2m_kc^2)([\hbar c\,\mathrm{grad}_k\psi-ie_k\mathbf{A}_k\psi],\cdot[\hbar c\,\mathrm{grad}_k\psi-ie_k\mathbf{A}_k\psi])+\sum_k\sum_{j<k}\left(\psi, J_{jk}e\left\{[i(e_k-e_j)/\hbar c]\times\int_{r_j}^{r_k}A^s ds\right\}P_{jk}\psi\right). \quad (29)$$

The corresponding Euler-Lagrange differential equation is

$$i\hbar\partial\psi/\partial t=-\sum_k(1/2m_kc^2)(\hbar c\,\mathrm{grad}_k-ie_k\mathbf{A}_k)^2\psi+\sum_k e_k\varphi_k\psi+\sum_k\sum_{j<k}e\left\{[i(e_k-e_j)/\hbar c]\times\int_{r_j}^{r_k}A^s ds\right\}P_{jk}\psi. \quad (30)$$

This is the required, gauge-invariant modification of the Schroedinger equation. From Eq. (28) it follows that the equation for ψ^* may be obtained by taking the conjugate complex of Eq. (30).

The complete expression for the current density may now be obtained in the usual manner from consideration of an infinitesimal gauge transformation. Since L given by Eq. (29) is invariant under the gauge transformation Eq. (4), it will in particular be invariant if G is an infinitesimal. That is, for the variation

$$\begin{aligned}\delta\mathbf{A}&=-\mathrm{grad}G,\\ \delta\varphi&=\partial G/\partial(ct),\\ \delta\psi&=-(i/\hbar c)\textstyle\sum_j e_jG_j\psi,\\ \delta\psi^*&=(i/\hbar c)\textstyle\sum_j e_jG_j\psi^*,\end{aligned} \quad (31)$$

we have

$$\delta\int L dt d\tau_1 d\tau_2\cdots d\tau_N=0.$$

The variation in the integral produced by $\delta\psi$ and $\delta\psi^*$ vanishes in virtue of the equations of motion, Eq. (30) or Eq. (3). Thus we are left with

$$\int\left(\frac{\delta L}{\delta\mathbf{A}}\cdot\delta\mathbf{A}+\frac{\delta L}{\delta\varphi}\delta\varphi\right)dt d\tau_1\cdots d\tau_N=0. \quad (32)$$

Now, from Eq. (29)

$$(\delta L/\delta\varphi)\delta\varphi=(\psi,\ \textstyle\sum_k e_k\delta\varphi_k\psi), \quad (33)$$

and

$$(\delta L/\delta\mathbf{A})\cdot\delta\mathbf{A}=-\textstyle\sum_k(he_k/2m_kc)[(i\delta\mathbf{A}_k\psi,\cdot\operatorname{grad}_k\psi)$$
$$+(\operatorname{grad}_k\psi,\cdot i\delta\mathbf{A}_k\psi)-(2e_k/hc)\mathbf{A}_k\cdot\delta\mathbf{A}_k(\psi,\psi)]$$
$$+\textstyle\sum_k\sum_{j<k}[i(e_k-e_j)/\hbar c]\int_{r_j}^{r_k}\delta A^s ds$$
$$\left(\psi,\ J_{jk}e\left\{[i(e_k-e_j)/\hbar c]\int_{r_j}^{r_k}A^s ds\right\}P_{jk}\psi\right). \quad (34)$$

We consider the limit of these expressions as $\mathbf{A}\to 0$, $\varphi\to 0$ since we are not interested in the small currents produced by the external fields. Then

$$(\delta L/\delta\mathbf{A})\cdot\delta\mathbf{A}=\textstyle\sum_k(i\hbar e_k/2m_kc)\delta\mathbf{A}_k$$
$$\cdot[(\psi,\operatorname{grad}_k\psi)-(\operatorname{grad}_k\psi,\psi)]+(i/\hbar c)\textstyle\sum_k$$
$$\times\sum_{j<k}(e_k-e_j)\int_{r_j}^{r_k}\delta A^s ds(\psi,\ J_{jk}P_{jk}\psi). \quad (35)$$

Inserting the expressions for $\delta\mathbf{A}$ and $\delta\varphi$ from Eq. (31), we find

$$(\delta L/\delta\varphi)\delta\varphi=(\psi,\ \textstyle\sum_k e_k\partial G_k/\partial(ct)), \quad (36)$$

and

$$(\delta L/\delta\mathbf{A})\cdot\delta\mathbf{A}=-\textstyle\sum_k(i\hbar e_k/2m_kc)$$
$$\times[(\psi,\operatorname{grad}_k\psi)-(\operatorname{grad}_k\psi,\psi)]\cdot\operatorname{grad}_k G_k$$
$$-(i/\hbar c)\textstyle\sum_k\sum_{j<k}(e_k-e_j)$$
$$\times(G_k-G_j)(\psi,\ J_{jk}P_{jk}\psi), \quad (37)$$

where $G_k=G(\mathbf{r}_k)$. The last term can be put into a more useful form by noting that

$$G_j=P_{jk}G_k=e\{D_{jk}\}G_k=\sum_{n=0}^{n=\infty}\frac{1}{n!}(\mathbf{r}_{jk}\cdot\operatorname{grad}_k)^n G_k. \quad (38)$$

Introducing Eqs. (36)–(38) into Eq. (32) and integrating by parts, we find

$$\textstyle\sum_k\int dt d\tau_1\cdots d\tau_N G_k\Big\{-e_k\dfrac{\partial}{\partial t}(\psi,\psi)$$
$$+(ie_k\hbar/2m_k)\operatorname{div}_k[(\psi,\operatorname{grad}_k\psi)-(\operatorname{grad}_k\psi,\psi)]$$
$$+(i/\hbar)\textstyle\sum_{j<k}(e_k-e_j)\sum_{n=1}^{n=\infty}\dfrac{(-1)^n}{n!}(\operatorname{div}_k\mathbf{r}_{jk})^n$$
$$\times(\psi,\ J_{jk}P_{jk}\psi)\Big\}=0, \quad (39)$$

where the operator

$$(\operatorname{div}_k\mathbf{r}_{jk})=-3+\mathbf{r}_{jk}\cdot\operatorname{grad}_k.$$

Now by making use of the fact that G_k has an arbitrary functional form, Eq. (39) may be written as the conventional equation of continuity

$$\partial\rho/\partial t+\operatorname{div}(\mathbf{S}_0+\mathbf{S}_x)=0, \quad (40)$$

with

$$\rho(\mathbf{r})=\textstyle\sum_k e_k\int(\psi,\psi)_{r_k=r}$$
$$\times d\tau_1\cdots d\tau_{k-1}d\tau_{k+1}\cdots d\tau_N, \quad (41)$$

$$\mathbf{S}_0(\mathbf{r})=\textstyle\sum_k(e_k\hbar/2im_k)\int[(\psi,\operatorname{grad}_k\psi)$$
$$-(\operatorname{grad}_k\psi,\psi)]_{r_k=r}d\tau_1\cdots d\tau_{k-1}d\tau_{k+1}\cdots d\tau_N, \quad (42)$$

and

$$\mathbf{S}_x(\mathbf{r})=-(i/\hbar)\textstyle\sum_k\sum_{j<k}(e_k-e_j)$$
$$\times\int\left[\mathbf{r}_{jk}\sum_{n=1}^{\infty}\frac{(-1)^n}{n!}\right.$$
$$\left.\times(\operatorname{div}_k\mathbf{r}_{jk})^{n-1}(\psi,\ J_{jk}P_{jk}\psi)\right]_{r_k=r}$$
$$\times d\tau_1\cdots d\tau_{k-1}d\tau_{k+1}\cdots d\tau_N. \quad (43)$$

The expressions for ρ and $\mathbf{S}_0$ are the conventional charge and current densities and $\mathbf{S}_x$ may clearly be interpreted as the exchange current density.

In order to complete the description of the exchange current, it will be shown that the energy of interaction between a weak external field and the exchange current has the conventional form

$$U=-(1/c)\int \mathbf{A}\cdot\mathbf{S}_x d\tau. \tag{44}$$

From the Schroedinger equation, Eq. (30), the average value of the exchange energy is found to be

$$\sum_k \sum_{j<k}\int (\psi, J_{jk}P_{jk}\psi)e\Big\{(i/\hbar c)(e_k-e_j) \times\int_{r_j}^{r_k} A^s ds\Big\}d\tau_1\cdots d\tau_N.$$

For weak external fields the exponential may be expanded. The linear term then yields the interaction U in the desired approximation. Thus

$$U=\sum_k \sum_{j<k}(i/\hbar c)\int\Big[(\psi, J_{jk}P_{jk}\psi)(e_k-e_j) \times\int_{r_j}^{r_k} A^s ds\Big]d\tau_1\cdots d\tau_N. \tag{45}$$

The line integral in Eq. (45) can be re-expressed by making use of the expansion of $A^s(\mathbf{r})$ about the point $\mathbf{r}_k$:

$$A^s(\mathbf{r})=\sum_{n=0}^{\infty}\frac{1}{n!}(\Delta\mathbf{r}_k\cdot\mathrm{grad}_k)^n A^s(\mathbf{r}_k) =\sum_{n=0}^{\infty}\frac{1}{n!}|\Delta\mathbf{r}_k|^n\left(\frac{d^n}{ds^n}A^s\right)_{r_k=r},$$

where $\Delta\mathbf{r}_k=\mathbf{r}-\mathbf{r}_k$ so $|\Delta\mathbf{r}_k|=s$, the length of the path measured from the point $\mathbf{r}_k$. Thus

$$\int_{r_j}^{r_k} A^s ds=-\sum_{n=0}^{\infty}\frac{1}{n!}\left(\frac{d^n}{ds^n}A^s\right)_{r_j}\int_{r_k}^{r_j} s^n ds \tag{46}$$

$$=-\sum_{n=0}^{\infty}\frac{1}{(n+1)!}(\mathbf{r}_{jk}\cdot\mathrm{grad}_k)^n(\mathbf{r}_{jk}\cdot\mathbf{A}_k).$$

Inserting this expression in Eq. (45) and integrating by parts n times, we obtain

$$U=-(i/\hbar c)\sum_k\sum_{j<k}(e_k-e_j) \times\int\Big[(\mathbf{A}_k\cdot\mathbf{r}_{jk})\sum_{n=0}^{\infty}\frac{(-1)^n}{(n+1)!}(\mathrm{div}_k\mathbf{r}_{jk})^n \times(\psi, J_{jk}P_{jk})\Big]d\tau_1\cdots d\tau_N.$$

The introduction of $\mathbf{S}_x$ from Eq. (43) leads immediately to the desired result, Eq. (44).

This result indicates that variation with respect to the potentials of the total Lagrangian describing both the particles and the electromagnetic field will lead to Maxwell's equations involving the total current $\mathbf{S}_0+\mathbf{S}_x$ in the usual way.

VI. THE EXCHANGE MOMENT

In a uniform magnetic field the interaction energy with the exchange current can also be expressed as

$$U=-(\mathbf{M}_x\cdot\mathbf{H}), \tag{47}$$

where $\mathbf{M}$ is the exchange magnetic moment. Since the vector potential for such a field is $\mathbf{A}=-(1/2)[\mathbf{r}\times\mathbf{H}]$, we find from Eq. (44) the usual expression

$$\mathbf{M}_x=(1/2c)\int[\mathbf{r}\times\mathbf{S}_x]d\tau. \tag{48}$$

However, because of the complicated form of $\mathbf{S}_x$, it is somewhat simpler to deal directly with the expression, Eq. (45). Inserting the value of $\mathbf{A}$ in Eq. (45) we find that the line integral can be immediately evaluated since $[\mathbf{r}\times\mathbf{H}]^s$ is constant along the path of integration:

$$\int_{r_j}^{r_k} A^s ds=-\tfrac{1}{2}([\mathbf{r}_k\times\mathbf{r}_j]\cdot\mathbf{H}). \tag{49}$$

Thus

$$U=-(i/2\hbar c)\sum_k\sum_{j<k}(e_k-e_j) \times\int(\psi, J_{jk}P_{jk}\psi)([\mathbf{r}_k\times\mathbf{r}_j]\cdot\mathbf{H})d\tau_1\cdots d\tau_N,$$

or, comparing Eq. (47)

$$\mathbf{M}_x=(i/2\hbar c)\sum_k\sum_{j<k}(e_k-e_j) \times\int(\psi, J_{jk}P_{jk}\psi)[\mathbf{r}_k\times\mathbf{r}_j]d\tau_1\cdots d\tau_N. \tag{50}$$

It is to be noted that in the double sum defining $\mathbf{M}_z$ those terms vanish for which both j and k refer to neutrons or those for which both j and k refer to protons, since in such cases $e_k - e_j = 0$.

Equation (50) may therefore be replaced by

$$\mathbf{M}_z = (ie/2hc)\sum_\nu \sum_\pi \int [\mathbf{r}_\pi \times \mathbf{r}_\nu] \times (\psi, J_{\pi\nu} P_{\pi\nu}\psi) d\tau_1 \cdots d\tau_N, \quad (51)$$

where the indices π refer only to protons and the indices ν to neutrons. This expression is antisymmetric for interchange of neutrons and protons, therefore *the exchange moments of conjugate pairs of nuclei* (i.e., those that can be obtained from one another by interchange of neutrons and protons) *are equal in magnitude and opposite in sign.* It also follows that *the exchange moments of self-conjugate nuclei vanish.* Thus one cannot expect to explain the anomalies[7] in the moments of H^2, Li^6, B^{10}, N^{14} by the introduction of an exchange current.

VII. APPLICATION TO H^3 AND He^3

The exchange moments of the nuclei H^3 and He^3 may now be obtained from Eq. (51). As an immediate consequence of the theorem stated at the end of the foregoing paragraph we find that the exchange moments of H^3 and He^3 are equal in magnitude and opposite in sign. Villars[2] obtained the same result in his field theoretical treatment of the moments. One can conclude that the sum of the moments of the two nuclei does not involve the exchange moments so the validity of the general theorem[8] concerning the sum of the moments is not affected:

$$\mu(H^3) + \mu(He^3) = \mu_p + \mu_n - 2(\mu_p + \mu_n - \tfrac{1}{2})(3D^2 - {}^4P^2 + 2\,{}^2P^2)/3. \quad (52)$$

Thus, for a given nuclear wave function it is necessary to calculate the exchange moment for only one of the two nuclei. The calculation will be carried through for H^3.

In order to evaluate the integral in Eq. (51) it will be necessary to make some assumption concerning the nature of the potential, $J_{\pi\nu}$, and the form of the wave functions. It will be assumed that the potential is the sum of a spin-independent and a tensor interaction. The functional form of the potential will be taken to be Gaussian with the constants determined from the properties of the deuteron.[9] The wave function which has been found[10] using this potential will be used here. No serious difference would be expected if the Gerjuoy-Schwinger[11] functions were used. This wave function contains four percent ^4D function and no ^2P or ^4P function. In the calculation which produced this function the tensor interaction was treated as an ordinary potential rather than an exchange potential, but either of these potentials will give about the same result for the D state probability. The present considerations are based on the assumption that the tensor interaction involves a Majorana exchange operator.

If the positions of the neutrons in H^3 are $\mathbf{r}_1$ and $\mathbf{r}_2$, and the position vector of the proton is $\mathbf{r}_3$, Eq. (51) gives for the exchange moment

$$\mathbf{M}_z = (ie/2hc)\int \{[\mathbf{r}_3 \times \mathbf{r}_1](\psi, J_{13}P_{13}\psi) + [\mathbf{r}_3 \times \mathbf{r}_2](\psi, J_{23}P_{23}\psi)\} d\tau_1 d\tau_2 d\tau_3. \quad (53)$$

Now the wave function ψ is the sum of an S function and a D function. The integrand will involve a product of two S functions, a product of an S and D function, and the product of two D functions. Since $(\mathbf{r}_3 \times \mathbf{r}_1)$ and $(\mathbf{r}_3 \times \mathbf{r}_2)$ have the transformation properties of a P function under space rotations, the only contribution to the integral from the spin independent term in J arises from the product of the two D functions. The tensor interaction term in J has the transformation properties of a D function so this term will make a contribution for the product of S and D functions as well as the product of the two D functions. If we denote by S and D the amplitudes of the S and D wave functions, then $S^2 = 0.96$, $D^2 = 0.04$. A direct calculation of the average exchange movement based on Eq. (53), using the above-mentioned wave functions,[10]

[7] R. G. Sachs, Phys. Rev. **69**, 611 (1946).
[8] R. G. Sachs and J. Schwinger, Phys. Rev. **70**, 41 (1946).
[9] S. Moszkowski and R. G. Sachs, Phys. Rev. **73**, 184 (1948).
[10] M. Goeppert-Mayer and R. G. Sachs, Phys. Rev. **73**, 185 (1948).
[11] E. Gerjuoy and J. Schwinger, Phys. Rev. **61**, 138 (1942).

leads to the result

$$M_x=[0.080\gamma SD+0.038D^2-0.073\gamma D^2]\times(J_0a_0^2M/\hbar^2) \quad (54)$$

if the magnetic moment is measured in units of nuclear magnetons. Here, J_0 is the strength of the Gaussian neutron-proton interaction, a_0 is the range of the interaction, M is the mass of the proton, and γ is the strength of the tensor interaction in the notation of Rarita and Schwinger.[12] The numerical coefficients depend explicitly on the H^3 wave functions, but in such an insensitive manner that Eq. (54) should yield a fair estimate of the exchange moment for values of J_0 and γ different from those used to determine the wave functions. It seems likely that Eq. (54) can also be used to estimate the moment for a square well potential. For the Gauss potential we take[9] $\gamma=0.53$, $J_0a_0^2M/\hbar^2=4.29$ and find

$$M_x=0.035 \text{ n.m.} \quad (55)$$

If we assume that Eq. (54) is adequate to represent the exchange moment for a square well potential, the Rarita-Schwinger[12] values $\gamma=0.775$, $J_0a_0^2M/\hbar^2=2.80$ lead to the estimate

$$M_x\approx 0.041 \text{ n.m.} \quad (56)$$

VIII. CONCLUSION

The exchange moments given by Eq. (55) or Eq. (56) are much too small to account for the difference of 0.27 n.m. between the observed moment and that to be expected,[8] neglecting exchange, on the basis of a four percent D state probability. This result is to be contrasted to that obtained by Villars,[2] using the pseudoscalar symmetric meson theory. The principal difference between the two theories arises from the fact that Villars' exchange current has a non-vanishing average value in the S state, while the phenomenological theory leads only to contributions which are proportional to the small amplitude of the D function. This is a consequence of the dependence of one term in the Villars exchange moment operator on the spins of the nucleons. Villars also finds an orbital contribution to the exchange moment which is very similar in form to that obtained here. He ignores the latter contribution, since he treats the wave function of the nucleus as an S function.

This situation is analogous to that which obtains in the theory of the magnetic moment of the electron. If one bases the theory of the interaction of the electron with the electromagnetic field on the non-relativistic Schroedinger equation, no information is obtained concerning the intrinsic magnetic moment of the electron which is associated with the spin. On the other hand, the Dirac theory in the non-relativistic limit leads directly to an expression for the intrinsic moment. Similarly, a relativistic formulation of the theory of interacting nucleons is required to give, even in the non-relativistic limit, an expression for the spin dependent part of the exchange moment. The meson field theories provide a possible formulation of the theory. Unfortunately, the pseudoscalar symmetric theory which accounts for the observed exchange moment does not give a reasonable account of nuclear forces since it leads to the undesirable r^{-3} potential. On the other hand, work which has been carried out by Villars and Thellung,[5] indicates that modifications of the meson theories which eliminate the undesirable potential do not lead to the correct exchange moment.

It can be concluded that the orbital exchange moment which is obtained here on phenomenological grounds is well founded, but not adequate to account for the observations. The principal contribution to the exchange moment would appear to depend in a detailed way on the nature of the field describing the interaction between nucleons. Therefore, the magnetic moments of H^3 and He^3 may prove to be a means for obtaining direct information concerning the nature of the field.

This investigation was carried out as a direct consequence of a very interesting discussion with Professor Fermi.

[12] W. Rarita and J. Schwinger, Phys. Rev. 59, 436 (1941).

PHYSICAL REVIEW VOLUME 74, NUMBER 4 AUGUST 15, 1948

Relative Yields of Some X-Ray Induced Nuclear Reactions

M. L. PERLMAN AND G. FRIEDLANDER*
General Electric Company, Research Laboratory, Schenectady, New York

(Received May 10, 1948)

X-rays from the 100-Mev betatron and 80-Mev synchrotron were used to induce (γ,n), (γ,p), $(\gamma,2n)$, and $(\gamma,2p)$ reactions. Relative yields for a number of these reactions were determined by measurement of the activities of the products. Yields of (γ,n) reactions appear to be about an order of magnitude larger for $Z \geq 29$ than for lower Z; the transition seems to be abrupt. The five (γ,p) reactions studied have approximately equal yields, and these are about the same as (γ,n) yields below the transition. Values for the few $(\gamma,2p)$ yields measured are about one-twentieth those for the (γ,p) reactions. Yields for the $(\gamma,2n)$ reactions vary, but are much smaller than (γ,n) yields. The most probable number of particles emitted as the result of the interaction of a high energy quantum with a nucleus is one.

I. INTRODUCTION

QUANTITATIVE studies of yields of various nuclear reactions involving the emission of a single particle under excitation by 17-Mev and 12-Mev gamma-rays have been made by several investigators.[1-3] Measurements made in this laboratory[4] have shown that many nuclear reactions can be induced by the x-rays produced in the 100-Mev betatron.

In the experiments reported in this paper various elements were irradiated with x-rays generated by the 100-Mev betatron in order to study relative yields of (γ,n), (γ,p), $(\gamma,2n)$, and $(\gamma,2p)$ reactions and to see how the yields vary with atomic or mass number. The yield was determined essentially by identification and measurement of the beta-activity of the isotope expected to result from a particular reaction on one of the target isotopes. Experiments were made with x-rays produced in a tungsten target by 50-Mev and by 100-Mev electrons.

In all experiments the beta-activity of the product was distinguished from other activities by analyses of decay curves. Cases for investigation were chosen so as to eliminate or minimize the following possibilities: First, the product could have been made from the target isotopes or impurities by processes other than the particular one of interest; second, other products of half-life similar to the one sought could have been made either from the target elements or from impurities. In order that relative yield values based on counting data might be reliable, insofar as available information permitted, cases were chosen in which decay schemes are known and in which no significant fraction of the counting rates could be ascribed to gamma- or x-ray emission.

II. EXPERIMENTAL DETAILS

Monitors

Irradiations were monitored by measurement of the C^{11} or F^{18} activity induced in a standard square piece of polystyrene or lithium fluoride which was bombarded together with each target. The use of a monitor whose half-life approximates that of the product to be measured reduces errors caused by fluctuations in the x-ray intensity. The two monitors were carefully intercalibrated at both x-ray energies by measurements of the activities produced in them when they were bombarded together for ten minutes at nearly constant intensity. The monitors presented to the beam the same cross section as did targets, and monitor and target were always mounted in tandem. Typical monitor decay plots are shown in Figs. 1 and 2. Except for some short-lived activities in the lithium fluoride, which were not evident one hour after bombardment, only a single radioactive species was observed in each monitor over at least five half-lives.

* Present address, Brookhaven National Laboratory, Upton, Long Island, New York.

[1] W. Bothe and W. Gentner, Zeits. f. Physik **106**, 236 (1937), and Zeits. f. Physik **112**, 45 (1939).

[2] O. Huber, O. Lienhard, P. Scherrer, and H. Wäffler, Helv. Phys. Acta **16**, 33 (1943).

[3] O. Huber, O. Lienhard, and H. Wäffler, Helv. Phys. Acta **17**, 195 (1945); (a) O. Hirzel and H. Wäffler, Helv. Phys. Acta **20**, 373 (1947).

[4] G. C. Baldwin and G. S. Klaiber, Phys. Rev. **70**, 259 (1946).

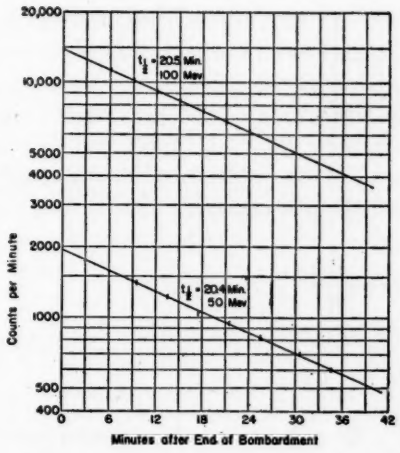

FIG. 1. Decay of polystyrene monitor after irradiation with 100-Mev and with 50-Mev x-rays.

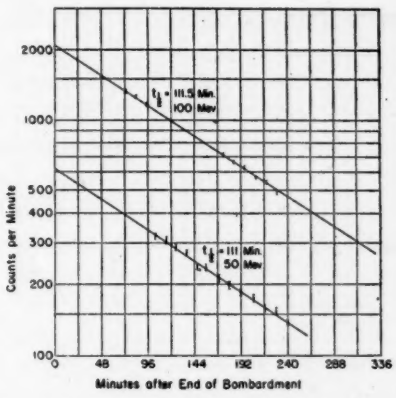

FIG. 2. Decay of lithium fluoride monitor after irradiation with 100-Mev and with 50-Mev x-rays.

The ratio of the saturation activity of the polystyrene monitor to that of the lithium fluoride monitor was 4.39 ± 0.1 at 100 Mev; at 50 Mev it was 3.98 ± 0.1 It happens that monitor activities in all experiments reported here were measured with a lead tetramethyl filled, Eck and Krebs type, cylindrical, thin glass Geiger counter, whose efficiency was checked before each experiment and remained essentially unchanged throughout this research.

Targets and Samples

Most target materials were in the form of powders, which were packed for irradiation in plastic boxes $\frac{3}{4}$ inch by $\frac{3}{4}$ inch in inside section. In the standard bombardment geometry the axis of the x-ray beam passed through the centers of both box and monitor. The distance from the x-ray source was 80 centimeters. After irradiation the powder or a part of it was poured into a short vertical brass cylinder $\frac{7}{8}$ inch in inside diameter, which was previously positioned on a plastic sample mounting board. A closely fitted, flat-faced plunger, hand operated, served to form the powder into a fairly uniform pill even when the thickness was not over 0.2 millimeter. After removal of plunger and cylinder the samples were covered with thin Cellophane.

After the counting experiments on a given sample had been concluded, the weight of target material in the sample was determined. In most cases the sample was dried to constant weight, either in a desiccator or an oven, and weighed. Where a different method of assay was used this will be indicated in the discussion of the individual results below.

Counters and Recorder

For measurement, samples were always placed in a standard position very close to the mica window of a G-M tube of $1\frac{1}{16}$-inch inside diameter filled with argon and ethyl alcohol. The pulses from the counter, after amplification, were put into a scaler whose factor could be chosen from the powers of two up to a maximum of 4096. The output of the scaler was recorded on the moving paper tape of a Brush Type BL-201 oscillograph. The tape used on this machine is ruled, and it is moved under the galvanometer pen by a geared synchronous motor at one of three speeds. By proper choice of scaling factor and paper speed it was possible to follow the decay of activities with half-lives as short as a few seconds. The combination of instruments proved convenient also for recording measurements over extended periods on long-lived samples.

Counting measurements were corrected for small day-to-day variations in counter sensitivity, for back-scattering, for self-absorption, and for absorption in the Cellophane covering and mica window. For the latter absorption correction the mass absorption coefficients of Cellophane and of mica were taken to be the same as that of aluminum.

Absorption and Scattering Measurements

Self-absorption corrections were determined experimentally. Samples of nickel, lithium flu-

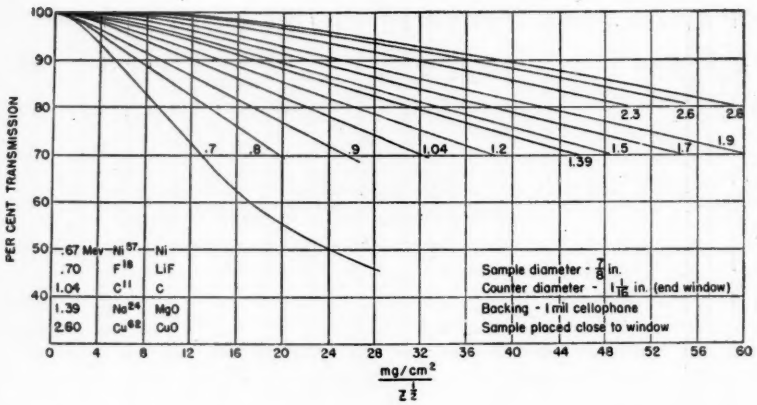

FIG. 3. Self-absorption of beta-radiations of various energies (Mev).

oride, carbon, magnesium oxide, and cupric oxide were irradiated to produce in them, respectively, the activities of $Ni^{57}(\beta^+$ 0.67 Mev), $F^{18}(\beta^+$ 0.7 Mev), $C^{11}(\beta^+$ 0.99 Mev),[5] $Na^{24}(\beta^-$ 1.39 Mev), and $Cu^{62}(\beta^+$ 2.6 Mev). A number of samples of different thicknesses were made from each of the active substances. These samples were mounted by the standard technique except that they were supported on 0.001-inch Cellophane to decrease back-scattering. In some cases it was necessary to allow interfering activities to die so that substantially a single radioactive species might be present in each of the substances at the time of measurement. The activities of the different samples from a single bombardment were measured in the standard geometry under a mica-window counter, and their specific activities, after correction for decay, were plotted against their weights per unit area. The curve obtained was extrapolated to zero thickness. The specific activities were then converted to transmission values. This procedure was followed for each of the substances listed above. Since this list, however, did not include all the active substances measured in the yield experiments, it was assumed that the mass absorption for a given energy is inversely proportional to $\bar{Z}^{\frac{1}{2}}$, the square root of the average atomic number of the absorbing substance. For a compound the average atomic number is the weighted average of the atomic numbers of the elements composing the compound; for example, $\bar{Z}^{\frac{1}{2}}$ for antimony trioxide (Sb_2O_3) is $(2\times122\times51^{\frac{1}{2}}+3\times16\times8^{\frac{1}{2}})/292$ or 6.42. The validity of this assumption is supported by the fact that the two self-absorption curves—transmission *vs.* $(mg/cm^2)/\bar{Z}^{\frac{1}{2}}$—for the 0.67-Mev positron of Ni^{57} in nickel metal and for the 0.7-Mev positron of F^{18} in lithium fluoride were the same within experimental error. By interpolation, curves were obtained for beta-radiations of energies other than those listed. The final results are shown in Fig. 3.

Back-scattering was determined for many of the samples used in the self-absorption experiments by measurement of their activities with thin Cellophane backing and with the standard plastic sheet backing. This small correction, whose maximum value was six percent, was assumed to be a function of transmission only.

The experiments for the determination of the absorption and back-scattering effects are not refined; however, the corrections to observed counting rates contributed by these effects are nearly always under 30 percent. The inaccuracy in these corrections probably gives rise to an error in the final results no greater than five percent.

III. CALCULATION OF RESULTS

The decay curves of most irradiated samples showed the presence of more than one component, as had been expected. The activity at the end of bombardment of the component sought was determined by extrapolation. This value was used to calculate the activity which would be measured under the standard conditions at the end of a saturation bombardment if there were no absorption or back-scattering and if the product from one milligram-atom of the parent isotope were present.

[5] Actually a value of 1.04 Mev for the maximum energy of the C^{11} positron would be more consistent with our other results than the value of 0.99 Mev found by K. Siegbahn and E. Bohr, Ark. f. Mat. Astr. Fys. **30B**, No. 3 (1943).

The procedure for the monitor was simply to determine its activity at the end of bombardment and to calculate the activity for saturation bombardment. The ratio of the saturation product activity per milligram-atom of parent isotope to the saturation activity of C^{11} in the polystyrene monitor was taken as a measure of the yield of a reaction.

IV. RESULTS[6]

Relative yield values are given in Tables I, II, and III. Unless otherwise noted, each yield value listed is the average of at least two independent experiments.

A. (γ,n) Reactions

$C^{12}(\gamma,n)C^{11}$.—Spectroscopically pure graphite powder was used as target material. A typical bombardment lasted 15 minutes. The activity produced decayed with the C^{11} period over at least five half-lives; no other periods were observed.

$N^{14}(\gamma,n)N^{13}$.—In 15-minute bombardments of ammonium chloride the only activities observed were those of N^{13} (9.9 minutes) and Cl^{34} (33 minutes).

$O^{16}(\gamma,n)O^{15}$.—Boric acid was used as the target material. It was analyzed for oxygen by the titration of a weighed quantity with NaOH after the addition of mannitol. In addition to the strong O^{15} activity a weak activity whose half-life was approximately 20 minutes was observed (perhaps C^{11}). Bombardments were of five minutes duration.

$F^{19}(\gamma,n)F^{18}$.—Pure LiF powder made from optical crystal scrap was bombarded for two hours in a typical case. An unidentified 15-minute activity, a 1-minute activity (probably F^{17}), and the strong 110-minute F^{18} were observed. The shorter periods were unobservable after they had decayed for 90 minutes.

$Al^{27}(\gamma,n)Al^{26}$.—For the measurement of the 7-second Al^{26} the counting equipment was placed in a small room off the betatron space. It was not possible to redistribute the target material before counting. The target was in the form of a very pure aluminum disk whose diameter was $\frac{7}{8}$ inch, the same as that of a standard counting sample. The standard monitor was not used; instead a thin $\frac{7}{8}$-inch disk of polythene, $(CH_2)_n$, was bombarded for two minutes together with the aluminum. It proved possible to have the aluminum under the counter within 8 to 10 seconds after the end of irradiation. The 7-second Al^{26} and 62-second Na^{25} activities were easily measurable in the aluminum. The pure C^{11} activity of the polythene was determined with an end-window counter, and the ratio of the yield of the reaction $Al^{27}(\gamma,n)Al^{26}$ to that of the reaction $C^{12}(\gamma,n)C^{11}$ was calculated. This in turn made it possible to calculate the $Al^{27}(\gamma,n)$ yield in terms of the usual polystyrene monitor activity.

$P^{31}(\gamma,n)P^{30}$.—Red phosphorus, which had been washed to remove oxides and acids, was bombarded for five to ten minutes. The activities of P^{30} (2.5 minutes) and Al^{29} (6.7 minutes) were observed, perhaps together with a very small activity of longer half-life.

$Cl^{35}(\gamma,n)Cl^{34}$.—Data on yields of this reaction were obtained from the ammonium chloride bombardments described under $N^{14}(\gamma,n)N^{13}$ and from 10-minute bombardments of potassium chloride. In the potassium chloride the activities of K^{38} and Cl^{34} were the only ones observed.

$K^{39}(\gamma,n)K^{38}$.—Cf. $Cl^{35}(\gamma,n)Cl^{34}$.

$Ni^{58}(\gamma,n)Ni^{57}$.—Pure nickel powder was bombarded for two or three hours. In addition to an unidentified activity of comparatively short half-life only 36-hour Ni^{57} and 1.73-hour Co^{61} were observed.

$Cu^{63}(\gamma,n)Cu^{62}$.—Irradiation of reagent grade CuO for ten minutes produced in measurable quantities the activities of Cu^{62} and O^{15}. A longer period of very low intensity was also present.

$Ga^{69}(\gamma,n)Ga^{68}$ and $Ga^{71}(\gamma,n)Ga^{70}$.—Ga_2O_3 was used as the target material for irradiations of five to twenty minutes duration. In addition to a short-lived activity, only 68-minute Ga^{68} and 20-minute Ga^{70} were observed to be present.

$Pd^{110}(\gamma,n)Pd^{109}$.—After the shorter-lived products formed in the irradiation of $PdCl_2$ had disappeared, the 13-hour Pd^{109} and 35-hour Rh^{105} remained. Because of the thickness of the samples used and because of the presence of conversion electrons in the radiation from Rh^{105}, no (γ,p) yield was calculated on the basis of the

[6] Preliminary reports on some of these results have been made. Cf. M. L. Perlman and G. Friedlander, Phys. Rev. **72**, 1272 (1947); G. Friedlander and M. L. Perlman, Bull. Am. Phys. Soc. **23**, No. 2, 38 (Jan. 1948).

TABLE I. Relative yields of (γ,n) reactions; $N^{14}(\gamma,n)N^{13}=1.00$ at each energy.

Parent isotope	Product isotope	Product[a] half-life	Product[b] betas and energies (Mev)	Relative yield 100 Mev	Relative yield 50 Mev
$_6C^{12}$	C^{11}	20.5 min.	β^+ 1.04[h]	2.3	2.3
$_7N^{14}$	N^{13}	9.9 min.	β^+ 1.2[g]	*1.00*	*1.00*
$_8O^{16}$	O^{15}	2.1 min.	β^+ 1.7	2.2	2.4
$_9F^{19}$	F^{18}	1.87 hr.	β^+ 0.7	2.7	2.8
$_{13}Al^{27}$	Al^{26}	7.0 sec.	β^+ 2.99	2.3	3.1
$_{15}P^{31}$	P^{30}	2.5 min.	β^+ 3.0	7.2	7.1
$_{17}Cl^{35}$	Cl^{34}	33.0 min.	β^+ 5.1 (80%)[c] 2.4 (20%)	2.4	2.4
$_{19}K^{39}$	K^{38}	7.6 min.	β^+ 2.5[d]	2.6	2.6
$_{28}Ni^{58}$	Ni^{57}	36.0 hr.	β^+ 0.67	6.3	6.0
$_{29}Cu^{63}$	Cu^{62}	9.9 min.	β^+ 2.6	33	35
$_{31}Ga^{69}$	Ga^{68}	68.0 min.	β^+ 1.9	42	44
$_{31}Ga^{71}$	Ga^{70}	20.0 min.	β^- 1.7	43	44
$_{46}Pd^{110}$	Pd^{109}	12.7 hr.	β^- 1.1[e]	33	39
$_{47}Ag^{109}$	Ag^{108}	2.33 min.	β^- 2.8	41	46
$_{51}Sb^{121}$	Sb^{120}	16.6 min.	β^+ 1.53	42	46
$_{75}Re^{187}$	Re^{186}	92.0 hr.	β^- 1.07[f]	85	86

[a] Values observed in these experiments.
[b] Unless noted data from G. T. Seaborg, Rev. Mod. Phys. 16, 1 (1944).
[c] Ho Zah-Wei, Phys. Rev. 70, 782 (1947).
[d] M. M. Ramsey, J. L. Meem, and A. C. G. Mitchell, Phys. Rev. 72, 639 (1947).
[e] W. Rall, Phys. Rev. 70, 112A (1946).
[f] D. C. Hess, Jr., R. J. Hayden, and M. G. Inghram, Phys. Rev. 72, 730 (1947); L. J. Goodman and M. L. Pool, Phys. Rev. 71, 288 (1947).
[g] K. Siegbahn and S. E. Peterson, Ark. f. Mat. Astr. o Fys. 32A, No. 9 (1945); 32B No. 5 (1945); L. M. Langer, C. S. Cook, and M. B. Sampson, Phys. Rev. 71, 906 (1947).
[h] See reference 5.

35-hour activity. Duration of bombardments was two to three hours.

$Ag^{109}(\gamma,n)Ag^{108}$.—In short irradiations (one to two minutes) of pure silver powder only 2.3-minute Ag^{108} and 24.3-minute Ag^{106} were observed.

$Sb^{121}(\gamma,n)Sb^{120}$.—The target material was antimony trioxide (Sb_2O_3); duration of bombardment was ten minutes. Three products were observed, 2-minute O^{15}, 16.6-minute Sb^{120}, and a long-lived activity of very low intensity which may have been Sb^{122}. No 117-minute In^{117}, which would be produced in the reaction $Sb^{121}(\gamma,\alpha)In^{117}$, was observed.

$Re^{187}(\gamma,n)Re^{186}$.—Rhenium estimated to be 99.99 percent pure[7] was bombarded for five hours. Two LiF monitors were used, one for the first half and one for the last half of the irradiation. After approximately three days the samples decayed with the 92-hour half-life characteristic of Re^{186}.

In Table I are given yield values for the (γ,n) reactions observed in the irradiations described above. The yield value of the reaction $N^{14}(\gamma,n)N^{13}$ has arbitrarily been taken as unity at each x-ray energy, and all other yield values are relative to it. Limits of errors are estimated to be ±15 percent. Figure 4 shows the relative yields of the (γ,n) reactions plotted against mass number.

[7] Obtained from Jarrell-Ash Company, Boston, Massachusetts.

B. (γ,p) Reactions

$Si^{30}(\gamma,p)Al^{29}$.—In very pure elementary silicon which was bombarded for 15 minutes the activities of Al^{29} (6.7 minutes) and of Al^{28} (2.4 minutes) only were observed. A small amount of 10-minute Mg^{27} may have been present. As in many of these experiments, activities of half-life shorter than approximately 30 seconds decayed to a quite low level during the time interval between the end of bombardment and the start of measurement.

$Fe^{57}(\gamma,p)Mn^{56}$.—The target material chosen was metallic iron powder, which was analyzed for oxide content. Bombardment time was two hours. Besides some short periods (probably those of Fe^{53} and Mn^{52}) the only activities observed were 2.6-hour Mn^{56} and perhaps[15] 8-hour Fe^{52}.

$Ni^{62}(\gamma,p)Co^{61}$.—Cf. $Ni^{58}(\gamma,n)Ni^{57}$.

$Mo^{98}(\gamma,p)Cb^{97}$.—In samples of MoO_3 bombarded for one hour there were observed activities of 15-minute and 75-minute half-lives (the latter Cb^{97}) and an activity of low intensity and comparatively long half-life.

$Ru^{102}(\gamma,p)Tc^{101}$.—Ruthenium metal was bombarded for ten minutes. In addition to the

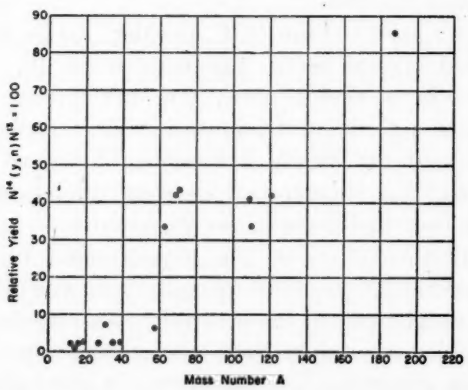

FIG. 4. Relative yields of (γ,n) reactions induced by 100-Mev x-rays.

[15] Cunningham, Hopkins, Lindner, Miller, O'Connor, Perlman, Seaborg, and Thompson, Phys. Rev. 72, 739 (1947).

14-minute Tc^{101}, activities of the following half-lives were present: approximately 3 minutes, 80 minutes, comparatively long.

Yields of the (γ,p) reactions relative to the (γ,n) yield of N^{14} are given in Table II.

C. $(\gamma,2n)$ and $(\gamma,2p)$ Reactions

$C^{12}(\gamma,2n)C^{10}$.—Polystyrene targets in the form of disks were irradiated for 20 seconds. The experimental arrangements and monitoring were similar to those used for the $Al^{27}(\gamma,n)Al^{26}$ measurements. An aluminum absorber of 110-mg/cm² thickness served to decrease the background C^{11} activity. Very little, if any, C^{10} decay (8.8-second half-life) was observed in the curve obtained by the addition of five experiments. Only an upper limit could therefore be set for the relative yield of the reaction.[8]

$F^{19}(\gamma,2n)F^{17}$.—Measurements on the production of the 70-second F^{17} activity from F^{19} were made on LiF samples which were irradiated for two minutes. See $F^{19}(\gamma,n)F^{18}$.

$P^{31}(\gamma,2n)P^{29}$.—The half-life of P^{29} (4.6 seconds) precluded the use of the usual mechanical transfer of samples to the counter. Red phosphorus with one percent of polystyrene to act as binder was formed into flat pellets $\frac{7}{8}$ inch in diameter whose transmission for the radiations both of P^{29} and P^{30} was over 90 percent. Several pellets were placed side by side in a line along the axis of the 80-Mev x-ray beam of the synchrotron. Just above the phosphorus there was mounted a cylindrical thin-walled counter which was shielded from the direct beam by several inches of lead. The samples were irradiated for ten seconds and counted automatically immediately afterwards. A decaying background, measured in irradiations made without phosphorus, was taken into account. The observed P^{30} activity was used as an "internal" monitor. Little or no 4.6-second P^{29} was observed, and the value for the relative yield given is an upper limit. This value is calculated on the assumption that the relative yield of the reaction $P^{31}(\gamma,n)P^{30}$ is about the same at 80-Mev as at 50-Mev and at 100-Mev.

[8] If the half-life of C^{10} is 20 seconds (rather than 8.8 seconds), as has been recently suggested (R. Sherr, H. R. Muether, and M. G. White, Bull. Am. Phys. Soc. **23**, No. 3, 45 (1948)), the upper limit of the yield is affected very little.

TABLE II. Relative yields of (γ,p) reactions; $N^{14}(\gamma,n)N^{13}=1.00$ at each energy.

Parent isotope	Product isotope	Product half-life	Product betas and energies (Mev)	Relative yield 100 Mev	50 Mev
$_{14}Si^{30}$	Al^{29}	6.8 min.	β^- 2.5	5.8	6.6
$_{26}Fe^{57}$	Mn^{56}	2.62 hr.	β^- 0.75 (20%) 1.04 (30%)[a] 2.81 (50%)	7.6	7.6
$_{28}Ni^{62}$	Co^{61}	1.74 hr.	β^- 1.1	5.4	5.0
$_{42}Mo^{98}$	Cb^{97}	76.0 min.	β^- 1.4[b]	5.0	3.1
$_{44}Ru^{102}$	Tc^{101}	14.5 min.	β^- 1.2	3.7	3.6[c]

[a] K. Siegbahn, Arkiv f. Mat. Astr. o. Fys. **33A**, No. 10 (1946).
[b] Plutonium Project, J. Am. Chem. Soc. **68**, 2411 (1946).
[c] Value based on one experiment.

$Cu^{63}(\gamma,2n)Cu^{61}$.—Cupric oxide which was irradiated for two hours showed, in addition to the short-period activities previously described, the activities of Cu^{61} (3.2 hours) and Cu^{64} (12.8 hours). Because of the large self-absorption of the radiations of Cu^{64} in the sample, its activity was not used to calculate the (γ,n) yield on Cu^{65}. In order to see whether the 3.2-hour Cu^{61} might not be masking 1.75-hour Co^{61} produced by $(\gamma,2p)$ reaction, in one experiment a chemical separation was carried out. The cobalt fraction at saturation was only about 7 percent as active as the Cu^{61}.

$Al^{27}(\gamma,2p)Na^{25}$.—Cf. $Al^{27}(\gamma,n)Al^{26}$.

$P^{31}(\gamma,2p)Al^{29}$.—Cf. $P^{31}(\gamma,n)P^{30}$.

$Cu^{63}(\gamma,2p)Co^{61}$.—Cf. $Cu^{63}(\gamma,2n)Cu^{61}$. It is not clear how much of the Co^{61} was produced by the (γ,α) reaction on Cu^{65}.

In Table III there are given yields of the two-particle reactions, again relative to that of the $N^{14}(\gamma,n)$ reaction.

TABLE III. Relative yields of $(\gamma,2n)$ and $(\gamma,2p)$ reactions yield of $N^{14}(\gamma,n)N^{13}=1.00$ at each energy.

Reaction	Product half-life	Product betas and energies (Mev)	Relative yield 100 Mev	50 Mev
$C^{12}(\gamma,2n)C^{10}$	not observed	β^+ 3.4	<0.003	
$F^{19}(\gamma,2n)F^{17}$	72.0 sec.	β^+ 2.1	0.22	0.15
$P^{31}(\gamma,2n)P^{29}$	not observed	β^+ 3.6	<0.1[c]	
$Cu^{63}(\gamma,2n)Cu^{61}$	3.2 hr.	β^+ 0.9 (78%)	3.3	2.5
$Al^{27}(\gamma,2p)Na^{25}$	62.0 sec.	β^- 2.7 (45%)[a] 3.7 (55%)	0.15	0.14
$P^{31}(\gamma,2p)Al^{29}$	6.7 min.	β^- 2.5	0.20	0.15[d]
$Cu^{63}(\gamma,2p)Co^{61}$	1.8 hr.	β^- 1.1[b]		0.16[d]

[a] E. Bleuler and W. Zünti, Helv. Phys. Acta, **20**, 195 (1947).
[b] T. J. Parmley and B. J. Moyer, Phys. Rev. **72**, 82 (1947).
[c] 80-Mev x-ray energy.
[d] Value based on one experiment.

V. DISCUSSION

Preliminary measurements[9] indicate that the spectral distribution of quanta in the 100-Mev x-radiation from the betatron is in at least approximate agreement with theoretical predictions; that is, the number of quanta in a small energy interval is inversely proportional to the mean energy of the interval. As yet accurate measurements are not available of relative intensities, in terms of quanta, at various x-ray energies. For this reason it is difficult to compare on an absolute basis yields obtained at different energies, and therefore one of the (γ,n) yields has been taken as unity at each energy.

The neutrons and protons produced by the x-rays in the target and in the surroundings do cause some nuclear reactions. The yields of two such secondary reactions, $Cu^{63}(p,n)Zn^{63}$ and $Al^{27}(n,p)Mg^{27}$, in thick targets have been found[10] to be about 2×10^{-4} times those of primary (γ,n) reactions on copper and zinc. It is unlikely, therefore, that secondary processes can be responsible for any significant fraction of the yields of even the relatively improbable reactions studied. Another experiment involving the simultaneous exposure of samples in and outside the center of the x-ray beam set an upper limit at 1 percent for the fraction of the apparent "(γ,n) yields" which may actually be due to $(n,2n)$ reactions.

The apparently sudden increase in the (γ,n) yield, which occurs in the neighborhood of mass 60, is unexplained. It has been suggested that it may be related to the fact that in the cases investigated (Table I) the neutron excess $(A-2Z)$ is two or less for the target nuclei with masses below 60 and five or more for target nuclei with masses above 60. This explanation would not seem to agree with the fact that the yields for the two gallium isotopes are the same and the fact that no substantial changes in (γ,n) yields were observed between Cu^{63} with a neutron excess of five and Pd^{110} with a neutron excess of eighteen. Additional measurements should help to clarify this point. The high yield of the $Re^{187}(\gamma,n)$ reaction (about twice that of any other reaction studied) suggests that other cases above $A=120$ should also be investigated.

Although the five (γ,p) reactions studied involve target elements whose (γ,n) yields differ by large factors, no such differences appear in the (γ,p) yields. The values for the (γ,p) yields are of the same order as the (γ,n) yields for the species below copper. It seems hard to reconcile this result with the idea of evaporation from a compound nucleus.

The $(\gamma,2p)$ and $(\gamma,2n)$ yields are much lower than single-particle yields. That at least some three-particle yields are quite low also is evident from the fact that the (γ,n) yields from the two gallium isotopes are the same. The magnitudes of the relative (γ,n) yields from Cl^{35}, Cu^{63}, and Sb^{121}, in which cases the product could have been produced by $(\gamma,3n)$ reaction from the accompanying isotopes richer by two neutrons, also show that $(\gamma,3n)$ is a relatively improbable reaction.

The fact that the relative yields for the various (γ,n) and (γ,p) reactions follow, within experimental error, the same trend at 50-Mev as they do at 100-Mev maximum energy suggests either that quanta above 50-Mev in energy do not contribute very much to the (γ,n) yield or that the excitation curves (cross section *versus* photon energy) are similar except for an energy independent parameter. The first possibility is substantiated by some excitation measurements[11] for the reactions $Cu^{63}(\gamma,n)Cu^{62}$ and $C^{12}(\gamma,n)C^{11}$.

Further work on the yields of photo-nuclear reactions is clearly necessary. In particular, an extension of this research to reactions involving the emission of more than two nucleons, further studies on the dependence of yield on mass number, and investigations of excitation functions appear desirable.

ACKNOWLEDGMENTS

We wish to express our appreciation to Dr. E. E. Charlton and to the operators of the betatron for their cooperation and to Mr. G. Jaffe for his valuable assistance. It has been a pleasure to cooperate with Dr. R. V. Langmuir on the experiments which involved synchrotron irradiations.

[9] Private communication from Dr. J. L. Lawson.

[10] N. A. Bonner, G. Friedlander, L. P. Pepkowitz, and M. L. Perlman, Phys. Rev. **71**, 511 (1947).

[11] G. C. Baldwin and G. S. Klaiber, Phys. Rev. **73**, 1156 (1948).

An Extension of the Polarizability Theory of Raman Effect

FRANK MATOSSI AND ROBERT MAYER*
Naval Ordnance Laboratory, Washington, D. C.

(Received May 13, 1948)

The polarizability theory of Raman effect has two defects: (a) The depolarization factor ρ of Raman lines of totally symmetric oscillations of molecules can be given only by the indefinite statement $\rho<6/7$; additional utilization of the Silberstein model of optical anisotropy for a more precise prediction leads to wrong results. (b) The depolarization factor of the totally symmetric lines of calcite and aragonite should be zero for every orientation of the crystals, whereas finite values are observed for some orientations. The following cure is proposed. It is assumed that the atomic polarizability α is dependent on the exciting field strength E ($\alpha=\alpha_0+\beta E^2$). In the crystals, it is furthermore assumed that a disturbing field exists which depends on crystal symmetry. With these assumptions, it is possible to account for the observed results without changing the fundaments of the polarizability theory.

I. INTRODUCTION

THE well-known Placzek theory of Raman effect is based upon the suggestion that Raman scattering is due to changes in polarizability of molecules during vibration or rotation. This theory was very successful in describing and explaining many observed facts of importance, and it was also very helpful in giving information about molecular structure. There are, however, some topics apparently resisting this theory in its usual form. Some of these can easily be described in terms of this theory, without altering any of its main features other than by addition of such well founded concepts as anharmonic forces, quantum-resonance energy, and others. Of the remaining discrepancies, some minor ones may be due to the approximate character of some theoretical statements, but there are at least two items where observation and theory essentially disagree, so that for a long time it seemed hopeless to account for them in terms of the Placzek theory even if slight modifications or better approximations might be possible. These two main problems may be stated as follows.

(a) It is known that the depolarization factor[1] ρ of the coherent Rayleigh scattering can be computed from the assumption that scattering is produced by the induced dipole oscillating with the frequency of the incident radiation and that in addition to this the induced dipole moment is different in different directions of the molecule because of the mutual influence of the dipoles induced in the atoms of the molecule (Silberstein's model of optical anisotropy). According to theory, we should be able to compute the depolarization of Raman lines in a similar way by substituting the change of the polarizability for the induced moment into the equations of Rayleigh scattering. This treatment, though wholly in agreement with the fundamental principles of Placzek's theory and though successful in general statements, nevertheless fails if it is applied even to such simple molecules as H_2, O_2, and others.[2] E.g., for O_2 we observe $\rho=0.26$; the general theory gives $\rho<6/7$ as for all totally symmetric oscillations; computation as indicated above, with the aid of the Silberstein model, however, yields $\rho=0.63$. If it is not possible to explain this apparent failure of the polarizability theory in terms of this theory itself, we must abandon either the simple notion of mutual dipole action or the polarizability theory itself, each of which is very efficient in other respects.

An attempt to elucidate this problem in the light of existing theories has been made by Matossi,[2] in assuming that not only the molecular polarizability but also the atomic one depends on the distance between the atoms. In this purely phenomenological way, we are able to account

* Institute of Physics, University of Graz, Austria.

[1] ρ is defined as ratio of the intensity components of scattered rays vibrating perpendicular and parallel to the direction of incident rays.

[2] Cf. J. Cabannes and A. Rousset, J. de phys. et rad. 1, 155, 181, and 210 (1940); F. Matossi, Physik. Zeits. 45, 304 (1945) (see supplement).

for the observed depolarization factors. The change of atomic radius during the vibration, corresponding to the change of atomic polarizability, is only two to five percent (cf. the supplement). But a stronger foundation for the just-mentioned assumption was still missing.

(b) The normal theoretical treatment of the depolarization of those Raman lines which correspond to the totally symmetric pulsation of the CO_3 group in carbonates (1087 cm^{-1}) always leads to $\rho=0$, regardless of what orientation of crystal axes with respect to directions of incidence and observation is chosen. Experimental observation, however, indicates the contrary.[3] According to Michalke, we have for calcite $\rho_x=0$, $\rho_y=0.4\pm0.1$, $\rho_z=0.2\pm0.05$, where the indices x, y, z indicate the orientation of the optic axis, this being, respectively, parallel to the direction of incidence (x), observation (y), and perpendicular to both (z).

(c) It will be shown that it is possible to account for both of these discrepancies, if we assume that the atomic polarizability is not independent of the inducing electric field, but that the induced moment $\mathbf{p}$ may be written

$$\mathbf{p}=(\alpha_0+\beta E^2)\mathbf{E}, \quad \text{with} \quad \beta E^2 \ll \alpha_0. \tag{1}$$

In this equation, $\mathbf{E}$ is the electric field strength, $E=|\mathbf{E}|$. The justification (and necessity) of this hypothesis,[4] particularly the quadratic dependence of the polarizability on E, follows from the dispersion theory of anharmonic oscillators in third approximation.[5]

Furthermore, in the case of the carbonates, there must be assumed a disturbing field, homogeneous over the region of a CO_3 group, and not dependent on time (or at most slowly variable), its direction being determined by symmetry conditions. One might at first attribute the disturbance to a field emerging from the central atom of the plane CO_3 group, but here again the symmetry prevents an influence of this non-homogeneous field on the depolarization factor—hence the assumption of a homogeneous field, which may alter its strength and direction slowly compared with the time of oscillation.

We may imagine the disturbing field as representative of the deviations of the central field from exactly trigonal symmetry or as the resultant field of the neighboring atoms, these never being perfectly regularly distributed because of their vibrations and the non-ideal lattice.

We shall show that in the case of the crystals it will be sufficient to take notice only of the disturbing field without considering the mutual influence of the atoms. Taking the latter condition also into account would make computation very laborious and difficult to survey. We shall be content to obtain at least a possibility of explaining the above-mentioned results of observation without going into a too detailed quantitative treatment.

II. DIATOMIC MOLECULES

A simple calculation in a first approximation applied to Eq. (1) according to Silberstein's procedure,[6] leads to the following expressions for A_1 and B_1, the polarizabilities of the molecule of type X_2 parallel and perpendicular to its axis, respectively (we omit the index 0 at α_0 for sake of simplicity):

$$A_1=A_0\left\{1+\epsilon\left(1+\frac{A_0}{r^3}\right)\times\left[E_r^2\left(1+\frac{A_0}{r^3}\right)^2+E_n^2\left(1-\frac{B}{2r^3}\right)^2\right]\right\}, \tag{2a}$$

$$B_1=B_0\left\{1+\epsilon\left(1-\frac{B_0}{2r^3}\right)\times\left[E_r^2\left(1+\frac{A_0}{r^3}\right)^2+E_n^2\left(1-\frac{B}{2r^3}\right)^2\right]\right\}, \tag{2b}$$

in which $A_0=[2\alpha/1-(2\alpha/r^3)]$ and $B_0=[2\alpha/1+(\alpha/r^3)]$ are the polarizabilities for $\epsilon\equiv\beta/\alpha=0$, i.e., the normal Silberstein formulae. E_r and E_n are the components of the field strength of the

[3] D. Osborne, Thèses (Paris 1932); H. Michalke, Zeits. f. Physik **108**, 748 (1938). These authors disagree in the details but agree in the statement that ρ is not always vanishing. We use Michalke's data.

[4] Originally (cf. Naturwiss. **33**, 190 (1946)), we had used a linear function for α, $\alpha=\alpha_0+\beta E$, for which there is no theoretical foundation. The results (not published) are different only in quantitative respect.

[5] Cf. F. Matossi, Physik. Zeits. **40**, 323 (1939); the underlined terms of Eq. (8) of this paper, neglected there, are essential now.

[6] L. Silberstein, Phil. Mag. **33**, 92, 521 (1917); cf. also S. Bhagavantam, *Scattering of Light and the Raman Effect* (Chemical Publ. Company, Inc., New York, 1942), p. 101 ff.

In deriving the Eqs. (2), the induced dipole moment is given its value for $\epsilon=0$ in all terms containing ϵ as a factor.

incident wave parallel and perpendicular to the molecular axis; r is the distance between the two atoms.

Because of the smallness of ϵ, the terms containing ϵ are irrelevant for the computation of A_1 and B_1 themselves; therefore, the depolarization factor of Rayleigh scattering still is practically determined by A_0 and B_0. But for Raman scattering, the depolarization factor of which is given by the derivatives of A and B with respect to the normal coordinate, the case is different.

Abbreviating

$$\epsilon\left(1+\frac{A_0}{r^3}\right)=\epsilon_1, \quad \epsilon\left(1-\frac{B}{2r^3}\right)=\epsilon_2, \qquad E_r/E=v, \quad E_n/E=w, \tag{3}$$

we obtain

$$A_1=A_0\left(1+\frac{\epsilon_1^3}{\epsilon^2}v^2E^2+\frac{\epsilon_1\epsilon_2^2}{\epsilon^2}w^2E^2\right), \tag{4a}$$

$$B_1=B_0\left(1+\frac{\epsilon_1^2\epsilon_2}{\epsilon^2}v^2E^2+\frac{\epsilon_2^3}{\epsilon^2}w^2E^2\right). \tag{4b}$$

Differentiating these expressions with respect to the normal coordinate q of the vibration and denoting these derivatives by a prime, we have

$$A_1'=A_0'+2\left[\frac{\epsilon_1^3}{\epsilon^2}v^2+\frac{\epsilon_1\epsilon_2^2}{\epsilon^2}w^2\right]A_0EE', \tag{5a}$$

$$B_1'=B_0'+2\left[\frac{\epsilon_1^2\epsilon_2}{\epsilon^2}v^2+\frac{\epsilon_2^3}{\epsilon^2}w^2\right]B_0EE'. \tag{5b}$$

In these equations, we have neglected all terms of higher order which do not contain E' because of their smallness compared with A_0' and B_0'. However, it is not permissible to neglect terms with ϵ_1E' and ϵ_2E', since it is possible that $E'A_0$ and $E'B_0$ may become large relative to EA_0' and EB_0'. For if we have

$$E=E_0|\sin\omega t|, \quad q=q_0\sin(\omega_0t+\Delta), \tag{6}$$

E_0 and q_0 being the amplitudes of light-wave and molecular vibration and Δ being an arbitrary phase constant, we obtain

$$E'=(dE/dq)_{q=0}=(E_0\omega/q_0\omega_0)\cos(\omega/\omega_0)(n\pi-\Delta), \tag{7}$$

in which n is an integer. By comparing E' with $E_{q=0}=E_0|\sin(\omega/\omega_0)(n\pi-\Delta)|$, we obtain for the ratio $E'A_0/EA_0'$ the expression $\omega A_0/\omega_0q_0A_0'\approx10^2$ to 10^3, ignoring the sine and cosine functions.

To compute the depolarization factor of a gas consisting of molecules with the polarizability components (5), we proceed as usual;[7] however, we have to consider that A_1 and B_1 are themselves dependent on the orientation of the molecule on account of the factors v and w. But it is a sufficient approximation, to substitute for v^2 and w^2 their mean values, $\frac{1}{3}$ and $\frac{2}{3}$, respectively; then A_1' and B_1' are constant polarizability components, and the result of Born can be adopted immediately.

The result is:

$$\rho=(6\Omega/5\Omega_0+7\Omega), \tag{8}$$

with

$$\Omega=\langle(A_1'-B_1')^2\rangle_{Av}=(A_0'-B_0')^2+\epsilon'^2E_0^4(\epsilon_1A_0-\epsilon_2B_0)^2(\omega^2/\omega_0^2q_0^2), \tag{9}$$

$$\Omega_0=\langle(2B_1'+A_1')^2\rangle_{Av}=(2B_0'+A_0')^2+\epsilon'^2E_0^4(2\epsilon_2B_0+\epsilon_1A_0)^2(\omega^2/\omega_0^2q_0^2). \tag{10}$$

In these equations, it is written

$$\langle E^2E'^2\rangle_{Av}=\tfrac{1}{4}E_0^4(\omega^2/\omega_0^2q_0^2),$$

according to (6) and (7). Furthermore,

$$\epsilon'=(\epsilon_1^2+2\epsilon_2^2)/3\epsilon^2.$$

Estimating the value of q_0 for oxygen[8] to be $q_0=7\times10^{-10}$ cm and supposing $x=\epsilon E_0^2$ to be 0.01 and $\omega/\omega_0=16$ (for violet light), we calculate $\rho=0.27$, whereas $\rho=0.26$ is observed with oxygen. $\epsilon=0$ would give the result $\rho=0.63$. That $x=0.01$ is not too large a value is demonstrated by comparing the computed depolarization factors of Rayleigh scattering for $x=0.01$ and for $x=0$. We obtain with $\alpha=0.73\times10^{-24}$ cm^3, $r=1.5\times10^{-8}$ cm

$$\text{for } x=0.01: \quad \rho_{Rayl}=0.084, \qquad \text{for } x=0: \quad \rho_{Rayl}=0.082,$$

i.e., only an alteration by two percent, not exceeding the deviations of different measurements. In the case of Raman scattering, the assumption

[7] Cf. M. Born, *Optik* (Verlag Julius Springer, Berlin, 1933), pp. 81 and 82.

[8] Cf. K. W. F. Kohlrausch, *Ramanspektren, Hand- und Jahrbuch d. chem. Physik* (Becker und Erler, Leipzig, 1944), Vol. 9, Part IV, p. 65.

TABLE I.

	$\alpha\times10^{24}$ (cm³)	$r\times10^{8}$ (cm)	$\varrho_0\times10^{10}$ (cm)	ω_0 (cm^{-1})	ρ_{obs}.[2]	$\rho_{calc.}$ ($x=0.01$)	$\rho_{calc.}$ ($x=0$)
N_2	0.88	1.6	6.4	2330	0.19	0.26	0.63
O_2	0.73	1.5	7.3[5]	1555	0.26	0.27	0.63
H_2	0.40	1.44	17	4160	0.05	0.11 ($x=0.1$)	0.74
CO_2	1.0	2.0 (O−O)	7.0 estimated	1335	0.21	0.10 [0.21 for $x=0.0022$]	0.75
CS_2	3.2	2.52 (S−S)	7.0 estimated	660	0.15	0.23	0.65

$x=0.01$, however, leads to changing the depolarization factor by about 50 percent and therefore to a far better agreement with observation.

The results for those diatomic molecules, for which data are available, are recorded in Table I, which includes also CO_2 and CS_2, these molecules being treated as diatomic ones, because their C atom can be considered as unpolarizable. For the computation, ω is always taken as about 25000 cm^{-1}. There is, in principle, a dependence of ρ on ω but only in a very small amount. The values of α and r are taken from data for Rayleigh scattering for sake of consistency.

In general, the calculated values are still too high, but the agreement between observation and theory seems to be satisfactory.

Only the absolute value of ϵ is determined by Eqs. (7) to (9). In the next section, we find a negative ϵ; therefore here ϵ may be negative too.

Another interesting example is OCS. This molecule has two symmetric vibrations, at 860 and 2050 cm^{-1}. The former one has a very strong Raman line with $\rho=0.10$; it corresponds to the totally symmetric vibration of CO_2 (S and O in opposite phases).[9] But for the much weaker Raman line at 2050, we have $\rho=0.77$; this vibration corresponds to the antisymmetric one of CO_2 (S and O in equal phases). It is understandable that the theory developed here applies only to the 860 line, in which the distance O−S changes appreciably. The other vibration approximately lets this distance unchanged. We can assume that only this distance is relevant for Raman effect, treating OCS as a diatomic molecule OS because of $\alpha_C=0$, and that for 2050 the normal theory with $\epsilon=0$ will be accurate enough. Then the theoretical value of ρ for this line is $\rho=0.80$, in sufficient agreement with the experiment. The lower value for the other line may be explained qualitatively in the same manner as above for the diatomic molecules.

Other unsymmetric linear molecules, as ClCN, have both symmetric Raman lines strongly polarized ($\rho=0.20$ and 0.24, respectively). Probably they cannot be treated in the same manner as OCS, because the assumption $\alpha=0$ for C might not be fulfilled in this case (different bonds at the C atom).

III. CALCITE AND ARAGONITE

As mentioned in the introduction, the assumption that the polarizability is dependent on the field strength is not sufficient to account for the observed results concerning the depolarization factors of the Raman lines of the totally symmetric vibration of the CO_3 group. This arises from the trigonal symmetry of this group, the general theory here giving unequivocal results independent of assumptions about the polarizability. Therefore, a field-dependent α alone cannot help, and we have assumed the disturbing field, also mentioned above, neglecting here the mutual influence of the atoms because, on one hand, the greater distance of the O atoms in the CO_3 group reduces this mutual action and because, on the other hand, it is unnecessary for explaining the main features of the observations. In any case, the polarizability of the central atom can be considered as small enough to be irrelevant. The experimental data are not yet sufficiently reliable to justify going into greater detail.

We characterize the calcite crystal by one of its CO_3 groups. The x axis of the coordinates may be one of the altitudes of the CO_3 group, the y axis being parallel to the corresponding triangle side. The normal of the group plane corresponds to the optic axis of the crystal. The incident light-wave may have the components E_y and E_z of the electric field strength $\mathbf{E}$; the disturbing field $\mathbf{E}_d$ may have the components E_{dz} and E_{dy}, $\mathbf{E}_d$ being in the CO_3 plane. Denoting the components of the total moment of all three oxygen atoms as $P_x=p_{1x}+p_{2x}+p_{3x}$, P_y, P_z, we have $\rho_z=\langle P_x'^2\rangle_M/\langle P_z'^2\rangle_M$, the primes indicating differentiation with respect to the normal coordinate of vibration, the bars indicating aver-

[9] J. Wagner, Zeits. f. physik. Chemie **193**, 55 (1943).

aging. Interchanging y axis and z axis, we obtain $\rho_y=\langle P_z'^2\rangle_{Av}/\langle P_y'^2\rangle_{Av}$. Interchanging x axis and z axis, we obtain $\rho_z=\langle P_z'^2\rangle_{Av}/\langle P_x'^2\rangle_{Av}$.

However, in this case, $\mathbf{E}$ has only the components E_x and E_y. Hence $\rho_x=0$, because P_x is proportional to E_x. $\rho_x=0$ is also the result obtained by all observers.

The assumptions mentioned above lead to

$$\begin{aligned} P_x&=3\{\alpha+\beta|\mathbf{E}+\mathbf{E}_d|^2\}E_{dx},\\ P_y&=3\{\alpha+\beta|\mathbf{E}+\mathbf{E}_d|^2\}(E_y+E_{dy}),\\ P_z&=3\{\alpha+\beta|\mathbf{E}+\mathbf{E}_d|^2\}E_z, \end{aligned} \tag{11}$$

in which α and β refer to a single atom.

From (11), we get

$$\begin{aligned} P_x'&=6\beta E_{dx}(EE'+E_{dy}E_y'),\\ P_y'&=3\alpha E_y'+6\beta(E_y+E_{dy})(EE'+E_{dy}E_y')\\ &\quad+3\beta(E_d^2+E^2+2E_{dy}E_y)E_y',\\ P_z'&=3\alpha E_z'+6\beta E_z(EE'+E_{dy}E_y')\\ &\quad+3\beta(E_d^2+E^2+2E_{dy}E_y)E_z'. \end{aligned} \tag{12}$$

In calculating the mean squares of these components, the average values with respect to t (in E), to Δ (in E'), and to the orientation (in E_y, E_z) are taken independently. Then, after some elementary calculations, the depolarization factors ρ_y and ρ_z are

$$\begin{aligned} \rho_y&=\frac{4\beta^2E_{dx}^2(E_0^2+E_{dy}^2)}{\alpha^2+\beta^2(E_d^4+(27/8)E_0^4+4E_{dy}^4+3E_d^2E_0^2+4E_d^2E_{dy}^2+24E_0^2E_{dy}^2)+2\alpha\beta(E_d^2+\frac{3}{2}E_0^2+2E_{dy}^2)},\\ \rho_z&=\frac{4\beta^2E_{dx}^2(E_0^2+E_{dy}^2)}{\alpha^2+\beta^2(E_d^4+(27/8)E_0^4+3E_d^2E_0^2+2E_0^2E_{dy}^2)+2\alpha\beta(E_d^2+\frac{3}{2}E_0^2)}. \end{aligned} \tag{13}$$

It is seen at once that ρ vanishes if $E_{dx}=0$. This is quite understandable, since only a component of the disturbing field in the x direction may cause an induced moment in this same direction, if mutual action is neglected. If $E_{dy}=0$, it is $\rho_y=\rho_z$.

A difference of ρ_y and ρ_z, as it is observed experimentally, may only occur if E_{dy} does not vanish. Indeed, it must be supposed that the disturbing field does not remain parallel to the x direction, the direction of one altitude of the triangle. It will rather change its direction irregularly, or the field direction may be different at different CO_3 groups. Therefore, we should average with respect to all possible field directions. According to the individual features of the disturbing field, which might be different for each individual crystal, these mean values of ρ might be different also in different samples.

$\mathbf{E}_d$ may be supposed to remain constant in value, only the direction varying. If the field assumes all directions in the CO_3 plane or only those parallel to the altitudes of the CO_3 triangle, as it seems natural for a calcite crystal, we have, with the abbreviations

$$\epsilon E_0^2=x,\quad \epsilon E_d^2=y; \tag{14}$$

$$\begin{aligned} \bar\rho_y&=\frac{2xy+\frac{1}{2}y^2}{1+(27/8)x^2+(9/2)y^2+15xy+3x+4y},\\ \bar\rho_z&=\frac{2xy+\frac{1}{2}y^2}{1+(27/8)x^2+y^2+4xy+3x+2y}. \end{aligned} \tag{15}$$

With $x=-0.02$ and $y=-0.35$, we obtain, in sufficient agreement with the observations

$$\begin{aligned} &\bar\rho_y=0.39,\quad \bar\rho_z=0.19\\ (\text{observed:}\quad &0.4,\qquad 0.2\ ). \end{aligned}$$

Slight changes in y cause great changes in $\bar\rho_y$. The numerical value of y seems to be reasonable, but in view of the qualitative character of the treatment, its exact value is not of essential importance. As is seen from Eq. (11), it is not necessary to assume $\epsilon|\mathbf{E}+\mathbf{E}_d|^2$ to be very small because, in the approximation expressed by (11), β does not influence the depolarization of the Rayleigh scattering at all.[10]

[10] Equation (11) does not give correct values of ρ for Rayleigh scattering (cf. the complete theory of Rayleigh scattering in crystals, F. Matossi, Zeits. f. Physik **92**, 425 (1934) and the observations of S. Bhagavantam and J. V. Narayana, Proc. Ind. Acad. Sci. **A16**, 366 (1942); therefore, it may be doubted, whether (11) should be used in the treatment of Raman effect. But what is important in our considerations is the influence of β, which nevertheless may be obtained in a fair approximation.
There may be one objection more: $\alpha+\beta|\mathbf{E}+\mathbf{E}_d|^2$ is the

The depolarization factors for polarized excitation may be obtained starting from (12) in the same manner as above. The final formulae are for $E_z=0$:

$$\rho_y=E_{dx}^2/E_{dy}^2,$$

$$\rho_z=\infty$$

and for $E_y=0$:

$$\rho_y=\frac{4\beta^2E_{dx}^2(\frac{1}{2}E_0^2+E_{dy}^2)}{\alpha^2+\beta^2(E_d^4+(27/8)E_0^4+4E_{dy}^4+3E_d^2E_0^2+4E_d^2E_{dy}^2+24E_0^2E_{dy}^2)+2\alpha\beta(E_d^2+\frac{3}{2}E_0^2+2E_{dy}^2)},$$

$$\rho_z=\frac{2\beta^2E_0^2E_{dx}^2}{\alpha^2+\beta^2(E_d^4+(27/8)E_0^4+3E_d^2E_0^2)+2\alpha\beta(E_d^2+\frac{3}{2}E_0^2)};$$

or, after averaging with respect to the directions of $\mathbf{E_d}$ in the CO_3 group as above,

for $E_z=0$:

$$\bar\rho_y=1,$$

$$\bar\rho_z=\infty;$$

for $E_y=0$:

$$\bar\rho_y=\frac{xy+\frac{1}{2}y^2}{1+(27/8)x^2+(9/2)y^2+15xy+3x+4y},$$

$$\bar\rho_z=\frac{xy}{1+(27/8)x^2+y^2+3xy+3x+2y}.$$

With the same values of x and y as before, calculated ρ values are

for $E_z=0$:

$$\bar\rho_x=0,\qquad \bar\rho_y=1\qquad \bar\rho_z=\infty;$$

observed is,[11] respectively:

$$0.4,\qquad 2,\qquad 10;$$

for $E_y=0$:

$$\bar\rho_x=0,\qquad \bar\rho_y=0.35,\quad \bar\rho_z=0.02;$$

observed respectively:

$$0.05,\qquad 0.6,\qquad 0.5.$$

Considering the approximative character of the theory, the utilization of only two adjustable magnitudes (x and y) and the difficulty of measuring depolarization factors of crystals, the agreement between theory and experiment is not inacceptable. The values measured by Bhagavantam do not seem to be very reliable; at least the first one is certainly too high ($\rho=\infty$ and $\rho=10$ are quite compatible values).

Also for aragonite there are observations[12] which are anomalous for the Raman line at 1087 cm^{-1}. Because of the rhombic symmetry (D_{2h}) of aragonite, we have six different crystal positions with respect to the x-y-z system. Designating with ζ the axis perpendicular to the CO_3 groups, with ξ, a direction parallel to one altitude of a CO_3 triangle perpendicular to a symmetry plane of the crystal, the different positions may be characterized by the following scheme, which at the same time contains the observed ρ values:

1	2	3	4	5	6
$x\ y\ z$	$x\ y\ z$	$x\ y\ z$	$x\ y\ z$	$x\ y\ z$	$x\ y\ z$
$\zeta\ \xi\ \eta$	$\zeta\ \eta\ \xi$	$\xi\ \zeta\ \eta$	$\eta\ \zeta\ \xi$	$\xi\ \eta\ \zeta$	$\eta\ \xi\ \zeta$
$\rho=0$	0	0.3	0.3	0.3	0.3

According to the D_{2h} symmetry, we assume $\mathbf{E_d}$ to have finite values approximately only in directions 90° apart ($E_{dz}=0$ or $E_{dy}=0$). Then we obtain the following theoretical expressions for ρ, in the same manner as above:

$$\bar\rho_1=\bar\rho_2=0,$$

$$\bar\rho_3=\bar\rho_4=\frac{2xy}{1+(27/8)x^2+5y^2+15xy+3x+4y},$$

$$\bar\rho_5=\bar\rho_6=\frac{2xy}{1+(27/8)x^2+y^2+4xy+3x+2y}.$$

polarizability of the molecule in the solid state, which differs from that in gaseous state, $\alpha+\beta E^2$, appreciably, if γ is not very small. Normally, the difference of polarizabilities, determined by the Lorentz-Lorenz-formula, is only small; but just in the cases we are dealing with, it is not possible to measure the refractive indices for gaseous and fluid states without destroying the substance. Therefore, we cannot finally decide this question from observational data.

[11] S. Bhagavantam, Proc. Ind. Acad. Sci. **A8**, 345 (1938).

[12] L. Couture, Comptes Rendus **218**, 669 (1944).

It is not possible to regain the observed values exactly. One of the best theoretical values is reached for $x=y=-0.22$. Then $\bar{\rho}_3=0.16$ and $\bar{\rho}_5=0.32$. In spite of the discrepancy for $\bar{\rho}_3$, which is not too serious (Couture does not give the limits of accuracy, she only states $\rho=\sim 0.3$), these results may be accepted as another qualitative indication that the theory is able to account in principle for anomalous depolarization factors.

It should be mentioned, however, that the total intensities of the Raman lines are not described accurately by this theory. But there might be other factors influencing the excitation of Raman lines in different crystal orientations, affecting the absolute values but not the ratios of the scattered intensity components. These factors are not yet understood. Another possibility of explaining the anomalies of ρ in calcite and aragonite, deviation of the CO_3 group from strictly trigonal symmetry, is unable as well to account for the intensities.[13] It is uncertain whether a combination of both theories (field dependency and deviation of symmetry) would give better results in this respect.

There remain at least two questions: Why do such anomalies or such disturbing fields occur just in calcite and aragonite, while for other crystals we have no indication for a similar behavior? Is the neglection of mutual influence really justified? A negative answer to the last question might change the numerical conclusions but hardly the qualitative result, the necessity of a field-dependent polarizability and of a disturbing crystal field.

IV. SUMMARY

Assuming a small dependence of atomic polarizability on inducing field strength and utilizing the Silberstein concept of mutual interaction of induced dipoles, it is possible to compute the depolarization factors of Raman lines of diatomic molecules as well as those of Rayleigh scattering in agreement with observation.

Furthermore, assuming a disturbing field in $CaCO_3$ crystals, it is possible to account for the observed non-vanishing depolarization factors of the Raman lines of the totally symmetric vibration.

SUPPLEMENT

Because the issue of the Physikalische Zeitschrift cited in reference 2 is not easily available, the results of that paper may be reviewed shortly.

It was assumed that α be dependent on the distance r between the atoms of linear molecules, α being the *atomic* polarizability. Then

$$\rho=\frac{6b^2}{45a^2+7b^2}$$

with $b^2=(A'-B')^2$, $a=\frac{1}{3}(A'+2B')$, and

$$A'=\frac{2(d\alpha/dr)[1-(2\alpha/r^3)]}{[1-(2\alpha/r^3)]^2},$$

$$B'=\frac{2(d\alpha/dr)[1+(\alpha/r^3)]}{[1+(\alpha/r^3)]^2}.$$

From the observed ρ values and these formulae, $d\alpha/dr$ is computed. The result is contained in the following table, together with the relative change of atomic radius R which corresponds to the change of α for $dr=q_0$, the amplitude of the oscillation. dR/R is small enough to justify the procedure.

	H_2	O_2	CO_2	CS_2	
$10^{16}(d\alpha/dr)$	0.27	0.6	0.76	3.3	cm^2
dR/R	0.05	0.02	0.02	0.02	

Dr. G. B. Sabine and Dr. L. Mundie have given valuable aid in the English formulation.

Note added in proof.—Independent from us, H. Senftleben and H. Gladisch recently [Naturwiss. **34**, 187 (1947)] suggest the same hypothesis as we to explain some results about the dependence of heat transfer on electric fields.

[13] H. Michalke, see reference 3; F. Matossi, Zeits. f. Physik **64**, 34 (1930).

PHYSICAL REVIEW VOLUME 74, NUMBER 4 AUGUST 15, 1948

On the Classical Equations of Motion of Point Charges

PETER HAVAS
Department of Physics, Lehigh University, Bethlehem, Pennsylvania
(Received February 9, 1948)

Recent attempts to obtain the force of radiative reaction in the classical equations of motion of point charges have proceeded from two different viewpoints. Each of these has to introduce one basic assumption in addition to Maxwell's equations, namely the conservation law for the electromagnetic energy-momentum tensor in field theory and the relation between the Lorentz force and the momentum of the particle in action-at-a-distance theory. In previous field-theoretical derivations the Lorentz-Dirac equations including radiation damping are obtained only if one takes the field produced by the particle to be the retarded field; but equations of motion without the damping term are obtained if one uses half the sum of retarded and advanced fields. On the other hand, the theory of action at a distance as developed by Wheeler and Feynman was able to obtain the radiation damping using fields symmetric in time. It is noted that the need for the exclusive use of retarded fields arose only in the field-theoretical derivations for the one-particle problem. The considerations of Wheeler and Feynman on the total field due to all particles of the universe are, however, applicable to field theory in the symmetric form as well as to action-at-a-distance theory. The acceptance of their condition of "complete absorption" again leads to the radiation damping term in the equations of motion of the many-body problem. Some implications of this result are discussed.

I. INTRODUCTION

ONE of the major problems of classical electrodynamics has been to account for the force experienced by a charge as a result of its motion. The first attempt at a solution due to Lorentz[1] was based on a model of an extended charge and attributed the force of radiative reaction to the action of one part of the particle on another. It appeared as the first term in a series in powers of the radius of the particle, and all higher terms depended upon the charge distribution assumed. This, and the fact that it appears to be very difficult to fit finite-sized elementary particles into the schemes of relativity and of quantum mechanics makes it desirable to treat these particles as mathematical points.[2] In Lorentz' theory, however, infinities appear in the equations if the radius goes to zero.

Recent attempts to obtain the force of radiative reaction have proceeded from two different viewpoints. One is that of field theory, which considers the *total* field at all points in space to be the fundamental physical quantity and the point charges as singularities of the field. The other is that of action at a distance, which considers only the forces exerted on a charge by *other* charges to be physically meaningful.

The field theoretical point of view was first applied successfully to this problem by Dirac,[3] who showed that the equations of motion are suggested by the conservation law for the electromagnetic energy-momentum tensor. He clearly stated it as follows: "The usual derivation of the stress-tensor is valid only for continuous charge distributions and we are here using it for point charges. This involves adopting as a fundamental assumption the point of view that energy and momentum are localized in the field in accordance with Maxwell's and Poynting's ideas." Using this conservation law and Maxwell's equations he obtained Lorentz' equations of motion, but whereas these equations were considered by Lorentz to be only approximate, Dirac concluded that "there is good reason for believing them exact, within the limits of the classical theory."

Another field theoretical derivation of these equations was given by Infeld and Wallace,[4] who succeeded in linking it with the general method of obtaining equations of motion in general relativity of Einstein, Infeld and Hoffmann.[5] The main interest of their paper for the present purpose is that they showed explicitly that, for the case of a single particle, the Lorentz-Dirac equations including radiation damping are ob-

[1] H. A. Lorentz, *Collected Papers* (M. Nijhoff, The Hague, 1936), Vol. II, pp. 281 and 343. Also *The Theory of Electrons* (Teubner, Leipzig, 1909), pp. 49 and 253.
[2] Cf. J. Frenkel, Zeits. f. Physik **32**, 518 (1925).
[3] P. A. M. Dirac, Proc. Roy. Soc. **A167**, 148 (1938). In the following quoted as D.
[4] L. Infeld and P. H. Wallace, Phys. Rev. **57**, 797 (1940). In the following quoted as IW.
[5] A. Einstein, L. Infeld and B. Hoffmann, Ann. Math. **39**, 65 (1938).

tained only if one takes the field produced by the particle to be the *retarded* field; but equations of motion without the damping term are obtained if one uses half the sum of retarded and advanced fields.

The first derivation of the force of radiative reaction on the basis of action at a distance is due to Wheeler and Feynman.[6] As it is necessary in any action-at-a-distance theory to introduce an assumption on the basic equations of motion, they had to assume that the Lorentz force acting on a particle equals its rate of change of momentum. On the other hand, they were able to obtain the Lorentz-Dirac equations taking the forces on the charges as determined by half the sum of the retarded and the advanced field.

It was of considerable importance to show that the fundamental law of force is symmetric with respect to past and future, and to settle the question first raised in 1909, in which "Ritz considers the limitation to retarded potentials as one of the foundations of the second law of thermodynamics, while Einstein believes that the irreversibility of radiation depends exclusively on considerations of probability."[7] It appeared that the theory of action at a distance was preferable to the point of view of field theory, which seemed incapable of explaining the radiation reaction using fields symmetric in time.

However, we shall show that this is actually not the case. The need for the exclusive use of retarded fields for the explanation of the radiative reaction arose only in the field-theoretical derivations for the *one-particle* problem. The considerations of WF on the total field due to *all* particles are, however, applicable to field theory as well as to the theory of action at a distance. The acceptance of their condition of "complete absorption" does not yield any new results in field theory if the retarded field alone is used, but in the case of half-advanced, half-retarded fields it does provide the radiation-damping term in the equations of motion. Therefore, subject to this condition, *one can obtain the Lorentz-Dirac equations in both theories starting with fields symmetric in time, in spite of the fundamentally different underlying physical ideas.*[8]

II. FIELD THEORY: THE FORMULATION OF INFELD AND WALLACE

We shall first outline the field theoretical derivation of the equations of motion due to Infeld and Wallace.[4] We write down the conservation laws for the electromagnetic energy-momentum tensor:

$$T_{mn,n}=T_{mo,o} \qquad \text{(IW 2.1)}$$

$$T_{on,n}=T_{oo,o} \qquad \text{(IW 2.2)}$$

where

$$T_{mn}=\text{Maxwell stress tensor}=F_{ms}F_{ns}-F_{mo}F_{no}-1/4\delta_{mn}F_{rs}F_{rs}+1/2\delta_{mn}F_{so}F_{so} \qquad \text{(IW 2.3)}$$

$$T_{on}=\text{Poynting vector}=F_{so}F_{sn} \qquad \text{(IW 2.4)}$$

$$T_{oo}=\text{Energy density}=1/2F_{so}F_{so}+1/2F_{rs}F_{rs} \qquad \text{(IW 2.5)}$$

$F_{so}=E_s$ and $F_{mn}=\epsilon_{mns}H_s$ where E_s and H_s are the electric and magnetic field respectively, δ_{mn} is the Kronecker symbol, and ϵ_{mns} is the permutation symbol (Levi-Civita tensor density). Latin letters run from 1 to 3 and repetition of an index implies summation over this range. "$,n$" and "$,o$" denote partial derivatives with respect to the coordinates x^n and time, respectively. The velocity of light is taken as unity.

The conservation laws break down only at points occupied by a singularity. We shall choose a Lorentz frame of reference in which the point charge is instantaneously at rest at the origin at some moment t. Then if we take any surface enclosing the singularity it can be shown that the four surface integrals

$$\int(T_{mn}+\psi_{m,n})\lambda^n dS \qquad \text{(IW 2.10)}$$

$$\int(T_{on}+\psi_{o,n})\lambda^n dS \qquad \text{(IW 2.11)}$$

[6] J. A. Wheeler and R. P. Feynman, Rev. Mod. Phys. **17**, 157 (1945). In the following quoted as WF.

[7] W. Ritz and A. Einstein, Phys. Zeits. **10**, 323 (1909).

[8] In talking of the "equivalence" of the theory of action at a distance and field theory, WF refer only to the formal equivalence of the final equations of motion obtained in the two theories. However, the derivation of the Lorentz-Dirac equations requires, as noted above, in addition to Maxwell's equations common to both theories, assumptions which are fundamentally different for these theories, and which differentiate them by more than just "language". By treating Dirac's results as a "prescription", WF do not enter into an examination of these assumptions at all. This is the object of the present paper, which will show that the equivalence extends to the use of fields symmetric in time.

are independent of the shape and size of the surface chosen, and hence can depend only on quantities characterizing the singularity, in particular the coordinates of the singularity and their time derivatives. Here λ^n are the direction cosines of the normal to the surface of integration,

$$\psi_m = \Psi_m - \bar{\psi}_m \qquad \text{(IW 2.14)}$$

$$\psi_o = \Psi_o - \bar{\psi}_o \qquad \text{(IW 2.15)}$$

where $\bar{\psi}_m$, $\bar{\psi}_o$ are arbitrary harmonic functions and Ψ_m, Ψ_o are solutions of the Poisson equation which do not contain in their development with respect to r an harmonic function of the type $1/r$.

The motion of the singularity is determined by the assignment of consistent values to the four surface integrals. We can assume that they are equal to zero and shift the task of determining the motion to the choice of the arbitrary harmonic functions. Calling the coordinates of the singularity $\eta^r(t)$, and indicating derivatives with respect to time by dots, we have as the simplest non-trivial choice[9]

$$\bar{\psi}_m = m_o(\ddot{\eta}^m/r)$$

and obtain then for the equations of motion

$$m_o\ddot{\eta}^m = -1/4\pi \int (T_{mn} + \Psi_{m,n})\lambda^n d\xi. \qquad \text{(IW 2.16)}$$

We note that up to this stage it did not matter if retarded or advanced fields were used. We are only concerned with this problem when we evaluate the integral over T_{mn}.

The integrals over $\Psi_{m,n}$ can be shown to be zero. For the fields determining T_{mn} we have to take the total fields

$$F_{mn} = \gamma_{m,n} - \gamma_{n,m} + {}_{\text{ext}}F_{mn} \qquad \text{(IW I.1)}$$

$$F_{mo} = \gamma_{m,o} - \gamma_{o,m} + {}_{\text{ext}}F_{mo} \qquad \text{(IW I.2)}$$

where γ_o is the electromagnetic scalar potential, and γ_m the vector potential of the field of the point charge itself, and ${}_{\text{ext}}F_{\mu\nu}$ is the external field (including the fields of other point charges).

If we take for γ_μ half the sum of the retarded and advanced potentials, we obtain for the equations of motion

$$m_o\ddot{\eta}^m = e\ {}_{\text{ext}}E_m \qquad \text{(IW 2.17)}$$

where ${}_{\text{ext}}E_m$ is the external electric field (the fields of the other point charges also being taken as 1/2 (retarded+advanced) field) evaluated at the position of the singularity at the moment t. These are just the usual equations of motion without radiation reaction, *except for the special form of the fields of the other charges.*

If we choose for γ_μ retarded potentials only, we obtain

$$m_o\ddot{\eta}^m = e\ {}_{\text{ext}}E_m + 2/3e^2\dddot{\eta}^m \qquad \text{(IW 2.18)}$$

where we have to take in ${}_{\text{ext}}E_m$ the contribution due to other charges as retarded fields only. These equations do contain the radiation reaction.

The above equations held in a special coordinate system only. We consider a four-space with coordinates x^μ and signature $+ - - -$, Greek letters taking the values 0, 1, 2, 3 where x^0 is the time coordinate and x^1, x^2, x^3 are the space coordinates. The vector v^μ is defined as the four-dimensional velocity vector of the point charge. Accents indicate differentiation with respect to arc length in space-time. Then it may be shown that in the first case (from now on referred to as the symmetric case) the equations of motion become

$$m_o v'^\mu = e\ {}_{\text{ext}}F_\nu{}^\mu v^\nu \qquad \text{(IW 2.19)}$$

and in the second case (from now on referred to as the retarded case)

$$m_o v'^\mu = e\ {}_{\text{ext}}F_\nu{}^\mu v^\nu + 2/3e^2 v''^\mu + 2/3e^2 v'^2 v^\mu \qquad \text{(IW 2.20)}$$

where ${}_{\text{ext}}F_\nu{}^\mu$ is evaluated at the world point of the singularity and contains symmetric contributions from the other charges in the symmetric case and retarded contributions only in the retarded case.[10] Equations (IW 2.20) are just the Lorentz-Dirac equations.

[9] It has been shown in IW that this choice corresponds to the choice of an energy-momentum tensor for matter and that the arbitrariness can be removed by an appeal to the general relativity theory. The same argument holds also for the choice necessary at the corresponding stage of the derivation in *D*. Equations of motion based on the derivation of *D*, but using a different choice of the "arbitrary" functions, have been suggested by C. J. Eliezer, Proc. Camb. Phil. Soc. 42, 278 (1946). It appears from the above that while these equations are perfectly consistent with the special theory of relativity, they are in conflict with the general theory.

[10] This distinction in the meaning of ${}_{\text{ext}}F_\nu{}^\mu$ in the two sets of equations has not been made explicit in IW, as that paper was not concerned with any application of those equations, but it is obvious from their derivation.

For future reference we shall make the distinction between the meaning of ${}_{\text{ext}}F_\nu{}^\mu$ in Eqs. (IW 2.19) and (IW 2.20) explicit by writing it as

$$ {}_{\text{ext}}F_\nu{}^\mu = \sum_{k\neq a} 1/2({}_{\text{ret}}F_\nu{}^{\mu(k)} + {}_{\text{adv}}F_\nu{}^{\mu(k)}) + {}_eF_\nu{}^\mu \quad (1) $$

in the symmetric case and

$$ {}_{\text{ext}}F_\nu{}^\mu = \sum_{k\neq a} {}_{\text{ret}}F_\nu{}^{\mu(k)} + {}_eF_\nu{}^\mu \quad (2) $$

in the retarded case. Here ${}_{\text{ret}}F_\nu{}^{\mu(k)}$ and ${}_{\text{adv}}F_\nu{}^{\mu(k)}$ are the retarded and advanced fields of the k-th charge, and ${}_eF_\nu{}^\mu$ is a solution of Maxwell's equations for empty space, which of course is not necessarily the same in the retarded and in the symmetric case.

We obtain, therefore, for the equations of motion

$$ m_a v_a{}'^\mu = e_a \sum_{k\neq a} 1/2({}_{\text{ret}}F_\nu{}^{\mu(k)} + {}_{\text{adv}}F_\nu{}^{\mu(k)}) v_a{}^\nu + e_a\, {}_eF_\nu{}^\mu v_a{}^\nu \quad (3) $$

for the symmetric case, and

$$ m_a v_a{}'^\mu = e_a \sum_{k\neq a} {}_{\text{ret}}F_\nu{}^{\mu(k)} v_a{}^\nu + e_a\, {}_eF_\nu{}^\mu v_a{}^\nu + 2/3 e_a{}^2 v_a{}''^\mu + 2/3 e_a{}^2 v_a{}'^2 v_a{}^\mu \quad (4) $$

for the retarded case. All F's are evaluated at the world point of the a-th singularity, whose rest mass we have denoted by m_a now instead of m_o, its velocity vector by $v_a{}^\mu$, and its charge by e_a.

Dirac's results are entirely equivalent to those of Infeld and Wallace. As Dirac states, however, of Eq. (4) that it has been "obtained in a theory which is fundamentally symmetrical between retarded and advanced potentials", we shall show in the Appendix that actually he did not use any symmetry relations in his derivation of the above equations, but retarded fields only.

III. ACTION AT A DISTANCE: THE WHEELER-FEYNMAN THEORY

In the theory of action at a distance as developed by Fokker[11] and Wheeler and Feynman[6] the equations of motion of the a-th charge are assumed to be[12]

$$ m_a v_a{}'^\mu = e_a F_\nu{}^\mu v_a{}^\nu \quad (5) $$

where the right-hand side is the Lorentz force acting on the particle, and F is the field

$$ \sum_{k\neq a} 1/2({}_{\text{ret}}F^{(k)} + {}_{\text{adv}}F^{(k)}). \quad \text{(WF 38)} $$

Therefore, we have

$$ m_a v_a{}'^\mu = e_a \sum_{k\neq a} 1/2({}_{\text{ret}}F_\nu{}^{\mu(k)} + {}_{\text{adv}}F_\nu{}^{\mu(k)}) v_a{}^\nu. \quad (6) $$

The expression (WF 38) can be broken down into three parts

$$ \sum_{k\neq a} {}_{\text{ret}}F^{(k)} + (1/2\ {}_{\text{ret}}F^{(a)} - 1/2\ {}_{\text{adv}}F^{(a)}) - \sum_{\text{all } k} 1/2({}_{\text{ret}}F^{(k)} - {}_{\text{adv}}F^{(k)}). \quad \text{(WF 39)} $$

The second term of this will contribute to the force an expression

$$ e_a(1/2\,{}_{\text{ret}}F_\nu{}^{\mu(a)} - 1/2\,{}_{\text{adv}}F_\nu{}^{\mu(a)}) v_a{}^\nu. $$

This reduces, according to Dirac, to the form

$$ 2/3 e_a{}^2 (v_a{}^\mu v_{a\nu}{}'' - v_a{}''^\mu v_{a\nu}) v_a{}^\nu \quad \text{(WF 41)} $$

which can also be written

$$ 2/3 e_a{}^2 (v_a{}''^\mu + v_a{}'^2 v_a{}^\mu). $$

The third term has no singularities anywhere and is, therefore, a solution of Maxwell's equations for empty space, which we shall call ${}_fF$ to distinguish it from the empty-space solutions introduced in (1) and (2), or

$$ {}_fF = \sum_{\text{all } k} 1/2({}_{\text{ret}}F^{(k)} - {}_{\text{adv}}F^{(k)}). \quad (7) $$

Then we obtain for the final equations of motion

$$ m_a v_a{}'^\mu = e_a \sum_{k\neq a} {}_{\text{ret}}F_\nu{}^{\mu(k)} v_a{}^\nu + 2/3 e_a{}^2 (v_a{}''^\mu + v_a{}'^2 v_a{}^\mu) + e_a {}_fF_\nu{}^\mu v_a{}^\nu \quad \text{(WF 44)} $$

for the case which WF call "incomplete absorption". The case which they call "complete absorption" is characterized by

$$ \sum_{\text{all } k} ({}_{\text{ret}}F^{(k)} - {}_{\text{adv}}F^{(k)}) = 0 \text{ (everywhere)}. \quad \text{(WF 37)} $$

Using this relation,[13] we obtain for the equations

[11] A. D. Fokker, Zeits. f. Physik **58**, 386 (1929). We are not concerned here with other formulations of action at a distance using retarded interactions only.

[12] Here and in the following we shall change the notation of WF slightly to conform to the one employed above.

[13] While (WF 37) was obtained in WF from the relation $\sum_{\text{all } k} (1/2\ {}_{\text{ret}}F^{(k)} + 1/2\ {}_{\text{adv}}F^{(k)}) = 0$ (outside the absorber) (WF 33), it is only (WF 37) which is used in the equations of motion. As (WF 33) necessitates a division of the universe into a part "inside" the absorber and a part "outside" it, it appears irreconcilable with any current cosmological

of motion

$$m_a v_a'^{\mu} = e_a \sum_{k \neq a} {}_{\text{ret}}F_{\nu}^{\mu(k)} v_a^{\nu} + 2/3 e_a^2 (v_a''^{\mu} + v_a'^2 v_a^{\mu}). \quad \text{(WF 42)}$$

IV. FIELD THEORY AND THE CONSIDERATIONS OF WHEELER AND FEYNMAN

Following Infeld and Wallace we obtained two different sets of equations of motion for the retarded and the symmetric case (Eqs. (3) and (4)) respectively. If we considered the equations significant for the case of a single particle, we would obtain a force of radiative reaction in the retarded case only. However, it is clear that we can only compare those equations with experiment which take account of the existence of a large number of particles in the universe (which may or may not lead to the same conclusions as the simpler equations for the one-particle case). We shall show that we can take over the considerations of Wheeler and Feynman on the field of all particles in the universe into field theory and we shall then obtain the radiative reaction *also in the symmetric case* just as in the theory of action at a distance.

Except for its last term, Eq. (3) of field theory is of the same form as Eq. (6), the starting point of the theory of action at a distance. Its first term on the right-hand side is just the expression (WF 38) and we can break it down into three different fields exactly as WF have done, for none of their arguments (once Eq. WF 38 is accepted) involves any distinction between field theory and action at a distance. Therefore, we we obtain finally, corresponding to (WF 44),

$$m_a v_a'^{\mu} = e_a \sum_{k \neq a} {}_{\text{ret}}F_{\nu}^{\mu(k)} v_a^{\nu} + 2/3 e_a^2 (v_a''^{\mu} + v_a'^2 v_a^{\mu}) + e_a ({}_{e}F_{\nu}^{\mu} + {}_{f}F_{\nu}^{\mu}) v_a^{\nu} \quad (8)$$

where the sum in the last term is due to two fields each of which is a solution of Maxwell's equations for empty space and, therefore, still a solution for empty space.

If we accept (WF 37), we obtain corresponding to (WF 42)

$$m_a v_a'^{\mu} = e_a \sum_{k \neq a} {}_{\text{ret}}F_{\nu}^{\mu(k)} v_a^{\nu} + 2/3 e_a^2 (v_a''^{\mu} + v_a'^2 v_a^{\mu}) + e_a \, {}_{e}F_{\nu}^{\mu} v_a^{\nu}. \quad (9)$$

Equation (4) (the retarded case) is already of the form of Eq. (8) (except that the term involving ${}_{f}F$ if absent), and nothing new is obtained if one takes into account all particles in the universe.

We have considered in outline the derivation of the equations of motion from the point of view of field theory first in order to show that, starting from the *total* field, one may obtain the Eqs. (3) or (4) which apparently do not involve the total field, but only the "external" one, and are therefore of the same form as in action at a distance. This, then, enabled us to show that the application of the WF considerations to the symmetric case yields the radiation damping term which appears in the retarded case already without these considerations.

However, we could have seen without any calculation that under the so-called "complete absorption" conditions *any* results of field theory must be the same in the symmetric and in the retarded (and also the advanced) case. For the condition (WF 37) can also be written

$$\sum_{\text{all } k} {}_{\text{ret}}F^{(k)} = \sum_{\text{all } k} {}_{\text{adv}}F^{(k)} = \sum_{\text{all } k} (1/2 \, {}_{\text{ret}}F^{(k)} + 1/2 \, {}_{\text{adv}}F^{(k)}), \quad (10)$$

and these are the fields (due to sources) which have to be inserted into the energy-momentum tensor at the start of any field-theoretical calculation in the retarded, advanced and symmetric cases, respectively. As these are equal, it is obvious that the equations of motion must also be the same in all cases.[14]

While this demonstrates the equality of the equations of motion arrived at in the various cases, the explicit form of the equations must be obtained by a calculation such as those of Dirac or Infeld and Wallace.

It should be noted that in the theory of action at a distance, contrary to field theory, Eqs. (10) or (WF 37) do *not* lead to the same equations of

theory, while (WF 37) holds everywhere and is therefore consistent with, and might even be a consequence of cosmological considerations. Also (WF 33) does not have to hold for (WF 37) to be true. This makes it more plausible at present simply to take (WF 37) as an additional assumption of the WF-theory.

[14] The relation (10) was suggested by A. Einstein, Phys. Zeits. **10**, 185 (1909). Cf. also reference 7.

TABLE I.

	Field theory			Action at a distance	
	Maxwell's equations				
Basic assumptions	Conservation laws for the electromagnetic energy-momentum tensor (IW 2.1, 2.2)			Lorentz Eq. (5)	
Fields used	Retarded	Symmetric		Symmetric	
Equations obtained	(4)	(3)		(6)	
Additional assumption	None	None	(WF 37)	None	(WF 37)
Final equations	(4)	(8)	(9)	(WF 44)	(WF 42)
Terms common to all final equations	$m_a v_a'^{\mu} = \sum_{k \neq a} {}_{\text{ret}}F_{\nu}^{\mu(k)} v_a^{\nu} + 2/3\, e_a^2 (v_a''^{\mu} + v_a'^2 v_a^{\mu})$				
Additional terms (to be multiplied by $e_a v_a^{\nu}$)	${}_{e}F_{\nu}^{\mu}$	${}_{e}F_{\nu}^{\mu} + {}_{f}F_{\nu}^{\mu}$	${}_{e}F_{\nu}^{\mu}$	${}_{f}F_{\nu}^{\mu}$	None

motion in all cases. As it is not the total field which enters the starting equations (5), the final equations (WF 42) can be obtained in the symmetric case only.

If one does not assume condition (WF 37), we have from (7)

$$\sum_{\text{all } k} {}_{\text{ret}}F^{(k)} = \sum_{\text{all } k} (1/2\ {}_{\text{ret}}F^{(k)} + 1/2\ {}_{\text{adv}}F^{(k)}) + {}_{f}F$$

$$= \sum_{\text{all } k} {}_{\text{adv}}F^{(k)} + 2\,{}_{f}F. \quad (11)$$

Therefore, the total fields in the three cases differ only by solutions of Maxwell's equations for empty space, and the equations of motion will only differ in the terms involving such solutions (cf. Eqs. 4 and 8).

In short, the mathematical reason for the similarity of (4) and (8) is simply that two solutions of the inhomogeneous wave equation can at most differ by a solution of the homogeneous one.

V. DISCUSSION

We shall now inquire into the relationship between the five different sets of equations of motion: Eqs. (4), (8) and (9) from field theory and (WF 42) and (WF 44) from action at a distance.

To facilitate the comparison we summarize the assumptions and results in Table I. The last row shows that these equations differ mathematically only in fields which represent empty-space solutions. However, physically the fields ${}_{e}F$ and ${}_{f}F$ do not have the same significance. ${}_{e}F$ is a solution of the homogeneous wave equation, which arises only in field theory and may be due wholly, partly, or not at all to sources; but at present field theory is unable to analyze it any further. ${}_{f}F$ on the other hand is uniquely determined by the sources according to relation (7), which states that it is half the difference of the retarded and advanced fields of all particles. As shown in section III, the term $e_a v_a^{\nu}\,{}_{f}F_{\nu}^{\mu}$ contains a part which just cancels the radiation damping term $2/3 e_a^2 (v_a''^{\mu} + v_a'^2 v_a^{\mu})$. Therefore, the similarity of Eqs. (8) and (WF 44) to (4), (9) and (WF 42) is purely formal and (8) and (WF 44) actually do *not* describe radiating particles (cf. the discussion of "incomplete absorption" in WF).

If we adopt the assumption frequently used in field theory that ${}_{e}F = 0$, Eqs. (4) and (9) reduce to (WF 42). However, it should be kept in mind that while the solutions of the equations of the symmetric case (9) and (WF 42) are subject to the restriction (WF 37), those of the retarded case (4) are not. Therefore, we (and also WF) have *not* shown the complete equivalence of the retarded and symmetric cases.

Keeping the assumption ${}_{e}F = 0$, we have, on the other hand, complete equivalence of Eq. (9) and (WF 42) of field theory and action-at-a-distance theory, respectively, describing the motion of radiating charges. These identical equations have been obtained from two basically different starting points, while using in common Maxwell's equations, fields symmetric in time, and the condition (WF 37).

In both theories we have to introduce one additional assumption, namely, either the conservation law for the electromagnetic energy-momentum tensor, or the relation between Lorentz force and momentum. The advantage of action at a distance is the plausibility of the physical idea of reducing everything to the interaction of particles. But this is balanced by the difficulties connected with the conservation[11] and transmission of energy and momentum. Therefore, none of the viewpoints appears to be preferable to the other from considerations of simplicity.

Clearly a *direct* verification of the fundamental assumptions of the two viewpoints is impossible, as one cannot observe a field without a test charge, the effect of which, however, would have to be included in the total field. The only experimentally verifiable conclusions are precisely the equations of motion.

Comparing these equations, we see that there is *no* effect which would *require* the point of view of action at a distance. On the other hand, the demonstration of a non-vanishing ${}_eF$ would show an effect which can only be explained by field theory.

Such a demonstration, while possible in principle, appears to be impossible in practice, as it would amount to finding whether the observed field is "only" due to the retarded fields of all the charges in the universe, or whether there is still another part.

Therefore, as far as the symmetric case is concerned, there do not seem to be any compelling reasons at present to prefer either of the two points of view. It appears possible, however, that the application of these viewpoints to general relativity or to quantum mechanics will provide such reasons.

The author wishes to thank Professors J. A. Wheeler and R. P. Feynman for a stimulating discussion, and Professor R. J. Emrich for his valuable criticism of the manuscript.

APPENDIX

We want to show that Dirac's formulation of the field theory for the one-particle problem leads to the same conclusions as that of Infeld and Wallace, namely that one does obtain the term of radiative reaction only in the retarded, but not in the symmetric case. Dirac takes the actual field as[15]

$$ {}_{\text{act}}F = {}_{\text{ret}}F + {}_{\text{in}}F \qquad \text{(D 8)} $$

where ${}_{\text{in}}F$ is the incident field, a solution of the homogeneous wave equation, as is ${}_{\text{out}}F$, which is defined by

$$ {}_{\text{act}}F = {}_{\text{adv}}F + {}_{\text{out}}F. \qquad \text{(D 9)} $$

The difference

$$ {}_{\text{rad}}F = {}_{\text{out}}F - {}_{\text{in}}F \qquad \text{(D10)} $$

or

$$ {}_{\text{rad}}F = {}_{\text{ret}}F - {}_{\text{adv}}F \qquad \text{(D 11)} $$

is called the field of radiation in D. The equations of motion are obtained by substituting the actual field (D 8) into the energy-momentum tensor. After a rather long calculation, which, however, involves only the use of Maxwell's equations, his stress-tensor and (D 8), Dirac obtains the result

$$ mv'^{\mu} = ev^{\nu} f_{\nu}{}^{\mu} \qquad \text{(D 22)} $$

where

$$ f = {}_{\text{act}}F - 1/2({}_{\text{ret}}F + {}_{\text{adv}}F), \qquad \text{(D 13)} $$

or

$$ f = 1/2({}_{\text{ret}}F - {}_{\text{adv}}F) + {}_{\text{in}}F $$

from which we get (see (WF 41) above)

$$ mv'^{\mu} - 2/3e^2(v''^{\mu} + v'^2 v^{\mu}) = ev^{\nu}\, {}_{\text{in}}F_{\nu}{}^{\mu}. \qquad \text{(D 24)} $$

If we had used the field of what we called above symmetric case, we would have had

$$ {}_{\text{act}}F = 1/2({}_{\text{ret}}F + {}_{\text{adv}}F) + {}_{\text{in}}F. $$

It can be easily seen, following Dirac's calculations, that the introduction of this expression would still have led to (D 22) with the definition (D 13) or with

$$ f = {}_{\text{in}}F $$

and, therefore, we would have obtained as our equations of motion

$$ mv'^{\mu} = ev^{\nu}\, {}_{\text{in}}F_{\nu}{}^{\mu}, $$

which do not include the term of radiative reaction.[16]

[15] Here, and in the following, we shall change the notation of D slightly to conform to the one employed above. Also, as we shall only have to follow the argument of D without any detailed calculations, we shall omit sub- and superscripts for convenience wherever there is no danger of confusion.

[16] This result has also been obtained by C. J. Eliezer, Rev. Mod. Phys. 19, 147 (1947) (case $k = -\frac{1}{2}$), in a different connection.

For the case of several particles, analogous considerations would lead to our Eqs. (4) and (3) respectively.

Therefore Dirac's derivation is in accord with the one of Infeld and Wallace outlined previously. However, we noted that Dirac himself calls his theory fundamentally symmetrical between retarded and advanced potentials. The contradiction seems to come from the fact that Dirac considers his theory symmetrical due to the apparent symmetry of the use of retarded and advanced fields in definitions (D 8) and (D 9) (and the analogous definitions (D 38) and (D 39) for the many-body problem).

However, it should be noted that in the derivation by Dirac outlined above, he is only using (D 8) (respectively D 38). The definition (D 9) never enters into any of his calculations which lead to his equations of motion. It is only used in a purely formal manner to introduce the notion of ${}_{\text{rad}}F$ (see (D 10)) into some of the equations;[17] but the results themselves are independent of it.

[17] The purely formal character of any definition of the radiation field can be seen also from the fact that in WF the term "radiation field" is used for just $1/2\ {}_{\text{rad}}F$ of D, without in any way leading to contradictions, as the only physically significant equations are the equations of motion of the point charges.

PHYSICAL REVIEW VOLUME 74, NUMBER 4 AUGUST 15, 1948

The Photo-Voltaic Effect

K. LEHOVEC
Signal Corps Engineering Laboratories, Fort Monmouth, New Jersey

(Received March 19, 1948)

The *Schottky-Mott* theory of the barrier layer rectification is extended with respect to the action of light absorbed in the barrier layer. The essential physical assumptions to be used are as follows: (a) The barrier layer is a boundary layer of a semiconductor with a reduced density of mobile charges (either electrons or "holes"); (b) both positive *and* negative mobile charges are released by light; (c) the recombination within the barrier layer is negligible; and, (d) the electrons and "holes" have the same properties whether released by light or by thermal agitation. Thus an "equation of state" connecting photo-voltage, photo-current, light intensity, wave-length, external resistance, etc., is derived. Among others the regularities of short circuit current, open circuit voltage, photo-characteristic, dark characteristic (barrier layer rectification), power output, and spectral distribution of the quantum yield are involved.

I. INTRODUCTION

THE most successful theory in the explanation of the barrier rectification is the theory of W. Schottky[1] and N. F. Mott.[2] In his discussion of the action of light in a barrier layer of the nature described by the above theory, N. F. Mott has already succeeded in explaining the sign of the photo-voltage.[3] In this paper we generalize the fundamental assumptions of W. Schottky and N. F. Mott and derive a comprehensive formula for the barrier layer photo-effect.[4] The establishment of one formula for the manifold of barrier layer photo-cells varying in peculiarities is possible since the peculiarities of minor importance enter only into the parameters of the formula, which remain open to a further discussion in special cases.

We shall treat explicitly the photo-effect in semiconductors only for the case where the mobile carriers of charge are electrons (n-type semiconductors) and shall state the corresponding results for semiconductors with "hole" conductance (p-type semiconductors).[5]

II. BASIC CONCEPTS ABOUT THE BARRIER LAYER

In principle both barrier layer rectifiers and barrier layer photo-cells consists of a semicon-

[1] W. Schottky, Zeits. f. Physik **113**, 367 (1939); Zeits. f. Physik **118**, 539 (1942), and other publications.
[2] N. F. Mott, Proc. Roy. Soc. London **A171**, 27 (1939).
[3] N. F. Mott, Proc. Roy. Soc. London **A171**, 281 (1939).
[4] This formula has been communicated in a previous note by the author in Optik **1**, issue 3 (1946).
[5] K. Lehovec, Zeits. f. Naturforsch. **2**, 398 (1947).

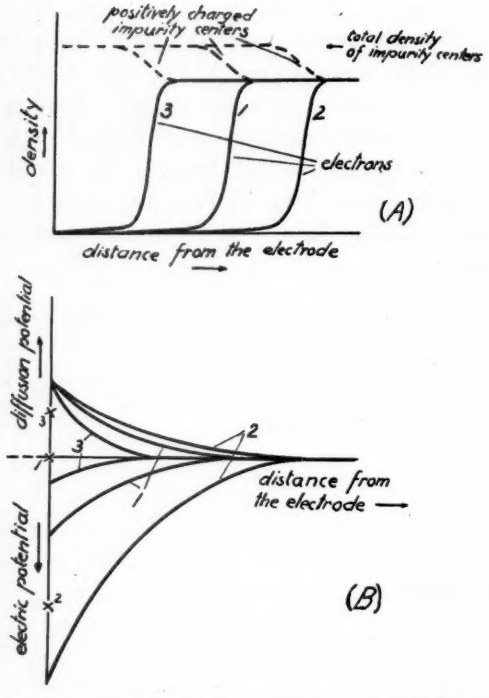

FIG. 1. A. Distribution of the densities of free electrons and of charged impurity centers in the barrier layer. B. Distribution of the diffusion potential and of the electric potential in the barrier layer. × is the potential appearing outside. Curve 1: balance; curve 2: current flowing in the high resistance direction; curve 3: current flowing in the low resistance direction.

ductor sandwiched between two metal electrodes. The d.c. resistance of a suitable combination depends on the amount and the direction of the current. The rectification is located at one of the contacts between the electrode and semiconductor,[6] the other contact having a low and negligible resistance. Therefore, it will be sufficient to deal with the system semiconductor-barrier layer-electrode, and "electrode" refers hereafter to the "electrode at the barrier layer." The rectifying contact has a considerable capacity as shown by a.c. measurements.[7] Using the formula for a plate condensor (with a dielectric constant of about 10), we get a thickness of the order of 10^{-5} cm corresponding to the capacity. A layer of this thickness with a lattice structure different from both metal and semiconductor could not generally be detected by chemical methods or x-ray diffraction. Moreover, the change of capacity with the applied voltage points to a physical effect. Considering the numerical values of capacity and resistance of this so called "barrier layer" or "blocking layer," it is found that the conductance of the semiconductor decreases by many orders of magnitude in approaching the electrode. Since a change of electronic mobility of that order seems out of question, we have to assume that the density of free electrons in the semiconductor decreases considerably in approaching the electrode.

There is still some question about the cause of this decrease in electron density. It has been explained by the differences in the work functions of metal and semiconductor[8] and by surface states.[9] The influence of tunnel effect, image force, and discontinuous distribution of space change have been treated as secondary effects.[1,10] However, for our general theory of the photovoltaic effect we may leave this question open noticing that the parameter "density of free electrons at the border of the electrode" may well depend on several influences.

Except for intrinsic semiconductors, the free electrons come from disturbance or impurity centers in the semiconductor lattice. The dissociation equilibrium is determined by the mass action law

$$(N^+ n/N^0) = \text{const}; \quad (N^+ + N^0 = N_{\text{total}}). \quad (1)$$

n is the density of the free electrons, N^+ and N^0 is the density of the positively charged and of the undissociated impurity centers, respectively.[11] In the bulk of the semiconductor we have no space charge and, therefore, $n = N^+$. In the barrier layer n decreases and therefore N^+ increases, effecting a positive space charge and a negative potential relative to the bulk semiconductor. Thus an electric field already existing without any external voltage drives the electrons in the barrier layer from the metal toward the semiconductor. On the other hand, the density gradient drives the electrons toward the elec-

[6] Schottky, Waibel, and Stoermer, Zeits. f. Hochfrequenztechnik **37**, 162 (1931).
[7] W. Schottky and W. Deutschmann, Physik. Zeits. **30**, 839 (1929); L. A. Wood, Rev. Sci. Inst. **4**, 434 (1933) and others.
[8] W. Schottky, Physik. Zeits. **41**, 570 (1940).
[9] J. Bardeen, Phys. Rev. **71**, 717 (1947).
[10] E. Courant, Phys. Rev. **69**, 684 (1946).
[11] To avoid cumbersome formulations, the total density of impurity centers, N_{total}, may be considered as approximately constant though this is not a necessary assumption for our calculations.

trode. Both currents compensate each other, if no external voltage is applied. Then the electric potential is just compensated by the diffusion potential (see Fig. 1B, curve 1).

The volume charge in the barrier layer is compensated by a "surface charge" which extends over a few angstroms at both sides of the interface metal/semiconductor. In this zone the density of the free electrons decreases from the high value in the metal to the small value in the barrier layer.[12] This is shown in Fig. 2, and for the purpose of comparison a graph of the electron density at metal-vacuum boundary is also sketched. The striped areas mark, respectively, the positive and negative resulting charges. In the region of the semiconductor between the metal surface and the minimum of electron density in the barrier layer the electrons are still in close interaction with the metal and the "effective metal border" might, therefore, be considered as being at the position of the minimum of the density of free electrons in the barrier layer. Even before the semiconductor is placed in contact with a metal, the surface states may already have caused the formation of a barrier layer.[9]

From this point of view the rectification can be understood.[13] If an external voltage is applied at the barrier layer the positive space charge is increased, or respectively, decreased depending on whether the applied electric field has the same or opposite direction as the existing inner electric field. Since the space-charge density is limited by the density of the disturbance centers, a change in the space charge will result essentially in a change of the thickness of the space-charge layer. If the metal is the negative terminal the space charge is increased, the barrier layer gets thicker, and the resistance increases (high resistance direction); the field current is larger than the diffusion current and the electric potential is larger than the diffusion potential (Fig. 1, curves 2). If the metal is the positive terminal, the space charge is decreased, the barrier layer gets thinner, and the resistance decreases (low resistance direction); the diffusion current is larger than the field current and the diffusion potential is larger than the electric potential (Fig. 1, curves 3). The external voltage at the barrier layer in the low resistance direction is limited by the diffusion potential. At this value the thickness of the barrier layer approaches zero and the current infinity. However, the other resistances of the circuit limit the current and, therefore, this condition will never be reached practically.

For p-type semiconductors the signs of low resistance direction and high resistance direction change in full agreement with the experiments. In intrinsic semiconductors a barrier layer with very high resistance cannot exist since the total density of mobile charges would always be higher in layers with space charge than in layers without space charge. In intrinsic semiconductors at thermal equilibrium the product of the densities of free electrons and holes is constant; consequently the sum of the densities is a minimum if both densities are equal.

III. BASIC CONCEPTS ABOUT THE PHOTO-EFFECT IN THE BARRIER LAYER

After having considered the fundamental properties of the barrier layer, the behavior of additional free carriers of charge released by light has to be discussed.[14] For every kind of carriers of charge the following balance exists in each volume unit and for each time interval (formulated for electrons): Total change = number of electrons released by light, minus the number of electrons carried away by (necessarily space dependent) electron currents, minus the number of electrons recombining. We will con-

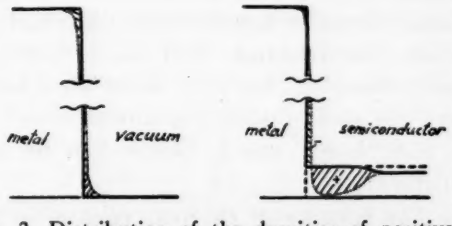

FIG. 2. Distribution of the densities of positive ions (——) and of free electrons (· · · ·) in the boundary metal/vacuum and metal/semiconductor. The ordinate is interrupted, since the density of free electrons in the metal is very much higher than in the bulk semiconductor. The area of the negative charge in the right figure would just compensate the positive area.

[12] For a more complete treatment see H. Y. Fan, Phys. Rev. 62, 388 (1942).

[13] A comprehensive mathematical treatment is given by W. Schottky and E. Spenke, Wiss. Veroff. Siemenswerke 18, 225 (1939).

[14] K. Lehovec, Zeits. f. Naturforsch. 1, 258 (1946).

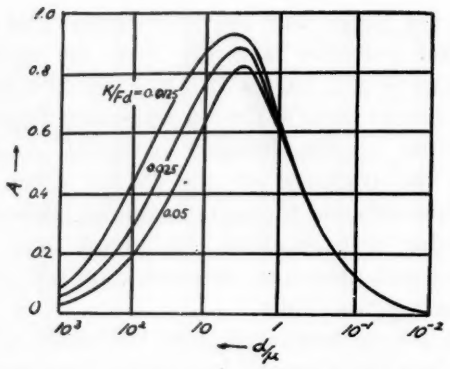

FIG. 3. Spectral distribution of the front wall photo-effect referring to the same amount of light quanta. Abscissa: thickness of the barrier layer/absorption length (the values of d/μ are drawn decreasing from left toward right, because small d/μ corresponds with long wave-lengths, generally).

sider only the stationary state where the total change is zero.

(a) *The release of electrons by light.* Let us first assume that the light releases free electrons and immobile ions only. For constant density of positive ions, as postulated in the stationary state, an equal number of electrons has to recombine in the same unit volume as are released by light and no additions to a spontaneous photocurrent could result. For the same reason the thermal dissociation and recombination of electrons from immobile impurity centers have not been mentioned in our balance, since these two terms always compensate each other. In the following we shall neglect such "ineffective absorptions" and shall only deal with the "effective absorptions" where each absorbed light quantum releases an equal number, say α, of free electrons and *mobile* positive charges.

Usually it will be an absorption in the semiconductor lattice where for each absorbed light quantum one electron and one "hole" are released. However, for very short wave-lengths (x-rays) for each absorbed quantum many electrons and "holes" can be released in the semiconductor.[15]

(b) *The behavior of electrons released by light.* Unlike most of the former theories[16] about the photo-voltaic effect which are based on a surplus of energy of the electrons released by light (according to Einstein's relation), we assume the other limiting case: the surplus energy is soon dissipated by collisions with the lattice, and there is no difference from the other free electrons.[17] Moreover, we assume that the energy distribution of the free electrons is not changed essentially either by the light or by the strong fields in the barrier layer so that Ohm's law (field current proportional to the density of free electrons times field intensity) and the ordinary diffusion law (diffusion current proportional to the gradient of electron density) may be applied.

Because of the high field intensity in the barrier layer (thickness about 0.1μ; voltage about 0.5 volt; field intensity about 50,000-volt/cm) the average gain of electron energy between two collisions with the lattice is already of the order of the energy equivalent to the lattice temperature. Therefore, deviations from Ohm's law may well take place which will increase with increasing external voltage in the high resistance direction and also with decreasing temperature. Fortunately the photo-voltage corresponds to a voltage in the low resistance direction, as we shall see, where the mentioned effect does not seem to be very significant though already present.

(c) Recombination of free carriers of charge. Since a quantum yield as high as almost 100 percent has been reached,[18] the recombination within the barrier layer must be very small (assuming that each light quantum has released one electron). This can be understood since the barrier layer is a layer with small concentration of free electrons. Therefore, the assumption that the recombination within the barrier layer is negligible seems reasonable for a first approximation of the problem.

(d) An additional assumption for distinguishing between photo-effect of the barrier layer and that of the bulk semiconductor. A comprehensive calculation would require not only the treatment of the barrier layer region but also the treatment of the bulk semiconductor region nearby, where a negative space charge may be built up and the recombination has to be considered. However, it seems reasonable for many purposes to neglect the action of light in the bulk semiconductor.[3]

[15] K. Scharf and O. Weinbaum, Zeits. f. Physik **80**, 465 (1933).

[16] For instance, E. Perucca and R. Deaglio, Zeits. f. Physik **72**, 102 (1931); G. Liandrat, Ann. de physique **6**, 419 (1936); V. Körösy and P. Selenyi, Physik. Zeits. **32**, 847 (1931).

[17] Cf. N. F. Mott and R. W. Gurney, *Electronic processes in ionic crystals* (Oxford University Press, London, 1940), p. 190.

[18] H. Schröppel, Sitzber, Phys. Med. Sozietät Erlangen **70**, 87 (1938).

Moreover, this photo-effect has a considerable time lag, which allows its experimental separation from the barrier layer photo-effect.[19] For our calculations we separate the barrier layer photo-effect from the bulk photo-effect by the somewhat deliberate assumption that there will be an "effective thickness" d of the barrier layer with the following properties: (a) the recombination within this layer is negligible; (b) the additions to photo-current and voltage by the semiconductor outside this thickness may be neglected; (c) the boundary conditions valid for the bulk semiconductor a large distance from the electrode may already be applied to the border of the barrier layer $x=d$.

It will be noticed that this "effective thickness" is an idealized mathematical concept and may not coincide with the layer with diminished density of free electrons (or with positive space charge) or with the "capacity length," though these might be good first approximations.

IV. DERIVATION OF THE "EQUATION OF STATE" OF THE PHOTO-VOLTAIC EFFECT

Compilation of the symbols to be used:

- x space coordinate perpendicular to the surface, increasing toward the semiconductor; $x=0$ ("effective") metal semiconductor interface
- d "effective thickness" of the barrier layer
- n density of free electrons; n_0 and n_d density for $x=0$ and $x=d$ respectively
- V electric potential; V_0 electric potential at $x=0$; $V=0$ electric potential at $x=d$
- F absolute value of the field intensity at $x=0$
- E photo-voltage or external voltage at the barrier layer
- I photo-current or current through the barrier layer
- e electron charge
- v mobility of electrons
- D diffusion constant for electrons
- K voltage equivalent of temperature ($=kT/e$)
- J intensity of light when entering the semiconductor
- $h\nu$ energy of one light quantum
- α number of electrons released by one light quantum
- μ absorption length (distance in the semiconductor in which the intensity of light is decreased to the 2.73th part)
- ρ reflection coefficient of light coming from semiconductor to electrode
- Λ thickness of the semiconductor
- R resistance in the external circuit

In the following the front wall effect in excess semiconductors (electron conduction) is considered explicitly. The thermodynamical potential at the barrier layer which gives the voltage appearing outside is the sum of an electric potential and a diffusion potential:

$$E=V_0+K\ln(n_d/n_0). \tag{2}$$

The corresponding current will be calculated by means of the following relation:

$$\frac{J}{h\nu}\cdot\alpha\cdot\frac{1}{\mu}\cdot\exp\left(-\frac{x}{\mu}\right) = -\frac{1}{e}\frac{\partial}{\partial x}\left[-nev\frac{\partial V}{\partial x}+eD\frac{\partial n}{\partial x}\right]. \tag{3}$$

The left side represents the amount of free electrons released by the absorbed light quanta in a unit volume at the distance x from the electrode. In the brackets on the right side there is the total current carried by electrons (positive sign means an electron current from the semiconductor toward the electrode); the first term is the current by the field (directed toward the semiconductor) and the second term is the current by diffusion (directed toward the electrode). In other words, Eq. (3) expresses the fact that each absorbed light quantum adds α-free electrons to the current. Therefore, the electron current is dependent on space. The independence on space of the total current is guaranteed by an additional current of positive charges released by the light. For these positive charges an equation very similar to (3) may be written. However, for our purposes the treatment of (3) is sufficient. The boundary conditions for (3) are the densities of

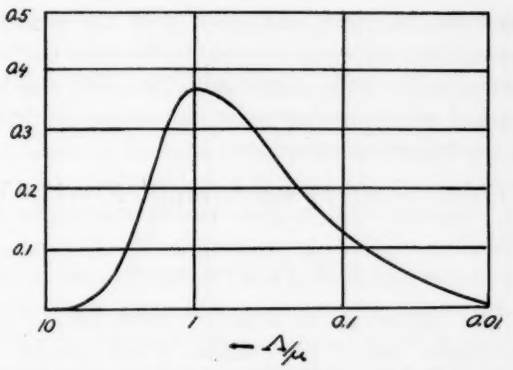

FIG. 4. Spectral distribution of the rear wall photo-effect referring to the same amount of light quanta. Abscissa is the ratio: thickness of the semiconductor/absorption ength.

[19] H. Kerschbaum, Naturwiss. 18, 39 (1930).

electrons for $x=0$ and $x=d$ and the electron current at $x=d$ which is equal to the total current through the bulk semiconductor. The mathematical treatment given in the appendix leads to the following equation:

$$(Je/h\nu)\cdot\alpha\cdot A+I=n_0evF\cdot[\exp(E/K)-1], \quad (4)$$

with

$$A=[1+(K/F\mu)]^{-1}-\exp(-d/\mu). \quad (5)$$

The factor A is closely connected to the quantum yield. The value $A=1$ would be reached if (a) all light quanta were absorbed within the barrier layer, and (b) all released electrons were carried by the electric field toward the semiconductor. The second term of (5) which is especially significant for weak absorption of light gives the amount of light quanta which are not absorbed within the barrier layer. The difference between the first term and unity is especially significant for strongly absorbed light and refers to the electrons carried by diffusion toward the electrode. A is given in Fig. 3 as a function of d/μ; parameter is $K/(Fd)$.

In rear wall photo-cells only the light of wavelengths which are weakly absorbed reaches the barrier layer and (5) reduces to d/μ. Considering further the absorption of light in the semiconductor located before the barrier layer and the reflection of light at the rear electrode, we have

$$A_{\text{rear wall}}=\exp(-\Lambda/\mu)\cdot d/\mu\cdot(1+\rho). \quad (6)$$

The expression $A_{\text{rear wall}}\cdot(\Lambda/d)\cdot(1/1+\rho)$ is given in Fig. 4. Notice that the factor $A_{\text{rear wall}}$ will reach only values of a few percent since d/Λ is generally very small compared with 1.

For p-type photo-cells ("hole" conduction) E and I change only their signs. Denoting with $|E|$ and $|I|$ the absolute values of photo-voltage and photo-current, the formula

$$(Je/h\nu)\cdot\alpha\cdot A-|I|=n_0evF[\exp(|E|/K)-1] \quad (7)$$

may be written for both n-type and p-type photo-cells; of course n_0 and v refer to electrons or "holes," respectively.

Equation (4) has been derived with considerable generality. The result would not be influenced if n_0 were dependent on the field or on the light; there has been no need for assumptions about the distribution of the disturbance centers or about their balance with the electrons. Even a small mobility of the charged impurity centers would not change the general form of (4) but only influence the parameters, especially F and d, and make them dependent on time.

Of course the parameters E, F, and d are not independent, but they are connected by Poisson's equation and this connection is influenced by the distribution of the disturbance centers and their dissociation. Formulae for simplified cases might be of some value. In general, E, F, and d can be derived from experimental data and the distribution of the disturbance centers can then be calculated.

V. GENERAL DISCUSSION

In this chapter we discuss only some of the basic connections among E, I, and J, as they are involved explicitly in (4). We shall not mention minor deviations which might be effected by changes in the dielectric constant, in the dissociation equilibrium of the disturbance centers, or in the electron density at the border of the metal, though these deviations may well have a certain significance in special cases. References to the experiment will be made only where disagreements seem to exist.

(a) *Sign of photo-voltage and photo-current.* Combining (4) with $-E=RI$ (the negative sign refers to the fact that the total voltage drop in a closed circuit is zero), it is found in every case that $E\geq 0$ and $I\leq 0$ for semiconductors with electron conduction. For semiconductors with "holes" in every case $E\leq 0$ and $I\geq 0$. Therefore, the electrode at the barrier layer becomes the positive (negative) terminal by illumination if the semiconductor is of the n-type (p-type), and this corresponds in every case to a voltage in the low resistance direction. The photo-current corresponds to a current of electrons ("holes") from the electrode at the barrier layer to the semiconductor for n-type (p-type) semiconductors and this corresponds in every case to a current through the photocell in the high resistance direction.

(b) For vanishing illumination ($J=0$) Eq. (4) gives *the d.c. characteristic of the unilluminated barrier layer*. The formula is practically equivalent to an equation given by W. Schottky,[20]

[20] W. Schottky, Zeits. f. Physik **118**, 539 (1942), (Eq. (12)).

where a more comprehensive discussion may be found.

For our purposes the low resistance direction is of particular value because this part of the characteristic is closely related to the photo-characteristic (see h). The theory requires an increase of I approximately proportional to $\exp(E/K)$, but the experiments show mostly somewhat slower increases. This might be due to the effect of an increase of the average electron energy in the strong electric fields of the barrier layer.

(c) *The short circuit current* ($R=0$, $E=0$) is proportional to the intensity of light.

(d) *The open circuit voltage* ($R=\infty$, $I=0$) is approximately proportional to the light intensity or to the logarithm of the light intensity according to whether the photo-voltage is small or large in comparison with the voltage equivalent of temperature.

(e) *The spectral distribution* is determined by the factor A (see Figs. 3 and 4), if the incident light is referred to the same amount of light quanta. From Eqs. (5) and (6) it will be noted that A decreases slightly with increasing voltage E, since the field intensity F and the thickness d decrease. Therefore, only the spectral distribution of the short circuit current where $E=0$ is independent from the light intensity. It will be noted that the spectral distribution of a barrier layer photo-effect can be calculated, if the absorption curve of the semiconductor is known (with some not critical assumptions about the thickness of the barrier layer, etc.).

(f) *The dependence of photo-current and photo-voltage on the external resistance* (at constant light intensity) may be calculated by combining (4) with $-E=RI$. This curve has approximately the shape of a step function according to the exponential function on the right side of (4). Starting from small external resistances, the photo-current remains at first practically equal to the short circuit current, and the voltage increases proportional to the external resistance. Then, after a narrow transition region, the photo-voltage becomes practically equal to the open circuit voltage and the photo-current decreases inversely proportional to the external resistance.

(g) Based on the above, the *maximum power output* might be set equal approximately to the product of the short circuit current and the open circuit voltage. The deviation of this approximation from the correct value might well be as high as a factor 4, but the right order of magnitude is given by it. Considering (c) and (d), we find that the maximum power output will increase approximately with the square of the light intensity or with the product of the light intensity and the log of light intensity, respectively. The corresponding external resistance is approximately constant, or decreases proportionally with the ratio of the log of the light intensity to the light intensity, respectively. The transition from the one approximation to the other takes place in a range of the light intensity, for which the corresponding open circuit voltage is of the order of the voltage equivalent of temperature.

(h) *The relation between the open circuit voltage and the short circuit current for different light intensities* (photo-characteristic) can be derived by eliminating the light intensity from the formulae for open circuit voltage ((4) with $I=0$) and short circuit current ((4) with $E=0$); namely,

$$|I|[A(E)/A(0)]=n_0 evF\cdot[\exp(|E|/K)-1]. \quad (8)$$

Equation (8) differs from the d.c. characteristic of the unilluminated barrier layer in the low resistance direction ((4) with $J=0$) only by the deviation of the ration $A(E)/A(0)$ from 1. Since $A(E)$ decreases with increasing E, the open circuit voltage at an illumination J will always be a little lower than the voltage required to send through the unilluminated cell a current equal to the short circuit current at the said illumination. The deviations between the photo-characteristic and dark characteristic are hence a function of the wave-length.

Some authors[21] are opposed to any connection between rectifier effect and photo-voltaic effect, since a photo-voltaic effect has sometimes been observed in photo-cells which did not show any rectifying action. However, it is necessary to consider that the rectifying qualities of the photo-cell need not to be the same as the recti-

[21] Foster C. Nix and Arnold W. Treptow, J. Opt. Soc. Am. **29**, 457 (1939); M. Borisow, C. Sinelnikow, and A. Walther, Phys. Zeits. Sowjetunion **3**, 146 (1933); L. A. Wood, Rev. Sci. Inst. **6**, 196 (1935); Mme. Roy-Pochon, Comptes Rendus **198**, 2083 (1934).

fying qualities of the barrier layer. For instance, a sufficiently high resistance (bulk semiconductor resistance) in series with the barrier layer will diminish the rectifying action of the photo-cell by any desired amount without changing the open circuit voltage. On the other hand, some spots within the barrier layer of resistance low compared with the average resistance may diminish the rectifying action too. However, the short circuit current will not be diminished considerably as long as the resistances of these "shorts" are still large compared with the resistance of the bulk semiconductor.

(i) *If the light is not monochromatic* then the factor $J/h\nu\cdot\alpha\cdot A$ has to be replaced by

$$\int J(\nu)/h\nu\cdot\alpha(\nu)\cdot A(\nu)\partial\nu.$$

As it might be seen from Eq. (4), only the short circuit current is a linear superposition of the currents resulting from each individual wavelength interval; the photo-voltage effected by an illumination with different wave-lengths at the same time is always smaller than the sum of the single wave effects.

(j) *If the light intensity varies along the surface* of the cell an Eq. (4) might be written for each element of area of the surface. If the photo-cell is homogeneous and if the voltage drop along the surface of the electrode and of the bulk semiconductor can be neglected, the voltage at the right side of each equation will be the same. Summing up all these equations, it is found that the effect will be the same as if the whole light intensity were distributed homogeneously over the whole surface.

(k) At small light intensities where the zero current voltage is small compared with the voltage equivalent of temperature, Eq. (7) yields:

$$|E| = \rho_0(Je/h\nu)\cdot\alpha\cdot A - \rho_0|I|, \qquad (9)$$

where $\rho_0=(K/n_0evF)$ is the zero current resistance of the unilluminated barrier layer. Equation (9) corresponds to an e.m.f. of $\rho_0(Je/h\nu)\alpha\cdot A$ and of an internal resistance ρ_0.

(l) Generally, Eq. (7) may be interpreted simply in the following way (formulated for an n-type semiconductor): $(Je/h\nu)\cdot\alpha\cdot A$ is the current due to the holes released by the light in the barrier layer and following the electric field toward the electrode. An increasing accumulation of positive charge is avoided by an equal electron current to the electrode partially through the barrier layer (the term on the right side of Eq. (7) is equal to the current through the unilluminated barrier layer at the voltage E) and partially through the external resistance ($|I|$). Thus Eq. (7) is merely an extension of Eq. (38), page 195 of Mott and Gurney.[17] However, the theory presented goes much farther in that it gives a concrete expression for the factor A describing the spectral distribution, etc.

These selected examples show that the theory presented here is well adapted to deal with the various problems encountered by the barrier layer photo-effect.

ACKNOWLEDGMENT

I wish to express my thanks to the members of the Micro-Optical Section, Components and Materials Branch of the Squier Signal Laboratory, Signal Corps Engineering Laboratories, for many helpful discussions.

APPENDIX

The first integral of Eq. (3) of the text is:

$$J/h\nu\cdot\alpha\cdot[\exp(-x/\mu)-\exp(-d/\mu)] = -nv\partial V/\partial x+D\partial n/\partial x-I/e.$$

The integration constant has been expressed by the values at $x=d$. This is a linear differential equation of the first order in n; its integral has the general form

$$n=[\text{const}+L]\exp(V/K),$$

where the relation $K=D/v$ and the abbreviation

$$L=J/h\nu\cdot\alpha/D\cdot\int_0^x\left\{\exp(-x/\mu)-\exp(-d/\mu)+\frac{I\cdot h\nu}{J\cdot e\cdot\alpha}\right\}\exp(-V/K)\partial x$$

have been used.

According to the boundary conditions we have

$$\text{const}=n_0\exp(-V_0/K)$$

and

$$n_d=n_0\exp(-V_0/K)+L_{x=d}.$$

Appreciable contributions to the integrand of L are given only by the lowest values of the voltage V (which is negative); for $V_0 \ll -K$, we may, therefore, use the approximation

$$V \approx V_0 + Fx + \cdots.$$

and extend the limits of the integral from 0 to ∞. (A second approximation will be given below.) Then we get

$$L_{x=d} = \frac{J \cdot \alpha \cdot K}{h\nu \cdot D \cdot F} \cdot \exp\left(-\frac{V_0}{K}\right) \cdot \left\{\left(1+\frac{K}{F_\mu}\right)^{-1} - \exp\left(-\frac{d}{\mu}\right) + \frac{I \cdot h\nu}{J \cdot e \cdot \alpha}\right\}.$$

Using the connection between n_d and $L_{x=d}$ mentioned above, we have with regard to Eq. (2) of the text:

$$\frac{Je}{h\nu} \cdot \alpha \cdot \left[\left(1+\frac{K}{F_\mu}\right)^{-1} - \exp\left(-\frac{d}{\mu}\right)\right] + I = n_0 evF\left[\exp\left(\frac{E}{K}\right) - 1\right].$$

which can be split up into the basic equations (4) and (5) of the text.

The second approximation

$$V \approx V_0 + Fx - Mx^2 + \cdots$$

gives with

$$\exp(Mx^2/K) \approx 1 + Mx^2/K$$

and

$$\int_0^d x^2 \exp(-Fx/K)\partial x \approx 2K^3/F^3:$$

$$L_{x=d} = \frac{J \cdot \alpha \cdot K}{h\nu \cdot D \cdot F} \cdot \exp\left(-\frac{V_0}{K}\right) \cdot \left\{\left(1+\frac{K}{F_\mu}\right)^{-1} + 2\frac{MK}{F^2}\left(1+\frac{K}{F_\mu}\right)^{-3} - \left[\exp\left(-\frac{d}{\mu}\right) - \frac{I \cdot h\nu}{J \cdot e \cdot \alpha}\right]\left(1+2\frac{MK}{F^2}\right)\right\}.$$

Then we have

$$\frac{Je}{\nu} \cdot \alpha \cdot A + I = \frac{n_0 evF}{1+2MK/F^2} \cdot \left[\exp\left(\frac{E}{K}\right) - 1\right],$$

with

$$A = \left(1+\frac{K}{F_\mu}\right)^{-1} \frac{1+2MK/F^2 \cdot (1+K/F_\mu)^{-2}}{1+2MK/F^2} - \exp\left(-\frac{d}{\mu}\right).$$

For $M=0$ obviously Eq. (4) appears. If the density of the impurity centers is approximately constant within the barrier layer, it can be shown that $2MK/F^2$ is of the order $-K/2V_0$ which is very small compared with 1, if $V_0 \ll -K$. Therefore, in the text only the first approximation is used.

The assumption $V_0 \ll -K$ excludes only comparatively high voltages in the low resistance direction, being closer to the diffusion potential than about $4K$ ($4K \sim 100$ mv at room temperature). These voltages are generally not reached by measurements.

Theory of Elliptically Polarized Photons

GENTARO ARAKI
Department of Industrial Chemistry, Kyoto University, Kyoto, Japan
(Received February 2, 1948)

The unitary transformation from linearly to elliptically polarized states of photons is determined in a scheme of the second quantization (§1). It is given by $\mathbf{e}_l=\mathbf{e}_1\cos\varphi+i\mathbf{e}_2\sin\varphi$, $\mathbf{e}_r=i\mathbf{e}_1\sin\varphi+\mathbf{e}_2\cos\varphi$ where $\mathbf{e}_1$ and $\mathbf{e}_2$ are orthogonal unit vectors corresponding to linearly polarized states of photons and $\mathbf{e}_l$ and $\mathbf{e}_r$ are those corresponding to left and right elliptically polarized states of photons. A general formula for a probability of an emission of light from an atom is deduced on the basis of the Dirac electron theory so as to include up to both a magnetic dipole and an electric quadrupole term (§2). Its general form is improved as compared with the hitherto obtained one. The general theory is applied to electric dipole and quadrupole and magnetic dipole spectral lines (§3 and §4). Polarization states of the Zeeman components corresponding to all combinations of magnetic and orbital magnetic quantum numbers of an atom are completely determined for an arbitrary given direction of an observation on the basis of quantum mechanics.

INTRODUCTION

THE relation between various polarization states of photons has not yet been fully discussed, because scientists have been little interested in this line from the theoretical point of view. However, it becomes necessary to know this relation if one wishes to apply the theory to practical cases. For example, in order to discuss polarizations of spectral lines emitted from an atom on the basis of quantum mechanics of light it is necessary to know in what way elliptically polarized states of photons are represented in the scheme of the second quantization.

Kramers[1] discussed the quantization of free radiation, taking circularly polarized states as its bases. A detailed discussion on the circularly polarized states of photons was given later by the author.[2] It was shown that the spin angular momentum[3] of a system consisting of an assemblage of circularly polarized photons has a normal form and this assemblage is only a system having a normal form of its spin angular momentum.[4] It was also found that a left circularly polarized photon has a spin $+1$ in a direction of its momentum and a right circularly polarized photon has a -1.[5]

The general theory was applied to the longitudinal Zeeman effect of electric dipole spectral lines.[6] When Zeeman components of spectral lines are oblique to an applied magnetic field, their polarization states vary in a complex way as a direction of the observation changes.[7] Such a change for quadrupole lines was discussed by Rubinowicz.[8] However, his theory was based on the classical electrodynamics. A theory of this phenomenon based on the quantum mechanics of light has not yet been worked out.

The theory contained in the present paper is a generalization of the previous paper.[2,6] Its purpose is to work out a complete theory of polarizations of photons and spectral lines, to determine an elliptically polarized state of a photon in a scheme of the second quantization, and to apply the general theory thus obtained to the above-mentioned special phenomena.

[1] H. A. Kramers, "Theorien des Aufbaues der Materie," *Hand-und Jahrbuch der chem. Phys.* (Eucken-Wolf, Leipzig, 1938), Vol. 1, p. 429.

[2] G. Araki, Prog. theor. Phys. **1**, 125 (1946). This paper will be referred to as I.

[3] The separation of angular momentum into orbital and spin was first carried out by Darwin, but in a form of special representation for a field of light as an assemblage of linearly polarized plane waves. The separation in a form which is independent of such a representation is also given in I. C. G. Darwin, Proc. Roy. Soc. London **A136**, 36 (1932). W. Pauli, *Handbuch der Physik* (Verlag-Julius Springer, Berlin, 1933), 24/1, p. 247.

[4] An unitary transformation between polarization states also discussed briefly from another standpoint by W. Pauli, reference 3, p. 252.

[5] It is cited, in W. Heitler, *Quantum Theory of Radiation* (Clarendon Press, Oxford, 1936), p. 63, that the angular momentum of light is discussed by N. Bohr, C. Mannebeck, G. Placzek, and L. Rosenfeld.

[6] G. Araki, Prog. theor. Phys. **2**, 1 (1947). This paper will be referred to as II.

[7] E. Segré, Zeits. f. Physik **66**, 827 (1930); E. Segré und C. J. Bakker, Zeits. f. Physik **72**, 724 (1931).

[8] A. Rubinowicz, Naturwiss. **18**, 227 (1930); Zeits. f. Physik **61**, 338 (1930); **65**, 662 (1930). A. Rubinowicz und J. Biaton, Ergeb. d. exakt. Naturwiss. **11**, 176 (1932).

It was shown in I[2] that a unitary transformation of polarization vectors of a photon has two parameters except for a trivial transformation, and the values of these parameters corresponding to linearly and circularly polarized states were determined. The values of these parameters which correspond to elliptically polarized states of a photon will be determined in the following.

To apply the general theory to a problem of polarizations of spectral lines, a general formula for a probability of an emission of light will next be deduced on the basis of the Dirac electron theory so as to include up to both a magnetic dipole and an electric quadrupole term. The expression of the formula will be improved in a general form compared with the one formerly obtained.

These general theories will finally be applied to electric dipole and quadrupole and magnetic dipole spectral lines. Polarization states of the Zeeman components corresponding to all combinations of magnetic or orbital magnetic quantum numbers will be completely determined for an arbitrary given direction of an observation.

1. ELLIPTICALLY POLARIZED STATES OF A PHOTON

A system of photons is described by a vector potential[9] (an operator) in a scheme of the second quantization. We shall denote this potential by **A**. If the photons are characterized by the energy $\hbar\omega$ and momentum $\hbar\mathbf{k}$ the vector potential is written in the following form:

$$\mathbf{A}=c(2\pi/V)^{\frac{1}{2}}\sum_{\mathbf{k}}\mathbf{A}(\mathbf{k}), \tag{1.1}$$

where

$$\mathbf{A}(\mathbf{k})=(\hbar/\omega)^{\frac{1}{2}}\{\mathbf{a}(\mathbf{k})\exp(i\mathbf{kx}) +\mathbf{a}\dagger(\mathbf{k})\exp(-i\mathbf{kx})\} \tag{1.2}$$

is a monochromatic constituent and † means an adjoint (a Hermitian conjugate). In this representation the Hamiltonian and momentum of the whole system have normal forms [cf. (2.4) of I]. These expressions are independent of the way in which polarizations of photons are represented.

TABLE I.

	Direction of major axis	Eccentricity	
$\dot{\mathbf{b}}_l$ $\begin{cases}0<\varphi<\pi/4\\ \pi/4<\varphi<\pi/2\end{cases}$	$\mathbf{e}_1$ $\mathbf{e}_2$	$(1-\tan^2\varphi)^{\frac{1}{2}}$ $(1-\cot^2\varphi)^{\frac{1}{2}}$	(1.10a)
$\dot{\mathbf{b}}_r$ $\begin{cases}0<\varphi<\pi/4\\ \pi/4<\varphi<\pi/2\end{cases}$	$\mathbf{e}_2$ $\mathbf{e}_1$	$(1-\tan^2\varphi)^{\frac{1}{2}}$ $(1-\cot^2\varphi)^{\frac{1}{2}}$	(1.10b)

[9] A longitudinal part of the vector potential and a scalar potential are omitted by a gauge transformation.

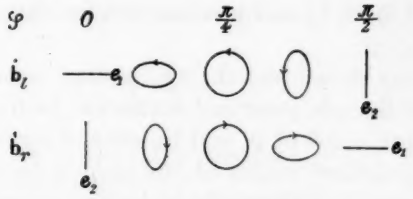

FIG. 1. Polarization ellipses.

We shall now introduce modes of polarizations. The operator $\mathbf{a}(\mathbf{k})$ is represented in two different ways as follows:

$$\mathbf{a}(\mathbf{k})=\mathbf{e}_1(\mathbf{k})a_1(\mathbf{k})+\mathbf{e}_2(\mathbf{k})a_2(\mathbf{k}) =\mathbf{e}_1'(\mathbf{k})a_1'(\mathbf{k})+\mathbf{e}_2'(\mathbf{k})a_2'(\mathbf{k}), \tag{1.3}$$

where $\mathbf{e}_1$ and $\mathbf{e}_2$ are real unit vectors which are perpendicular to each other and to $\mathbf{k}$, and $\mathbf{e}_1'$ and $\mathbf{e}_2'$ are normalized complex vectors which are orthogonal to each other and to $\mathbf{k}$ in the sense of a unitary geometry. The transformation from $(\mathbf{e}_1, \mathbf{e}_2)$ to $(\mathbf{e}_1', \mathbf{e}_2')$ is then unitary, and a Hermitian unit form of components of $\mathbf{a}$ is its invariant. These normalized vectors will be referred to as polarization vectors of $\mathbf{k}$ photons. Hermitian operators $a_1\dagger(\mathbf{k})a_1(\mathbf{k})$ and $a_2\dagger(\mathbf{k})a_2(\mathbf{k})$ represent numbers of linearly polarized photons, and $a_1'\dagger(\mathbf{k})a_1'(\mathbf{k})$ and $a_2'\dagger(\mathbf{k})a_2'(\mathbf{k})$ are those characterized by the polarization vectors $\mathbf{e}_1'(\mathbf{k})$ and $\mathbf{e}_2'(\mathbf{k})$. $a_j(\mathbf{k})$ and $a_j'(\mathbf{k})$ $(j=1, 2)$ will be referred to as number amplitude operators.

The most general unitary $2\cdot 2$ matrix is given by

$$\begin{pmatrix}\cos\varphi\exp i\theta_1 & \sin\varphi\exp i(\theta_1+\theta)\\ -\sin\varphi\exp i(\theta_2-\theta) & \cos\varphi\exp i\theta_2\end{pmatrix} \tag{1.4}$$

[cf. (3.11) of I]. A transformation such as

$$\begin{pmatrix}\exp i\theta_1 & 0\\ 0 & \exp i\theta_2\end{pmatrix} \tag{1.5}$$

is trivial for polarization vectors. Consequently, we can omit this type. The most general unitary transformation of polarization vectors can thus be written as follows:

$$\begin{aligned}\mathbf{e}_1'&=\mathbf{e}_1\cos\varphi-\mathbf{e}_2\sin\varphi\exp(-i\delta),\\ \mathbf{e}_2'&=\mathbf{e}_1\sin\varphi\exp(i\delta)+\mathbf{e}_2\cos\varphi,\end{aligned} \tag{1.6}$$

where δ is equal to $\theta+\theta_1-\theta_2$ [cf. (3.1), (3.4),

and (3.5) of I] and $\mathbf{k}$ is omitted for the sake of simplicity.

It was shown in I that $\mathbf{e}_1'$ and $\mathbf{e}_2'$ correspond to two linearly polarized states for $\delta=0$ and an arbitrary value of φ, and to left and right circularly polarized states of the photon for $\delta=\pi/2$ and $\varphi=\pi/4$. Elliptically polarized states must correspond to another set of values for δ and φ. We shall now determine values of these parameters which correspond to elliptically polarized states with given major axes and eccentricities.

In the previous paper $\mathbf{A}(\mathbf{k})$ was represented by two linearly polarized orthogonal states or by left and right circularly polarized states as its base. Now we adopt, as the base, left and right elliptically polarized plane waves as follows:

$$\begin{aligned}\mathbf{b}_l(\mathbf{k})&=\mathbf{e}_1\cos\varphi\,\sin(\omega t-\mathbf{kx}+\epsilon_l)\\&\qquad-\mathbf{e}_2\sin\varphi\,\cos(\omega t-\mathbf{kx}+\epsilon_l),\\\mathbf{b}_r(\mathbf{k})&=-\mathbf{e}_1\sin\varphi\,\cos(\omega t-\mathbf{kx}+\epsilon_r)\\&\qquad+\mathbf{e}_2\cos\varphi\,\sin(\omega t-\mathbf{kx}+\epsilon_r),\end{aligned}\tag{1.7}$$

where

$$0\leqq\varphi\leqq\pi/2.\tag{1.8}$$

The monochromatic constituent of the vector potential is then given by

$$2^{-\frac{1}{2}}\mathbf{A}(\mathbf{k})=A_l(\mathbf{k})\mathbf{b}_l(\mathbf{k})+A_r(\mathbf{k})\mathbf{b}_r(\mathbf{k}).\tag{1.9}$$

If we assume for the sake of convenience that $\mathbf{e}_1$, $\mathbf{e}_2$, and $\mathbf{k}$ form a right-handed system, vector potentials given by $\mathbf{b}_l(\mathbf{k})$ and $\mathbf{b}_r(\mathbf{k})$, correspond, in general, to left and right elliptically polarized plane waves of monochromatic lights, respectively, because an electric field of light is given by $\dot{\mathbf{A}}-/c$. Particularly in the cases where $\varphi=0$ or $\varphi=\pi/2$ linearly polarized lights are given whose directions of oscillations are perpendicular to each other, and for $\varphi=\pi/4$ they correspond to left and right circularly polarized lights, respectively. When φ is not equal to 0, $\pi/4$, or $\pi/2$, ends of electric vectors derived from $\mathbf{b}_l(\mathbf{k})$ and $\mathbf{b}_r(\mathbf{k})$ describe ellipses. Directions of their major axes and their eccentricities are given in Table I. This is shown in Fig. 1 (against light). These ellipses will be referred to as polarization ellipses.

Now we put

$$\begin{aligned}\mathbf{q}_l(\mathbf{k})&=A_l\{\mathbf{e}_1\cos\varphi\,\sin(\omega t+\epsilon_l)\\&\qquad-\mathbf{e}_2\sin\varphi\,\cos(\omega t+\epsilon_l)\},\\\mathbf{q}_r(\mathbf{k})&=A_r\{-\mathbf{e}_1\sin\varphi\,\cos(\omega t+\epsilon_r)\\&\qquad+\mathbf{e}_2\cos\varphi\,\sin(\omega t+\epsilon_r)\},\\\mathbf{p}_l(\mathbf{k})&=\dot{\mathbf{q}}_l(\mathbf{k}),\quad\mathbf{p}_r(\mathbf{k})=\dot{\mathbf{q}}_r(\mathbf{k}).\end{aligned}\tag{1.11}$$

$$\mathbf{a}(\mathbf{k})=(\omega/2\hbar)^{\frac{1}{2}}\{\mathbf{q}(\mathbf{k})+i\mathbf{p}(\mathbf{k})/\omega\},\tag{1.12a}$$

$$\mathbf{a}_j(\mathbf{k})=(\omega/2\hbar)^{\frac{1}{2}}\{\mathbf{q}_j(\mathbf{k})+i\mathbf{p}_j(\mathbf{k})/\omega\}\quad(j=l,r),\tag{1.12b}$$

and substitute these expressions for the right-hand side of (1.9). Comparing the result with (1.2) and (1.12a) we find that $\mathbf{a}$, $\mathbf{q}$, and $\mathbf{p}$ are decomposed as follows:

$$\mathbf{a}(\mathbf{k})=\mathbf{a}_l(\mathbf{k})+\mathbf{a}_r(\mathbf{k}),\tag{1.13a}$$

$$\mathbf{q}(\mathbf{k})=\mathbf{q}_l(\mathbf{k})+\mathbf{q}_r(\mathbf{k}),\quad\mathbf{p}(\mathbf{k})=\mathbf{p}_l(\mathbf{k})+\mathbf{p}_r(\mathbf{k}).\tag{1.13b}$$

The operators with a suffix l correspond to a system of left elliptically polarized photons characterized by (1.10a), and the operators with a suffix r correspond to a system of right elliptically polarized photons characterized by (1.10b).

Further, if we introduce

$$\begin{aligned}q_l(\mathbf{k})&=A_l\sin(\omega t+\epsilon_l),\\q_r(\mathbf{k})&=A_r\sin(\omega t+\epsilon_r),\\p_l(\mathbf{k})&=\dot{q}_l(\mathbf{k}),\quad p_r(\mathbf{k})=\dot{q}_r(\mathbf{k}),\end{aligned}\tag{1.14}$$

(1.11) has the following form:

$$\begin{aligned}\mathbf{q}_l&=\mathbf{e}_1q_l\cos\varphi-\mathbf{e}_2(p_l/\omega)\sin\varphi,\\\mathbf{p}_l&=\mathbf{e}_1p_l\cos\varphi+\mathbf{e}_2\omega q_l\sin\varphi,\end{aligned}\tag{1.15a}$$

$$\begin{aligned}\mathbf{q}_r&=-\mathbf{e}_1(p_r/\omega)\sin\varphi+\mathbf{e}_2q_r\cos\varphi,\\\mathbf{p}_r&=\mathbf{e}_1\omega q_r\sin\varphi+\mathbf{e}_2p_r\cos\varphi,\end{aligned}\tag{1.15b}$$

where $\mathbf{k}$ is omitted for the sake of simplicity. In this transformation operators with a suffix l or r are substituted, respectively, by those with the same suffix and do not mix with those with different suffices. Consequently, the operators with a suffix l or r still correspond to left or right elliptically polarized photons, respectively. The relation between (a_1, a_2) and (q_1, p_1, q_2, p_2) is given by an isomorphic equation of (1.12):

$$a_j(\mathbf{k})=(\omega/2\hbar)^{\frac{1}{2}}\{q_j(\mathbf{k})+ip_j(\mathbf{k})/\omega\}\quad(j=1,2),\tag{1.16}$$

where (q_1, p_1) and (q_2, p_2) are canonically conjugate Hermitian operators of linearly polarized photons which are, respectively, characterized by $\mathbf{e}_1(\mathbf{k})$ and $\mathbf{e}_2(\mathbf{k})$.

By (1.3), (1.12b), (1.13a), (1.15), and (1.16) the transformation from $(q_1, \underline{p}_1, q_2, p_2)$ to (q_l, p_l, q_r, p_r) can be obtained as follows:

$$\begin{aligned}q_l&=q_1\cos\varphi+(p_2/\omega)\sin\varphi,\\p_l&=p_1\cos\varphi-\omega q_2\sin\varphi,\\q_r&=q_2\cos\varphi+(p_1/\omega)\sin\varphi,\\p_r&=p_2\cos\varphi-\omega q_1\sin\varphi.\end{aligned}\tag{1.17}$$

A commutation relation between q_1, p_1, q_2, and p_2 is that

$$q_1p_1-p_1q_1=q_2p_2-p_2q_2=i\hbar \qquad (1.18)$$

and other pairs are commutative. This relation is invariant for the transformation (1.17):

$$q_lp_l-p_lq_l=q_rp_r-p_rq_r=i\hbar, \qquad (1.19)$$

other pairs being commutative. Moreover, it is also invariant for the transformation (1.15):

$$\mathbf{q}_l\mathbf{p}_l-\mathbf{p}_l\mathbf{q}_l=\mathbf{q}_r\mathbf{p}_r-\mathbf{p}_r\mathbf{q}_r=i\hbar, \qquad (1.20)$$

other pairs being commutative. By (1.15) and (1.19), $\mathbf{q}_l$, $\mathbf{p}_l$, $\mathbf{q}_r$, and $\mathbf{p}_r$ satisfy

$$\mathbf{p}_l\mathbf{p}_r+\omega^2\mathbf{q}_l\mathbf{q}_r=0. \qquad (1.21)$$

Therefore, the Hamiltonian and the momentum of a system of photons take normal forms for the representation given by (1.13b):

$$\mathbf{p}^2(\mathbf{k})+\omega^2\mathbf{q}^2(\mathbf{k})=\mathbf{p}_l^2(\mathbf{k})+\omega^2\mathbf{q}_l^2(\mathbf{k}) +\mathbf{p}_r^2(\mathbf{k})+\omega^2\mathbf{q}_r^2(\mathbf{k}), \qquad (1.22)$$

[cf. (1.15) of I].[10] This normal form is invariant for both the transformations (1.15) and (1.17):

$$\mathbf{p}_l^2+\omega^2\mathbf{q}_l^2=p_l^2+\omega^2q_l^2, \quad \mathbf{p}_r^2+\omega^2\mathbf{q}_r^2=p_r^2+\omega^2q_r^2. \qquad (1.23a)$$

$$p_l^2+\omega^2q_l^2+p_r^2+\omega^2q_r^2 =p_1^2+\omega^2q_1^2+p_2^2+\omega^2q_2^2. \qquad (1.23b)$$

Consequently, the real transformations (1.15) and (1.17) are canonical. Two pairs (q_l, p_l) and (q_r, p_r) are canonically conjugate Hermitian operators of left and right elliptically polarized photons, respectively, because of the invariant relation given by (1.23a). A transformation from canonically conjugate coordinates and momenta to number amplitude operators is therefore given by (1.12) and

$$a_l=(\omega/2\hbar)^{\frac{1}{2}}(q_l+ip_l/\omega), \quad a_r=(\omega/2\hbar)^{\frac{1}{2}}(q_r+ip_r/\omega), \qquad (1.24)$$

[cf. §§2 and 3 of I]. The Hermitian operators $\mathbf{a}_l\dagger\mathbf{a}_l$ and $a_l\dagger a_l$ represent the number of left elliptically polarized photons characterized by a polarization ellipse specified by (1.10) (a), and $\mathbf{a}_r\dagger\mathbf{a}_r$ and $a_r\dagger a_r$ represent that of right elliptically polarized photons characterized by (1.10) (b).

The relations (1.12) (b), (1.13) (a), (1.15) and (1.24) give the following transformations of polarization vectors and number amplitude operators:

$$\mathbf{e}_l=\mathbf{e}_1\cos\varphi+i\mathbf{e}_2\sin\varphi, \quad \mathbf{e}_r=i\mathbf{e}_1\sin\varphi+\mathbf{e}_2\cos\varphi, \qquad (1.25)$$

$$\mathbf{a}_l=\mathbf{e}_la_l, \quad \mathbf{a}_r=\mathbf{e}_ra_r. \qquad (1.26)$$

The transformation of number amplitude operators is contragredient to that of polarization vectors [see (1.3)]. Therefore, we have

$$a_l=a_1\cos\varphi-ia_2\sin\varphi, \quad a_r=-ia_1\sin\varphi+a_2\cos\varphi. \qquad (1.27)$$

The Hermitian unit form of number amplitude operators is invariant for the transformations (1.26) and (1.27).

Comparing (1.25) with (1.6) we see that elliptically polarized states correspond to $\delta=\pi/2$ and an arbitrary value of φ, where directions of major axes and eccentricities of polarization ellipses are characterized by φ according to (1.10). The other values of δ correspond to the other complex basic states of polarizations, in which we are interested not from a practical but only from a theoretical standpoint. The expression (1.25) of polarization vectors includes thus all practical cases of polarizations: linearly, circularly, and elliptically polarized states. The result discussed in I is naturally involved in the present case: $\mathbf{e}_l=\mathbf{e}^+$ and $\mathbf{e}_r=i\mathbf{e}^-$ for $\varphi=\pi/4$; the transformations (1.15) and (1.17) reduce to (4.8) and (3.23) of I, respectively, by putting $\varphi=\pi/4$, where p_r/ω and $-\omega q_r$ in I are to be replaced, respectively, by q_r and p_r in the present paper.

2. PROBABILITY FOR EMISSION OF PHOTON

A semirelativistic formula for an intensity of light emitted from an atom was discussed in §7 of II.[6] A probability per second per unit solid

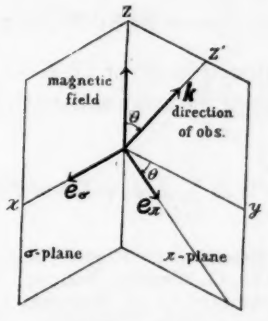

FIG. 2.

[10] The spin of the system does not take a normal form unless φ is equal to $\pi/4$. This was shown in §§3 and 4 of I.

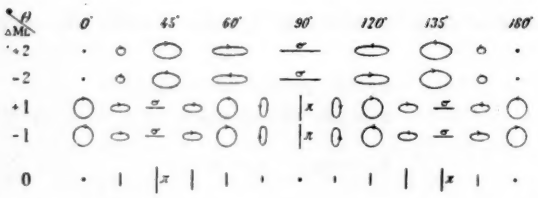

FIG. 3. Polarization states of quadrupole lines.

angle for an emission of a photon from the atom is given by

$$W=(2\pi)^2(\nu/c)^3|(\psi_b, O\psi_a)|^2, \tag{2.1}$$

where

$$O=1/(2\pi\nu)\sum_{j=1}^{N}\exp(-i\mathbf{kx}_j)\{\mathbf{e}\nabla^{(j)}+\mathbf{S}^{(j)}[\mathbf{ke}]\} \tag{2.2}$$

and $2\pi\nu$, $\mathbf{k}$, and $\mathbf{e}$ are, respectively, an energy, a momentum, and a complex conjugate of a polarization vector of the emitted photon. ($\mathbf{e}$ is not a polarization vector itself but its complex conjugate!) The Hartree atomic unit is used throughout this and the following sections ($\hbar=e=m=1$). ψ_a and ψ_b are normalized eigenfunctions of the atom in its initial and final states, respectively. N is the number of electrons contained in the atom.

It is well known that electric dipole and quadrupole parts are included in the above formula.[11] A magnetic dipole part has, however, not been separated in the form corresponding just to the fact that an electron has a magnetic moment of unit Bohr's magneton, although it was imagined from a correspondence to the classical electrodynamics.[12] The separation of these parts can be carried out as follows.

We expand O in a power series in $|\mathbf{k}|$. We have then

$$O=1/(2\pi\nu)\sum_{j=1}^{N}\{\mathbf{e}\nabla^{(j)}+\mathbf{S}^{(j)}[\mathbf{ke}] -i(\mathbf{kx}_j)(\mathbf{e}\nabla^{(j)})+\cdots\}. \tag{2.3}$$

As was mentioned in §7 of II, if we assume that eigenfunctions of the atom satisfy the Schrödinger equation

$$-(1/2)\sum_{j=1}^{N}\Delta_j\psi_a+U\psi_a=E_a\psi_a, \tag{2.4}$$

where U is a point function, it can be shown that

$$1/(2\pi\nu)\sum_{j=1}^{N}(\psi_b, \nabla^{(j)}\psi_a)=-(\psi_b, \mathbf{P}\psi_a), \tag{2.5}$$

where E_a-E_b is replaced by $2\pi\nu$, and $\mathbf{P}=-\sum_{j=1}^{N}\mathbf{x}_j$ is an electric dipole moment of the atom. Using an identity

$$2(\mathbf{kx})(\mathbf{e}\nabla)=[\mathbf{ke}]\cdot[\mathbf{x}\nabla]+(\mathbf{ex})(\mathbf{k}\nabla) +(\mathbf{kx})(\mathbf{e}\nabla), \tag{2.6}$$

the second and third terms of (2.3) can be transformed into the following form:

$$1/(2\pi\nu)\sum_{j=1}^{N}\{\mathbf{S}^{(j)}[\mathbf{ke}]-i(\mathbf{kx}_j)(\mathbf{e}\nabla^{(j)})\} =-[\mathbf{ke}/|\mathbf{k}|]\mathbf{M}-i/(4\pi\nu) \times\sum_{j=1}^{N}\{(\mathbf{ex}_j)(\mathbf{k}\nabla^{(j)})+(\mathbf{kx}_j)(\mathbf{e}\nabla^{(j)})\}, \tag{2.7}$$

where a pseudovector

$$\mathbf{M}=-(\mathbf{L}+2\mathbf{S})\alpha/2 \tag{2.8}$$

is a magnetic dipole moment of the atom, α is the Sommerfeld fine structure constant, and pseudovectors

$$\mathbf{L}=-\sum_{j=1}^{N}i[\mathbf{x}_j\nabla^{(j)}], \quad \mathbf{S}=\sum_{j=1}^{N}\mathbf{S}^{(j)} \tag{2.9}$$

are, respectively, orbital and spin angular momenta of the atom.

From the Schrödinger equation (2.4), it follows on account of a Hermitian property of a Laplacian operator that

$$2\pi\nu(\psi_b, (\mathbf{ex}_k)(\mathbf{kx}_k)\psi_a) =(1/2)\sum_{j=1}^{N}\{(\psi_b, \Delta_j(\mathbf{ex}_k)(\mathbf{kx}_k)\psi_a) -(\psi_b, (\mathbf{ex}_k)(\mathbf{kx}_k)\Delta_j\psi_a)\} =(\psi_b, \{(\mathbf{ex}_k)(\mathbf{k}\nabla^{(k)})+(\mathbf{kx}_k)(\mathbf{e}\nabla^{(k)})\}\psi_a). \tag{2.10}$$

This equation enables us to write the second term of (2.7) as follows:

$$-i/(4\pi\nu)\sum_{j=1}^{N}(\psi_b, \{(\mathbf{ex}_j)(\mathbf{k}\nabla^{(j)}) +(\mathbf{kx}_j)(\mathbf{e}\nabla^{(j)})\}\psi_a)=(i/2)(\psi_b, \mathbf{e}Q\mathbf{k}\psi_a), \tag{2.11}$$

where a tensor Q of the second rank with its

[11] H. Bethe, *Handbuch der Physik* (Geiger-Scheel, 1933), 24/1 pp. 429, 473; G. Wentzel, *ibid.*, pp. 779, 783.

[12] E. U. Condon and G. H. Shortley, *Theory of Atomic Spectra* (University Press, Cambridge, 1935), p. 90; O. Klein, Zeits. f. Physik 41, 407 (1927).

components

$$Q_{zz}=-\sum_{j=1}^{N} x_j^2, \quad Q_{xy}=-\sum_{j=1}^{N} x_j y_j, \cdots \quad (2.12)$$

is an electric quadrupole moment of the atom.

From (2.1), (2.3), (2.5), and (2.11) we have

$$W=(2\pi)^2(\nu/c)^3|(\psi_b, O'\psi_a)|^2, \quad (2.13a)$$

$$O'=\mathbf{eP}+[\mathbf{ke}/|\mathbf{k}|]\mathbf{M}+(1/2i)\mathbf{e}Q\mathbf{k}+\cdots. \quad (2.13b)$$

This agrees, except for the second term, with an expression derived by Bethe,[13] but his expression is referred to special axes. The magnetic moment included in the second term is given by (2.8). This involves a spin term which is missing in Bethe's. This term is due to the second term in the brace of (2.2), and the latter follows from a semirelativistic term[14] in an approximation of the Dirac interaction between an atom and photons (cf. §6 of II)) and it is omitted from the usual expressions. The third term in (2.13b) is more general than Wentzel's expression.[15] Energy radiated per second per solid angle from the atom is given by $2\pi\nu W$. This intensity formula has a complete analogy with a classical one. According to the classical electrodynamics, a time average of an energy of a monochromatic light radiated from a point source with oscillating electric dipole and quadrupole and magnetic dipole moments per unit solid angle per second is given by[16]

$$I_{Cl}=(1/4)(2\pi/c)^3\nu^4\{\mathbf{e}_0\mathbf{P}_0+[\mathbf{ke}_0/|\mathbf{k}|]\mathbf{M}_0 +(1/2)\mathbf{e}_0Q_0\mathbf{k}\}^2, \quad (2.14)$$

where $\mathbf{e}_0$ is an unit real vector parallel to an electric field of the emitted light, and $\mathbf{P}_0$, $\mathbf{M}_0$, and Q_0 are amplitudes of electric dipole, magnetic dipole, and electric quadrupole moments of the source.

3. POLARIZATION STATES OF QUADRUPOLE LINES

We shall consider polarization states of electric quadrupole spectral lines emitted from an atom placed in a magnetic field. Let a direction of the magnetic field be z axis, a direction of an observation be z' axis, an angle between z and z' axes be $\theta(0\leqq\theta\leqq\pi)$, a plane determined by z and z' axes be π-plane, and y axis be in π-plane. The xz plane will be referred to as σ-plane. If we assume $\mathbf{e}_1$ to be parallel to x axis, $\mathbf{e}_2$ must then be in π-plane and it makes an angle θ with y axis. We shall write $\mathbf{e}_\sigma$ and $\mathbf{e}_\pi$, respectively, instead of $\mathbf{e}_1$ and $\mathbf{e}_2$. Lines parallel to these vectors will be referred to as σ-axis and π-axis, respectively (see Fig. 2).

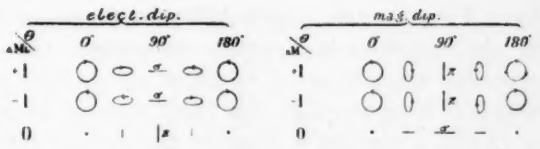

FIG. 4. Polarization states of dipole lines.

Complex conjugates of the polarization vectors given by (1.25) are then

$$\mathbf{e}_l^*=\mathbf{e}_\sigma\cos\varphi-i\mathbf{e}_\pi\sin\varphi,$$
$$\mathbf{e}_r^*=-i\mathbf{e}_\sigma\sin\varphi+\mathbf{e}_\pi\cos\varphi. \quad (3.1)$$

The electric quadrupole part of the operator O' takes then its explicit form as follows:

$$\begin{aligned}1/(2i)\mathbf{e}_l^*Q\mathbf{k}&=(|\mathbf{k}|/8)\{Q^{++}\sin\theta(\cos\theta\sin\varphi-\cos\varphi)\\&\quad+Q^{--}\sin\theta(\cos\theta\sin\varphi+\cos\varphi)\\&\quad+2iQ^{z+}[(2\cos^2\theta-1)\sin\varphi-\cos\theta\cos\varphi]\\&\quad-2iQ^{z-}[(2\cos^2\theta-1)\sin\varphi+\cos\theta\cos\varphi]\\&\quad+Q^0\sin2\theta\sin\varphi\}, \quad (3.2a)\end{aligned}$$

$$\begin{aligned}1/(2i)\mathbf{e}_r^*Q\mathbf{k}&=(|\mathbf{k}|/8)\{iQ^{++}\sin\theta(\cos\theta\cos\varphi+\sin\varphi)\\&\quad+iQ^{--}\sin\theta(\cos\theta\cos\varphi-\sin\varphi)\\&\quad-2Q^{z+}[(2\cos^2\theta-1)\cos\varphi+\cos\theta\sin\varphi]\\&\quad+2Q^{z-}[(2\cos^2\theta-1)\cos\varphi-\cos\theta\sin\varphi]\\&\quad+iQ^0\sin2\theta\cos\varphi\}, \quad (3.2b)\end{aligned}$$

where

$$Q^{++}=-\sum_{j=1}^{N}(x_j^+)^2, \qquad Q^{--}=-\sum_{j=1}^{N}(x_j^-)^2,$$

$$Q^{z+}=-\sum_{j=1}^{N}z_jx_j^+, \qquad Q^{z-}=-\sum_{j=1}^{N}z_jx_j^-, \quad (3.3a)$$

$$Q^0=-\sum_{j=1}^{N}(2z_j^2-x_j^+x_j^-),$$

$$x_j^+=x_j+iy_j, \qquad x_j^-=x_j-iy_j. \quad (3.3b)$$

From these expressions we shall now be able to determine a polarization state of the emitted

[13] H. Bethe, see reference 11, p. 473.
[14] This also follows from a correspondence to the classical electrodynamics. See reference 1, p. 460.
[15] G. Wentzel, reference 11, p. 783.
[16] A. Rubinowicz and J. Blaton, Ergeb. d. exakt. Naturwiss. 11, 176 (1932).

light. For example, a probability for an emission of the quadrupole Zeeman component corresponding to $\Delta M_L=+1$ is given by (2.13a) in which $0'$ is replaced by the third term of (3.2a) or (3.2b), according to whether the emitted light is left elliptically or right elliptically polarized. Matrix elements of other terms vanish because selection rules for inner and azimuthal quantum numbers of a matrix of Q^{z+} are different from dipole terms and that for an orbital magnetic quantum number is also different from other quadrupole terms. If the coefficient of Q^{z+} in (3.2a) vanishes for a value of θ and that in (3.2b) does not for the same value of θ, there is no probability for an emission of a left elliptically polarized light, and the emitted light in this direction must be right elliptically polarized. The other cases can be examined in the same way.

Non-vanishing matrix elements of Q^{++}, Q^{--}, Q^{z+}, Q^{z-}, and Q^0 are given,[17] respectively, by $\Delta M_L=+2$, -2, $+1$, -1, and 0, where ΔM_L is an increment (not a difference!) of an orbital magnetic quantum number of the atom. Changes of polarization states, with θ, of the Zeeman components of electric quadrupole lines corresponding to these ΔM_L can conveniently be determined according to the following procedure. For this purpose we use the following two conditions for a coefficient of Q^{++}, Q^{--}, Q^{z+}, Q^{z-}, or Q^0 in (3.2): condition L—the coefficient in (3.2b) vanishes and that in (3.2a) does not; condition R—the coefficient in (3.2a) vanishes and that in (3.2b) does not.

Using these conditions we can proceed as follows:

1°. For $\varphi=0$ condition L gives directions in which σ-component is emitted, and condition R gives directions in which π-component is emitted.

2°. For $\varphi=\pi/4$ condition L gives directions in which a left circularly polarized component is emitted, and condition R gives directions in which a right circularly polarized component is emitted.

3°. For $0<\varphi<\pi/4$ or $\pi/4<\varphi<\pi/2$ condition L gives directions in which a left elliptically polarized component is emitted, and condition R gives directions in which a right elliptically polarized component is emitted. Eccentricities of polarization ellipses of these components are $(1-\tan^2\varphi)^{\frac{1}{2}}$ for $0<\varphi<\pi/4$ and $(1-\cot^2\varphi)^{\frac{1}{2}}$ for $\pi/4<\varphi<\pi/2$. The major axis in the left elliptically polarized case is σ-axis for $0<\varphi<\pi/4$ and π-axis for $\pi/4<\varphi<\pi/2$. In the right elliptically polarized case it is π-axis for $0<\varphi<\pi/4$ and σ-axis for $\pi/4<\varphi<\pi/2$.

For example, conditions L and R for $\Delta M_L=+1$ are as follows.

Condition L:

$$\left.\begin{aligned}(2\cos^2\theta-1)\cos\varphi+\cos\theta\sin\varphi=0\\(2\cos^2\theta-1)\sin\varphi-\cos\theta\cos\varphi\neq 0\end{aligned}\right\}, \tag{3.4a}$$

Condition R:

$$\left.\begin{aligned}(2\cos^2\theta-1)\sin\varphi-\cos\theta\cos\varphi=0\\(2\cos^2\theta-1)\cos\varphi+\cos\theta\sin\varphi\neq 0\end{aligned}\right\}. \tag{3.4b}$$

For $\varphi=0$ they give

Condition L: $\theta=\pi/4,\ 3\pi/4$; (3.5a)

Condition R: $\theta=\pi/2$. (3.5b)

The quadrupole Zeeman component corresponding to $\Delta M_L=+1$ is, therefore, σ-component for $\theta=\pi/4$, $3\pi/4$, and π-component for $\theta=\pi/2$. In the other directions of an observation the emitted light is not linearly polarized.

For $\varphi=\pi/4$ the conditions (3.4) give

Condition L: $\theta=\pi/3,\ \pi$; (3.6a)

Condition R: $\theta=0,\ 2\pi/3$. (3.6b)

The emitted light is therefore left circularly polarized for $\theta=\pi/3$, π, and right circularly polarized for $\theta=0$, $2\pi/3$. Thus when θ is not equal to 0, $\pi/4$, $\pi/3$, $\pi/2$, $2\pi/3$, $3\pi/4$, and π, the emitted light is elliptically polarized. It is not in agreement with the result by Rubinowicz and Blaton[18] that the emitted light is circularly polarized for $\theta=\pi/3$, $2\pi/3$.

For $0<\varphi<\pi/4$ the conditions (3.4) give

Condition L:

$$\pi/4<\theta<\pi/3 \quad \text{and} \quad 3\pi/4<\theta<\pi; \tag{3.7a}$$

Condition R:

$$\pi/2<\theta<2\pi/3. \tag{3.7b}$$

[17] E. U. Condon and G. H. Shortley, *Theory of Atomic Spectra* (University Press, Cambridge, 1935), p. 59.

[18] A. Rubinowicz und J. Blaton, Ergeb. d. exakt. Naturwiss. 11, 176 (1932), Tables I and III.

For $\pi/4<\varphi<\pi/2$ they give

Condition L:

$$\pi/3<\theta<\pi/2; \quad (3.8a)$$

Condition R:

$$0<\theta<\pi/4 \quad \text{and} \quad 2\pi/3<\theta<3\pi/4. \quad (3.8b)$$

The emitted light is left elliptically polarized in the range given by (3.7a) and (3.8a), and right elliptically polarized in the range given by (3.7b) and (3.8b). Their polarization ellipses are characterized by the values of φ which are determined as functions of θ by Eq. (3.4).

Polarization states of the other components, corresponding to the other selection rules, can be determined in the same way. The result is represented in Fig. 3 (against light). In this figure a point means that the intensity vanishes.

4. ELECTRIC AND MAGNETIC DIPOLE LINES

Polarization states of the Zeeman components of electric and magnetic dipole lines can also be determined in the same way. The result is represented in Fig. 4 (against light). In the case of the magnetic dipole lines figures are arranged according to selection rules of a magnetic quantum number M of the atom, instead of an orbital magnetic quantum number M_L.

PHYSICAL REVIEW VOLUME 74, NUMBER 4 AUGUST 15, 1948

Measurements of Thomson Coefficients for Metals at High Temperatures and of Peltier Coefficients for Solid-Liquid Interfaces of Metals

J. J. LANDER
Bell Telephone Laboratories, Murray Hill, New Jersey

(Received April 30, 1948)

Apparatus has been devised for measuring and measurements made of Thomson coefficients of metals at high temperatures. It is found that in the range from 400°C to the melting point the approximation $\sigma=\beta T$ is adequate for platinum, palladium, copper, and silver but not for gold, molybdenum, and tungsten.

Experimental results for the Peltier coefficients for solid-liquid interfaces of gold, silver, and copper are also reported. An experimental sensitivity of 0.1 millivolt revealed no effect in gold and silver, but +10.2 millivolts were obtained for copper.

I. INTRODUCTION

ALTHOUGH the thermoelectric Peltier and Thomson effects are usually of secondary importance in practical electrothermal phenomena they may become of immediate importance when thermal or electrical symmetry is a primary consideration. Thus such effects may play significant parts in contact phenomena; for example, in contact erosion and in the low frequency behavior of a circuit containing metal-semiconductor junctions. These thermoelectric effects are also of theoretical interest since they provide important clues to the electronic structure of conductors.

This article describes apparatus devised for measuring and measurements made of: (a) the liquid-solid Peltier coefficients of Au, Ag, and Cu; and (b) the Thomson coefficients for solid Pt, Pd, Ag, Au, Cu, W, and Mo at high temperatures.

II. THE LIQUID-SOLID PELTIER EFFECT OF Au, Ag, AND Cu

A. Theory

An electric current flowing through the boundary between two materials not having the same composition or structure produces heat in proportion to the current flowing. The Peltier coefficient between materials A and B at temperature T may be defined by

$$_AP_B(T)=\Delta Q/i\times t,$$

where ΔQ is the heat evolved at the junction when current i flows for time t across the junction. Here a positive sign is taken to mean that heat is absorbed by the junction when electrons flow from B to A. This is the usual convention.

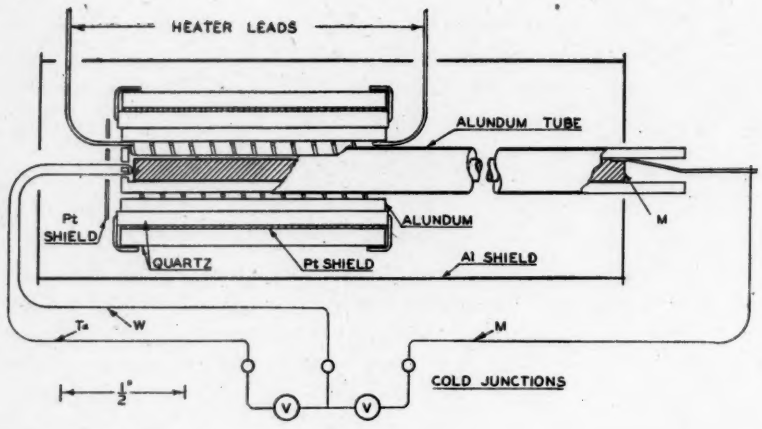

FIG. 1. Schematic diagram of apparatus for measuring the Peltier coefficient for a solid and its melt.

Pelier heat can be measured directly although its separation from Joule heat, conduction heat, radiation heat, and Thomson heat is not easy. The direct measurement of the Peltier heat between a solid melting at a high temperature and its liquid appears to be highly impractical. Therefore, we resort to an indirect method which makes use of a thermodynamic relation derived by J. J. Thomson. This relation,

$$_AP_B(T) = T\,{}_A(dE/dT)_B,$$

requires a measurement of the thermoelectric power at temperature T. If now A is a solid metal and B is its melt, the liquid-solid interface is necessarily at the melting point T_m which cannot be conveniently varied in order to obtain dE/dT. However, in a circuit containing A, its melt B, and a third material C, insoluble in both A and its melt B,

$$_AP_C(T_m) = T_m{}_A(dE/dT)_C,$$

and, since the junction between A and B is at constant temperature and therefore contributes a constant voltage,

$$_BP_C(T_m) = T_m{}_B(dE/dT)_C.$$

The difference of these equations is the required coefficient and is

$$_AP_B(T_m) = T_m[{}_A(dE/dT)_C - {}_B(dE/dT)_C]. \quad (1)$$

Experimentally, therefore, one obtains Peltier coefficients between the solid of interest and a third material and between the liquid of interest and the third material. The difference of these values at the melting point is the desired Peltier coefficient between the solid and its melt. In principle, the third material can be chosen indifferently but, practically, it must meet certain experimental requirements. The method has been used by Harrison and Foote,[1] Linder,[2] Boydston,[3] and others for low melting metals. In experiments described below it has been applied to Au, Ag, and Cu. Measurements upon higher melting point metals would be much more difficult and these have not been attempted.

B. Apparatus

The apparatus sketched in Fig. 1 was constructed in order to measure Peltier coefficients for liquid-solid interfaces of higher melting metals. The specimen, a rod about 100 mils in diameter and five inches long, is mounted along the axis with one end in the furnace. A large thermal gradient runs down the specimen to the outside end where a wire of the test metal is attached. The other end of the wire acts as a cold junction. A tungsten-tantalum thermocouple made of five-mil wires is plugged into the high temperature end of the specimen. The thermocouple serves the double purpose of measuring the temperature of a small region in the specimen and measuring the thermoelectric power between either wire (actually tungsten was chosen in all experiments) and the specimen in that small region. Tests were carried out in an atmosphere of palladium-purified hydrogen flow-

[1] T. R. Harrison and P. D. Foote, J. Opt. Soc. Am. **7**, 389 (1923).
[2] E. G. Linder, Phys. Rev. **29**, 554 (1927).
[3] R. W. Boydston, Phys. Rev. **30**, 918 (1927).

ing through the apparatus at about 2 liters per second at a pressure of about 5 mm of mercury.

The W-Ta thermocouple was calibrated against a Pt-Pt (+10 percent Rh) thermocouple. It was found that after a short anneal at a temperature higher than the experimental range, reproducible readings were obtained for the W-Ta couple and that these were fitted to better than one percent between 800 and 1400°C by the equation

$$ {}_{W}E_{Ta}(\mu V) = 11.82(T-30) + 8.8\times10^{-4}(T-30)^2 - 3.5\times10^{-7}(T-30)^3. \quad (2) $$

Both thermocouple e.m.f. and tungsten to specimen e.m.f. were measured with a Type K potentiometer and a low resistance high sensitivity galvanometer. The over-all sensitivity was 0.1 μV.

C. Experimental Results

Representative results obtained with Ag, Au, and Cu (C.P. grade) are plotted in Fig. 2. The abscissae are voltages of the W-Ta thermocouple, transformable directly into temperatures by Eq. (2). The ordinates are voltages between M, the metal under test, and tungsten. Melting points are marked by vertical bars on the curves for gold and silver. Each test rod was cycled three times through an interval of about 150°C on each side of its melting point. The time per cycle was about two hours. The beginning of melting was best observed by an abrupt increase in efficiency of heating (due to a decrease of approximately 50 percent in the thermal conductivity of the liquid). The slopes of successive runs were very well reproduced, although occasionally an abrupt change in temperature of a fraction of a degree did occur within a run probably due to a sudden small movement of the thermocouple with respect to the test material. The slope of subsequent points always fitted the previous slope.

The curves for Ag and Au reveal no discontinuity in slope at the melting point. Since the average deviation of experimental points from a straight line over a range of about 1 millivolt and more than 100°C is about 1.0 microvolt and relative temperature is measured with a sensitivity of about 0.01°C, the sensitivity of measure of $T(dE/dT)$ is about 20 microvolts. It is concluded that the Peltier coefficients between solid silver and its melt and between solid gold and its melt are less than 0.1 millivolt.*

A marked change of slope at the melting point was observed in the case of copper. Measurements of three cycles furnished values of (dE/dT) for solid copper equal to 13.21, 12.46, and 13.39 μV/°C, the average being 13.02 μV/°C. The corresponding measurements of (dE/dT) for liquid copper gave 3.50, 3.21, and 3.94, the average being 3.55 μV/°C. The calculated Peltier coefficient ${}_{s}P_{l}$ is +10.25 millivolts. The marked (greater than hundredfold) difference between copper, and silver or gold is notable in view of the marked similarities of their first order electrical properties.

III. THOMSON COEFFICIENTS FOR SOLID Pt, Pd, Ag, Au, Cu, W AND Mo AT HIGH TEMPERATURES

A. Theory

An electric current flowing in a conductor with a temperature gradient produces heat in proportion to the current flowing and to the gradient. The Thomson coefficient of a material A, in which current i flowing for time t through a

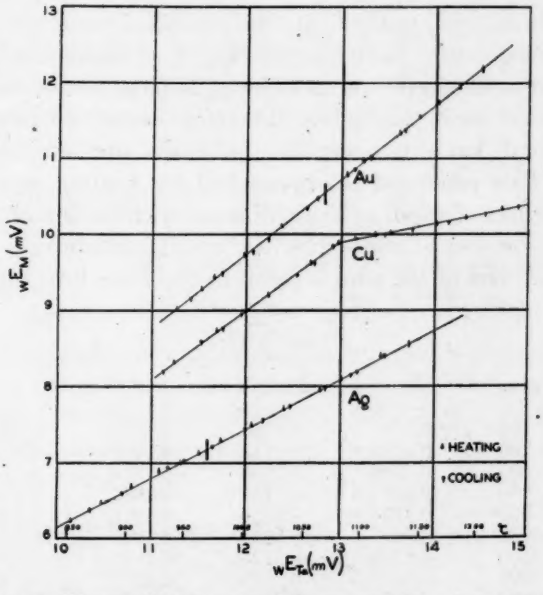

FIG. 2. Thermoelectric potentials measured in the neighborhood of melting points.

* Comparison of this value with that of potentials required to produce observed amounts of contact erosion leads to the conclusion that this effect is negligible in the erosion of gold and silver contacts.

temperature difference ΔT produces a quantity of heat ΔQ, may be defined by

$$\sigma_A(T)=\Delta Q/(\Delta T\times i\times t).$$

If heat is *evolved* as *electrons* go to places of *higher* temperature, the *positive* sign is chosen for the coefficient. This is the convention in more general usage, although opposite to that of the International Critical Tables.

In this case an indirect experimental method based on the thermodynamic relation

$$\sigma_B-\sigma_A=T_A(d^2E/dT^2)_B$$

is not feasible. Two difficulties are immediately obvious. Use of the relation to obtain a Thomson coefficient implies that one Thomson coefficient has been obtained by some other method. Moreover, an extraordinary precision of measurement would be required to obtain accurate results at high temperatures. Because of these two difficulties, the use of a direct method is indicated. More or less satisfactory direct methods have been used for low temperature measurements, but these do not appear to be readily adaptable to high temperature measurements.

In trying to measure Thomson heat directly one is of necessity also concerned with Joule heat, conduction heat, and radiation heat. Since conduction heat has the virtue of being easily measured one wants to make it large and radiation heat negligible. Therefore small surfaces and large temperature gradients are wanted. This condition is approached by heating short wires of small cross section electrically. If radiation loss is negligible, the conduction heat out an end of the wire is equal to the Joule heat plus the Thomson heat developed between that end and the surface of maximum temperature.

TABLE I.

T* °K	a	b	c	d
400	0.1712	0.1458	0.1248	0.1076
500	0.2796	0.2133	0.1607	0.1326
600	0.3546	0.2500	0.1824	0.1375
700	0.4099	0.2722	0.1937	0.1388
800	0.4524	0.2864	0.1946	0.1386
1000	0.5137	0.3033	0.1967	0.1376
1200	0.5558	0.3124	0.1976	0.1365
1400	0.5862	0.3179	0.1977	0.1360
1600	0.6096	0.3216	0.1977	0.1355
1800	0.6284	0.3240	0.1976	0.1351
2000	0.6432	0.3256	0.1974	0.1348
2200	0.6550	0.3271	0.1974	0.1344
2400	0.6660	0.3281	0.1973	0.1340
2600	0.6748	0.3289	0.1972	0.1336

In the absence of Thomson heat, the conduction heats flowing out the ends of an isotropic wire are equal if these ends are at the same temperature. Adding Thomson heat on one side and subtracting it on the other produces, in general, an asymmetric temperature condition, but one in which Thomson heat is partially compensated by a change in Joule heat produced by a readjustment of potential. It turns out, however, that the difference in heat outputs at the ends of the wire can be used as a sufficiently sensitive measure of Thomson heat.

Consider a wire with ends held at absolute temperature T_0 heated electrically to a maximum temperature T^*. Assume the wire so short that radiation loss is negligible at all values of T^* which are of interest. It will be convenient to make use of the Wiedemann-Franz law $k/\lambda=AT$, where k is thermal conductivity, λ electrical conductivity, and A a constant. Let the electrical potential at any point φ with the potential at the two ends, respectively, O and E. The heat flowing per second through the surface with zero potential and temperature T_0 is, in the steady state,

$$Q_1=\varphi^*I+I\int_{T_0}^{T^*}\sigma dT,$$

where φ^* is the potential at T^* and I is the electrical current flowing through the wire. Through the surface at potential E and temperature T_0 the heat flowing per second is

$$Q_2=(E-\varphi^*)I-I\int_{T_0}^{T^*}\sigma dT.$$

The difference between these divided by the total heat output is

$$(Q_1-Q_2)/(Q_1+Q_2)=\Delta Q/Q=[(2\varphi^*-E)/E]+(2/E)\int_{T_0}^{T^*}\sigma dT. \quad (3)$$

One sees that φ^* must be evaluated if σ is to be obtained from experimental measurements of $\Delta Q/Q$ as a function of E and T^*.

Neglecting the Thomson effect, the differential

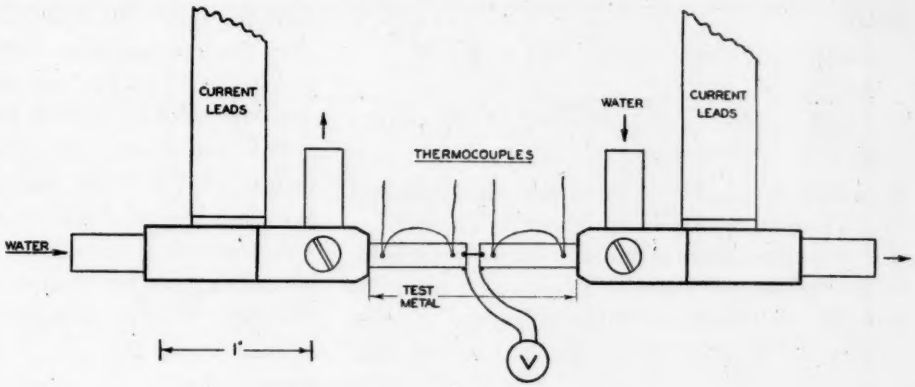

FIG. 3. Schematic diagram of apparatus for measuring Thomsom coefficients at high temperatures.

equations to be satisfied are

$$\nabla\cdot k\nabla T+\lambda(\nabla\varphi)^2=0, \quad \nabla\cdot\lambda\nabla\varphi=0,$$

which may be written in the single equation

$$\nabla(\lambda\varphi\nabla\varphi+k\nabla T)=0. \tag{4}$$

This equation determines a relation $T=f(\varphi)$ uniquely under conditions general enough to include our problem.[4] The solution under the prescribed conditions is

$$\int_{T_0}^{T}(k/\lambda)dT=A\int_{T_0}^{T}TdT=\int_0^{\varphi}(\varphi^*-\varphi)d\varphi. \tag{5}$$

Taking Thomson heat into consideration, the term $\sigma\lambda\nabla\varphi\cdot\nabla T$ is added to the left of Eq. (4) and the solution becomes

$$A\int_{T_0}^{T}TdT=\int_0^{\varphi}\left[(\varphi^*-\varphi)+\int_{T(\varphi)}^{T}\sigma dT\right]d\varphi.$$

On the low potential side of T^*

$$A\int_{T_0}^{T^*}TdT=\int_0^{\varphi^*}\left[(\varphi^*-\varphi)+\int_{T}^{T^*}\sigma dT\right]d\varphi,$$

and on the high potential side

$$A\int_{T_0}^{T^*}TdT=\int_E^{\varphi^*}\left[(\varphi^*-\varphi)+\int_{T}^{T^*}\sigma dT\right]d\varphi.$$

Subtracting, obtain

$$(E/2)(E-2\varphi^*)=\int_0^{\varphi^*}d\varphi\int_T^{T^*}\sigma dT-\int_E^{\varphi^*}d\varphi\int_T^{T^*}\sigma dT. \tag{6}$$

In general, σ is small and produces a small perturbation of the symmetric function $T=f(\varphi)$ of Eq. (5). Therefore the integrals on the right of Eq. (6) can be evaluated by integrating to the average limit $E/2$ over the path

$$d\varphi=[(AT)^{\frac{1}{2}}/(T^{*2}-T^2)^{\frac{1}{2}}]dT$$

obtained from (4). This yields

$$(2\varphi^*-E)/E=-[4(A)^{\frac{1}{2}}/E^2]\times\int_T^{T^*}d(T^{*2}-T^2)^{\frac{1}{2}}\int_T^{T^*}\sigma dT, \tag{7}$$

the quantity needed in Eq. (3). After substituting (7) in (3), integrating by parts, and substitution of $E=2(A)^{\frac{1}{2}}(T^{*2}-T_0^2)^{\frac{1}{2}}$ from Eq. (5) one obtains the relation

$$(\Delta Q/Q)(E/2)=[1/(T^{*2}-T_0^2)^{\frac{1}{2}}]\int_{T_0}^{T^*}\sigma(T^{*2}-T^2)^{\frac{1}{2}}dT.$$

This is simply evaluated if σ is proportional to the temperature, but unfortunately this assumption is not justified in general. Represent σ by a power series, $\sigma=\alpha+\beta T+\gamma T^2+\cdots$. It is then found[5] that

$$(\Delta Q/Q)(E/2)=\alpha aT^*+\beta bT^{*2}+\gamma cT^{*3}+\delta dT^{*4}+\cdots \tag{8}$$

[4] Two excellent papers concerned with relations between potential and temperature in steady-state problems and in which the mathematical foundations for the above analysis is given detailed attention are: F. Kohlrausch, Ann. d. Physik 1, 132 (1900) and H. Diesselhorst, Ann. d. Physik 1, 312 (1900).

[5] Alternatively the experimental values of $(\Delta Q/Q)(E/2)$ may be expressed as a power series and the integral equation solved for σ. The equation has been reduced to Abel's form and solved by J. M. Richardson.

where

$$a=\tfrac{1}{2}[[((\pi/2)-\sin^{-1}r)/(1-r^2)^{\frac{1}{2}}]-r],$$
$$b=\tfrac{1}{3}[1-r^2],$$
$$c=\tfrac{1}{4}[[((\pi/2)-\sin^{-1}r)/2(1-r^2)^{\frac{1}{2}}]+r(\tfrac{1}{2}-r^2)],$$
$$d=\tfrac{1}{5}[1-r^2][r^2+\tfrac{2}{3}],$$

in which $r=T_0/T^*$. Values for these factors with T_0 equal to 300°K are given in Table I.

If the experimental metal obeys the Wiedemann-Franz Law well, T^* is obtained from (5) and the observed potential difference E. For small σ the accuracy of the method should then be limited only by experimental accuracy. Actually, the law has been found to be well obeyed by Ag, Au, Cu, Pt, and Pd. In the case of W and Mo, the law seemed well enough obeyed to permit substitution of pyrometrically observed values of T^*. This amounts to choosing an average value of A different for each T^*.

A theoretical sensitivity for the method can be calculated by comparing $\Delta Q/Q$ with the Thomson heat contribution to $\Delta Q/Q$. The ratio of these quantities,

$$\frac{\alpha aT^*+\beta bT^{*2}+\gamma cT^{*3}+\cdots}{\alpha(T^*-T_0)+(\beta/2)(T^{*2}-T_0^2)+(\gamma/3)(T^{*3}-T_0^3)+\cdots},$$

is about $\frac{2}{3}$ if $\sigma=\alpha$, $\frac{2}{3}$ if $\sigma=\beta T$, and about 6/10 if $\sigma=\gamma T^2$. Thus the compensating shift in potential does not seriously reduce the sensitivity of $\Delta Q/Q$ to the Thomson heat evolved. If this compensating shift in potential had very greatly reduced the sensitivity, a better experimental method would have been to measure this potential shift by means of a probe electrode attached to the center of the test metal.

B. Apparatus

A diagram of the experimental apparatus is given in Fig. 3. The test material, which is heated electrically to the maximum temperature

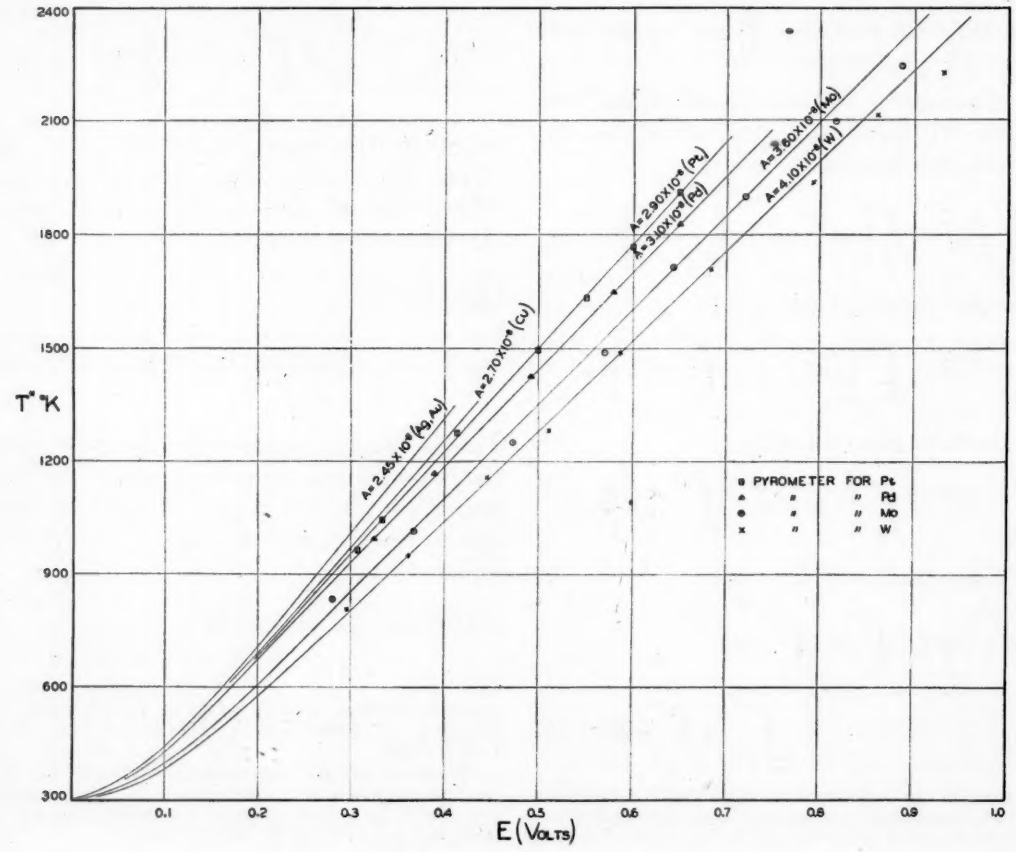

FIG. 4. Temperature *vs.* voltage data.

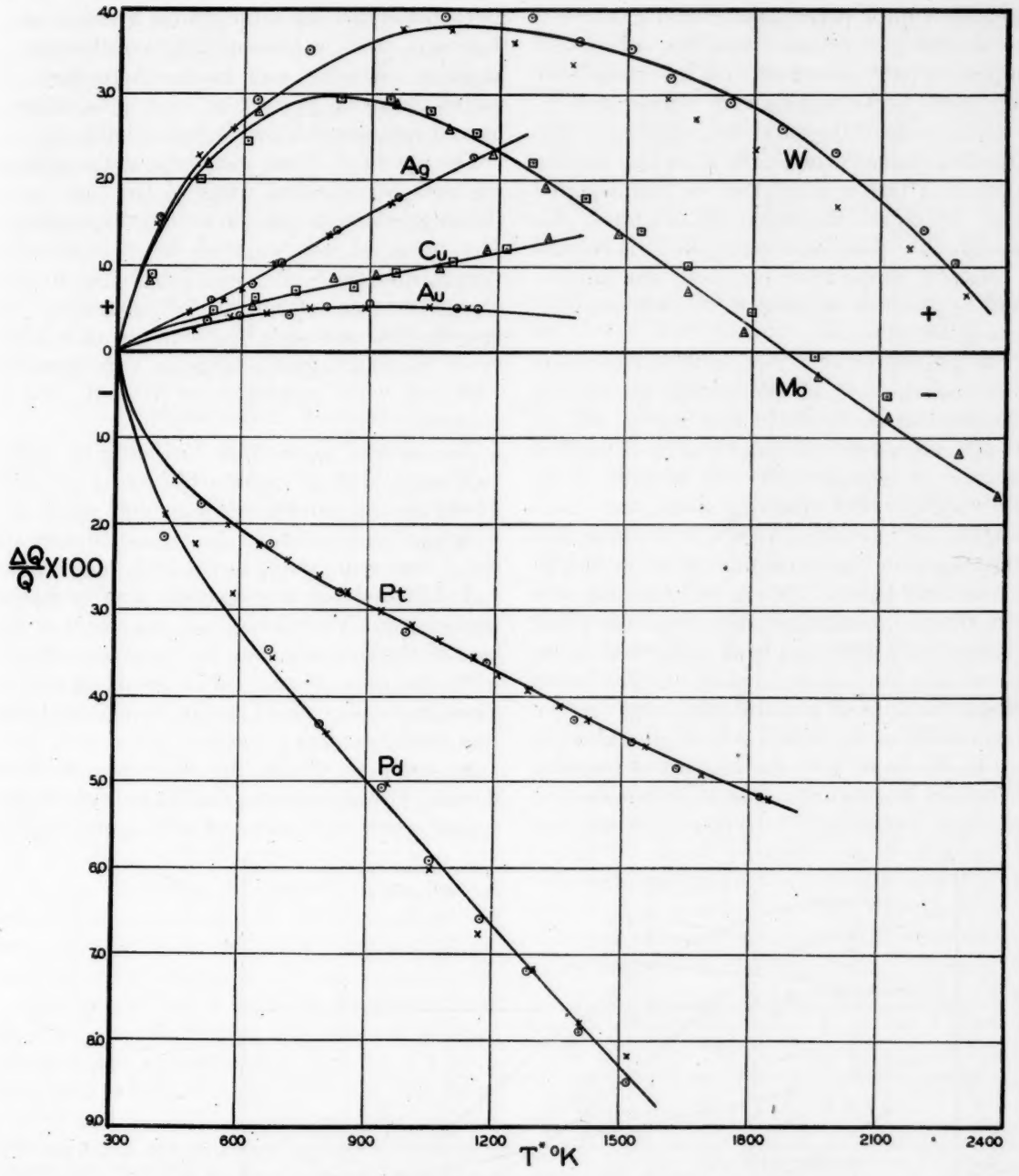

FIG. 5. Experimental values of $(\Delta Q/Q)\times 100$ plotted against temperature.

T^*, is the small wire at the center. In order to measure heat output easily, the ends of this wire are beaded and welded to bars of the same metal. Beading and welding insure good thermal and electrical contact. The bars are made of the test metal to eliminate Peltier heating at the welds. The design is such that the temperature rise in the bars was approximately 2° per 100° maximum temperature rise. Temperature gradients in the bars were measured by Chromel-Alumel couples of 5-mil wire coated with 5 mils of glass and set with silver paste in 30-mil holes at the ends of the bars. The electrical resistance between bars and thermocouples was 10^8 ohms or more. The two couples of one bar were connected in opposition, and the resulting potential

measured with a potentiometer and galvanometer sensitive to 0.1 μv. Thus the differential temperature was measured with a sensitivity of about 0.002°C. To maintain the temperature T_0 at the far ends of the bars, they were set firmly in the large copper clamps, the important feature of which is fast internal flow of thermostated water. To obtain the maximum accuracy it is essential only that the ends of the rods be held at constant temperature for about one minute, which is the time required to make a measurement of $\Delta Q/Q$.

The limiting ratio of the length l of test wire to its diameter d which insures that the ratio of radiation loss Q_r to conduction loss Q_c will be less than a prescribed amount was calculated, in the case of copper, from the formula $Q_r/Q_c \simeq T^{*3}l^2 \times 2 \times 10^{-12}/d$. Allowing a maximum radiation loss of 2 percent at 1000°C $l^2/d \simeq 10$ so that a 0.02-cm wire can be about 0.4 cm in length. On the other hand a 0.02-cm molybdenum wire (with thermal conductivity about one-third that of copper) at 2500°C can be no more than about 0.06 cm long. An experimental check on radiation loss was made in all tests by measuring current. The measure of the electrical heat generated can then be compared with the measure of the total conduction loss and this ratio must remain constant with increasing T^*. In no case in the data given below did the ratio change by more than 3 percent. In a few cases reduction of the data to absolute amounts was made. Agreement to better than one percent at high temperatures proved convection losses to be negligible.

The potential E was measured at the ends of the rods by attached wires of the test metal connected through a switch to the potentiometer. The potential was supplied by a number of storage batteries in series connected to the clamps through a reversing switch and an adjustable low resistance. Currents up to a maximum of about thirty amperes were required with test wires ranging from 6 to 10 mils in diameter.

The change in thermal conductivity in the rods amounted at most to about 1 percent. Therefore the potentiometer reading alone is a sufficient measure of the heat flow through the rod if the termocouple in the high temperature end of the rod does not lag badly with increasing temperature. A small lag (e.g., 5 percent at the highest temperature) does not interfere seriously with the measurement of a small $\Delta Q/Q$. In separate measurements the maximum lag found was much less than 5 percent.

In order to obtain the difference in heats flowing through the rods, the like pair of thermocouple wires from one rod were connected in

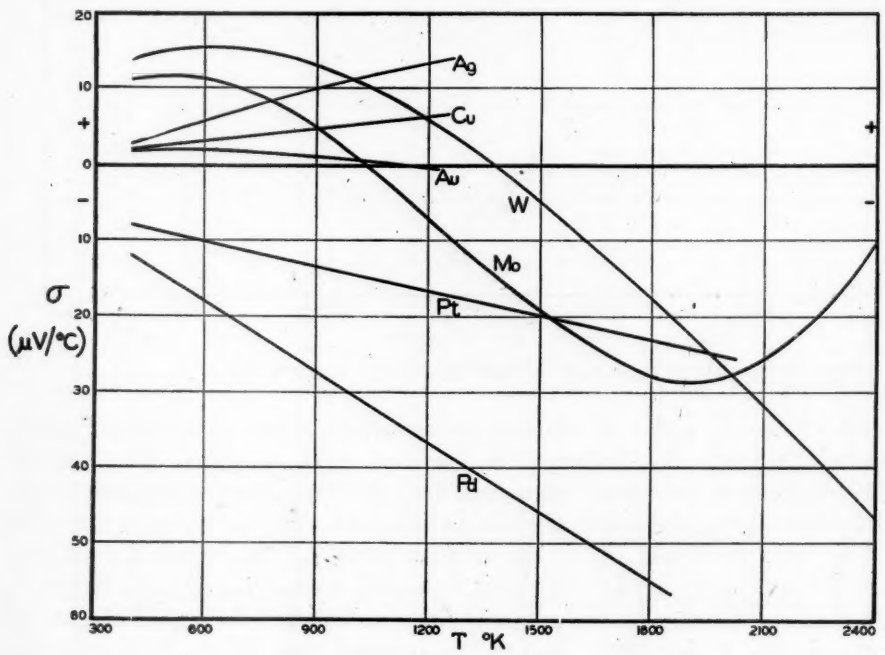

FIG. 6. Calculated Thomson coefficients.

opposition to the like pair from the other, the difference measured, then measured again with the current reversed. The difference of these differences is twice the required ΔQ and this procedure automatically corrects for unavoidable small asymmetry.

Ag, Au, Pt, and Pd were measured in air. Cu, Mo, and W were measured in hydrogen, and this was done simply by fitting a small glass tube over the wire around the ends of the rods and providing the glass tube with hydrogen input and output tubes. The flow of hydrogen was made slow to avoid convection losses.

C. Experimental Results

The dependence of T^* on E is given by $E=2(A)^{\frac{1}{2}}(T^{*2}-T_0^2)^{\frac{1}{2}}$ if the Wiedemann-Franz law holds. Variation in A of the order of ten percent produces a variation of five percent in T^* and can be tolerated if great accuracy is not sought. Experimental data in the literature confirm the constancy of A within this limit in the case of Au, Ag, and Cu. Observation of the voltage which just melts a wire is available as an experimental check. It was found that Au wires melt at 0.410 volt, Ag wires at 0.365 volt, and Cu wires at 0.435 volt. Combining these values with data in the literature, $A_{Ag}=A_{Au}$ was chosen equal to 2.45×10^{-8} watt ohm/(deg.) and A_{Cu} equal to 2.70×10^{-8}. Pt, Pd, Mo, and W do not obey the Wiedemann-Franz law so well. Therefore, pyrometric observations of T^* were made for these metals and the results are plotted against voltage in Fig. 4. The data for Pt fit a curve with A equal to 2.90×10^{-8} and this value is confirmed by the observed melting voltage equal to 0.690. The data for Pd fit a curve with A equal to 3.10×10^{-8} and this value is confirmed by the observed melting voltage equal to 0.645. Pyrometric data for Mo are well fitted below 2000°K by the curve with A equal to 3.60×10^{-8} and W below 2000°K by the curve with A equal to 4.10×10^{-8}. The value for Mo is somewhat higher than data in the literature would lead one to expect. Above 2000°K, T^* for these two metals was weighted in favor of the pyrometric data. The W and Mo wires used did not melt without significant radiation loss, and therefore their melting voltages are not recorded. The corresponding curves for Ag, Au, and Cu, as determined by the method described, are drawn here also for the purpose of comparison. Below the lower limit of the pyrometric observations (about 800°K) the values of A for Pt, Pd, Mo, and W continue to decrease with decreasing temperature so that, in using the fixed values of A indicated, one is effectively using an A which is averaged for the range from 800° to 2000°K. Data for Mo and W are probably more seriously affected by this treatment than are those for Pt and Pd. One observes also in Fig. 4 considerable deviation of experimental values from the averaged curves for W and Mo above 2000°K.

TABLE II.

Metal	$\alpha\times10^6$	$\beta\times10^8$	$\gamma\times10^{10}$	$\delta\times10^{14}$
Au	+0.454	+0.507	−4.95	——
Ag	−4.21	+1.868	−3.45	——
Cu	−0.29	+0.544	——	——
Pt	−3.66	−1.083	——	——
Pd	——	−3.03	——	——
Mo	−7.96	+8.46	−1.042	+2.86
W	——	+5.19	−0.486	+0.792

Observed values of $\Delta Q/Q$ are plotted against T^* in Fig. 5. T^* has been obtained from Fig. 4 and the observed voltage E. The results of two runs are plotted in each case, and except for Mo and W, these check each other very well. No systematic search for the cause of Mo and W variations was made, but it was found that the results of a second run with the same wire (therefore with a well annealed wire) agreed with the results of the first run.

The curves drawn in Fig. 5 were obtained from Eq. (3) using values of α, β, γ, and δ given in Table II.** The Thomson coefficients calculated from these values of α, β, γ, and δ are plotted against temperature in Fig. 6.***

D. Discussion

With the apparatus described $\Delta Q/Q$ is measured with a sensitivity of the order of 10 percent per 100°C rise in temperature, the sensitivity

** Values for directly observed Thomson coefficients given in the I.C.T. are given in the same form but with opposite sign and for different temperature intervals.

*** The large negative values obtained for platinum and palladium, if representative of values for the liquid metals, lead to the conclusion that under some conditions Thompson heat may be a significant source of erosion in platinum and palladium contacts.

being lowest for Au and highest for Pd. As the temperature span of measurement increases the accuracy of measurement of $\Delta Q/Q$ for this span increases, thus average values are obtained with accuracy for a sufficiently wide temperature range. The method is obviously not sensitive to abrupt changes in the Thomson coefficient such as might result, for example, from a phase transition. Similarly, the average values assigned to the ends of the range of measurement are not well determined.

There are few high temperature data for Thomson coefficients available in the literature and extrapolated low temperature values do not agree, in general, with the results reported above. Thus Berg[6] finds σ_{Pt} numerically decreasing with increasing temperature in the range 0°C to 128°C. Borelius and Gunneson[7] find σ_{Au} increasing with increasing temperature in the range 0°C to 300°C, but Lecher[8] reports values for Cu and Ag which have the same trend as the values reported above although about half as large in the neighborhood of 300°C. Fair agreement with the literature is obtained by extrapolation of the above results to 0°C. Worthing[9] reports σ_W increasing numerically from -10 at 1500°K to -35 at 2200°K, and these values are in fair agreement with those found here.

The high temperature reversal found for σ_{Mo} (Fig. 6) may be exaggerated due both to reduction in accuracy at the ends of the region of measurement and to a failure to determine and use a more accurate temperature-voltage relation. The data for $\Delta Q/Q$ strongly indicate an inflection point at about 2000°K and this produces zero slope of $d\sigma dT$ in this neighborhood. A more accurate study of this metal is, however, required before the sharp reversal reported can be accepted confidently. The curve for W above 2000°K does not excite suspicion, but is subject to the same sort of error.

It is to be noticed that Pt, Pd, Cu and Ag confirm the theoretical prediction that to a first approximation σ should be proportional to the absolute temperature, and that either sign is possible.[10] Negative values are reported in the case of Pt and Pd, and positive values in the case of Cu and Ag. More complicated behavior is observed with Au, Mo, and W. In the case of Au, however, σ is comparatively small. Thus at higher temperatures Au should be used to replace Pb when using the method of measuring σ based on the thermodynamic equation.

ACKNOWLEDGMENT

In the course of this work the author has received valuable suggestions from L. H. Germer, C. Herring, and J. Bardeen and to them he wishes to express sincere thanks.

[6] O. Berg, Ann. d. Physik **32**, 447 (1910).
[7] G. Borelius and F. Gunneson, Ann. d. Physik **65**, 520 (1921).
[8] E. Lecher, Ann. d. Physik **20**, 480 (1906).
[9] A. G. Worthing, Phys. Rev. **5**, 448 (1915).
[10] Mott and Jones, *The Theory of the Properties of Metals and Alloys* (Clarendon Press, Oxford, 1936), p. 310.

Letters to the Editor

PUBLICATION of brief reports of important discoveries in physics may be secured by addressing them to this department. The closing date for this department is five weeks prior to the date of issue. No proof will be sent to the authors. The Board of Editors does not hold itself responsible for the opinions expressed by the correspondents. Communications should not exceed 600 words in length.

Magnetic Variable Stars as Sources of Cosmic Rays

HORACE W. BABCOCK
Mount Wilson Observatory, Pasadena, California
July 8, 1948

RECENT observations confirm the variations in the general magnetic field previously reported for the peculiar A-type spectrum variable star HD 125248 (BD-18° 3789).[1] In a regular period of 9.295 days, the polar magnetic field changes from +7800 gauss to −6500 gauss and back. At maximum, the magnetic moment is roughly 2×10^{37} gauss cm³, and the energy in the magnetic field is probably of the order of 10^{-6} of the kinetic energy of rotation. The well-known changes in line intensity[2,3] are synchronous with the magnetic cycle, the maximum for the Eu II lines coinciding with maximum positive magnetic intensity, and the maximum for Cr I and Cr II coinciding with maximum negative magnetic intensity. Many of the abnormal line intensities and their variations can be explained, at least qualitatively, in terms of Zeeman broadening of narrow, strongly saturated, absorption lines. (Some lines of Eu II attain an actual width of 0.35A in a field of 8 kilogauss and may have their total absorption increased by a factor approaching 8.) About a score of type A spectrum variables brighter than the sixth magnitude are known,[3] and the existence of magnetic fields of the order of a few kilogauss has been established in some of these by observations of the Zeeman effect;[4] it may be inferred that all of these spectrum variables have varying magnetic fields and that the magnetic variations are more fundamental than the changes in line intensity. In some of the closely related "peculiar" stars, constant but abnormal line intensities are found, together with a magnetic field that is constant within the observational error. An example is γ-Equulei (FO_p) with $H_p=1900\pm250$ gauss.[5]

Davis has shown that a rotating star having a dipole magnetic field of constant intensity 5500 gauss at the poles should develop a quadrupole electrostatic field with potential V_p at the poles of the order of 10^{14} volts.[6] He further showed that cosmic rays should be temporarily ejected with energy eV_p along the polar axis, but that accumulation of ions that do not move along the axis will produce a space charge that will invalidate the model and suppress further ejection of cosmic rays. The observed alternating magnetic field of HD 125248, on the other hand, now suggests that at certain phases the suppressing effect of space charge will be eliminated and that alternate ejection of positive ions and electrons through electrostatic repulsion from the polar regions will recur in parts of each magnetic cycle.

A distinctly different process is that proposed by Swann to account for the acquirement of cosmic-ray energies by electrons, according to which the circular motion of an electron in an increasing magnetic field (such as a sunspot in the growing stage) gives it a magnetic moment opposed to the increasing field and results in outward acceleration.[7] (This mechanism has been dubbed the "Cygnatron" by Vallarta.) It now appears unnecessary to invoke the existence of stellar spots as sources of energetic cosmic rays as suggested by Swann, although such spots may, in fact, exist.[8]

The observed variations in the general magnetic field of HD 125248 and of some other spectrum variable stars constitute evidence for specific sources of cosmic rays according to either or both of the processes mentioned.

The number and distribution of magnetically active stars within the galaxy is as yet unknown, but they seem not to be scarce. Calculation shows that the path of a 10^{10}-volt proton passing a star having a surface field of 1 kilogauss at a distance of 0.01 light year (700 astronomical units) will have a radius of curvature of the order of 30 l.y.; this is small compared to the radius of the galaxy (35,000 l.y.). Deviations of this nature should contribute to the randomness of direction of cosmic rays.

[1] H. W. Babcock, Pub. Astr. Soc. Pac. **59**, 260 (1947).
[2] W. W. Morgan, Ap. J. **99**, 258 (1944).
[3] A. J. Deutsch, Ap. J. **105**, 283 (1947).
[4] H. W. Babcock, Ap. J. **105**, 105 (1947).
[5] H. W. Babcock, Ap. J. (*in press*).
[6] Leverett Davis, Jr., Phys. Rev. **72**, 632 (1947).
[7] W. F. G. Swann, Phys. Rev. **43**, 217 (1933).
[8] G. E. Kron, Pub. Astr. Soc. Pac. **59**, 261 (1947).

Pulse Characteristics of Anthracene Scintillation Counters

LOUIS F. WOUTERS
Radiation Laboratory, Department of Physics, University of California, Berkeley, California*
July 2, 1948

THE experiments of Bell and Davis[1] with regard to the superiority of anthracene for scintillation counters have been confirmed. In a representative arrangement, a transparent piece (1-in.×1-in.×¼-in. in dimension) of this material is fastened to the wall of a 1P21 photo-multiplier, facing the photosensitive surface. When operating at room temperature at 70 volts per stage, individual pulses up to 0.5-volt height (corresponding to the emission of about 100 electrons at the photo-surface) are observed at the output, upon exposure to a standard radium source. The signal-to-noise ratio of about 5:1 remains essentially constant up to 120 volts per stage applied to the first two stages of the

1P21, beyond which voltage it falls rapidly; it is independent of the potential applied to the remaining seven stages. An over-all gain of 25 million is then achieved by operating stages one and two at 120 volts each, and stages three through nine at 180 volts each. Pulse heights of 20 volts and more are then observed, which are sufficient to feed directly into oscilloscopes, coincidence, mixers, etc., without recourse to additional vacuum-tube amplification.

Since upwards of 1500 volts appear between adjacent anode and cathode pins, certain precautions were taken, such as slotting the base and socket, and wax impregnation. Since the peak current in the last few stages is quite high, these were by-passed with small mica capacitors.

For visual pulse observation, the photo-multiplier was mounted at the neck of an oscilloscope tube of the 5JP1 variety, with very short connections. The signal pulses showed a finite rise time of about 0.05 microsecond; this figure represents the period over which appreciable light emission by the anthracene takes place, the photo-multiplier output circuit being effectively an integrator of the photo-electrons. Variation of the decrement of the output circuit (by changing the load resistor) showed that pulse height attenuation became evident for decrements lower than 0.15 microsecond, in agreement with the rise time observation. This figure is indicative of the resolution time to be expected in normal practice. It is significant that the rise time of noise pulses originating at the photo-surface is visibly much more rapid, having no observable slope, and is much less affected by the circuit decrement.

Typical values for the output circuit elements:

circuit capacitance—15 micromicrofarads
load resistance —10,000 ohms.

The author wishes to acknowledge the encouragement and interest of Professors E. O. Lawrence and R. L. Thornton and the cooperation of the laboratory staff in pursuing these investigations. He also wishes especially to thank Messrs. Bell and DeBenedetti of the Oak Ridge National Laboratory for the clear, crystallized anthracene initially used in the described tests.

* This letter is based on work performed at the Radiation Laboratory under Contract No. W-4205-eng-48 with the Atomic Energy Commission.

[1] P. Bell and R. Davis, Bull. Am. Phys. Soc. **23**, No. 3 (1948).

Cloud-Chamber Study of Meson Disintegration*

R. W. THOMPSON
Physics Department and Laboratory for Nuclear Science and Engineering, Massachusetts Institute of Technology, Cambridge, Massachusetts
June 21, 1948

WE have recently obtained several cloud-chamber photographs at sea level showing mesons which come to rest and disintegrate. The apparatus is shown in Fig. 1. The cloud chamber (I.D.=11 inches; illuminated depth=3 inches) is filled with argon and ethyl alcohol to a total pressure of 100 cm Hg before expansion. A ½-inch thick

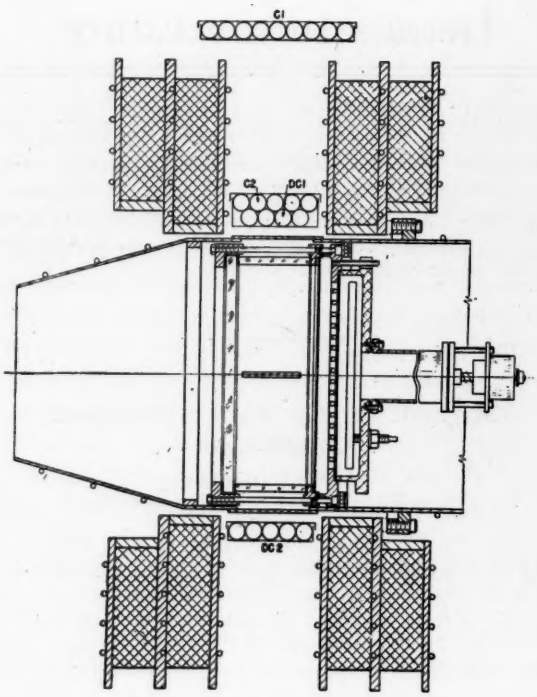

FIG. 1. Scale drawing of apparatus.

aluminum plate was placed across the diameter of the chamber to act as a slow meson absorber. The chamber is mounted between Helmholtz coils producing a field of 1680 gauss.

The counters are connected to a circuit which expands the cloud chamber when a simultaneous discharge in trays *C*1 and *C*2 is followed 0.7 μsec. to 4.7 μsec. later by the discharge of any one of the counters *DC*. This triggering arrangement heavily favors the detection of mesons which decay in or near the illuminated volume of the cloud chamber.

Figure 2 shows a positive meson which stops in the gas of the chamber after penetrating the plate. The track of the disintegration particle is clearly visible but is unfortunately short from the standpoint of curvature measurement.

We obtained six photographs showing positive mesons which stop in the plate. We also obtained a number of photographs in which heavily ionizing mesons which proba-

TABLE I. Momentum of the disintegration particle.

Film number	Sign of meson	Place of disintegration	Sagitta of track in mm	*pc* in Mev
77	+	plate	1.2	(20–50)
78	+	plate	3.3	42±12
84	−	glass	1.0	(70(?))
87	+	glass	3.5	53±15
89	+	gas	0.7	(20–50)
104	+	plate	3.5	43±9
106	+	plate	2.5	40±8
110	+	glass	1.5	(40±12)
111	+	plate	4.0	48±10
112	+	plate	4.0	42±8

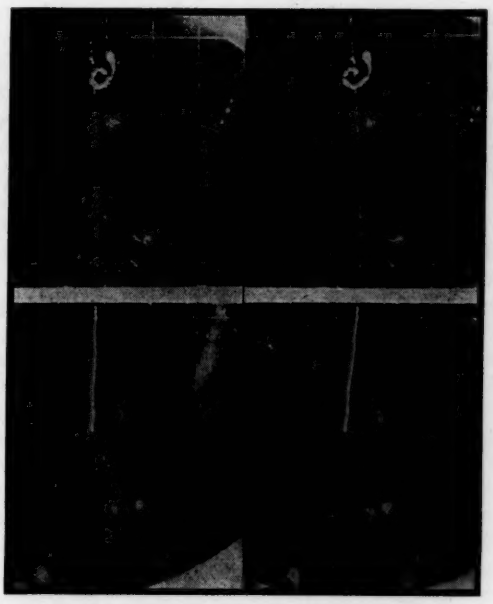

FIG. 2. Cloud-chamber photograph of a meson which penetrates a ¼-in. aluminum plate, stops in the gas (argon) of the chamber, and disintegrates with the emission of a lightly ionizing particle.

bly stop in the glass wall of the chamber are observed. In three of these, there is a thin track which is in line with the point in the glass where the respective meson stops and may therefore be the disintegration particle. Table I gives the momenta (corrected for energy loss in the plate) with estimated probable error for all the measurable photographs obtained. The momenta enclosed in parentheses are not considered very reliable because of short track length. The last five photographs were taken after improvement in technique and are considered most reliable.

The results seem to indicate a preponderance of momenta in the range 40–50 Mev/c in contrast to the results of Anderson *et al.*[1,2] who report two disintegration tracks of momenta 24 and 25 Mev/c, respectively.

The momentum of the disintegration particle is of particular interest because some information can be obtained therefrom concerning the disintegration scheme of the meson. If two particles are produced in the disintegration, conservation of energy and momentum requires that the charged disintegration particle (assumed of negligible rest mass) have a unique momentum given by the relation

$$pc=\frac{(\mu c^2)^2-(\mu_0 c^2)^2}{2\mu c^2}, \qquad (1)$$

where p is the momentum of the charged disintegration particle, c is the velocity of light, μ is the rest mass of the meson, and μ_0 is the rest mass of the neutral disintegration particle. If the disintegration gives rise to more than two particles it would not be unexpected for the charged disintegration particle to have a spectrum of momenta extending from zero to a maximum value given by Eq. (1), except that μ_0 should be replaced by the sum of the rest masses of all the neutral particles produced.

The present experiment will be continued with less absorbing material between the plate and the *DC* counters, so as to reduce the possibility that the triggering arrangement significantly discriminates against low momenta.

The writer wishes to acknowledge the constant support and kind encouragement of Professor Bruno Rossi who suggested the subject of this experiment.

* This work was supported in part by the Office of Naval Research.

[1] Anderson, Adams, Lloyd, and Rau, Phys. Rev. **72**, 724 (1947).
[2] Adams, Anderson, Lloyd, Rau, and Saxena, Rev. Mod. Phys. **20**, 334 (1948).

Excitation Time of Silver-Activated Zinc Sulfide on Electron Bombardment*

J. F. MULLANEY, F. REINES, AND H. G. WEISS
University of California, Los Alamos Scientific Laboratory, Los Alamos, New Mexico
July 1, 1948

AN experiment designed to study the promptness with which a phosphor excited by electron impact emits visible light was performed in this laboratory. In the specific case studied, the excitation by 4-kev electrons of a Dumont 5JP11 phosphor (silver-activated zinc sulfide), the rise time of visible radiation was found to be less than 10^{-8} second, the limit set by the amplifier system employed.

A laboratory-built oscilloscope was used employing a standard 5JP11 cathode-ray tube with a silver-activated zinc sulfide screen, and a vertical-deflection amplifier with a band width of 18 megacycles. The horizontal writing speed of the oscillograph was 8 inches per microsecond, and the sweep repetition rate was 1000 per second. The electron-accelerating potential was 4 kev.

The light from the cathode-ray tube was masked by a sheet of opaque paper pasted on the glass face. A vertical slit, approximately $\frac{1}{32}$ inch wide, was cut in this mask to allow the observation of a small portion of the horizontal sweep. A type 931 photo-multiplier tube was fitted with a one-inch diameter brass collimating tube approximately 8 inches long with a $\frac{1}{16}$-inch slit at its open end. The slit in the collimating tube was aligned with the vertical slit on the mask.

The output of the photo-multiplier tube was amplified in a wide-band preamplifier which, in turn, fed the wide-band, vertical-deflection amplifier of the oscilloscope. The opaque mask was arranged to allow the vertical deflection of the sweep to be visible to the observer but not to the photo-multiplier tube.

It was observed that the cathode-ray beam did not start to deflect directly at the masking slit, but was delayed along the sweep for a time corresponding to 0.04 ± 0.01 microsecond. The rise time of the pulse was approximately 0.015 microsecond.

The delay and rise times of the amplifier were determined as follows: A thin strip of copper foil, approximately $\frac{1}{16}$ inch wide, was cemented to the glass face of the cathode-ray tube, covering the slit in the paper mask which had provided the light source in the measurement described above.

The charge which the electron beam induced in this foil was coupled through the identical vertical-deflection amplifier system used above except for the omission of the 931 photomultiplier tube. It was observed that under these conditions, the deflection of the sweep was delayed approximately 0.04 ± 0.01 microsecond, and the rise time was about 0.015 microsecond. These values closely check the calculated delay and rise time for the 9-stage, 18-megacycle-wide amplifier system.

This experiment, therefore, definitely indicates that the light-emission delay in the phosphor was not observable to within the resolving time of this measurement technique, namely, 10^{-8} second. Variation in the electron beam current over wide limits produced no discernible variation in the phosphor excitation time.

* The work described in this article was done under the auspices of the Atomic Energy Project, and the information contained in this article will also be included in the National Nuclear Energy Series.

The Mean Life of Negative Mesotrons in Sulfur*

HAROLD K. TICHO
Department of Physics, University of Chicago, Chicago, Illinois
June 21, 1948

THE mean lives of positive and negative mesotrons stopping in sulfur were measured separately by means of the apparatus discussed previously.[1] Figure 1 shows the integral disintegration curves of positive and negative mesotrons. The curve marked τ_+, obtained when the magnetic lens was collecting positive mesotrons, has been plotted normalized with respect to the curve of negative mesotrons such that both curves represent the *same* number of mesotrons stopping in the absorber. The actual number of positive disintegration electrons observed was 202 and their mean life was $2.04\pm0.23\mu$ seconds.

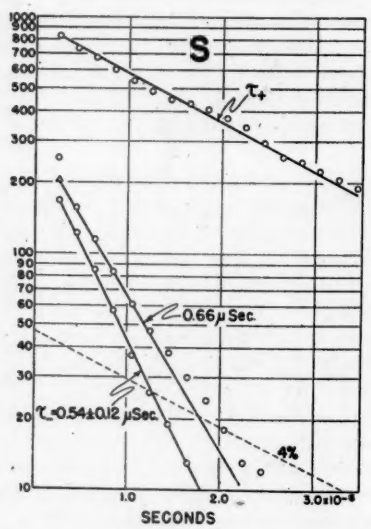

FIG. 1. Disintegration curves of positive and negative mesotrons in sulfur.

For negative mesotrons, the upper set of points shows the disintegration curve actually observed, and the triangular point at 0.25μ second represents the result when counter delays occurring without the absorber are subtracted. Beyond 1.5μ seconds, the curve departs from linearity. This must be due to the fact that the magnetic lens permits a fraction of the positive mesotrons to reach the absorber when it concentrates negative mesotrons. This fraction was found to be about 4 percent. The lower set of points shows the disintegration curve corrected for this positive admixture. From this curve, a value for the mean life of negative mesotrons in sulfur was obtained; $\tau_-=0.54\pm0.12\mu$ second. Hence, the ratio of mean lives in sulfur, τ_+/τ_-, is 4.0 ± 0.7. The ratio of the numbers of positive and negative disintegration electrons, N_+/N_-, corrected for a positive excess of 20 percent, is 3.5 ± 0.4.

The two ratios are the same within experimental error which is in agreement with the result previously obtained in sodium fluoride.[1] On the other hand, $N_+/N_-=3.5$ does not support the hypothesis[2] of an accelerated decay, in which case N_+/N_- should have been unity. This result also does not give any indication of the large discrepancy between the ratio τ_+/τ_- and the ratio N_+/N_- in aluminum which was reported by Valley and Rossi.[3]

The writer wishes to express his gratitude to Professor Marcel Schein for his continuing interest and advice during this investigation.

* The research described in this paper was supported in part by Contract N6ori-20, Task Order XVIII, U. S. Navy Department.
[1] H. K. Ticho and Marcel Schein, Phys. Rev. **73**, 81 (1948).
[2] S. T. Epstein, R. J. Finkelstein, and J. R. Oppenheimer, Phys. Rev. **73**, 1140 (1948).
[3] G. E. Valley and B. Rossi, Phys. Rev. **73**, 177 (1948).

Cosmic-Ray Showers Produced by Penetrating Particles*

C. Y. CHAO**
Physics Department and Laboratory for Nuclear Science and Engineering, Massachusetts Institute of Technology, Cambridge, Massachusetts
June 21, 1948

RECENT experiments[1] have established that cosmic-ray showers are initiated in some cases by penetrating particles, and that, of these showers, some contain at their origin both penetrating particles and fast electrons. Such showers are of interest because they probably typify the process in which the primary cosmic rays produce their secondaries in the atmosphere.

A series of cloud-chamber pictures has now been taken to investigate the production of showers by penetrating particles at sea level. The cloud chamber was rectangular, 20 inches square and 11 inches deep. For 10 percent of the pictures the chamber contained 9 horizontal lead plates, 12 inches by 10 inches by $\frac{1}{2}$ inch. For the rest of the pictures the lowest lead plate was replaced with an aluminum plate $\frac{1}{16}$ inch thick. The illuminated depth of the chamber was 8 inches. Stereoscopic pictures were taken. A tray of 6

Geiger-Müller counters, each 12 inches long and 1 inch in diameter, was placed just below the cloud chamber and a second tray of 4 similar tubes was placed 18 inches below the first. The cloud chamber was expanded when any 4 tubes of the upper tray were discharged simultaneously with two tubes of the lower tray. With this method of triggering, showers could be observed which were initiated by either ionizing or non-ionizing particles. A total of 545 pictures were obtained over a period in which the total sensitive time of the triggering apparatus was 184 hours.

We shall consider here only those showers which satisfy the following requirements: (a) the initiating particle traversed at least one lead plate before starting the shower, (b) at least 10 shower-particles were visible and (c) the shower propagated through at least one lead plate.† The showers so selected are classified according to whether they were produced by ionizing particles or non-ionizing particles and whether or not penetrating particles could be seen in the showers. The results are given in Table I. In the table we mean by "Electron showers" those in which no particles other than electrons are evident, and by "Mixed showers," those in which penetrating particles or heavily ionizing particles as well as electrons emerge from the origin. A penetrating particle is one which traverses at least one lead plate without multiplication. Most of the mixed showers, about 75 percent, show both penetrating particles and heavily ionizing particles. The columns labeled "By I.P." refer to showers in which the producing particle was an ionizing one, the columns labeled "By N.P." refer to showers in which the producing particle was definitely non-ionizing, and the columns labeled "By unknown" refer to showers in which the nature of the producing particle could not be established because the origin of the shower was either at the edge of the illuminated region or otherwise obscured. In each column are given the numbers of showers that originated in each of the lead plates below the first. Two shower photographs are reproduced in Fig. 1. Photograph (a) shows a mixed shower produced in plate 6 by an ionizing, penetrating particle. The shower has two electron cores; hence, it must have started with at least two fast electrons which may have been produced directly or indirectly through some intermediate agency; it contains also a number of penetrating particles, one of which leads to a star. Photograph (b) shows a mixed shower produced in Plate 6 by a non-ionizing, penetrating particle. The shower has a number of fast electrons, penetrating particles, and at least one heavily ionizing particle from the origin. The two other heavily ionizing particles may or may not belong to this shower. It is seen in the table that the electron showers produced by non-ionizing particles are more abundant in the upper lead plates than in the lower plates. Thus most of the non-ionizing particles responsible for the electron showers seem to be not very penetrating and may be high energy photons. If one takes this view, it appears that the contribution to both electron showers and mixed showers by non-ionizing, penetrating particles is

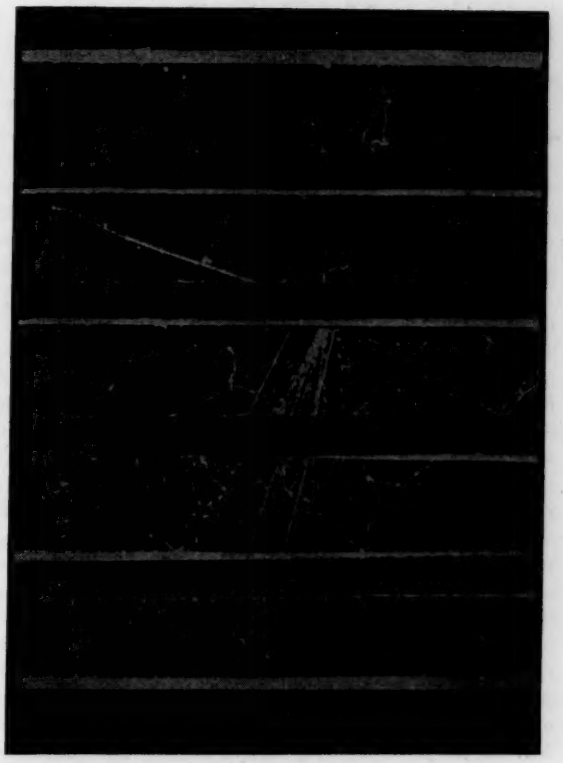

FIG. 1 (b). Photograph of a mixed shower produced in plate 6 by a non-ionizing penetrating particle.

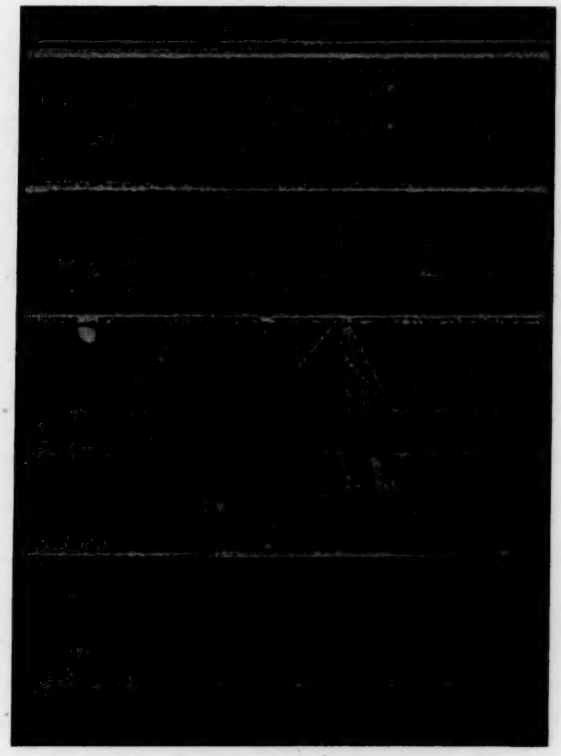

FIG. 1 (a). Photograph of a mixed shower produced in plate 6 by an ionizing penetrating particle.

TABLE I. Classification of showers.

Origin of showers	Electron showers By I.P.	By N.P.	By unknown	Mixed showers By I.P.	By N.P.	By unknown
Plate 2	0	6	1	0	0	0
Plate 3	0	1	0	3	0	0
Plate 4	2	1	1	1	1	0
Plate 5	3	1	0	5	0	0
Plate 6	6	1	7	4	1	2
Plate 7	11	1	1	1	0	0
Plate 8	2	0	1	1	0	0
Total	24	11	11	15	2	2

much smaller than that by ionizing, penetrating particles. This result is to be expected if the two types of showers are produced mainly by protons of the primary cosmic rays or by ordinary mesons. Although the contribution to the electron showers by ordinary mesons may be quite considerable, it seems probable in view of other evidence that the mixed showers observed in this experiment were largely produced by primary protons. It may be mentioned that the relative contributions of the two types of producing particles depend presumably on the energy of the showers selected and hence, on the particular arrangement of the experiment.

The author is grateful to Professor B. Rossi for his encouragement during the course of this experiment and to Mr. H. Bridge and Mr. R. J. Davisson for their suggestions and help. He is also indebted to Professor G. E. Valley and Mr. A. L. Jerrems, who designed and built the cloud chamber.

* This experiment was supported in part by the Office of Naval Research.

** On leave from Physics Department, National Central University and Institute of Physics, Academia Sinica, Nanking, China.

[1] H. Bridge, B. Rossi, and R. Williams, Phys. Rev. **72**, 257 (1947); W. B. Fretter, Phys. Rev. **73**, 41 (1948), also other references there; H. Bridge, W. Hazen, and B. Rossi, Phys. Rev. **73**, 179 (1948); H. Bridge and W. Hazen, Phys. Rev., to be published.

† Except the mixed shower produced in the 8th plate.

Coincidences Between Beta-Rays and Conversion Electrons in Europium

K. Y. CHU AND M. L. WIEDENBECK
Department of Physics, University of Michigan, Ann Arbor, Michigan
July 6, 1948

IT has been shown that the long-lived (5–8 years) isotope of europium decays with the emission of beta-spectra of upper energies of the order of 0.6–0.7 Mev and 1 Mev,[1] respectively. Using a double focusing spectrometer, Shull[2] has found the ratio of the two components to be approximately 4 to 1. In addition he has found a large number of conversion lines, the highest corresponding to a gamma-ray energy of 412 kev.

We have measured the beta-conversion electron coincidence rate for europium as a function of the absorber thickness. The lower curve in Fig. 1 was obtained by placing equal absorbers between the source and each of the counters. The point at which this curve becomes zero gives the maximum energy of the conversion electrons. For europium this value is about 375 kev.

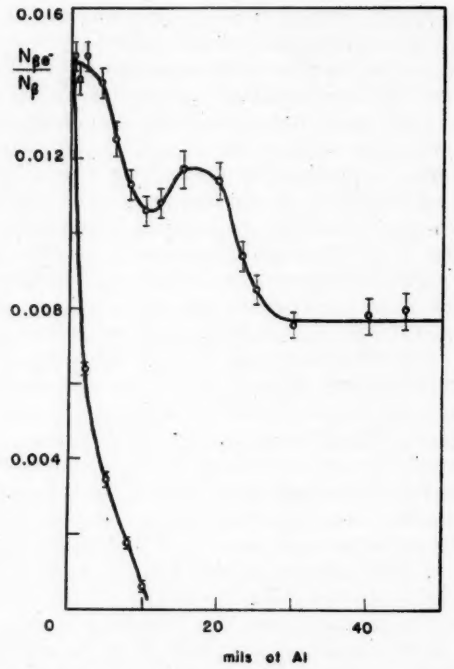

FIG. 1. Beta-conversion electron coincidence rate for europium. The lower curve was obtained by placing equal absorbers between the source and each counter. The upper curve was obtained by placing an absorber between the source and only one of the counters.

We have previously[3] published several curves obtained by placing an absorber between the source and only one of the counters. For cases of decay with the emission of a simple beta-spectrum a considerable amount of information can be obtained, including a fair estimate of the total conversion coefficient. The upper curve in Fig. 1 was obtained by this single absorber method. This curve is level at absorber thicknesses greater than 28 mils of aluminum at which point the lower energy beta-component has been completely absorbed. The equation for the curve beyond this point reduces to

$$R=\sigma_\beta \epsilon \sum_{K=1}^{n} \alpha_K,$$

in which σ_β is the fraction of the sphere subtended by the counter, ϵ is its efficiency, and $\sum_{K=1}^{n} \alpha_K$ the total conversion coefficient associated with the higher energy beta-rays. The value obtained for $\sum_{K=1}^{n} \alpha_K$ is 25 ± 5 percent. From the initial value of these curves and using a branching ratio of 4:1 one can give an estimate of 35 percent for the conversion coefficient of the gamma-rays following the lower energy beta-component. The peculiar shape of the curve appears to be real and is probably caused by the manner of absorption[3] of the many components involved in the coincidences.

[1] M. L. Wiedenbeck and K. Y. Chu, Phys. Rev. **72**, 1164 (1947).
[2] F. B. Shull, Doctorate Thesis, University of Michigan (1948).
[3] M. L. Wiedenbeck and K. Y. Chu, Phys. Rev. **72**, 1171 (1947).

Production of Li^8 in Boron-Loaded Photographic Emulsions

E. PICKUP
Division of Physics, National Research Council, Ottawa, Ontario, Canada
June 28, 1948

THE disintegration of B^{11} by fast neutrons to give Li^8 and an α-particle is now well known, and was first detected by Lawrance,[1] using an ionization chamber filled with boron trifluoride. The Q of the reaction, estimated from mass values in the Segrè chart is -6.7 Mev. For some time we have been working on the problem of trying to obtain Li^8 disintegrations in the gas in a cloud chamber with the object of getting information about the neutrino recoil. In the course of this work, and to obtain information about the yield of the $B^{11}(n, \alpha)Li^8$ reaction some Ilford C2, boron-loaded, photographic emulsions were exposed to the neutrons from a Li target bombarded with 600 kv deuterons, in the Ottawa ion accelerator. The neutron spectrum from such a target extends up to about 14.5 Mev with several peaks. This is well above the threshold for the B^{11} reaction, and examples of this disintegration have been observed in the emulsions as well as the usual B^{10} disintegrations. Measurements on the tracks are not yet complete, but one good typical case is shown in Fig. 1 below. This is a mosaic of four microphotographs, and shows clearly the recoil Li^8 nucleus together with the α-particle from the B^{11} disintegration, and the two oppositely directed α-particles of about equal range produced by the splitting of the Be^8 nucleus formed after β-decay of Li^8. This is a simple example of the so-called "hammer" tracks sometimes observed in cosmic-ray stars.

The total energy of the pair of α-particles in this particular case is 2.6 Mev, if we use the range energy data of Lattes, Fowler, and Cuer[2] for the emulsion. The energies of the other α-particle and the Li^8 recoil nucleus are 5.4 Mev and 1.7 Mev, respectively, the latter being extrapolated from the data of Lattes, Fowler, and Cuer for α-particles, assuming the Li^8 recoil to obey the range-energy relation $(m/Z^2)\cdot f(v)$, where $f(v)$ is the same as for α-particles in this energy region. Thus, the total energy of the incident neutron, taking into account the threshold energy for the reaction of -6.7 Mev, must have been 13.8 Mev, and this is consistent with its being a neutron from the high energy end of the Li-D spectrum.

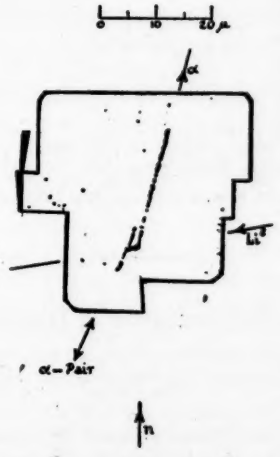

FIG. 1. Mosaic of photomicrographs showing $B^{11}(n,\alpha)Li^8$ reaction in Ilford C2, boron-loaded, photographic emulsion; Li^8 (β-decay; $t = 0.88$ sec.; electron not visible in emulsion) $\rightarrow Be^8$; $Be^8 \rightarrow \alpha$-pair. The direction of the incident neutron in this particular case was not very well defined because of proximity of neutron source and plate.

The ejection of Li^8 nuclei in cosmic-ray stars has been reported by Occhialini and Powell, and very recently in more detail by Franzinetti and Payne[3] of the Bristol group. In some observations by A. Morrison and myself here, on photographic emulsions exposed to cosmic radiation, which will be reported soon, we have obtained one definite example of a star showing a "hammer" track out of some 500 cosmic-ray stars. The estimated energy of the ejected Li^8 nucleus was 16 Mev, and the energy of the pair of α-particles was 3 Mev, these being about equal in length and oppositely directed.

The above work will be reported in more detail later.

[1] A. M. Lawrance, Proc. Camb. Phil. Soc. **35**, 304 (1939).
[2] Lattes, Fowler, and Cuer, Proc. Phys. Soc. **59**, 883 (1947).
[3] Franzinetti and Payne, Nature **161**, 735 (1948).

Experiments on He^3 at Low Temperatures

J. G. DAUNT, R. E. PROBST, AND S. R. SMITH
The Cryogenic Laboratory, Department of Chemistry and Department of Physics, The Ohio State University, Columbus, Ohio
June 24, 1948

THE first experimental indications of a new method of separation of the isotopes He^3 and He^4 were given by us in observing the effects accompanying the superfluid transfer of matter in liquid helium II both in supra-surface film transfer[1] and through channels in the bulk liquid.[2] We established that, within the limits of measurement, He^3 atoms do not partake in superfluid flow, characteristic of liquid helium II, and pointed out that the separation of the isotope He^3 by superfluid flow in the liquid phase is a process which could lead to its eventual isolation.

Repetitions of the preliminary experiments[1] on separation by the method of supra-surface film transfer have been made and have shown, as did the first experiments, that the relative abundances of He^3 in He^4 in the two reservoirs connected by the mobile film could be made to differ in the process by a factor of at least 200. Subsequent experiments, using techniques based on the same principle, have yielded samples with He^3/He^4 concentration of approximately 5.10^{-4}. We conclude, therefore, that this process of separation is satisfactory.

Based on evidence thus provided[1,2] for the non-superfluidity of He^3 in low concentration ranges, Lane and collaborators have adopted an elegant method[3] of concentrating the rare isotope by initiating the superfluid flow in the bulk liquid by thermal means, a technique used by us for initiating the flow through films rather than the bulk liquid. The variation of the results obtained at different temperatures by this method, however, together with some unpublished results obtained by us on separation processes

in the bulk liquid, have led us to believe that an exact interpretation of the mechanism involved cannot be obtained without information on the distribution of He^3 between vapor and liquid phases below the λ-point.

Early work[1] on the abundance ratio of He^3 to He^4 in the vapor in equilibrium with very dilute solutions of He^3 in He^4 in the liquid helium II phase showed that this ratio was equal to or less than that in the liquid solution. Subsequent work by Fairbank and Lane[4] with a similar method has shown that, within the limits of measurement, no He^3 exists in the vapor phase below 1.85°K, when the abundance ratio for the unrefrigerated gas was 1.2×10^{-6} (atmospheric helium gas). Using a new method in which precautions were taken to assure that any sampling of the vapor would not disturb the liquid-vapor equilibrium and to avoid any possible contamination of the results caused by unwanted film flow, we have measured the equilibrium abundance of He^3 between liquid and vapor phases. A description of the apparatus is left to a fuller article. The results are shown in Fig. 1 in which the ordinates give the logarithm of the ratio of the concentration of He^3 in He^4 in the vapor phase to the concentration in the liquid phase in equilibrium, $(\log C_V/C_L)$, i.e., the logarithm of the coefficient of distribution. Above the λ-point we have plotted in Fig. 1 observations made both by us for atmospheric helium and those previously reported by Lane and collaborators.[5] Satisfactory agreement is shown. Below the λ-point we obtain two sets of points which lie roughly along two straight lines, one set for a concentration of the liquid of between 30 to 40×10^{-6} (the upper curve) and the other for a liquid concentration of between 9 and 13×10^{-6}. The variation in the liquid concentration in each set is due to the gradual depletion of the total He^3 content of the solution by successive sampling.

It will be seen from the curves that only for the very lowest temperatures and smallest liquid concentrations did the value of the coefficient of distribution fall below unity.

One must conclude that the coefficient of distribution shows a marked variation with concentration, indicating a departure from the laws of perfect solutions even for such dilute solutions as here employed. As yet the variation of the coefficient of distribution with concentration cannot be established, but the general results indicate that with increasing concentration in the liquid solution, relatively more and more He^3 goes into the vapor phase, in agreement with the theory put forward by London and Rice.[6] Such a departure from ideality was already evident from our measurements[7] of the osmotic pressures developed in dilute solutions of He^3 and He^4.

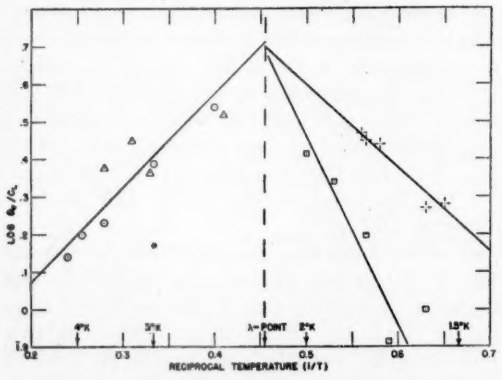

FIG. 1. Variation with temperature of the ratio, in the volume and liquid phases, of the concentration of He^3 in He^4. The triangles are for concentration He^3/He^4 in the liquid phase $=1\times10^{-6}$. The squares are for $He^3/He^4=10\times10^{-6}$. The crosses are for $He^3/He^4=30$ to 40×10^{-6}. The circles are the results of Lane and collaborators.[5]

If one applies the thermodynamic treatment of London and Rice,[6] one obtains for the difference of the enthalpies of condensation of He^3 and He^4: $\Delta\bar{H}_3-\Delta\bar{H}_4=-10$-cal. mole^{-1} for liquid concentrations of 30 to 40×10^{-6}, $\Delta\bar{H}_3-\Delta\bar{H}_4=-22$ cal. mole^{-1} for liquid concentrations of 9 to 13×10^{-6} and for liquid concentrations of 1×10^{-6} (not shown in Fig. 1) the value is approximately -25 cal. mole^{-1}. The latter figure, for atmospheric helium, as a result of the increased difficulty of mass spectrographic analysis for small concentrations, has not the same accuracy as the others. These values are a first approximation only since departures from ideality of the solutions have not been taken into account in the calculations; however, the marked difference between these results and those reported elsewhere[4] remains. Further experimental work on these measurements is being carried out to obtain the function giving the variation of C_V/C_L with initial concentration,[8] so that an exact computation can be made of the properties of pure He^3.

The results obtained so far, together with those on the osmosis,[7] have provided sufficient information for a large-scale separation process. For such a process, large superfluid flows through supra-surface films can be obtained by increasing the surface by wires[9] or foils. A technique for this has been outlined by us,[10] providing a film flow of 0.5 liter liquid per hour, and is being carried out here for continuous separation of He^3.

* This work was supported in part by the Office of Naval Research under a contract with the Ohio State Research Foundation.

[1] J. G. Daunt, R. E. Probst, H. L. Johnston, L. T. Aldrich, and A. O. Nier, Phys. Rev. **72**, 502 (1947).
[2] J. G. Daunt, R. E. Probst, and H. L. Johnston, J. Chem. Phys. **15**, 759 (1947).
[3] C. T. Lane, H. A. Fairbank, L. T. Aldrich, and A. O. Nier, Phys. Rev. **73**, 256 (1948).
[4] H. A. Fairbank, C. T. Lane, L. T. Aldrich, and A. O. Nier, Phys. Rev. **73**, 729 (1948).
[5] H. A. Fairbank, C. T. Lane, L. T. Aldrich, and A. O. Nier, Phys. Rev. **71**, 911 (1947).
[6] F. London and O. K. Rice, Phys. Rev. **73**, 1188 (1948).
[7] J. G. Daunt, R. E. Probst, and H. L. Johnston, Phys. Rev. **73**, 638, 1263 (1948).
[8] The importance of this is stressed by J. W. Stout in a private communication and is to be published in Phys. Rev.
[9] J. G. Daunt and K. Mendelssohn, Proc. Roy. Soc. **A70**, 423 (1939).
[10] J. G. Daunt and H. L. Johnston, The Ohio State University Research Foundation Report to U. S. Naval Office of Research, No. 6 (Jan. 1, 1948).

The Concentration of Helium 3

ALAN ANDREW AND W. R. SMYTHE
California Institute of Technology, Pasadena, California
July 6, 1948

WE have constructed a two-stage apparatus for concentrating the He^3 isotope. The first stage consists of four Clusius-Dickel columns of the concentric tube type connected in parallel. The second stage consists of 29 Hertz pumps connected in series.

Using the theory of Jones and Furry,[1] the Clusius-Dickel columns have a calculated performance of 0.036 gram per day concentrated 700 times above normal. The Hertz pumps have a calculated separation factor of approximately 1.8×10^6. The product of these is of the order of 10^9. This is high enough that the final percentage in the Hertz is a linear function of time.

Working with well helium on the basis of continuous operation and using the calculated characteristic time of 7 days, a 0.25-g product was taken from the first stage and transferred to the second stage where it was processed in 7 days. The first sample of 30 cc at a pressure of 10 mm had the following analysis:

Helium 3	0.5 percent,
Helium 4	59.5 percent,
Hydrogen	40.0 percent,

as analyzed by Consolidated Engineering Corporation of Pasadena on one of their mass spectrometers.

This initial run indicates that nearly a year would be required to produce 50 percent helium 3; however, theoretical considerations predict that this time can be materially shortened.

The helium was furnished by the U. S. Navy through Contract N6onr-102, Task Order V.

[1] R. C. Jones and W. H. Furry, Rev. Mod. Phys. 18, 151 (1946).

Fluctuations of Ionization and Low Energy Beta-Spectra

D. H. W. Kirkwood, B. Pontecorvo, and G. C. Hanna
National Research Council, Chalk River Laboratory, Chalk River, Ontario, Canada
June 29, 1948

USING an (n,γ) reaction in the Chalk River heavy water pile, we have prepared the nuclide A^{37}, which is known to decay by K-capture without emission of positrons.[1] A^{37} was introduced inside various proportional counters filled with a mixture of argon and methane: usually, though not always, 39 cm $A+12$ cm CH_4 were used. The cathode diameters, wire diameters, and effective lengths of two typical counters, 1 and 2, were, respectively, 4.67 cm, 0.0047 cm, 19.7 cm for No. 1 and 1.75 cm, 0.0047 cm, 6.9 cm for No. 2. The counters were connected to a linear amplifier, the output of which was fed either into a discriminator or into a 30-channel pulse analyzer. A typical differential curve is shown in Fig. 1, obtained with counter 1 working at 2520 volts. The noise was equivalent to 4500 pair of ions and the multiplication factor in this run was about 10^4. The curve is shown by a broken line below channel 2, because the effective width of channel 1 is not accurately known. The main peak corresponds to an energy of about 2800 ev, the binding energy of a K electron in the Cl^{37} atom. Since the Auger electron yield[2] for the K shell is about 90 percent, about 90 percent of the K-capture processes result in the emission of soft radiations dissipating the full 2800 ev in the counter.

The low energy peak corresponds to about 200 ev, as was

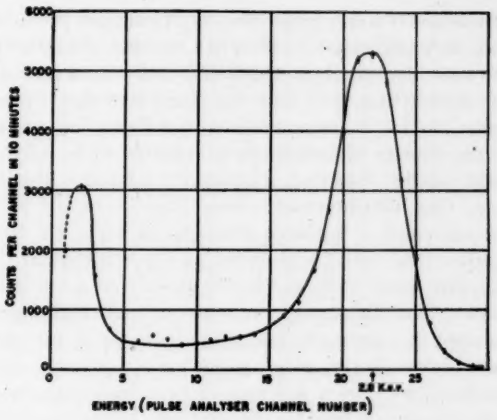

FIG. 1.

determined by runs at higher over-all gain. This is approximately the energy of ionization of the L shell. We believe that the following two mechanisms contribute in a comparable extent to the low energy peak: (*a*) Nuclear K-capture processes resulting in the $K-\alpha$-x-radiation being emitted by the Cl^{37} atom and not being absorbed in the counter. In such processes a photon of about 2600 ev would escape from the counter, while the remaining energy corresponding to the ionization of the L shell would be dissipated in the counter. (*b*) Nuclear absorption of an L electron, the so-called L-capture, which has been discussed in the literature but not yet observed experimentally.[3] While we plan to discuss in the near future the quantitative aspects of this question, we wish to turn now to the main peak.

1. While the main peak cut-off is very sharp on the high energy side, there is a "tail" on the other side. That this is partly due to the end effects of the counter, resulting in a small value of the multiplication factor near the end, has been shown by a few runs recently obtained with a counter (3) having a ratio of length to diameter three times as great as the one used in the run illustrated in Fig. 1. With counter 3 the cut-off on the low energy side is sharper.
2. That the mean energy necessary for an electron to produce a pair of ions is approximately independent of the electron energy was confirmed by experiments in which the $K-\alpha$-x-ray lines of copper were made to fall upon the counter. Although there was a wide distribution of pulses as a result of wall effects, the maximum size, caused by the full energy content of the copper $K-\alpha$-quantum ($\approx$8000 ev) could be measured on an oscilloscope. The ratio of this maximum pulse size to the main A^{37} pulse size was $2.8\approx8000/2800$. It is clear that A^{37} can provide an ideal "calibration line" for the proportional counter investigation of low energy beta-spectra such as that of H^3.
3. The width at 60.7 percent of the peak for the 2800-ev line is about 18 percent as determined in various runs. This corresponds to an observed standard deviation of the pulse size of ±9 percent. Yet the mean number of pairs of ions produced by a 2800-ev electron is about 100, and if we assume that the variance of the number of

ionizations is equal to the number of ion pairs produced, then we would expect to observe a standard deviation for the pulse size equal to $\pm(2\times100)^{\frac{1}{2}}/100=\pm14$ percent,* i.e., definitely greater than the observed value. In fact, according to a theoretical estimate[4] of Fano, the variance of the number of ionizations is expected to be substantially smaller than that governed by a Poisson distribution. Our measurements show that in our $A+CH_4$ mixture such a variance must be at least 2.4 times smaller; this value is obtained on the assumption that the only cause of spread in the peak is of a statistical nature. Such an assumption, under certain conditions, is justified in a proportional counter because of the negligible value of the noise in comparison with a signal produced by only a few pair of ions. It is this feature which has made possible the study of the fluctuations in the number of ionizations; in a pulse chamber without gas amplification, the minimum detectable pulse corresponds to such a great number of ion pairs that the spread in pulse size caused by fluctuations of ionization would be masked by instrumental spread.

In conclusion we wish to point out that the technique of the proportional counter at high multiplication factor should be useful not only in beta-ray problems such as orbital electron capture and continuous beta-spectra at low energy, but also in x-ray applications such as measurements of fluorescence yields.

[1] P. K. Weimer, J. D. Kurbatov, and M. L. Pool, Phys. Rev. **66**, 209 (1944).
[2] A. H. Compton and S. K. Allison, *X-Rays in Theory and Experiment* (D. Van Nostrand Company, Inc., New York, 1935), pp. 477–92.
[3] R. E. Marshak, Phys. Rev. **61**, 431 (1942); E. Segrè, Phys. Rev. **71**, 274 (1947); R. Bouchez, R. Daudel, P. Daudel, and R. Muxart, J. de Phys. et Rad. **8**, 336 (1947).
* The factor 2 arises from the variance introduced by the multiplication process in the counter (H. S. Snyder, Phys. Rev. **72**, 181 (1947); also "Statistics of multiplicative processes," an as yet unpublished paper by O. R. Frisch.
[4] U. Fano, Phys. Rev. **72**, 26 (1947).

The Magnetic Susceptibility of Uranium Tetrafluoride, UF_4*

NORMAN ELLIOTT
Brookhaven National Laboratory, Upton, New York
June 21, 1948

THE magnetic susceptibility of uranium tetrafluoride, UF_4 has been measured over the temperature range 74.5°K−294.5°K. The UF_4 was prepared by the conversion of Merck's "Reagent" Grade $UO_2(NO_3)_2\cdot6H_2O$ to UO_3, reduction of the UO_3 to UO_2, and subsequent hydrofluorination to form UF_4. These reactions were followed by measuring the changes in weight with each process. The UF_4 was analyzed gravimetrically for U. The result of three analyses was 76.08±0.43 percent U. The theoretical value is 75.80 percent, based on a molecular weight of 314.07. The magnetic measurements were made on a Gouy balance with the salt in the form of a powder. The results, corrected for diamagnetism, are shown in Fig. 1. A Weiss-Curie law is obeyed over the whole temperature range in which observations were made.

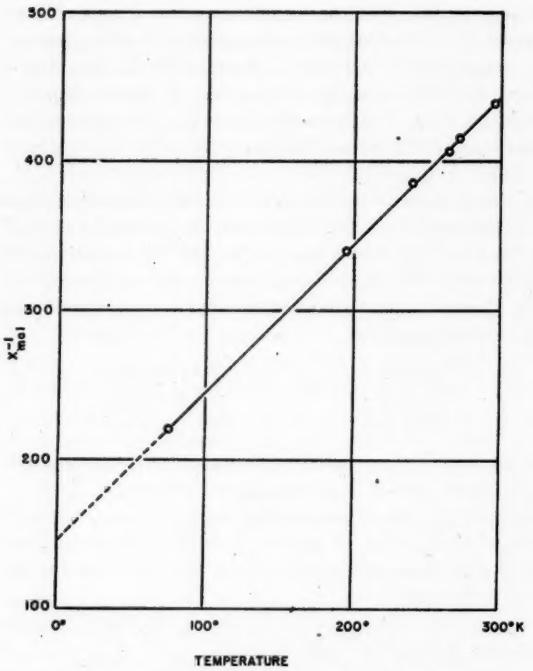

FIG. 1. Magnetic susceptibility of UF_4 as a function of temperature (corrected for diamagnetism).

Writing $\chi=C/(T+\Delta)$, Δ is calculated to be 146°K, and C to be 1.00. Using the equation $\mu=2.83(\chi_M(T+\Delta))^{\frac{1}{2}}$, the magnetic moment of the U^{4+} ion is found to be 2.83 Bohr magnetons, with an average deviation of 1 percent as determined by measurements on three samples.

If it is assumed that the U^{4+} ion has Russell-Saunders coupling, and evidence for this is furnished by the work of Kiess, Humphreys, and Laun,[1] one concludes from the experimental data that the crystalline field has broken down the spin-orbit coupling, and that a non-magnetic state lies considerably below all other states. The spin, S of two unpaired electrons remains free to contribute to the magnetic moment with a value $\mu=2(S(S+1))^{\frac{1}{2}}\beta=2.828\beta$, in good agreement with the observed moment.

The experimental results obtained for uranium tetrafluoride are similar to those found for compounds of the first row transition elements, and suggest that in this case the U^{4+} ion is in a $^3F_2$ state with two $6d$ electrons whose orbital contribution to the magnetic moment has been quenched by the crystalline field.

Basic states for the U^{4+} ion probably belong to the configuration $5f^2$, $5f6d$, or $6d^2$. Assuming the orbital moment to make its full contribution, no magnetic moment could be calculated for these states which was compatible with the above data. This is true for jj as well as for LS coupling.

The magnetic susceptibility of UF_4 does not provide a direct answer to the question of the spectroscopic state of the U^{4+} ion in this compound. The quenching of the orbital contribution to the moment is easily accounted for if the basic state is $^3F_2$, arising from the configuration $6d^2$, but not if it is $^3H_4$, coming from the $5f^2$ configuration. The investigations of Wu and Goudsmit[2] and of M. Goeppert Mayer[3]

show that the 5*f* levels of the heavy elements lie deep within the electronic structure. A crude calculation of the spin-orbit interaction for 5*f* electrons in uranium gives a value of 40,000 cm^{-1} for the energy. This is larger by factors of ten to one hundred than the crystalline field-orbit interactions which have been estimated in the case of the rare earths. Assuming the correctness of our present theoretical knowledge of the heavy elements, it is doubtful that 5*f* electrons are sufficiently accessible to crystalline field effects to give rise to a quenching of the orbital moment.

The magnetic susceptibility of uranium tetrachloride, UCl_4 has been measured by Bommer[4] who found a Weiss-Curie law obeyed above 300°K. The magnetic moment calculated from his data is 2.71 Bohr magnetons, and is in agreement with the "spin-only" formula also.

The magnetic behavior of the halides of tetravalent uranium is in pronounced contrast with that of the oxalate, sulfate, and acetylacetonate[5] whose magnetic moments are in agreement with the existence of a $^3H_4$ state, corresponding to trivalent praesodymium among the rare earths.

It is a pleasure to acknowledge the help and criticism of Dr. S. A. Goudsmit in writing this letter, and the opportunity to make some of the measurements while the author was a member of the Institute for Nuclear Studies at the University of Chicago.

* Research carried out at the Brookhaven National Laboratory under the auspices of the Atomic Energy Commission.
[1] Kiess, Humphreys, and Laun, J. Research Nat. Bur. of Stand. 37, 57 (1946).
[2] T. Y. Wu and S. Goudsmit, Phys. Rev. 43, 496 (1933); T. Y. Wu, Phys. Rev. 44, 727 (1933).
[3] M. Goeppert Mayer, Phys. Rev. 60, 184 (1941).
[4] H. Bommer, Zeits. f. anorg. allgen. Chemie 247, 249 (1941).
[5] C. A. Hutchison and N. Elliott, J. Chem. Phys. to be published.

The Disintegration of Cs^{137}

J. Townsend, Marshall Cleland, and A. L. Hughes
Department of Physics, Washington University, St. Louis, Missouri
July 6, 1948

IN a previous letter[1] it was reported that Cs^{137} (33 yr.) has a simple beta-spectrum with an end-point energy of 0.550 Mev and a gamma-ray of 0.663-Mev energy, partially internally converted (12 percent).

Subsequent coincidence-counting experiments revealed no beta-gamma-coincidences. However, coincidences were found between conversion electrons and the associated

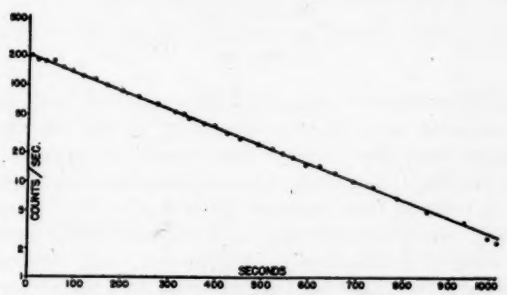

FIG. 1. Decay of Ba^{137} excited state.

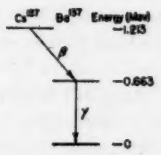

FIG. 2. Decay scheme of Cs^{137}.

x-rays. A critical absorption experiment to determine the x-ray energy was performed by placing aqueous solutions containing Sn, Sb, Te, and I between the source and one of the counters. The x-rays were found to be characteristic of Ba, indicating that the gamma-rays are emitted from the excited Ba nuclei which follow the beta-decay of Cs.

The large internal conversion coefficient and lack of beta-gamma-coincidences led to an investigation of the life of the Ba^{137} excited state. Sulfate ions were added to a solution containing the active cesium, which was then placed in contact with solid $BaSO_4$ (barite). The $BaSO_4$ was washed and examined for activity. The half-life of this gamma-activity, plotted in Fig. 1, is 158±5 sec.

The simple decay scheme of Fig. 2 is proposed. The long lifetimes of the Cs^{137} and excited Ba^{137} nuclei indicated that large spin changes are involved in both beta- and gamma-transitions. The spin of the ground state of Ba^{137} is known to be $\frac{3}{2}$. Although it is probably impracticable to measure directly the spin of the excited Ba nucleus, at least it would seem feasible to measure the spin of Cs^{137} directly by the atomic beam method used by Zacharias to measure K^{40}.[2] One millicurie of Cs^{137} contains about 5×10^{16} atoms, more than enough for such a determination.

We wish to thank Dr. H. Primakoff for the suggestion concerning the measurement of spin. This work was supported partly by the Office of Naval Research.

[1] J. Townsend, G. E. Owen, Marshall Cleland, and A. L. Hughes, Phys. Rev. 74, 99 (1948).
[2] J. R. Zacharias, Phys. Rev. 60, 168 (1941).

A Note on Ethylene Self-Quenching G-M Counters*

K. H. Morganstern, C. L. Cowan, and A. L. Hughes
Department of Physics, Washington University, St. Louis, Missouri
June 21, 1948

INVESTIGATIONS have been made on the effects of various quenching gases in varying percentages and total pressures on the characteristics of argon-filled G-M counters. Four polyatomic gases, alcohol, ether, ethylene, and cyclopropane, were used with argon in percentages of 10, 20, 30, and 40 and with total pressures from 6 to 14 cm. Four cylindrical G-M counters each with a different cathode (aluminum, gold, brass, and magnesium) were filled simultaneously with each of the filling mixtures, in turn, under conditions which were as nearly as possible identical and reproducible. This insured that for each counter the only variable was the gas filling.

After each filling, all the counters were examined for plateau slope and length, threshold, dead time, and multiple

counts. A one-shot sweep circuit was used to measure dead time[1] and gave a visual picture of the pulse. In addition, the pulses were examined on an oscilloscope for multiplicity.

Of the four quenching gases ethylene consistently gave the best results. It was found that with a partial pressure of 0.8 to 5 cm of ethylene a plateau was obtained with less than 0.10 percent rise per volt over a length of at least 200 volts. The plateau was definitely flatter than when the other polyatomic gases were used in the same tubes.

The ethylene not only gave long, flat plateaus over a wider range of partial pressures, but also had other decisive advantages over the other polyatomic gases. As a gas rather than a vapor (e.g., alcohol), it was much more dependable under temperature changes and easier to handle. It gave no multiple counts at all whereas occasional multiple counts were obtained on replacing the ethylene by alcohol. Ethylene did not react with counters employing Zapon as a thin window as did alcohol, amyl acetate, and ether. Finally the ethylene-filled counters were very stable with respect to counting rate and recovered rapidly even after a discharge through the counter.

* This work was supported in part by the Office of Naval Research.
[1] H. G. Stever, Phys. Rev. 61, 38 (1942).

Erratum: Electromagnetic Properties of Nuclei in the Meson Theory

[Phys. Rev. 62, 118 (1942)]
S. T. MA AND F. C. YU
Dublin Institute for Advanced Studies, Dublin, Eire

IN deriving Eq. (69) from Eq. (65) in our calculation of the exchange magnetic moment, a minus sign was left out by mistake. The result given by Eq. (69) should therefore be multiplied by a factor -1. After this correction this result agrees in magnitude and in sign with the result given in an earlier paper.[1] The present writer (S. T. Ma) was responsible for this mistake in our joint work.

[1] S. T. Ma, Proc. Camb. Phil. Soc. 36, 351 (1940), Eq. (25).

A Dynamic Method for the Determination of the Velocity Distribution of Thermal Atoms

IRVING L. KOFSKY AND HENRY LEVINSTEIN
Department of Physics, Syracuse University, Syracuse, New York
July 6, 1948

WE have investigated a new method for the determination of the velocity distribution of atoms evaporated from an oven. It differs from the methods described by Eldridge, Zartman, Estermann, and others[1] in that it can be performed rapidly and is readily adaptable to other measurements connected with atomic beams.

Atoms leaving the oven are pulsed by a single rotating sector disk and detected by a Langmuir-Taylor hot-wire detector[2] about 20 cm away. The velocity distribution of the atoms in the pulses leads to varying transit times for atoms of different velocities, and therefore to a time-dependent current in the detector circuit. This current is a measure of the number of atoms arriving per unit time, and, when it is applied to a cathode-ray oscilloscope with a linear sweep, one can "see" the rate of arrival of atoms at the hot wire. Figure 1 is a photograph of an oscilloscope trace of this curve, using a beam of indium atoms.

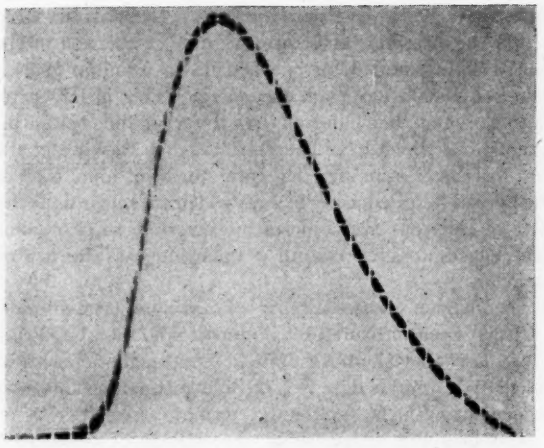

FIG. 1. Sample cathode-ray oscillogram showing the number of atoms arriving at the detector as a function of time.

Further improvements in the method may make it possible to determine the relaxation time, or the mean time an atom stays on the hot wire, if it is assumed that deviations from the atom velocities calculated from the Maxwell-Boltzmann theory are due to this effect. This will be accomplished by placing a photo-tube next to the detector and simultaneously observing the pulses produced on the oscilloscope by both the atoms and the light radiated from the oven. The time difference between the peak of the atom pulse and the peak of the light pulse may then be compared with the theoretically most probable transit time.

[1] J. A. Eldridge, Phys. Rev. 30, 931 (1927); I. F. Zartman, Phys. Rev. 37, 383 (1931); I. Estermann, O. C. Simpson, and O. Stern, Phys. Rev. 71, 238 (1947). The last-mentioned paper contains references to other researches on the subject of the velocity distribution in an atomic beam.
[2] I. Estermann, Rev. Mod. Phys. 18, 310 (1946).

On the Range of the Electrons in Meson Decay

J. STEINBERGER
Institute of Nuclear Studies, The University of Chicago, Chicago, Illinois
June 23, 1948

SOME preliminary data have been obtained in an experiment to determine the range of the electrons resulting from meson decay. The counter arrangement is shown in Fig. 1. The circuits record coincidences in trays 1 and 2, followed from between 0.6 and 4.5×10^{-6} second later by coincidences in trays 3 and 4. Presumably a meson has stopped in absorber 1, disintegrated, and traversed absorber 2. Both absorber 1 and absorber 2 are polystyrene, a hydrocarbon, except for weights of absorber 2 in excess of

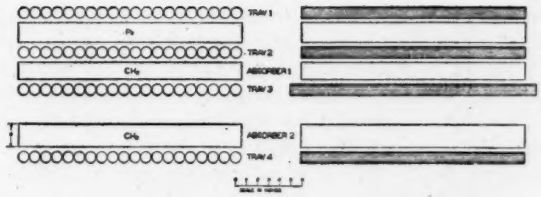

FIG. 1. Arrangement of counters.

16 g/cm², when it is partially carbon and partially polystyrene. The experiment consists of measuring the rate of occurrence of delayed coincidences as a function of the thickness of absorber 2.

The results are shown in Fig. 2. The solid curves show how 25- and 50-Mev electrons would appear in this apparatus. It can be seen that the majority of the electrons have an energy of ~25 Mev, but that an appreciable number have a larger energy. For energies greater than ~65 Mev, the counting rate is approximately that of the calculated background.

In computing the solid curves, the range distribution caused by scattering and geometry were taken into account. The effect of scattering was deduced from a measurement on the range in water of 16.5-Mev electrons. This was kindly communicated to me by Professor Skaggs. The energy loss of electrons has been taken to be 1.72 Mev/g/cm². This is an average value for this energy region for carbon, calculated by Halpern and Hall.[1]

The dashed curve in Fig. 2 is drawn on the basis of an electron spectrum given by

$$\{E[(\mu^2-\mu_0^2)c^4-2E\mu c^2]\}^{\frac{1}{2}}(\mu c^2-E)/[(\mu c^2-2E)\mu c^2]^3$$

where $\mu c^2=100$ Mev is the mass of the decaying meson, $\mu_0 c^2=45$ Mev the mass of a neutral meson, and E is the energy of the electron. The formula is obtained by making a phase space calculation for the three-particle disintegration meson$^{\pm}\rightarrow$meson^0+electron$^{\pm}$+neutrino.

Apparently the spectrum of decay electrons is quite complex. In drawing conclusions from the data, it should be kept in mind that the counting rate for the higher energy electrons is only about twice background, and the statistical errors are large. However, it seems as if the possibility that the meson decays via two competing processes should not be overlooked.

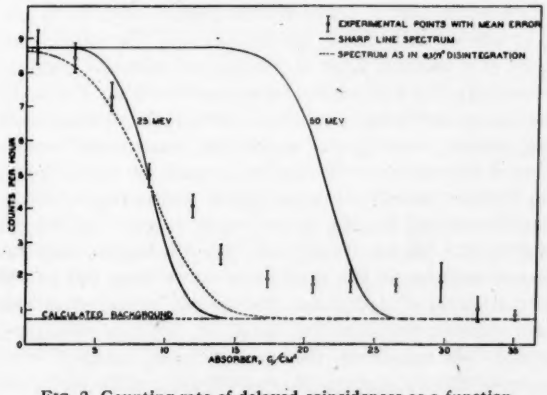

FIG. 2. Counting rate of delayed coincidences as a function of the weight of absorber 2.

I should like to thank Professor E. Fermi and Mr. H. Ticho for much help and advice, and Mrs. N. Woods for filling the counters.

[1] O. Halpern and H. Hall, Phys. Rev. **73**, 447 (1948).

Rate of Production of Helium in Meteorites by Cosmic Radiation

CARL AUGUST BAUER
University of Michigan, Ann Arbor, Michigan
July 2, 1948

THE evidences that cosmic radiation has produced helium in the metallic meteorites are: (1) The rate of production of helium by cosmic radiation in a small meteorite[1] is sufficient to produce the maximum observed helium content (4×10^{-5} cc/g) in a time less than the previously assigned "age" (7.6×10^9 yr.);[2] (2) this process gives a logical explanation to the mass-helium content diagram;[3] and (3) it completely resolves the severe difficulties introduced by the previously assigned "ages," namely, (*a*) the exceedingly great "age" of the "oldest" meteorites, (*b*) the great range in the "ages" of meteorites (from 60 million to 7600 million years), (*c*) the dividing of otherwise completely associated and similar meteorites into two or more groups on the basis of their helium contents alone,[2] (*d*) the variation of the helium content from point to point within the same meteorite,[4] and (*e*) the absence of a dependence of these "ages" on the nickel content of the meteorites and thus on their radial positions within the metallic core of their parent planet.

The 51 Bethany meteorites were all found in a limited region of Great Namaqualand, Southwest Africa. Table I gives, for five Bethany meteorites, the classification of the crystal structure, the percentage of nickel, Paneth's measurements[2] of the uranium, thorium, and helium contents, and his assigned ages. The similarity of these five masses in location, structure, and composition almost certainly establishes them as representing the same fall. However, Amalia (Krantz) has been assigned to a different fall because its helium content is so much greater than the others. These observations can be more satisfactorily accounted for by the assumption that cosmic radiation has produced the helium in Bethany, and therefore the difference in the helium contents of the different fragments arises from the difference in their radial positions within the original preatmospheric mass. The helium content of Goamus is equal to that predicted[3] at the center of a spherical preatmospheric mass of 50,000 kg. For this preatmospheric mass, Amalia (Krantz) must have been about 80 cm from the center, i.e., just on the edge of a spherical mass of 15,000 kg, the total known mass of the Bethany meteorites.

In Bethany Amalia (Krantz) two regions separated by about 7 cm have helium contents[4] that differ by 0.25×10^{-6} cc/g. If the two points were along a radial line and at a distance of 80 cm from the center of a 50,000-kg mass, the

TABLE I. Characteristics of several meteorites.

Name of Bethany meteorite	Class	Ni %	U in 10^{-9} g/g	Th in 10^{-9} g/g	He in 10^{-6} cc/g	Age in 10^9 years calculated from Individual measurements	Average activity
Goamus	Of	8	1	4	0.15	60	75
Amalia (Foote)	Of	8			0.2		110
Gröndorn	Of	8			0.2		110
Lion River	Of	8			0.2		110
Amalia (Krantz)	Of	8	1	4	3.0	1100	1500

predicted difference would be 0.90×10^{-6} cc/g. The observed difference should not be greater than the predicted difference, though it may be less if the two points do not lie along a radial line.

If these two observations, (1) the difference in the helium content of different fragments and (2) the difference from point to point within the same fragment, are accepted as indicating that cosmic radiation has produced the helium in Bethany, then two important conclusions follow: 1. The time since the solidification of the metallic core of the parent planet, and also the time since the disruption of the parent planet, are both less than 60 million years. This upper limit can be established because the U and Th contents of Bethany Goamus are sufficient to produce all of its helium in only 60 million years. 2. The rate of production of helium in meteorites by cosmic radiation is more than 70 times the rate predicted from the values of the observational quantities used in my previous paper.[1] This is true because cosmic radiation has to produce the helium in 60 million years rather than in 4 billion years. This high rate of production of helium in meteorites, as compared to the calculated rate just outside the earth's atmosphere, may arise from the effect of the sun's general magnetic field, as suggested previously,[1] or from secondary helium-producing processes that have not been considered.

[1] C. A. Bauer, Phys. Rev. **72**, 354 (1947).
[2] F. A. Paneth, Nature **149**, 235 (1942).
[3] C. A. Bauer, Phys. Rev. **74**, 225 (1948).
[4] F. A. Paneth, Roy. Astr. Soc., Occasional Notes, **No. 5**, 57 (1939).

Shape of the Positron Spectrum of N^{13}

C. S. COOK, L. M. LANGER, H. C. PRICE, JR., AND M. B. SAMPSON
Indiana University, Bloomington, Indiana
June 21, 1948

IN a recent letter,[1] we reported the results of an investigation of the shape of the positron spectrum of Cu^{61} (3.3 h). It was shown that the momentum distribution deviated markedly at low energies from that predicted by the Fermi theory for an allowed transition. In comparison with our earlier work on Cu^{64} (12.8 h),[2] it was noted that the deviation from the theoretical straight line Fermi plot began at an energy $W=2.0$ mc² for Cu^{61}, whereas the Cu^{64} plot was a straight line down to $W=1.53$ mc². The comparison between the Cu^{64} and Cu^{61} spectra is of interest because it involves two allowed transitions in isotopes having the same nuclear charge, Z, but different maximum energies, i.e., $W_0=3.36$ mc² for Cu^{61} and 2.29 mc² for Cu^{64}.

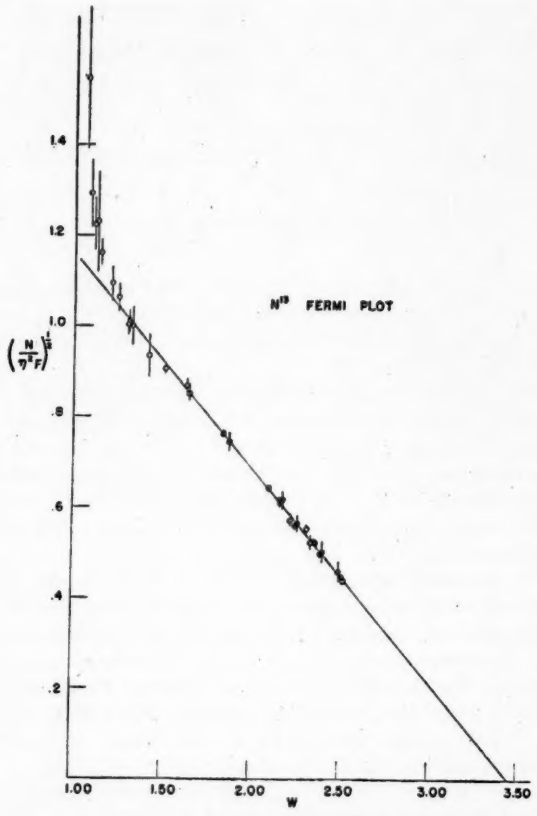

FIG. 1. Fermi plot of the positron momentum spectrum of N^{13}.

Our interest in the spectrum of N^{13} stems mainly from the fact that it is the result of an allowed transition with an energy release almost exactly the same as that in Cu^{61}, but in an isotope of much lower Z. The results of Siegbahn and Slätis[3] indicate that the N^{13} spectrum begins to deviate from theory at about the same energy as our data for Cu^{61} (i.e., 2.0 mc²). However, since their data were obtained with a relatively thick source, it was thought desirable to investigate the N^{13} distribution under more ideal conditions.

In the present experiment, the N^{13} was produced by $C^{12}(d,n)$ in the cyclotron. The sample was activated in such a form that it could be transferred directly to the spectrometer without further preparation. The source consisted of a uniform layer of 0.6-mg/cm² colloidal graphite (Aquadag) on a 0.18-mg/cm² aluminum backing. For bombardment, the sample, mounted on a skeleton aluminum ring support, was clamped against the water-cooled target plate of the cyclotron. An aluminum mask served to confine the 12-Mev deuteron bombardment to the region of the graphite desired for the spectrometer source, i.e., 0.4 cm wide by 2.5 cm long. Individual bombardments were for twenty minutes with a target current of from 100 to 130 microamperes of deuterons. The source, prepared in this way, was then transferred to the 40-cm radius of curvature, shaped field magnetic spectrometer,[4] and readings were begun within six minutes. No trouble was encountered from other activities present, since they are all negatron emitters

and since, because of the large size of the spectrometer and the absence of scattering, the background of the G-M detector was not increased by the presence of the source. The Zapon window counter transmits electrons down to 2.0 kev. The detecting slit width was 0.4 cm.

A decay curve of the positron activity taken over five half-lives in the spectrometer at an $H\rho = 2487$ gauss-cm shows a simple decay with a half-life of 10.2 ± 0.1 minutes. All parts of the spectrum were found to decay with a period consistent with this value.

In taking the data, counts were recorded at each field setting for three successive two-minute intervals. For each bombardment, a few points were taken in the lower energy region, and several points were taken at the high energy region of the spectrum. The individual runs were corrected for decay, and then all the runs were adjusted to the same intensity level at one energy, $W = 2.1$ mc^2.

Figure 1 shows the Fermi plot of the momentum distribution. It is seen that the experimental data are fitted by a theoretical straight line down to about $W = 1.3$ mc^2. This energy, at which the deviation from the Fermi theory begins, is much lower than the value indicated by the data of Siegbahn and Slätis and is indeed lower than that found by us for either Cu^{61} or Cu^{64}.

In the light of these measurements, it would appear that the deviation from theory depends on *both* the nuclear charge, Z, and the maximum energy, W_0, and may therefore be explainable in terms of Coulomb effects on the positron.

Our end point for N^{13}, determined from the straight-line extrapolation, is $E_0 = 1.25 \pm 0.03$ Mev, in good agreement with the value given by Siegbahn and Slätis.

This work is supported by a grant from the Frederick Gardner Cottrell Fund of the Research Corporation and by the U. S. Navy under Contract N6ori-48, T.O. I.

[1] C. S. Cook and L. M. Langer, Phys. Rev. **74**, 227 (1948).
[2] C. S. Cook and L. M. Langer, Phys. Rev. **73**, 601 (1948).
[3] K. Siegbahn and H. Slätis, Arkiv. f. Mat., Astr. o. Fys. **32A**, No. 9 (1945).
[4] L. M. Langer and C. S. Cook, Rev. Sci. Inst. **19**, 257 (1948).

A Process Aiding the Capture of Electrons Injected Into a Betatron

D. W. Kerst
Physics Department, University of Illinois, Urbana, Illinois
June 21, 1948

EARLY experience with the operation of a betatron showed that electrons could be trapped by the magnet although they were injected at energies far above that allowed by the early theory.[1] At these high injection energies the electrons should strike the electrode structure from which they came after completing a few revolutions around the magnet. A particle oscillating with amplitude a about the equilibrium orbit experiences a decrease of amplitude per revolution $da = adE/4E$ where E is the injection energy and dE is the energy gain per revolution. With the values taken from our 22-Mev betatron $a = 1$ cm, $E = 60{,}000$ volts, $dE = 90$ volts/turn; thus, $da = 0.0004$ cm per revolution. In several revolutions this damping is not sufficient to allow the electrons to pass the injector, which in practice can protrude several millimeters beyond the point of injection toward the equilibrium orbit. By tracing groups of electron paths around the machine R. A. Becker, N. Dimitriadis, L. Bess, and J. S. Blair of this physics department have shown that it is not possible to account for passage of the smallest injectors we have used.

The effect I wish to describe depends upon the electromagnetic energy associated with the electron beam circulating between the poles of the betatron. This electromagnetic energy is withdrawn from the kinetic energy of the beam after it leaves the injector. This causes the radius of the orbit to shrink. Since the energy in the electromagnetic field is proportional to the square of the circulating orbit current, the loss of energy per electron will be proportional to the circulating current.

The magnitude of the shrinkage in our 22-Mev betatron can be calculated from the fact that a wire placed at the position of the orbit has about 4×10^{-6} henries inductance mainly as a result of the large central flux. The injection current from the gun is 1 ampere. The voltage per turn is LdI/dt, neglecting retardation, and if one ampere circulating was established in the time for one revolution, 10^{-8} second, the loss per turn would be $4 \times 10^{-6} \pm 10^{+8} = 400$ electron volts. If several revolutions are required to establish this circulating current, the energy lost by the electrons is still 400 electron volts. The electrostatic energy associated with an ampere of circulating current is about 150 electron volts, making the total loss 550 electron volts.

The shift in the orbit radius, r, produced by this loss is $dr = rdE/(1-n)2E = 4$ mm with $r = 20$ cm, $E = 60{,}000$ volts, $dE = 550$ volts, and $n = \frac{3}{4}$. We know that we retain only 0.1 ampere in the beam,[2] but it is very likely that electrons destined to strike the wall or the injector rotate a few times about the magnet and build the current up to one ampere for a while.

The resistance of the tube coating and the time for penetration of magnetic flux into iron should influence the time dependence of this orbit contraction.

Injection from a gun placed at a radius smaller than the orbital radius works well. This also may be aided by the same effect. In this case electrons injected at about the time the circulating current has reached its maximum will increase in energy and orbital radius as the main part of the circulating current is lost by striking the injector.

Since this action described depends on the current circulating in the beam, it might be expected that the yield of x-rays from a betatron would increase more rapidly than the emission current from the injector. However, it is known that yield sometimes increases and sometimes decreases as the emission is decreased. The characteristics on the injector hinder a simple interpretation of an emission measurement.

It is frequently found that a so-called orbit contractor greatly assists the capture of electrons. It consists of one wire above and one wire below the orbit in which a rising current at injection time contracts the orbit.[3] This helpful action is very similar to the action of the beam on itself, and in cases where it is impossible to build up a high circu-

lating current in an accelerator the use of a contractor may prove to be valuable.

The magnetic and electrostatic fields of the beam also influence the focusing of electrons in the beam. Damping of oscillations about the equilibrium orbit results from decreasing electrostatic repulsion within the beam, as some of the circulating current is being lost to the walls. This damping is of the same order of magnitude as the orbit contraction in the example above.

[1] D. W. Kerst and R. Serber, Phys. Rev. **60**, 47 (1941); J. A. Rajchman and W. H. Cherry, J. Franklin Inst. **243**, 281 (1947).
[2] Leon Bess and A. O. Hanson, Rev. Sci. Inst. **19**, 108 (1948).
[3] In process of publication by G. D. Adams.

The Neutron Density in the Free Atmosphere up to 67,000 Feet*

LUKE C. L. YUAN
Princeton University, Princeton, New Jersey
June 22, 1948

SINCE neutrons in cosmic rays cannot be considered as primary particles because of their short lifetime, a maximum in the intensity distribution of neutrons as a function of the altitude must exist. Considerable work[1-4] has been done in the past to determine the neutron distribution in the atmosphere, and the results obtained thus far show that at low altitudes the slow neutron intensity increases exponentially with the altitude up to about 20 cm of Hg, with an absorption depth, λ, of the order of 150 g/cm^2, where λ is given by the expression $N=N_0\exp(-x/\lambda)$.

The following is a preliminary report on recent results obtained at high altitudes where a maximum in slow neutron intensity has been observed.

The measurements were carried out by sending aloft two identical BF_3 proportional counters to an altitude of 67,000 feet by means of free balloons. These counters were filled with enriched boron of 96 percent B^{10} to a pressure of 20 cm of Hg, and they were operated at a voltage plateau centered at 800 volts.

One counter was shielded with 0.030 inch of cadmium and the other counter was enclosed in a tin shield of the same thickness for the compensation of possible effects

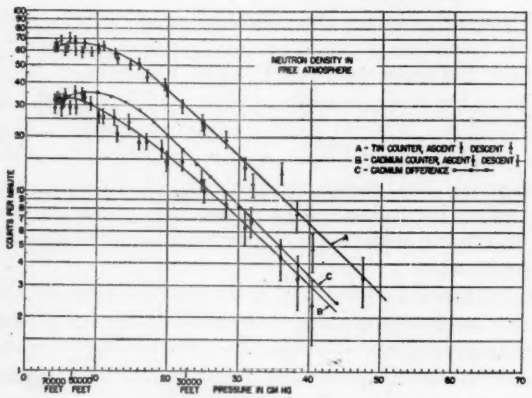
NEUTRON DENSITY IN FREE ATMOSPHERE
A - TIN COUNTER, ASCENT } DESCENT
B - CADMIUM COUNTER, ASCENT } DESCENT
C - CADMIUM DIFFERENCE
COUNTS PER MINUTE
PRESSURE IN CM HG

FIG. 1. Neutron density as a function of pressure in the free atmosphere.

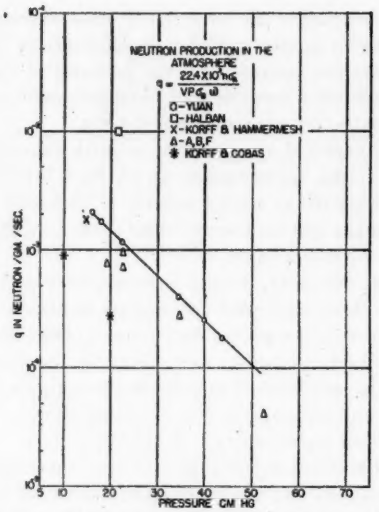

FIG. 2. Rate of neutron production in the atmosphere.

caused by stars produced in the cadmium shield. Both shields were sealed airtight and were maintained at atmospheric pressure throughout the flight, thus eliminating any possible effects caused by corona discharge at the high voltage terminals.

The measured neutron counts were radioed down by means of a frequency-modulated telemetering system.

A calibrated fixed signal of constant amplitude was switched on every 15 minutes for a period of 8 seconds. This served as a check on the constancy of the amplifier gain and the performance of the whole system.

The temperature and the pressure were measured by means of a thermal resistor and an aneroid barometer, respectively.

The measurements were recorded on a galvanometer-type oscillograph, as well as by a scaling circuit arrangement, whose readings were photographed automatically every minute.

The results of this flight are collected in Fig. 1. This shows the counting rate as a function of altitude. The upper curve (A) is for the tin-shielded counter and the lower one (B) for the cadmium-shielded counter. A maximum in the neutron intensity has been obtained for both counters at about 7 cm of Hg. The maximum intensity for slow neutrons, obtained by taking the cadmium difference ($E_n<0.4$ ev), occurs at approximately 9 cm Hg (center curve, C).

Up to 18 cm of Hg the neutron intensity increases exponentially with the altitude, with an absorption depth of 156 g/cm^2, which is in agreement with our previous measurements at lower altitudes.

Our counter sensitivity was calibrated experimentally through the courtesy of the Argonne National Laboratory by using their standardized neutron source. The result of the rather elaborate calibrations is that the efficiency of our 20-cm Hg counter for thermal neutrons is 6.8 percent. By means of this calibration, the absolute values of the rate of production of neutrons in the atmosphere per gram per second are calculated from the expression given by Bethe,

Korff, and Placzek.[2] These values, as well as those calculated from recent results of Korff and Cobas,[3] Agnew, Bright, and Froman,[4] are shown in Fig. 2. (The upper limit of q cannot exceed twice the calculated value.)

The cadmium ratio, i.e., the ratio between the unshielded and cadmium-shielded counters, is of the order of 2.2 over the depth from 22.8 cm of Hg to 4 cm of Hg. This is in agreement with Agnew, Bright, and Froman's[4] results.

The author wishes to express his gratitude to Professor R. Ladenburg for many helpful discussions, to Mr. D. B. Davis, who is responsible for the designing and building of the balloon equipment and to members of the Ordnance Research Laboratory who helped to make the flight a successful one.

* This report is based upon work performed under Contract N6onr-270 with the Office of Naval Research at the Ordnance Research Laboratory of Princeton University.

[1] E. Fünfer, Naturwiss. **25**, 235 (1937); E. Fünfer, Zeits. f. Physik **111**, 351 (1938); S. A. Korff and B. Hamermesh, Phys. Rev. **69**, 155 (1946).

[2] H. A. Bethe, S. A. Korff, and G. Placzek, Phys. Rev. **57**, 573 (1940).

[3] S. A. Korff and A. Cobas, Phys. Rev. **73**, 1010 (1940).

[4] H. M. Agnew, W. C. Bright, and Darol Froman, Phys. Rev. **72**, 203 (1947).

Neutron Absorption in Samarium

A. J. DEMPSTER
Argonne National Laboratory, Chicago, Illinois
June 28, 1948

IN a recent paper[1] it was shown that the large neutron absorption in samarium is due to the isotope at mass 149. Since the alteration produced by the neutrons was not very large, the experiment was repeated with a 4-mg sample exposed in a thin layer of approximately 1 mg per sq. cm to a much stronger neutron flux. The isotope at mass 149 was so reduced that it could not be detected. One of ten mass spectra made with one milligram of the sample is shown in Fig. 1, together with a mass spectrum of normal samarium. The intensity of the isotope at mass 150 was greatly increased so that it appears approximately equal to the one at 154. A faint gadolinium impurity showed on the long exposures, with the two absorbing isotopes at 155 and 157 missing.

Photometric measurements of the plates showed that the densities at the masses 147, 148, 152, and 154 fell on a normal photographic density curve indicating no changes as a result of neutron absorption in any of these isotopes. The new abundance at mass 150 was found from four spectra to have increased to 21.2±0.4 percent. The normal abundance at 150 is 7.47, and at 149, 13.84 percent, the sum being 21.3 percent. This shows that within the experimental error the isotopes that disappear at mass 149 reappear at mass 150. The absorbing cross sections of the other isotopes were estimated to be less than one percent of that of the isotope at mass 149.

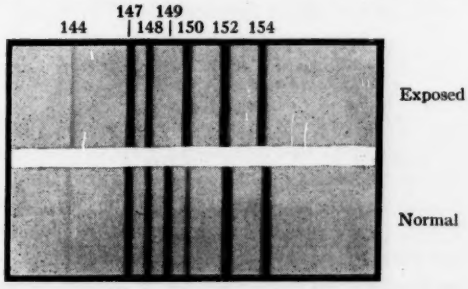

FIG. 1. Samarium isotopes altered by neutron absorption.

[1] R. E. Lapp, J. R. Van Horn, and A. J. Dempster, Phys. Rev. **71**, 745 (1947).

The Origin of Elements and the Separation of Galaxies

G. GAMOW
George Washington University, Washington, D. C.
June 21, 1948

THE successful explanation of the main features of the abundance curve of chemical elements by the hypothesis of the "unfinished building-up process,"[1,2] permits us to get certain information concerning the densities and temperatures which must have existed in the universe during the early stages of its expansion. We want to discuss here some interesting cosmogonical conclusions which can be based on these informations.

Since the building-up process must have started with the formation of deuterons from the primordial neutrons and the protons into which some of these neutrons have decayed, we conclude that the temperature at that time must have been of the order $T_0 \cong 10^9$ °K (which corresponds to the dissociation energy of deuterium nuclei), so that the density of radiation $\sigma T^4/c^2$ was of the order of magnitude of water density. If, as we shall show later, this radiation density exceeded the density of matter, the relativistic expression for the expansion of the universe must be written in the form:

$$\frac{d}{dt}\lg l = \left(\frac{8\pi G}{3}\frac{\sigma T^4}{c^2}\right)^{\frac{1}{2}} \tag{1}$$

where l is an arbitrary distance in the expanding space, and the term containing the curvature is neglected because of the high density value. Since for the adiabatic expansion T is inversely proportional to l, we can rewrite (1) in the form:

$$-\frac{d}{dt}\lg T = \frac{T^2}{c}\left(\frac{8\pi G\sigma}{3}\right)^{\frac{1}{2}} \tag{2}$$

or, integrating:

$$T^2 = \left(\frac{3}{32\pi G\sigma}\right)^{\frac{1}{2}}\cdot\frac{c}{t}. \tag{3}$$

For the radiation density we have:

$$\rho_{\text{rad.}} = \frac{3}{32\pi G}\cdot\frac{1}{t^2}. \tag{4}$$

These formulas show that the time t_0, when the temperature dropped low enough to permit the formation of deuterium, was several minutes. Let us assume that at that time the density of matter (protons plus neutrons) was $\rho_{\text{mat.}}{}^\circ$. Since, in contrast to radiation, the matter is conserved in the process of expansion, $\rho_{\text{mat.}}$ was decreasing as $l^{-3} \sim T^3 \sim t^{-\frac{3}{2}}$. The value of $\rho_{\text{mat.}}{}^\circ$ can be estimated from

the fact that during the time period Δt of about 10^2 sec. (which is set by the rate of expansion), about one-half of original particles were combined into deuterons and heavier nuclei. Thus we write:

$$v\Delta t n\sigma \cong 1 \tag{5}$$

where $v = 5 \cdot 10^8$ cm/sec. is the thermal velocity of neutrons at 10^9 °K, n is the particle density, and $\sigma \cong 10^{-29}$ cm^2 the capture cross section of fast neutrons in hydrogen. This gives us $n \cong 10^{18}$ cm^{-3} and $\rho_{\text{mat.}}{}^\circ \cong 10^{-6}$ g/cm^3 substantiating our previous assumption that matter density was negligibly small compared with the radiation density. (Thus we have $\rho_{\text{mat.}}{}^\circ \cdot \Delta t \cong 10^{-4}$ g·cm^{-3}·sec. and not 10^{+4} g·cm^{-3} sec. as was given incorrectly in the previous paper[2] because of a numerical error in the calculations.)

Since $\rho_{\text{rad.}} \sim t^{-2}$ whereas $\rho_{\text{mat.}} \sim t^{-1}$ the difference by a factor of 10^6 which existed at the time 10^9 sec. must have vanished when the age of the universe was $10^2 \cdot (10^6)^2 = 10^{14}$ sec. $\cong 10^7$ years. At that time the density of matter and the density of radiation were both equal to $[(10^6)^2]^{-2} = 10^{-24}$ g/cm^3. The temperature at that epoch must have been of the order $10^9/10^6 \cong 10^3$ °K.

The epoch when the radiation density fell below the density of matter has an important cosmogonical significance since it is only at that time that the Jeans principle of "gravitational instability"[3] could begin to work. In fact, we would expect that as soon as the matter took over the principal role, the previously homogeneous gaseous substance began to show the tendency of breaking up into separate clouds which were later pulled apart by the progressive expansion of the space. The density of these individual gas clouds must have been approximately the same as the density of the universe at the moment of separation, i.e., 10^{-24} g/cm^3. The size of the clouds was determined by the condition that the gravitational potential on their surface was equal to the kinetic energy of the gas particles. Thus we have:

$$\frac{3}{2}kT = \frac{4}{3}\pi R^3 \rho \frac{Gm_H}{R} = \frac{4\pi G m_H \rho}{3} R^2. \tag{6}$$

With $T \cong 10^3$ and $\rho \cong 10^{-24}$ this gives $R \cong 10^{21}$cm $\cong 10^3$ light years.

The fact that the above-calculated density and radii correspond closely to the observed values for the stellar galaxies strongly suggests that we have here a correct picture of galactic formation. According to this picture the galaxies were formed when the universe was 10^7 years old, and were originally entirely gaseous. This may explain their regular shapes, resembling those of the rotating gaseous bodies, which must have been retained even after all their diffused material was used up in the process of star formation (as, for example, in the elliptic galaxies which consist entirely of stars belonging to the population II).[4]

It may also be remarked that the calculated temperature corresponding to the formation of individual galaxies from the previously uniform mixture of matter and radiation, is close to the condensation points of many chemical elements. Thus we must conclude that some time before or soon after the formation of gaseous galaxies their material separated into the gaseous and the condensed (dusty) phase. The dust particles, being originally uniformly distributed through the entire cloud, were later collected into smaller condensations by the radiation pressure in the sense of the Spitzer-Whipple theory of star formation.[5] In fact, although there were no stars yet, there was still plenty of high intensity radiation which remained from the original stage of expanding universe when the radiation, and not the matter, ruled the things.

In conclusion I must express my gratitude to my astronomical friends, Dr. W. Baade, Dr. E. Hubble, Dr. R. Minkowski, and Dr. M. Schwartzschield for the stimulating discussion of the above topics.

[1] G. Gamow, Phys. Rev. **70**, 572 (1946).
[2] R. Alpher, H. Bethe, and G. Gamow, Phys. Rev. **73**, 803 (1948).
[3] J. H. Jeans, *Astronomy and Cosmogony* (Cambridge University Press, Teddington 1928).
[4] W. Baade, Astrophys. J. **100**, 137 (1944).
[5] L. Spitzer, Jr., Astrophys. J. **95**, 329 (1942); F. L. Whipple, Astrophys. J. **104**, 1 (1946).

Pressure Broadening in Ammonia at Centimeter Wave-Lengths*

DEFOREST F. SMITH
Sloane Physics Laboratory, Yale University, New Haven, Connecticut
June 28, 1948

THE intensities and shapes of microwave absorption lines in gases have been successfully correlated with the Van Vleck-Weisskopf[1] modification of the Lorentz impact-broadening theory. The absorption in the long wave-length tails of the ammonia inversion lines offers a severe test of this theory. Precise measurements of this absorption have been completed at wave-lengths 4.43 cm and 3.20 cm in the pressure range 0.1 to 7 atmospheres. These results are plotted in Fig. 1, together with the absorption coefficients computed by numerically summing the Van Vleck-Weisskopf expression over the rotational states, using the measured Bohr frequencies,[2] and a linear pressure variation of the measured half-widths.[2]

The discrepancy between theory and experiment is most severe at the higher pressures, but exceeds the measurement errors at pressures as low as 10 cm of mercury. The discrepancies are apparently inherent in the impact theory

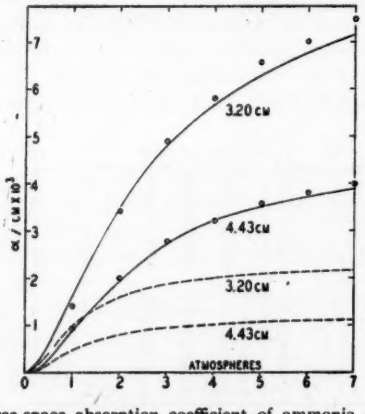

FIG. 1. Free-space absorption coefficient of ammonia at 20°C *vs.* pressure. Solid lines are experimental. Dashed lines are computed with impact theory. Circles are computed as discussed in text.

and cannot be removed by acceptable changes in the parameters.

At very high pressures, not collisions, but intermolecular perturbations, should be used in considering spectral line shapes, and a statistical type of theory should be employed. A crude form of this theory has been devised. The long-range perturbations partially developed by Margenau and Warren[3] suggested averaged perturbations that led to an expression for a statistical absorption coefficient α_s. This α_s differed from the Van Vleck-Weisskopf absorption coefficient α_i only in the shape factor term. The dispersion form in α_i was replaced by a triangular form in α_s.

The line widths in the expression for α_s were estimated from the r.m.s. perturbations, using intermolecular distances equal to the radius of the volume per molecule sphere.

At intermediate pressures the actual line shapes should depend on both statistical and impact processes. The behavior of the impact theory expression when a finite collision duration was introduced together with the assumption that the statistical processes are of importance only when the molecules are closer than the collision distance, suggested that in general the absorption coefficient at any pressure might be written as

$$\alpha=\alpha_i \exp(-ap)+\alpha_s[1-\exp(-ap)];$$

(ap) was taken to be the ratio of the volume of the collision sphere to the volume per molecule.

The absorption computed in this manner shows no substantial improvement over the impact theory itself, unless the Bohr frequencies used in α_s, and in α_s only, vanish. The circles in Fig. 1 are calculated on this basis. It should be pointed out that none of the parameters used in this computation were adjusted to fit the observed absorption. While calculations have not been carried out in detail, the above theory appears to be in agreement with published observations at shorter wave-lengths.[2, 4, 5, 6]

* Assisted by the Office of Naval Research under Contract N7onr-288, Task Order 1. This work was part of a dissertation presented for the degree of Doctor of Philosophy at Yale University.

[1] J. H. Van Vleck and V. F. Weisskopf, Rev. Mod. Phys. **17**, 229 (1945).
[2] B. Bleaney and R. P. Penrose, Proc. Phys. Soc. **60**, 83 (1948).
[3] H. Margenau and B. E. Warren, Phys. Rev. **51**, 748 (1937).
[4] J. E. Walter and W. D. Hershberger, J. App. Phys. **17**, 814 (1946).
[5] C. E. Cleeton and N. H. Williams, Phys. Rev. **45**, 234 (1934).
[6] B. Bleaney and Loubser, Nature **161**, 523 (1948).

On the Use of Nuclear Plates in a Magnetic Field

IAN G. BARBOUR
University of Chicago, Chicago, Illinois
July 1, 1948

SINCE present nuclear plate techniques do not allow direct determination of the sign of particles investigated and individual mass measurements are not very accurate magnetic deflection methods assume considerable importance in the study of cosmic rays. Powell and Rosenblum[1] have proposed that if two parallel emulsion surfaces separated by an air gap are placed perpendicular to a magnetic field, the curvature of a particle's path in air can be obtained from the tracks in the emulsions on either side. We have been using a similar arrangement, differing in several particulars from their method, to determine meson masses at balloon altitudes. Under Pb absorbers we have, in collaboration with J. J. Lord, obtained on our plates meson densities great enough to make measurements on such flights practicable.

In viewing the plates after development, accurate measurements can be made only if the two emulsions are exactly juxtaposed. With ordinary commercial plates, this involves viewing through the glass backing of 1 mm thickness, so that high magnification is impossible with refracting microscopes. Powell has therefore had to use a specially constructed reflecting microscope[2] with a large working distance. In our experiments, we have re-coated the original emulsions on very thin glass plates (150 microns and even down to 50 microns). Besides enabling the use of an ordinary microscope, this method has the additional advantage that if thin plates are coated with emulsion on both sides, several such plates separated by air gaps can be stacked as a "sandwich," and more than one curvature measurement made on the same particle as it crosses successive air gaps. Emulsions coated on thin plates, or on acetate film-backing, will be commercially obtainable in the near future.

The magnetic deflection can be measured by projecting as a straight line the last segment of a track as it leaves the top plate, and determining the distance from this line to the point at which the particle enters the lower emulsion. An independent deflection measurement is obtained by similarly projecting back the first segment of the lower track. Scattering very near the surface may introduce uncertainty in the direction of the projected line which would result in an error in the measured deflection proportional to the path length in air. Since, however, the magnetic curvature produces a deflection proportional to the square of the path length, a greater air gap will reduce the percentage error. Our air gap is 2000 microns wide. For a path length of 10,000 microns in air and our field of 12,500 gauss, the theoretical deflection of a 200 m_e meson of energy 4.5 Mev is 625 microns; for 1.2 Mev, 1250 microns, etc. Events with path length longer than this can readily be recorded, the only limit being the correct matching of tracks in the two emulsions caused by the same particle. The direction of an emergent track and its "dip angle" with the plane of the emulsion are found, and tracks in the lower emulsion in the region where the particle might be expected to strike are noted. We are simplifying this procedure by the use of a projection microscope, a tilting stage to measure dip angles, and a magnifying pantagraph attached to the stage with which the location and orientation of tracks can be traced on a large sheet of paper. Matching is checked by the equality of (a) the two deflection measurements obtained by projecting the upper and lower tracks, respectively, as indicated above; (b) the angles of dip, and (c) the grain densities, above and below. With proton tracks obtained by cyclotron bombardment and with plates exposed on balloon flights we are able to get good matching of tracks between the two emulsions.

[1] C. F. Powell and S. Rosenblum, Nature **161**, 473 (1948).
[2] Burch, Proc. Phys. Soc. **59**, 41 (1947).

Concentration of He^3 by Evaporation of Liquid Helium at Temperatures Below the λ-Point

B. V. ROLLIN AND J. HATTON
Clarendon Laboratory, Oxford, England
June 23, 1948

IN measurements made by Fairbank, Lane, Aldrich, and Nier[1] on the distribution of He^3 between the liquid and vapor phases in a dilute solution of He^3 in He^4, it was found that the concentration of He^3 in the vapor dropped to zero at a temperature just below the λ-point of He^4.

It is important to determine whether this represents a new property of solutions of He^3 in He^4 or whether it is a consequence of the fact that He^3 does not take part in superfluid flow.[2] The difficulty is to determine whether the gas sample collected has been evaporated from the main bulk of the liquid or from liquid transported up the connecting tube by the film phenomenon.[3] Fairbank, *et al.* calculated the contribution caused by evaporation from the film by using published values for the rate of film flow and concluded that film transport was insufficient to explain the observed results. However, it has been found that film effects may be very different with different experimental arrangements, and we have therefore thought it worth while to carry out experiments under conditions where it was quite certain that an appreciable fraction of the gas sample collected had been evaporated from the bulk liquid.

The cryostat consisted of two small vessels A and B in thermal contact, situated in an evacuated enclosure. About 1 cc of ordinary liquid helium was introduced into vessel A, while in vessel B we condensed about 0.1 cc of liquid helium from gas in which the He^3 content had been enriched by thermal diffusion to 0.15 percent.

The temperature of the cryostat was reduced to 1.3°K by pumping on A, and the evaporation rate from A was then 11 cc of gas at N.T.P. per minute. Heat was now supplied by a heating coil wound round B until the evaporation rate was doubled, and vessel B, the effective dead-volume of which (reduced to room temperature) was 600 cc, was connected with an external volume of 600 cc. The pumping of A was stopped and the vapor pressure in B increased slowly. When the pressure had risen to 5 mm, the external volume was cut off from vessel B which was then connected with a sampling bulb of 500 cc volume. The sampling bulb itself was closed off when the pressure in it had risen to 5 mm. The time taken in the flushing process was 80 seconds and the subsequent sampling occupied 1 minute.

Analysis of the gas sample showed it to contain 1.5 percent of He^3, representing a tenfold enrichment over the original concentration. The true enrichment factor for vapor in equilibrium with the liquid must be considerably greater than 10, because our sample was certainly diluted with He^4 as a result of the film effect and also because the concentration in the liquid was considerably depleted by the flushing and sampling processes.

It is possible that the discrepancy between this result and those obtained by Fairbank, *et al.*[1] is due to a fundamental difference between the properties of dilute and concentrated solutions of He^3 in He^4, as suggested by London and Rice.[4] However, it seems possible to us that the results of Fairbank, *et al.* may have been obscured by a predominance of the film effect.

Our result shows that by evaporation at very low temperatures, when the He^3 concentration is relatively high and when there is appreciable heat inflow, the He^3 tends to be concentrated in the vapor rather than in the residual liquid as suggested by Fairbank, *et al.*

[1] H. A. Fairbank, C. T. Lane, L. T. Aldrich, and A. O. Nier, Phys. Rev. **73**, 729 (1948).
[2] J. G. Daunt, R. E. Probst, H. L. Johnston, L. T. Aldrich, and A. O. Nier, Phys. Rev. **72**, 502 (1947).
[3] B. V. Rollin and F. Simon, Physica **6**, 219 (1939).
[4] F. London and O. K. Rice, Phys. Rev. **73**, 1189 (1948).

Beta-Beta-Coincidence Curves for Ir^{192} and Ta^{182}*

M. V. SCHERB AND C. E. MANDEVILLE
Bartol Research Foundation of the Franklin Institute, Swarthmore, Pennsylvania
June 25, 1948

THE writers have recently reported[1] on beta-beta-coincidence curves in the disintegration of Ir^{192} and Ta^{182}. These data were obtained by placing aluminum absorbers before *both* of the beta-ray counters. In discussing the curves it was remarked that in studying Ir^{192}, we did not observe the maximum in the region of low energy which was reported by Wiedenbeck and Chu.[2] It turns out that although the internal conversion coefficients of Table II of their paper were determined by placing absorbers before *both* counters, the curves shown for Ir^{192} and Au^{198} were obtained by inserting foils before only *one* of the two beta-ray counters. The comparison of curve shapes made by the writers was therefore without meaning. Dr. Wiedenbeck has kindly advised us of this oversight in a recent communication.

Beta-beta-coincidence rates for Ir^{192} and Ta^{182} are shown in Figs. 1 and 2 as a function of the aluminum absorber thickness placed before *one* of the beta-ray counters. Figure 1 shows that the "peculiar hump" is indeed present in the case of Ir^{192}. In Fig. 2, the beta-beta-coincidence rate of Ta^{182} remains constant at 1.2×10^{-3} coincidence per beta-

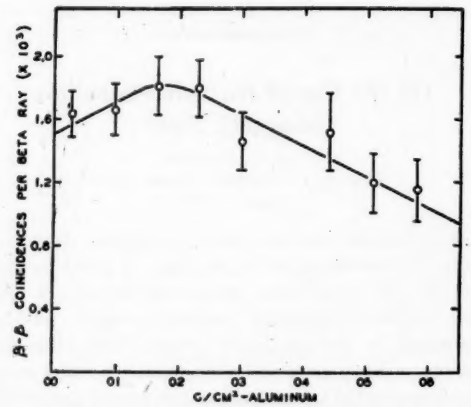

FIG. 1. Beta-beta-coincidences in the disintegration of Ir^{192}.

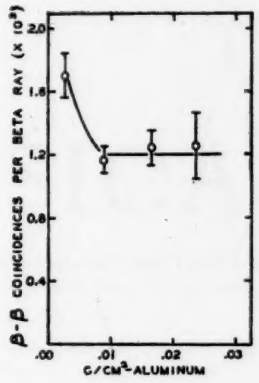

FIG. 2. Beta-beta-coincidences in the disintegration of Ta^{182}.

ray beyond 0.0085 g/cm² of aluminum. It seems reasonable to suppose that a rise of the curve to a peak in the low energy region was obscured by the thickness (2.5 mg/cm²) of the windows of the beta-ray counters.

* Assisted by the Office of Naval Research.
[1] M. V. Scherb and C. E. Mandeville, Phys. Rev. **73**, 1401 (1948).
[2] M. L. Wiedenbeck and K. Y. Chu, Phys. Rev. **72**, 1171 (1947).

Disintegration of Mesotrons in B^{10} *

NORRIS G. NERESON
Department of Physics, University of New Mexico, Albuquerque, New Mexico
and
Los Alamos Scientific Laboratory, Los Alamos, New Mexico
June 28, 1948

IN the fall of 1947 the suggestion was made by D. Froman, R. Landshoff, and F. Reines of the Los Alamos Laboratory that a comparison of the capture and disintegration processes of mesotrons in normal boron B^{11} and the boron isotope B^{10} would provide evidence as to a possible isotope effect. While this experiment was in progress, a further idea was expressed by Weisskopf[1] that negative mesotrons ought to be absorbed or captured in B^{10} if mesons interacted only as pairs with the nucleus. In order to clarify existing theories and ideas, the experiment described below was performed.

Results on the disintegration of positive and negative mesotrons in normal boron have been presented in a previous article.[2] The investigation of B^{10} was carried out simultaneously with B^{11} in the above mentioned experiment[2] and the same procedure followed as for the investigation of B^{11}. An iron container enclosing the B^{10} isotope accounted for 20 percent of the total weight of boron and container. The B^{10} employed was similar in size and quantity to that used in the case of B^{11} (approximately 11,000 grams).

The results for B^{10} are given in Table I as an addition to the table of results previously given. For convenience of comparison, the B^{11} results are also listed here again. In the extreme right column, the decay electron counting rate from positive mesotrons has been corrected (reduced) by a factor corresponding to the positive mesotron excess as derived from the anticoincidence rates. In the same column, the delayed counting rate from negative mesotrons has been corrected (increased) for the capture of negative mesotrons by the iron container; this correction has been made on a weight basis.

It is evident from the listed results that no significant difference is present in the delayed or decay electron counting rate from the two boron absorbers, demonstrating the absence of an isotope effect. The B^{10} data also provides additional evidence that the capture probability of negative mesotrons is very small in the case of boron.

The financial support of the Research Corporation of New York is gratefully acknowledged for work done at the University of New Mexico.

* The work described in this article was done under the auspices of the Atomic Energy Project, and the information contained in this article will also be included in the National Nuclear Energy Series (Manhattan Project Technical Section).
[1] Victor Weisskopf, Phys. Rev. **72**, 155–56 (1947).
[2] Norris Nereson, Phys. Rev. **73**, 565 (1948).

TABLE I. Comparison of results on disintegration of mesotrons in B^{10} and B^{11} absorbers.

Absorber material	Mesotron sign	Coincidences ($ABCD$) per hour	Ratio of positive to negative coincidence rate	Anticoincidences ($ABCD-X$) per hour	Ratio of positive to negative anticoincidence rate	Total running time for delayed counts	Total delayed counts	Delayed counts per hour	Delayed counting rates corrected for positive mesotron excess and iron container
Boron Isotope 95.5% B^{10} (In iron container)	Positive	46.0±0.5	1.10±0.02	17.7±0.3	1.15±0.03	185 hr.	26	0.14±0.03	0.12±0.03
	Negative	41.8±0.5		15.4±0.3		205 hr.	19	0.09±0.02	0.11±0.02
Normal Boron 81.6% B^{11} (In iron container)	Positive	46.7±0.4	1.10±0.01	18.5±0.2(5)	1.19±0.02	380 hr.	66	0.17±0.02	0.14±0.02
	Negative	42.5±0.4		15.5±0.2(5)		350 hr.	27	0.08±0.01(5)	0.11±0.01(5)